universität wien

DISSERTATION

Titel der Dissertation

Role of Lamina-associated polypeptide 2 alpha in striated muscle differentiation and regeneration

angestrebter akademischer Grad

Doktorin der Naturwissenschaften (Dr. rer.nat.)

Verfasserin:	Ivana Gotic
Matrikel-Nummer:	0448428
Dissertationsgebiet (lt. Studienblatt):	Molekulare Biologie
Betreuerin / Betreuer:	Univ.-Prof. Dr. Roland Foisner

Wien, im Juli, 2009

Table of Contents

Table of Figures

I. Abstract

Lamina-associated polypeptide 2α (LAP2α) is a mammalian nucleoplasmic protein implicated in cell cycle regulation through its interaction with A-type lamins and the retinoblastoma protein (pRb). Mutations in lamin A/C and LAP2α cause a variety of pathological human conditions, collectively termed laminopathies. One of the tissues most frequently affected by changes in genes encoding lamin A/C and LAP2α is striated muscle. To elucidate the molecular mechanisms underlying these severe conditions and study the role of LAP2α in striated muscle tissue, I analyzed the structural and functional properties of heart and skeletal muscle in complete and conditional tissue-specific LAP2α knockout mice.

Similar to the human condition caused by a mutation in LAP2α, complete knockout of the gene impaired heart function in mice and rendered the myocardium more susceptible to fibrosis with advancing age. At the molecular level, loss of LAP2α caused a deregulation of major cardiac transcription factors GATA4 and MEF2c, as well as their tissue-specific target genes. Activation of compensatory pathways in LAP2α-deficient hearts resulted in downregulation of β-adrenergic receptor signaling and reduced responsiveness of the myocardium to chronic β-adrenergic stimulation, stalling the progression from cardiac hypertrophy towards heart failure. On the other hand, dystrophin deficiency in an *Mdx* background resulted in a transient rescue of the *Lap2α*$^{-/-}$ phenotype.

Skeletal muscle of LAP2α-deficient mice showed no overt defects in muscle morphology, function and regeneration *in vivo*. Nevertheless, the absence of LAP2α caused an increase in the murine myofiber-associated muscle stem cell pool, which showed an enhanced stem cell-like phenotype and delayed myogenic differentiation *in vitro*. In addition, loss of LAP2α shifted the myofiber type ratios of adult slow muscles towards fast fiber types.

Altogether, these data suggest a novel role of LAP2α in maintenance of cardiac function under normal and stress conditions and demonstrate a dual function of the protein in skeletal muscle tissue, namely in satellite cell maintenance and early myogenic differentiation, as well as myofiber type-specification and muscle remodeling.

II. Zusammenfassung

Lamina-assoziiertes Polypeptid 2α (LAP2α) ist ein nucleoplasmatisches Protein, welches spezifisch in Säugerzellen expremiert wird. Durch die Interaktion mit A-Typ Laminen und dem Retinoblastoma Protein ist es in die Regulation des Zellzyklus involviert. Mutationen in Lamin A/C und LAP2α können zu Krankheiten im Menschen führen, die Laminopathien genannt werden und bei welchen am häufigsten die quergestreifte Muskulatur betroffen ist. Ich habe die strukturellen und funktionellen Eigenschaften von Herz-und Skelettmuskulatur in kompletten sowie gewebsspezifisch-konditionellen LAP2α knockout Mäusen analysiert, um einen Einblick in die molekularen Mechanismen zu bekommen, die den Erkrankungen zu Grunde liegen.

Das Fehlen von LAP2α in Mäusen verursachte einen ähnlichen Phenotyp, wie die Mutation des Genes im Menschen. Die Mäuse weisen eine verminderte Funktionalität des Herzens und eine erhöhte Anfälligkeit für Fibrose im Myokard im vorangeschrittenen Alter auf. Auf molekularer Ebene führte das Fehlen von LAP2α zu einer Deregulation der für die Herzentwicklung wichtigen Transkriptionsfaktoren GATA4 und MEF2c, sowie deren Zielgene. Die Aktivierung von Kompensationsmechanismen im Herz der *Lap2α*$^{-/-}$ Maus hatte eine verminderte Aktivität des β-adrenergen Rezeptors zur Folge. Die dadurch herbeigeführte reduzierte β-adrenerge Stimulationsfähigkeit des Myokards verhinderte eine weitere Progression der Hypertrophie, welche andernfalls zum Versagen der Herztätigkeit geführt hätte. Andererseits führte eine Dystrophin-Defizienz in einem genetischen *"Mdx"* Hintergrund zu einer transienten Aufhebung des LAP2α-null Phenotyps.

Die Morphologie, Funktion und Regeneration der Skelettmuskulatur in der *Lap2α*$^{-/-}$ Maus zeigte *in vivo* keine offensichtlichen Veränderungen. Nichtsdestotrotz führte das Fehlen von LAP2α zu einer erhöhten Anzahl von Muskelfaser-assoziierten Stammzellen, welche eine verzögerte myogene *in vitro* Differenzierung aufwiesen. Zusätzlich verschob sich durch die Abwesenheit von LAP2α das Verhältnis der unterschiedlichen Muskelfasertypen von langsamen zu schnellen Fasertypen.

Zusammenfassend weisen diese Ergebnisse auf eine neue Rolle von LAP2α in der Erhaltung der physiologischen Funktionen des Herzens unter Stress- und Normalbedingungen hin. Im Weiteren zeigen die erhaltenen Daten eine weitere Funktion von LAP2α in der Skelettmuskulatur, speziell in der Homöostase der Satellitenzellen und der frühen myogenen Differenzierung, sowie in der Determinierung des Muskelfasertyps und der Muskelremodellierung.

1 Introduction

1.1 The nuclear envelope

During the course of evolution, the lipid bilayer enclosing the genetic material of eukaryotic cells developed into a complex membrane structure called the nuclear envelope (NE). In higher eukaryotes, the nuclear envelope comprises three distinct membrane domains – the outer, the inner and the nuclear pore membrane (Figure 1). The pore membrane contains and associates with protein components of nuclear pore complexes (NPCs), the channel-type structures that allow diffusion of small and active transport of large molecules in- and out of the nucleus. The outer nuclear membrane (ONM), which is linked to the rough endoplasmic reticulum and therefore often coated with ribosomes, contains proteins involved in positioning of the nucleus within the cell by mediating contacts with the cytoskeleton. The inner nuclear membrane (INM) contains a subset of integral and peripheral membrane proteins that interact with the adjacent nuclear lamina and are implicated in maintenance and dynamics of the underlying chromatin structure (reviewed in [1]).

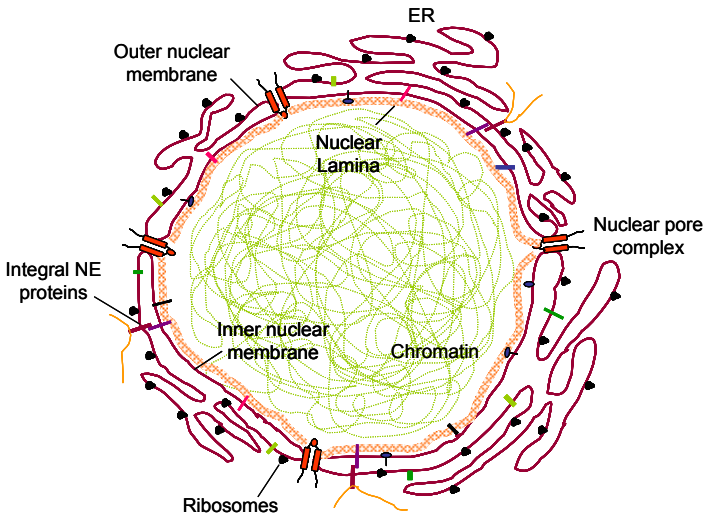

Figure 1. Schematic representation of a eukaryotic nucleus

1.1.1 The nuclear lamina

The nuclear lamina is a filamentous meshwork formed underneath the inner nuclear membrane of metazoan cells which, by providing mechanical stability for the nuclear envelope, maintains the integrity of the nucleus and supports nuclear function through the interactions with chromatin and numerous components of the nucleoplasm (reviewed in [2]). The major building blocks of the nuclear lamina are lamins – the nuclear type V intermediate filament (IF) proteins (reviewed in [3]). The IF family comprises numerous proteins (keratins, vimentin, desmin, synemin, syncoilin, peripherin, neurofilament proteins, nestin, α-internexin, glial fibrillary acid protein and

lamins) which, despite of their different expression and localization patterns, all share a similar structural organization, with a ~45 nm long central α-helical rod region flanked by non-α-helical N-terminal head and C-terminal tail domains (Figure 2) (reviewed in [1, 3, 4]). In contrast to cytoplasmic IF proteins, lamins have extra 42 residues in their coil 1B and a highly conserved 108 amino acid long C-terminal immunoglobulin fold structure[3, 5]. Additionally, the tail domain of lamins harbors the nuclear localization signal (NLS) and, in most cases, an iso-prenylation and carboxy-methylation motif called the CaaX-box (C, cysteine; a, aliphatic; X, any amino acid), which is modified by farnesylation in several sequential steps and mediates the interaction of lamins with the INM (reviewed in [3]). Although a precise assembly mechanism of these IF proteins is still elusive, the proposed models predict head-to-tail assembly of homodimers, formed by parallel alignment of single lamin molecules via the coiled coil-helix interactions, into protofilaments, which in turn align laterally to form a complex scaffold able to withstand the mechanical forces imposed upon the nucleus[6].

Lamin-encoding genes are absent from plant, as well as yeast cells and their evolution is

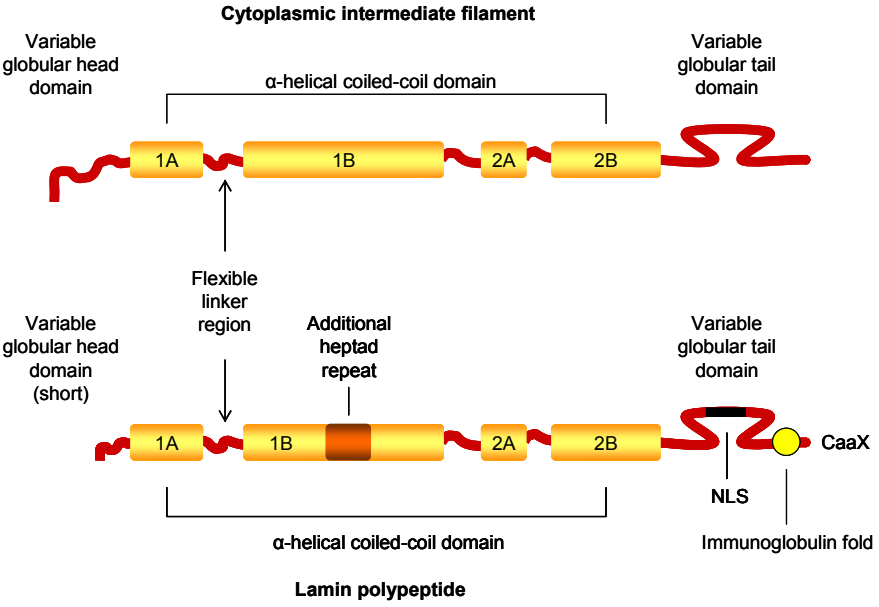

Figure 2. Lamins and cytoplasmic intermediate-filament proteins share the basic structural composition. 1A/B and 2A/B represent the α-helical coiled coil domains. Modified according to *C.J. Hutchinson and H.J. Worman, Nature Cell Biology, 2004.*

considered to coincide with the appearance of open mitosis in animal kingdom (reviewed in [7]). Whereas primitive metazoans possess a single lamin polypeptide, seven lamin variants, encoded by 3 genes (LMNA, LMNB1 and LMNB2), have been found in vertebrate nuclei and, based on their biochemical properties and expression patterns, organized into two major groups named A-type and B-type lamins (reviewed in [8]).

1.1.1.1 A-type lamins

A-type lamins (A, AΔ10, C and C2) are products of the alternatively spliced *LMNA* gene located on the human chromosome 1 q21.2-q21.3 (Chr 3 (42.6 cM) in the mouse). The *LMNA* spans 57.6 kb organized into 12 exons which encode the largest A-type variant, a 664 amino acid long protein named lamin A. Lamin C (572 aa) is a shorter isoform arising from the use of an alternative splicing site inside intron 10, which has no CaaX box, but contains 6 unique residues at its C-terminal end instead. The meiotic lamin C2 posesses only a short sequence of 6 aa substituting the complete N-terminal end and a part of the central rod domain of somatic lamins. A deletion of the *LMNA* exon 10 results in a 90 bp smaller variant named lamin AΔ10[8-11].

The production of the mature lamin A protein includes several posttranslational modifications and endoproteolytic cleavages (Figure 3)[8, 12]. The primary translational product of the lamin A mRNA, called prelamin A, bears the C-terminal CaaX box which is subject to farnesylation at the cysteine residue by a protein farnesyltransferase (FTase). In the second step, the -aaX residue is cleaved by an endopeptidase (Ras-converting enzyme (RCE1) or Zmpste24) before an isoprenyl carboxymethyl transferase (Icmt) places a carboxymethyl moiety onto the terminal cysteine. Such a product is then additionally cut by Zmpste24 15 residues upstream of the terminal farnesyl- and carboxymethylated cysteine to yield a mature lamin A protein, which has now lost the farnesyl moiety and its ability to integrate tightly into the INM[8, 12].

Although the majority of A-type lamins localizes to the nuclear periphery, a distinct portion of these proteins can also be found inside the nucleoplasm where it is thought to serve specific nuclear functions[13].

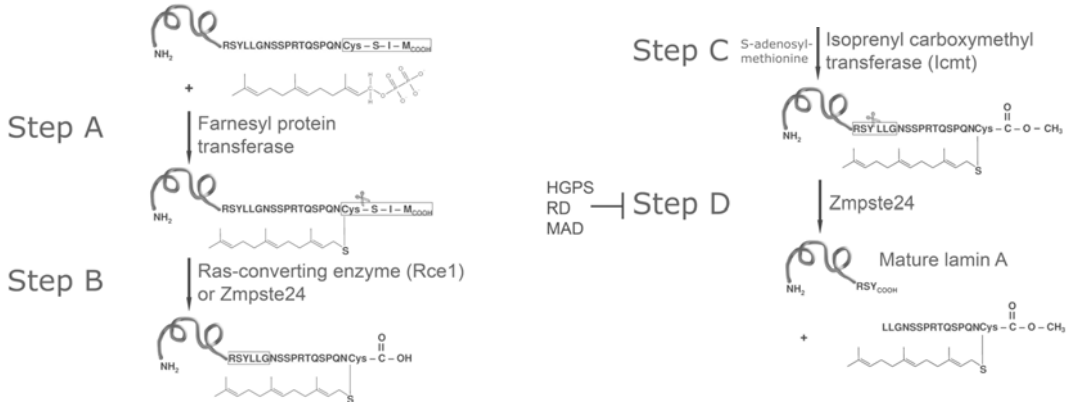

Figure 3. The maturation process of lamin A. Adapted according to *A.E. Rusiñol and M.S. Sinensky, Journal of Cell Science, 2006*.

The expression of A-type lamins is developmentally regulated and appears asynchronously in various tissues. During mouse development, their expression starts at about E9 within the visceral endoderm and the trophoblast[14], whereas all pre-implantation stage embryonic cells, as well as post-natal stem cells in the immune and hematopoietic system, cells of the neuroendocrine system and pancreatic island cells do not express A-type lamins or do so at very low levels[15].

1.1.1.2 B-type lamins

B-type lamins (B1, B2 and B3) are ubiquitously expressed at all developmental stages of an organism and the presence of at least one variant is essential for cell viability[1, 16]. Two B-type lamin genes have been described in mammalian cells: *LMNB1*, found on human chromosome 5 q23.3-q31.1 (mouse Chr 18 (29.0 cM)), encoding lamin B1 and *LMNB2*, maped to chromosome 19 p13.3 in human and chromosome 10 in mouse (43.0 cM), which encodes for lamin B2 and a smaller, male germline-specific lamin B3 variants[8]. All B-type lamins possess a terminal CaaX motif and are therefore subject to posttranslational isoprenylation[8]. In contrast to lamin A, B-type lamins do not go through the last enzymatic processing step (cleavage of the C-terminal 15 aa long peptide) and remain stably farnesylated. This permanent farnesylation of B-type lamins enables their association with the INM and restricts their subcellular localization to the nuclear periphery[8].

1.1.2 The lamin interactome

Lamins are not merely structural components of the nuclear lamina mechanically stabilizing the nucleus. Through the constantly growing number of interaction partners, they are implicated in various cellular processes, such as large scale chromatin organization, positioning of the nucleus, spacing of the nuclear pore complexes, nuclear reassembly after mitosis, DNA replication, RNA polymerase II-dependent gene expression and cell cycle control[17].

The LEM-domain protein family represents a major group of lamin-interacting factors. The LEM-domain (**L**AP2, **E**merin, **M**AN1) is a structural motif of approximately 40 amino acids organized into two loop-connected parallel α-helices, which defines a growing family of unrelated nucleoplasmic and inner nuclear membrane-associated proteins, including several lamina-associated polypeptide (LAP2) isoforms, emerin, MAN1, LEM2/5, ANKLE1/2, as well as *Drosophila*-specific proteins otefin and Bocksbeutelα/β (Figure 4)[18]. The special characteristic of the LEM-domain is the ability to bind a chromatin-associated protein conserved in multicellular organisms from flies to human called barrier-to-autointegration factor (BAF), which has been shown to cross-link double stranded DNA and function as a transcriptional co-repressor [18, 19].

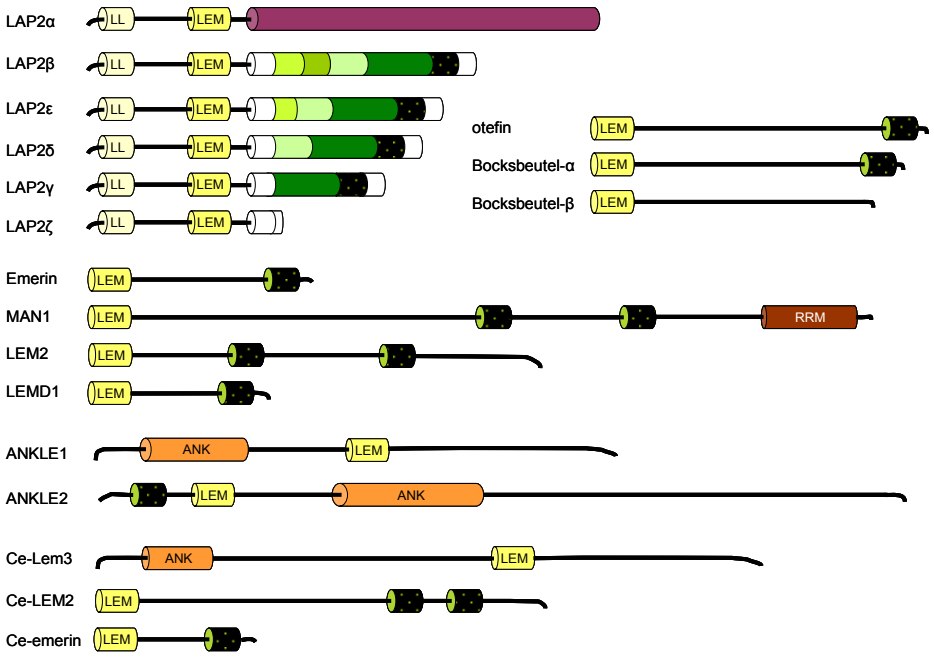

Figure 4. Schematic diagram of the LEM-domain protein family. LEM – LEM-motif, LL – LEM-like motif, ANK – ankyrin repeats, RRM – RNA recognition motif. The α-specific region of LAP2α is depicted in violet, the common C-terminal LAP2 domains in shades of green and white, and the transmembrane regions of all proteins in dotted-black.

The LAP2 protein family comprises six alternatively spliced products of the *LAP2* gene designated LAP2α, β, γ, δ, ε, and ζ[20]. All isoforms, except LAP2α and LAP2ζ, are inner nuclear membrane proteins characterized by the highly conserved 186 residues long N-terminal region which contains two globular chromatin-binding motifs – the BAF-interacting LEM and the DNA-associated LEM-like domain[21]. The C-terminal tails of nearly all LAP2 members are closely related and, in addition to the transmembrane sequence, contain a lamin B-binding region[21]. With its 693 amino acids, LAP2α represents the largest and the most distantly related nucleoplasmic LAP2 isoform which, instead of the membrane spanning domain, possesses a unique C-terminal chromatin-interacting segment and therefore differs from the other members in terms of expression, cellular localization, binding preference and supposed functions[21-23]. The high resolution structure of full length LAP2α has not been resolved yet. Although its N-terminal constant region seems to be monomeric, some studies predict a preference for the formation of full-length protein oligomers[24, 25]. The α-specific C-terminal tail, organized into 6 helices, has been shown to dimerize and thereby form an unusual structure with a central four-stranded coiled-coil, representing a previously unseen polypeptide fold (Figure 5)[25].

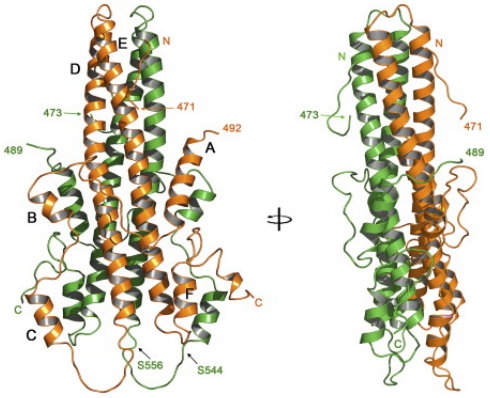

Figure 5. The structure of LAP2α C-terminal domain dimer. The central four-stranded coiled-coil of the dimer is formed by monomer helices (A-F) shown in orange and green. Modified according to *C.M. Bradley et al., Structure, 2007*.

So far, LAP2α has been found only in mammalian cells, whereas other isoforms exist also in other vertebrate classes[26, 27]. Together with the β-isoform, LAP2α is predominantly expressed in highly proliferating tissues and growing cultures, while LAP2γ seems to be up-regulated only in differentiating tissues[28]. Biological functions and expression patterns of smaller LAP2 isoforms are still largely unknown. In contrast to other LAP2 members which interact with both types of lamins, LAP2α preferentially binds to the nucleoplasmic pool of lamin A/C via its specific C-terminal tail – the residues 616-693 of LAP2α interact specifically with lamin A/C tail residues 319-572[22]. The complex of LAP2α/lamin A/C has been shown to bind the major cell cycle regulator and differentiation factor – the retinoblastoma protein (pRb) in its active, hypophosphorylated form and thus regulate cell cycle progression and differentiation in an E2F/pRb-dependent manner[29-31]. LAP2α complexes might even be directly acting on transcription of E2F target-genes, since they have been found associated with promoters of endogenous E2F/pRb-responsive sequences[30]. In addition, targeting of pRb for proteosomal degradation in *LMNA* knockout fibroblasts implies a role of LAP2α/lamin A/C complexes in nuclear anchorage and preservation of pRb stability[31]. Recently, LAP2α has been found to control the balance between proliferation and differentiation of transient amplifier cells during skin and hematopoietic tissue homeostasis by affecting pRb stability[32].

Other potential roles of LAP2α derive from studies on retroviral life cycle, where it was found essential for retroviral DNA integration into the host genome, as a cellular component of retroviral preintegration complexes, and replication of the Moloney murine leukemia virus (MMLV)[33]. However, the exact molecular mechanisms of these processes still remain unclear. Heat shock proteins Hsp70 and Hsc70 have also been found associated with LAP2α *in vivo*, suggesting a role of the protein in stress resistance[34]. As Hsp70 is thought to regulate the enzymatic activities of DNA base excision repair in human cells[35] and its loss leads to increased genomic instability in mouse[36], LAP2α might also be involved in DNA damage response.

LAP2β is a 451 residues long integral membrane protein that preferentially binds lamins at the nuclear periphery and is involved in the regulation of transcription[37]. It associates with germ cell-less (GCL), a factor that takes away the DP3 subunit from the DP3-E2F complexes and therefore represses E2F-mediated transcription[38]. Previous studies have introduced the possibility of a more general function of LAP2β in transcriptional repression of various members of the E2F protein family, as well as signaling pathways like p53 and NFK-κB. What is more, its repressive activity seems to be regulated through the intraction with HDAC3 (class I histone deacethylase)[39]. Overexpression of LAP2β induces deacethylation of histone H4 *in vivo* and *in vitro*, supporting the idea that membrane-anchored LEM proteins might directly be involved in large scale chromatin organization and transcriptional regulation at the nuclear periphery (reviewed in [[18]]). Interestingly, GCL knock out mice, although viable, exhibit nuclear abnormalities in various tissues and impaired sperm development[40], supporting the link between nuclear stability and regulation of gene expression. LAP2β also associates with the chromatin protein HA95 and thus contributes to the initiation of DNA replication by stabilizing cell-division-cycle protein-6 (cdc6), an important component of pre-replication complexes[41].

LAP2ζ, with its 224 residues, represents the smallest member of the LAP2 family. In contrast to the other isoforms, it lacks the membrane spanning domain as well as the nuclear localization signal, and is therefore predominantly found in the cytoplasm[20, 42]. A recent study showed that LAP2ζ, in excess, is able to relieve the chromatin of BAF-mediated repression by binding BAF and retaining this mainly nuclear protein in the cytoplasm. In addition, co-expression of LAP2ζ with either LAP2β or HDAC3 resulted in suppression of the inhibitory activity of the later two factors, which lead to the conclusion that LAP2ζ might present a transcriptional regulator, exerting its function through inhibition of BAF- and LAP2β-mediated gene silencing[42].

MAN1 is a ubiquitously expressed inner nuclear membrane-associated LEM-domain protein that interacts with both types of lamins[43]. In addition to the N-terminal LEM sequence, it possesses a C-terminal tail with two membrane-spanning domains and a RNA recognition motif (RRM), which directly binds to receptor-regulated Smads (R-Smad) and, by anchoring them at the nuclear periphery, inhibits the downstream path of the bone morphogenic protein (BMP)-induced signaling[18]. Overexpression of MAN1 was also shown to decrease receptor-mediated phosphorylation and oligomerization of the R-Smads, as well as influence the BMP and TGFβ signaling pathway in *Xenopus* development[44, 45]. The support for the MAN1-Smad interaction hypothesis came with the analysis of *MAN1*$^{\Delta/\Delta}$ mice that lack the C-terminal Smad-reacting domain[46]. The homozygous embryos died during development due to defects in TGF-β-dependent vascular remodeling. According to the predicted model the upregulation of R-Smad2/3 signaling in *MAN1*$^{\Delta/\Delta}$ mice could have caused an increase in deposition of extracellular matrix, which in turn could have lead to impaired migration of endothelial cells during angiogenesis[46].

Another member of the LEM-domain protein family is a small (254 aa), ubiquitously expressed integral membrane protein called emerin[47]. It was first discovered as a product of the human *EMD* gene mutated in Emery-Dreifuss muscular dystrophy[47]. Both emerin and MAN1 interact *in vitro* with several gene expression regulators, including GCL, BAF, as well as the apoptosis-promoting factor Btf, and probably have some overlapping functions[48]. In addition, emerin has been implicated in the regulation of the Wnt signaling[49], which controls various cellular processes such as proliferation, differentiation and apoptosis[50]. One of the Wnt signaling mediators, β-catenin, accumulates at adherens junctions and, upon activation of the Wnt cascade, transiently localizes to the nucleus to influence target gene expression[50]. Emerin has been shown to bind β-catenin and, by tethering it to the nuclear periphery or promoting its nuclear export, inhibit its transcriptional activity[49]. The retention of emerin at the nuclear periphery depends on the presence of either lamin A or C. While *LMNA* knockout cells show its re-localization to the endoplasmatic reticulum (ER)[51], lamin C-only cells and *Lmna*$^{-/-}$ cells ectopically expressing lamin A exhibit normal emerin distribution at the NE[52, 53]. This interaction indirectly involves lamins in the regulation of Wnt-mediated gene expression.

In addition, emerin was implicated in the regulation of actin dynamics by capping the pointed ends and stabilizing the polymeric filamentous F-actin *in vitro*[54]. It was also found in complexes with a specific nuclear form of αII-spectrin, a filamentous protein that binds to F-actin[54].

Despite the growing group of interaction partners and proposed functions, the physiological role of emerin and mechanistic details of its molecular interactions remain to be elucidated.

Lamin A and emerin have been found to associate with nuclear isoforms of the nesprin family, which comprises multiple alternatively spliced products of the human *SYNE1* and *SYNE2* genes[55]. Members of this protein family contain a spectrin-repeat rod domain linked to a C-terminal transmembrane KASH (Klarsicht-ANC-Syne-Homology) sequence, which mediates nuclear membrane localization, and/or N-terminal paired calponin-homology region that binds actin[56]. Nesprins are found in multiple sub-cellular compartments, such as the INM, ONM, mitochondria, Golgi apparatus, sarcoplasmic reticulum, muscle sarcomere and the plasma membrane, where they form networks which link these structures to the actin cytoskeleton[56]. The localization of specific, INM-bound isoforms like Nesprin 1α is dependent on their binding to lamin A[55]. Nesprins in the ONM interact with the SUN (Sad1/UNC-84 homology)-domain containing proteins (UNC-84, UNC-83, *Ce*-matefin) in the perinuclear space. These Nesprin-SUN-domain protein complexes, also called LINC complexes, bridge the luminal space between the INM and ONM and mechanically connect microtubules, actin and cytoplasmic intermediate filaments with the nuclear lamina, providing a structural link between the cytoskeleton and nucleoskeleton[57].

Lamin A and C have been found to bind and sequester cFos, a component of the AP1 complex that regulates transcription, differentiation, apoptosis and cell cycle progression in mammalian cells, and therefore inhibit its activity[58]. Constituents of the AP1 complex – cFos and Jun – are able to form heterodimers with unrelated DNA binding proteins like NFAT, Smads and bHLH transcription factors[59], thereby implicating lamins in the control of gene expression.

The immature form of lamin A – the pre-lamin A – has been shown to bind the adipocyte-specific transcription factor SREBP1 and, through its sequestration at the nuclear periphery, inhibit adipogenesis by preventing SREBP1-mediated activation of the peroxisome proliferator activator receptor gamma (PPARγ)[60].

Through their association with a range of nuclear bodies[61], as well as a constantly growing cohort of interaction partners such as LAP1, histon H2A or H2B dimers, monomeric actin, MOK2 and DNA, A-type lamins can be connected to almost all nuclear processes within a eukaryotic cell[17, 26].

One of the most prominent B-type lamin binding partners is the lamin B receptor (LBR), an integral membrane protein which also links lamins to organization of peripheral chromatin[62]. LBR interacts with double stranded DNA (*in vitro*), histone H3-H4 tetramers, chromatin associated protein HA95 and heterochromatin protein-1 (HP1), shown to bind the epigenetic mark of silent genes (unmethylated histone 3 at lysine 9)[63]. Mutations in LBR cause an autosomal dominant phenotype called Pelger-Huët anomaly, characterized by abnormal chromatin organization and decreased lobulation of white-blood-cell nuclei[64], providing further support for its role in chromatin organization. The membrane-embedded domain of LBR has a special sterol-reductase activity. A mutation affecting this region of LBR has also been linked to a severe human condition with impaired cholesterol biosynthesis called the Greenberg skeletal dysplasia[65]. However, the exact role of this enzyme activity and its relation to chromatin structure regulation remains unclear. Mice

with mutations in *Lbr* gene, called the *ichtyosis* locus, develop alopecia, variable syndactyly, hydrocephalus and abnormal granulocyte nuclear morphology[66], emphasizing the significance of this factor for normal mammalian cell function.

Lamin B1 in somatic cells binds the POU domain repressor protein Oct-1 which regulates the expression of collagenase genes[67, 68], implicating B-type lamins in the maintenance of extracellular matrix. Interestingly, MAN1, which also binds B-type lamins, was first identified by autoantibodies from a patient with collagen vascular disease[43].

Although the lamin interactome is extensive and intensively studied, the molecular details and physiological relevance of these networks remain to be discovered.

1.2 NE breakdown – mitosis time

In contrast to single-cell eukaryotes like *S. cerevisiae* whose nuclei retain their integrity during mitosis, the complex nuclear envelope of higher eukaryotes has to disassemble between prophase and prometaphase stages of the cell cycle to allow engagement of chromosomes with the cytoplasmic mitotic spindle (reviewed in [7]). In the process of opened mitosis, the NE breakdown is triggered by Polo-like kinase 1 (Plk1)-mediated phosphorylation of the G2-phase specific cyclin B1 (reviewed in [69]). Together with its binding partner Cdk1, Cyclin B1 forms the so called mitosis promoting factor (MPF), which shuttles between the nucleus and the cytoplasm during the G2 phase of the cell cycle. Phosphorylation of cyclin B causes the accumulation of MPF inside of the nucleus and enables the Cdk1 component to trigger phosphorylation of nucleoporins, lamins, integral INM proteins, as well as many other nuclear proteins, finally resulting in NE disassembly (reviewed in [7]).

In vertebrate cells, two specific serine residues (S22 and S392), which symmetrically flank the lamin rod domain, serve as substrates for a variety of protein kinases like PKC, PKA, MAPK and casein kinase II in the process of filament breakdown[70, 71]. LAP2α has up to seven serines clustered in its chromatin binding region, whose phosphorylation is necessary for dissociation of the protein from the chromatin during mitosis[72]. Binding of LAP2β to lamins and/or chromatin is also regulated by its phosphorylation by Cdk1[73].

Phosphorylated nucleoporins leave the NPCs early in mitosis. Subsequently, a subset of them associates with kinetochores forming holes in the NE and leading to the loss of NE barrier function. The phosphorylated lamin filaments and NE membranes are subsequently transported on spindle microtubules towards the centrosomes by dynein motors. In mammalian cells, A-type lamins dissociate from the nuclear lamina at early prophase, whereas B-type lamins do so only later. Following its dissociation from chromatin, the NE becomes completely disassembled and, according to the current models, its membranes either form special vesicles that are reused at the end of mitosis for reassembly, or fuse with the ER network (reviewed in [7]).

During final stages of mitosis, the NE reassembles around the segregated chromosomes in a highly regulated temporal fashion to form new daughter nuclei. Individual nucleoskeletal proteins initially targeted to the chromosomal surface attract the membranes, which fuse before the NPCs are able to assemble. The newly formed NPCs paw the way for import of lamins and the full reassembly of the nuclear lamina (reviewed in [7]). In the process of NE-reassembly, LAP2α and BAF initially accumulate at chromosomal telomeric regions during anaphase and form the, so called, core structures adjacent to the spindle pole and mid-spindle area[74]. Since these two proteins have been found to co-localize with the telomeric protein TRF2 at core structures, it was suggested that LAP2α might transiently serve to anchor telomeres to defined stable regions in the reforming nuclei[74]. Slightly after LAP2α and BAF, other proteins like emerin, LAP2β and a sub-fraction of lamin C, are targeted to the core regions (reviewed in [7]). LBR, in contrast, is initially

detectable at more peripheral chromatin regions indicating a different type of interaction with the chromatin[75].

B-type lamins can be detected on chromosomes shortly after LAP2β and, as they stay associated with the membranes during the NE breakdown, they could initially be targeted to chromosomes together with membrane structures. However, their assembly into a stable lamina occurs in subsequent stages at the inner surface of the newly formed membrane (reviewed in [7]). In contrast, A-type lamins are transported through the NPCs and redistribute inside the nucleus during telophase/G1 transition[74]. Consistent with this idea, inhibition of B-type lamin polymerization at the end of mitosis does not interfere with the assembly of A-type lamins. At early G1 phase the intact NE again fully encloses the chromatin which becomes decondensed during the nuclear growth (reviewed in [7]).

1.3 The nuclear envelope from a medical point of view

Mutations in genes encoding nuclear envelope proteins cause a group of pathological conditions in human called the nuclear envelopathies. At present, disease-causing mutations have been reported for 14 genes: *EDM* (*STA*), *LMNA*, *LMNB1*, *LMNB2*, *FACE-1* (*ZMPSTE24*), *LBR*, *MAN1*, *LAP2*, *AAAS*, *TOR1A*, *LIS1*, *SYNE1*, *SYNE2* and *NUP155* (Figure 6) (reviewed in [76-78]). Although symptoms caused by changes in proteins encoded by these genes vary greatly in severity and tissue type affected, many of them include nuclear dismorphology, as well as alteration in chromatin organization and gene expression.

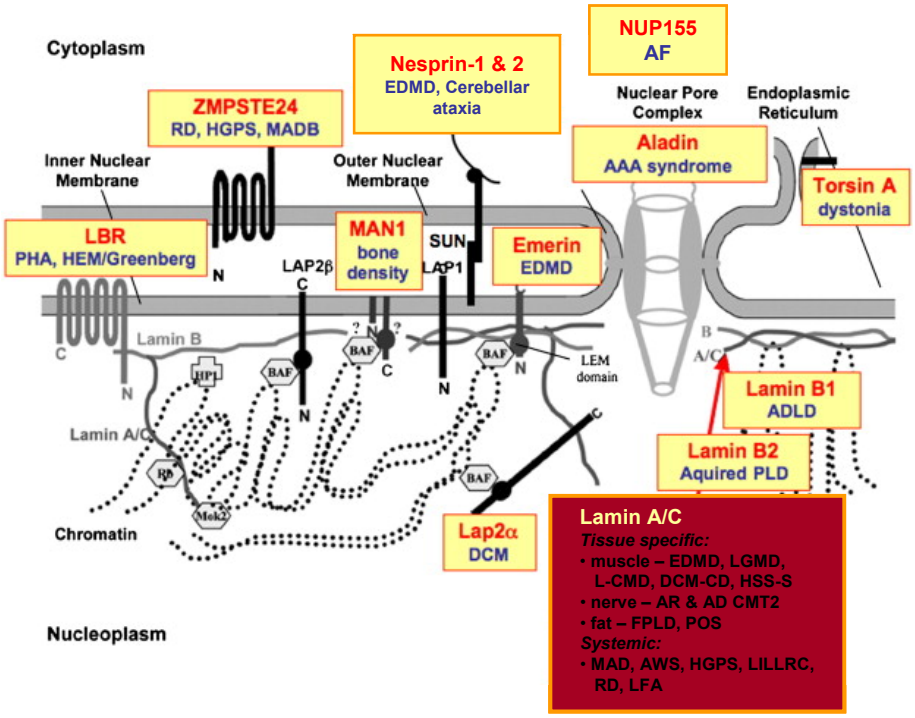

Figure 6. Schematic diagram of the nuclear envelope including pathological conditions caused by mutations in NE-associated proteins. RD – restrictive dermopathy; HGPS – Hutchinson-Gilford progeria syndrome; PHA – Pelger-Huët anomaly; EDMD – Emery-Dreifuss muscular dystrophy; ADLD – adult-onset autosomal dominant leukodystrophy; LGMD – limb girdle muscular dystrophy; DCM-DC – dilated cardiomyopathy with conduction system disease; CMT – Charcot-Marie-Tooth disorder; FPLD – familial partial lipodystrophy; MAD – mandibuloacral dysplasia; AWS – atypical Werner syndrome; POS – polycystic ovary syndrome; LFA – lethal foetal akinesia; L-CMD – lamin-associated congenital muscular dystrophy; HSS-S – heart-hand syndrome of Slovenian type; LILLRC - LIRLLC syndrome; AR – autosomal dominant; AD autosomal recessive; PLD – partial lipodystrophy; AAA – achalasia-addisonianism-alacrima; AF – atrial fibrillation. Modified according to *H.J. Worman and G. Bonne, Experimental Cell Research, 2007.*

1.3.1 Laminopathies

With more than 250 mutations reported so far, *LMNA* is the most frequently altered member of the nuclear envelope protein-encoding gene group linked to a disease (reviewed in [76]). Diseases caused by changes in lamin A/C protein or Zmpste24, one of the enzymes involved in lamin maturation, form a major subclass of envelopathies named laminopathies. Specific tissues selectively affected in primary laminopathies (caused by mutations in *LMNA*) include striated muscle, peripheral nerves and adipose tissue. Premature ageing syndromes and their related disorders, characterized by defects in multiple tissues, are classified as systemic laminopathies, although an increasing number of published *LMNA*-linked conditions with mixed symptoms suggests an overlapping continuum within different types of laminopathies (reviewed in [8]).

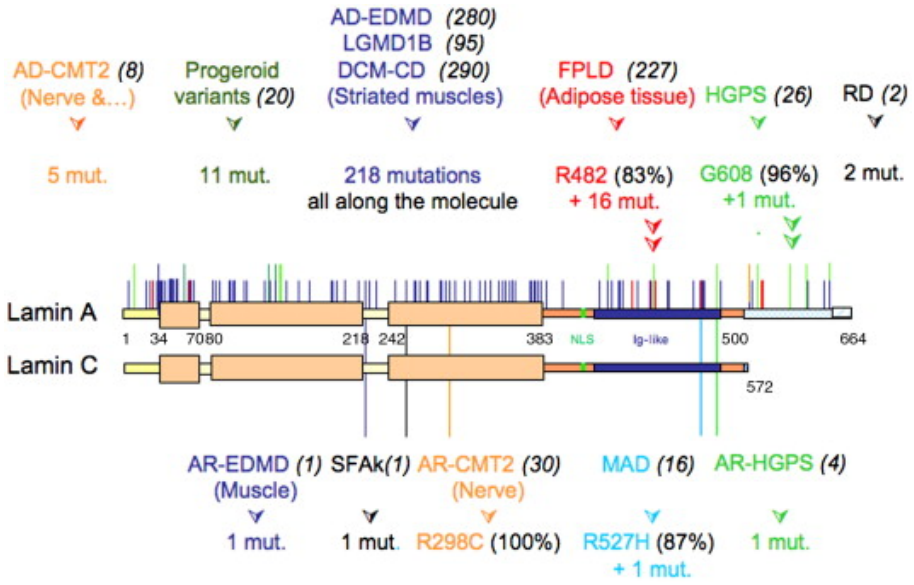

Figure 7. LMNA disease-causing mutations are spread along lamin A/C molecules. Dominant and recessive disorders are depicted on top and bottom of the scheme respectively. Numbers in parentheses in black indicate numbers of reported affected individuals carrying the specific mutation. Adapted according to *H.J. Worman and G. Bonne, Experimental Cell Research, 2007*.

1.3.1.1 Striated muscle laminopathies

LMNA mutations linked to striated muscle disorders are spread along the gene with no firm relation between the pathological phenotype, the type, and/or the localization of the mutation (Figure 7) (reviewed in [79]). Striated muscle defects account for ~60-70% of laminopathies and, according to their symptoms, fall into 5 distinct categories:

1.3.1.1.1 Limb-girdle muscular dystrophy type 1B (LGMD1B)

LGMD presents a clinically and genetically heterogeneous group of muscular disorders inherited in a dominant (LGMD1) or recessive (LGMD2) manner, which are characterized by slowly progressive weakness and wasting of the pelvic girdle. Additional age-related atrioventricular cardiac conduction disturbances and dilated cardiomyopathy distinguish a special subgroup of these disorders caused by mutations in *LMNA*, classified as LGMD1B[80, 81].

1.3.1.1.2 Emery-Dreifuss muscular dystrophy

EDMD is a rare pathological striated muscle condition characterized by early contractures of elbows, Achilles tendons and postcervical muscles, slowly progressive muscle weakness and wasting, initiating in the humeroperoneal region, as well as life-threatening cardiomyopathy with conduction blocks. It is linked to mutations in two genes: a) emerin-encoding *EMD*, which is passed on in an X-linked (XL-EDMD) fashion and b) *LMNA* inherited as autosomal dominant (AD-EDMD) or autosomal recessive (AR-EDMD) trait[47, 82].

1.3.1.1.3 Congenital muscular dystrophy (L-CMD)

Congenital muscular dystrophies are genetic myopathies specified by dystrophic features on muscle biopsy, as well as hypotonia, weakness, or delayed motor development from the first few months of life[83]. Mutations in 12 different genes and 2 loci have been associated with the currently recognized nine clinical subtypes of CMD[84]. Congenital muscular dystrophies share some symptoms with EDMD, such as spinal rigidity, hyperCKemia and contractures of elbows and Achilles tendons. However, the main feature of *LMNA*-related CMD (L-CMD) – the selective deficit of head support or axial muscle weakness – is not present in EDMD. Cardiac involvement in L-CMD is rarely observed, probably owing to the young age of most of the diagnosed patients. L-CMD presents a severe end of the spectrum of striated muscle laminopathies, as it develops within

the first year of life, in contrast to EDMD and LGMD1B, which have a later onset between mid-childhood and adulthood respectively[84].

1.3.1.1.4 Dilated cardiomyopathy with conduction system disease (DCM-CD)

Cardiac dilation and reduced systolic function are the two major characteristics of the largely heterogeneous group of inherited and acquired disorders classified as dilated cardiomyopathy (DCM). Among more than 20 candidates, *LMNA* and β-myosin heavy chain gene are the two most frequently mutated genes linked to the familial form of DCM (reviewed in [[79]]). Patients carrying a *LMNA* mutation are presented with the worst prognosis of all DCM cases and are at greater risk of sudden death.

A recent study identified new DCM-mutational hot spots in *LMNA*, affecting the lamin A/C coil 1B which is important for protein dimerization and interaction with lamin B[85]. Another potential explanation of the disease mechanism came from studies on posttranslational modifications of lamin A/C, which showed that DCM-linked mutations could affect sumoylation of lamin A at the residue K 201 and thus cause its abnormal nuclear localization[86]. Interestingly, a mutation in LAP2α (c. 2068C>T, p. R690C), which lowers the *in vitro* binding affinity of the protein to lamin A/C, has also been linked to dilated cardiomyopathy[28], emphasizing the role of lamins and their interaction partners in development and/or maintenance of striated muscle tissue.

1.3.1.1.5 Heart-hand syndrome of Slovenian type (HHS-S)

HHS is a clinically and genetically diverse disorder characterized by the co-occurrence of cardiac disease and limb malformations[87]. Recently, a new type of HSS was reported in a Slovenian family which presented a late onset progressive sinoatrial and atrioventricular conduction disease, tachyarrhythmias with high yield of sudden death, DCM and brachydactyly[88]. Upon exclusion of gene-perturbing changes in several known disease-causing candidates, such as *TBX5*, *TBX3*, *ROR2* and *SCN5A*, the study identified a new variant of *LMNA* intron 9 was identified[89]. This novel mutation (c. 1609-12 or IVS9-12, T>G) predicts an additional acceptor splice site, 11 nucleotides upstream of the wild type site, and introduces a frame shift in the *LMNA* mRNA, which leads to the premature termination and potential production of a truncated, 550 residues long, protein with a unique 14 aa long C-terminus. Analysis of cultured patient skin fibroblasts showed aberrant localization of lamin A/C and dysmorphic nuclei, which can be found in most of the *LMNA*-linked striated muscle conditions[89].

1.3.1.2 Partial lipodystrophies and related syndromes

In contrast to *LMNA*-linked striated muscle disorders, adipose tissue laminopathies are mainly linked to a specific site in the lamin A/C gene – the R482 codon[90]. *Familial partial lipodystrophy of Dunnigan type (FPLD)* is a rare condition characterized by a selective loss of adipose tissue. Patients with FPLD have normal fat distribution until the onset of puberty, when almost all subcutaneous adipose tissue from lower and upper extremities, as well as gluteal and truncal region disappears, and starts accumulating in the face and neck. Metabolic complications increase with the extent of fat loss and include insulin resistance, diabetes mellitus, hypertriglyceridemia and liver steatosis. The molecular pathway of this disease is predicted to involve accumulation pre-lamin A and its aberrant interaction with the adipose tissue-specific factor SREBP1 (reviewed in [79]).

A case of *A-type insulin resistance syndrome* including polycystic ovary syndrome with severe hyperandrogenism, acanthosis nigricans and marked insulin resistance was also linked to a mutation in *LMNA* (G602S). Skin fibroblasts of affected patients exhibited abnormalities of nuclear shape and several defects in the insulin transduction pathway[91].

1.3.1.3 Peripheral nerve disorders

1.3.1.3.1 Autosomal recessive Charcot-Marie-Tooth type 2 (AR-CMT2, CMTB1)

CMT disorder comprises a clinically and genetically heterogeneous group of hereditary motor and sensory neuropathies. According to electrophysiological criteria, CMT patients are divided in two major classes. Demyelinating forms of CMT, characterized by a motor median nerve conduction velocity <38 m/s constitute the type 1 and the axonal form, with a normal or slightly reduced nerve conduction velocity, the type 2 disorder. A unique homozygous *LMNA* mutation (R298C) was found to cause the CMT2B1 in a large Moroccan family. The main clinical symptomsin thios case included early onset symmetrical muscle weakness and wasting of distal lower limbs, foot deformities and walking difficulties associated with reduced or absent tendon reflexes. Interestingly, mice lacking lamin A/C present an axonal clinical and pathological phenotype highly similar to patient symptoms (reviewed in [79]).

1.3.1.3.2 Autosomal dominant axonal Charcot-Marie-Tooth disease (AD-CMT2)

LMNA has also been implicated in the development of autosomal dominant CMT disorder associated with muscular dystrophy, cardiac disease and leukonychia in one, as well as both – cardiac disease and partial lipodystrophy in two other families[92].

1.3.1.4 Premature ageing syndromes

1.3.1.4.1 Mandibuloacral dysplasia (MAD)

MAD is a rare autosomal recessive disorder characterized by postnatal growth retardation, mandibular and clavicular hypoplasia, acroosteolysis, delayed closure of the cranial suture, joint contractures, lipodystrophy and mottled cutaneous pigmentation. Currently, two mutations in *LMNA* (R527H[93] and A529V[94]) and one in its functionally-associated gene *FACE-1*[95],encoding a lamin A processing enzyme, have been found to cause this devastating human condition.

1.3.1.4.2 Hutchinson – Gilford progeria syndrome (HGPS)

HGPS, a rare fatal genetic disorder characterized by accelated aging in children, has been linked to 8 different *LMNA* mutations. The most common one represents a single base substitution (c. 1824C>T) in the *LMNA* exon 11, resulting in the activation of a cryptic splice site and an in-frame deletion of 50 amino acids from the C-terminal tail of the prelamin A. The aberrant lamin A variant called progerin can not be cut during the process of protein maturation, as it lacks the endoproteolytic cleavage site, and therefore remains farnesylated at its Caax box. HGPS skin fibroblasts and lymphoblasts show nuclear abnormalities, including altered size and shape, NE interruptions accompanied by chromatin extrusions, as well as defects in heterochromatin organization, genome stability and DNA repair (reviewed in [[79]]).

1.3.1.4.3 Atypical Werner syndrome

The clinical symptoms of Werner syndrome (WS) include premature appearance of features associated with normal aging as well as higher cancer predisposition. In the case of the typical WS, disease causing mutations are found in the DNA helicase-like gene (*RECQL2*), whereas the atypical WS arises from perturbing changes in the lamin A/C gene. Just like in other

laminopathy disorders, patient fibroblasts demonstrate altered nuclear morphology and lamin mislocalization (reviewed in [8]).

1.3.1.5 Restrictive dermopathy (RD)

A rare tight skin syndrome with neonatal lethal course within the first week of life, also known as RD, was found to develop due to mutations leading to a complete or partial in-frame loss of *LMNA* exon 11, as well as a unique mutation in the *FACE-1*[96].

1.3.1.6 Lethal foetal akinesia

A homozygous *LMNA* nonsense mutation (Y259X) was found to underlie a lethal foetal phenotype characterized by dysmaturity, facial dsymorphism with retrognathia, severe contractures of fingers and toes, long bone fractures, as well as generalized muscular dystrophy with almost complete absence of fibers in intercostal muscles. Patient skin fibroblasts showed nuclear abnormalities such as blebbing and protrusion of DNA into the cytoplasm, local absence of lamin B and NPCs, as well as a reduced level of emerin staining at the NE[92].

1.3.1.7 LIRLLC syndrome

Generalized lipoatrophy, insulin-resistant diabetes, leukomelanodermic papules, liver steatosis and hypertrophic cardiomyopathy, known as the LIRLLC syndrome, were found to co-segregate with the R113L mutation in the *LMNA* affecting the rod domain of lamin A/C protein, and cause nuclear abnormalities in primary patient fibroblast cultures[97].

1.4 Modeling human laminopathies – lessons learned from mice

In an attempt to disclose the molecular mechanisms underlying human laminopathies, several mouse lines bearing *Lmna* disease-specific gene alterations have been generated, giving an invaluable insight into lamin-dependent nuclear processes.

1.4.1 *Lmna*$^{-/-}$ mouse

While there is still no report of human patients completely lacking lamin A/C protein and a homozygous nonsense mutation that introduced a premature stop codon in *LMNA* caused prenatal lethality[98], *Lmna*$^{-/-}$ mice are able to survive until the age of 6-7 weeks[51]. These animals appear normal at birth but stop thriving after 2-3 weeks of age when clinical and histological signs of muscular dystrophy begin to appear. By the age of 4-6 weeks *Lmna*$^{-/-}$ mice developed DCM-DC which largely contributed to their early mortality[51, 99]. Nikolova et al. (2004)[99] found *Lmna*$^{-/-}$ mouse heart size to be similar to the wild type but the left ventricle (LV) remained thin-walled, globular-shaped and dilated, indicating that the severe functional defect, characterized by global reduction in LV contraction, was not accompanied by compensatory myocardial hypertrophy. In support of this finding, Northern blot analyses showed appropriate increases in LV expression of ANP and BNP, the factors usually upregulated during pathological heart conditions, whereas levels of α-skeletal actin and β-myosin heavy chain, involved in myocardial remodeling, remained unaltered. The isolated lamin A/C deficient cardiomyocytes were relatively short and thin, had reduced sarcomere length and exhibited contractile dysfunction. Although there was no obvious apoptosis at 2 weeks of age, myocardial tissue sections from 4-6 weeks old *Lmna*$^{-/-}$ hearts showed focal myocyte degeneration with destabilization of the nuclear lamina and the concomitant nuclear deformability. Electron microscopy revealed discernible disorganization of desmin filaments in *Lmna*$^{-/-}$ cardiomyocytes, as well as dilation of the nuclear envelope luminal space with distortion of nuclear pores. The perinuclear space was increased, with regions in which the nucleus and the adjacent cytoskeleton appeared completely disconnected. The nuclear morphological defects in *Lmna*$^{-/-}$ cardiomyocytes at 4-6 week of age were accompanied by an impaired translocation of the cleaved, active form of lamin A/C binding partner SREBP1 into the nucleus, and the consecutive reduction of its downstream target PPARγ, both of which play an important role in regulation of cholesterol and fatty acid synthesis in adipose tissue. Although defective lamin A/C-SREBP1 interaction has been postulated as a possible mechanism in the development of familial lipodystrophy, this probably does not represent the primary mechanism of lamin A/C-linked DCM[99]. The reductions in intranuclear SREBP1 and PPARγ in *Lmna*$^{-/-}$ mice are more likely caused by acquired defects in nuclear pore transport in LV myocytes. The extranuclear accumulation of SREBP1 in the heart might cause defects in myocardial energetics and exacerbate the LV contractile dysfunction[99] .

The causative connections to skeletal muscle dystrophy of *Lmna*$^{-/-}$ mice are still unclear, as *in vivo* muscle regeneration after cardiotoxin treatment, as well as *in vitro* primary myoblast differentiation appears normal[100]. In contrast, immortalized *Lmna*$^{-/-}$ myoblasts showed impaired differentiation, presumably due to downregulation of the major myogenic determinant MyoD and its targets, such as the muscle-specific intermediate filament desmin[101]. As a consequence, the immortalized *Lmna*$^{-/-}$ myoblasts upregulated another myogenic factor named Myf5, which can partially compensate for the loss of MyoD[102].

pRb plays a role in early steps of muscle differentiation possibly by preventing MyoD inactivation through HDAC1-mediated deacethylation[103], which also puts lamin A/C (the regulator of pRb stability and function[31]) into the context of muscle differentiation. Interestingly, protein levels of pRb are also affected in *Lmna*$^{-/-}$ myoblasts, pointing to a reduction of its stability, as described in *Lmna*$^{-/-}$ fibroblasts[104].

Interestingly, neurons of the sciatic nerve in *Lmna*$^{-/-}$ mice show extensive demyelination, suggesting that their muscular dystrophy phenotype could also be a consequence of neuronal degeneration and the subsequent loss of muscle innervation[105]. However, according to the recent study by Mejat et al. (2009), the primary cause of muscle innervation defects in AD-EDMD mouse models might be a destabilization of neuromuscular junctions due to mislocalization of lamin A/C and their NE-associated interacting proteins[106].

Another feature of *Lmna*$^{-/-}$ mice is the disrupted spermatogenesis characterized by apoptosis of pachytene stage spermatocytes, due to a failure in prophase I progression and defective sex chromosome pairing, presumably caused by the lack of the meiosis specific lamin C2 variant[107].

1.4.2 *Lmna*$^{H222P/H222P}$ mouse

A missense mutation (histidine-to-proline substitution at amino acid 222), originally identified in a family with AD-EDMD, was introduced into the mouse *Lmna* gene to study the effects of muscle disease-causing mutations on lamin A/C protein function[108]. Although indistinguishable from their WT siblings at birth, male *Lmna*$^{H222P/H222P}$ mice stopped thriving at the age of 3 months, exhibited reduced locomotion with abnormal stiff walking posture, as well as rapid shallow breathing. In addition to skeletal muscle dystrophy characterized by general fiber atrophy and type II fiber hypertrophy, they developed cardiac fibrosis, progressive LV and atrial dilation as well as hypokinesia with conduction defects, which lead to a premature death between 4 and 9 months of age. Similar to *Lmna*$^{-/-}$ mice, the LV dysfunction in *Lmna*$^{H222P/H222P}$ mice was not accompanied by cardiomyocyte hypertrophy, suggesting a role of lamin A/C in the process of cardiac stress-induced hyperthrophic growth. Cardiac and skeletal muscle cells of *Lmna*$^{H222P/H222P}$ mice showed alteration of heterochromatin distribution and an increased nuclear translocation of Smad proteins. These effects probably originated from a systemic rise in circulating TGF-β, generated by the failing heart and dystrophic muscles, rather than from a defect in nuclear shuttling of Smad proteins through nuclear pore complexes or an abnormal retention at the nuclear lamina, caused by mutated lamin

A/C proteins. Interestingly, female *Lmna*$^{H222P/H222P}$ mice developed the dystrophic phenotype later than males. At the age of 6 months, when the males already reached their terminal phase, *Lmna*$^{H222P/H222P}$ females only started showing the symptoms which became life threatening by the age of 13 months, implicating steroide hormones in the development of lamin A/C-linked striated muscle disorders. In contrast to human *LMNA* H222P mutation, which has an autosomal dominant effect, the mutation introduced into the mouse *Lmna* only results with a detrimental phenotype in the homozygous state[108].

1.4.3 *Lmna*$^{N195K/N195K}$ mouse

Lmna$^{N195K/N195K}$ mice were generated to model the autosomal dominant form of human dilated cardiomyopathy with conduction system disease[109]. Mice homozygous for the *Lmna* N195K mutation showed characteristics consistent with the DCM-CD1 and died at the age of 3 months due to heart arrhythmia, with minimal or no obvious skeletal muscle dystrophy. It was suggested that this *Lmna* mutation may cause the disease by influencing the structural organization of cardiomyocytes and/or altering the expression of essential heart-specific transcription factors during development and aging, since *Lmna*$^{N195K/N195K}$ hearts exhibited misexpression and/or mislocalization of muscle-specific structural proteins (desmin, connexin 40 and 43), as well as transcription factors (Hf1b)[109].

1.4.4 *Lmna M371K* mouse

Transgenic mice expressing a mutated EDMD-linked form of lamin A/C (M371K) under a heart-specific α-myosin heavy chain promoter showed extensive heart pathology (increased cytoplasmic eosinophilia of cardiomyocytes, focal edema, fragmented cardiomyofibrils and pyknotic-appearing nuclei), leading to premature death at 2-7 weeks of age[110]. Multifocal cardiac lesions, in the absence of fibrosis or inflammation in *Lmna M371K* hearts, pointed to an acute or sub-acute cardiac injury. *Lmna M371K* cardiomyocytes exhibited nuclear abnormalities demonstrating a potential dominant negative effect of mutant proteins on the endogenous wild type lamin A/C[110].

1.4.5 *Lmna*$^{LCO/LCO}$ mouse

In contrast to *Lmna*$^{-/-}$ mice which present a plethora of pathological symptoms and die at early age, mice expressing only the lamin C variant of the *Lmna* gene appear normal through their entire lifetime[52]. Although *Lmna*$^{LCO/LCO}$ cells exhibit a slight increase in abnormal nuclear morphology, it seems that the enhanced production of lamin C can in a way compensate for the loss of lamin A and thereby prevent the emergence of the disease phenotype. Interestingly, earlier reports suggesting an essential role of lamin A in the retention of emerin at the NE, are challenged by the normal localization of emerin in *Lmna*$^{LCO/LCO}$ cells.

1.4.6 Progeroid syndromes in mice

An in-frame deletion of the *Lmna* exon 9, due to the introduction of a splicing defect, resulted in the production of an aberrant lamin A/C protein, which caused a HGPS-like multiple tissue disorder in mice. The ***Lmna*$^{\Delta 9/\Delta 9}$** animals exhibited growth retardation, loss of subcutaneous fat, osteoporosis, as well as thin hyperkeratotic skin, and died by the age of 4 weeks[111].

Another mouse model of HGPS was generated by targeted deletion of the last 150 nucleotides of *Lmna* exon 11 together with introns 10 and 11[112]. The resulting ***Lmna*$^{HG/HG}$** mice expressed only an unprocessesed form of lamin A named progerin, with no lamin C, and developed severe osteoporosis followed by spontaneous bone fractures and early postnatal death. The symptoms of progeria had a later onset in heterozygous *Lmna*$^{HG/+}$ mice, which survived till the age of 6-7 months and did not present significant muscle weakness. Similar to *Lmna M371K* cardiomyocytes, heterozygous *Lmna*$^{HG/+}$ fibroblasts showed an increased frequency of misshaped nuclei, suggesting a dominant negative effect of progerin on endogenous lamin A/C[112].

A transgenic mouse line, created by the introduction of a 164-kb human bacterial artificial chromosome spanning four genes (*RAB25*, *UBQLN4*, *MAPBPIP* and *LMNA* with the HGPS-specific 1824C>T transition) into the mouse genome, failed to recapitulate any of the early hallmarks of progeria[113]. However, ***Lmna BAC G608G*** mice did show a loss of smooth muscle cells in the media of the aorta, present in some HGPS patients[113].

Mice lacking ZMPSTE24, an enzyme involved in the maturation of A-type lamins and associated with restrictive dermopathy in human, were independently created by two different groups[114, 115]. The ***Zmpste24*$^{-/-}$** animals appeared normal at birth and grew normally until weaning time, when the initial symptoms such as incisor abnormalities, alopecia, kyphosis and slow arthritic gait started to develop. By the age of 3-4 months the mice presented bone abnormalities leading to rib fractures near to costovertebral joint[115]. Muscle weakness and mild dystrophic skeletal muscle changes, observed in one independent mouse line[114], were presumably secondary effects of neuropathy and not directly caused by ZMPSTE24 absence in skeletal muscle. In culture, *Zmpste24*$^{-/-}$ cells exhibited enhanced senescence, possibly associated with an upregulation of p53-responsive genes (reviewed in [116]).

In an attempt to neutralize the toxic effects of accumulated farnesyl-prelamin A/progerin, *Zmpste24*$^{-/-}$ and *Lmna*$^{HG/+}$ mice were treated with inhibitors of farnesyltransferases (FTI)[117, 118], which were supposed to prevent farnesylation and the subsequent integration of prelamin A into the NE. The FTI treatment enhanced growth of the treated animals and improved the morphology of their nuclei, but although ameliorated to some extent, most of the symptoms persisted further (reviewed in [116]). A similar effect was observed in transgenic *Lmna*$^{nHG/+}$ mice expressing nonfarnesylated progerin, suggesting that the inhibition of farnesylation might be therapeutically useful, but also limited, as the protein is able to cause the disease, irrespective of its farnesylation state[119]. *Lmna*$^{HG/LCO}$ mice generated in another study indicated that the presence of the mature lamin A/C in *Lmna*$^{HG/+}$ animals could be additionally aggravating the toxic effect of progerin.

Lmna$^{HG/LCO}$ mice, expressing only progerin and lamin C, exhibited a milder phenotype than *Lmna*$^{HG/+}$ mice and had lower protein levels of progerin, possibly due to the altered composition of the lamina and a higher, more efficient, turnover of the protein in lamin C-only environment[120]. Interestingly, a 50% reduction of lamin A/C in *Zmpste24*$^{-/-}$*Lmna*$^{+/-}$ mice was sufficient to overrule the toxicity imposed by the presence of farnesylated prelamin A, and prevent the development of the disease[121]. *Zmpste*$^{-/-}$*Lmna*$^{LCO/+}$ and *Zmpste*$^{-/-}$*Lmna*$^{LCO/LCO}$ mice showed that already a prevention of prelamin A accumulation is able to fully rescue the progeria phenotype of *Zmpste24*$^{-/-}$ mice[52]. To this end, treatment of *Zmpste24*$^{-/-}$ cells with prelamin A-specific antisense oligonucleotides efficiently reduced the synthesis of the toxic protein and normalized the nuclear morphology of mouse fibroblasts[118].

1.4.7 *Emd*$^{-/-}$ mice

Mice lacking the integral NE protein emerin developed normally and were grossly indistinguishable from their wild type littermates[100, 122]. Although, in contrast to human patients with *EMD* mutations, *Emd*$^{-/-}$ and *Emd*$^{-/Y}$ mice did not exhibit any signs of muscular dystrophy or dilated cardiomyopathy[122], their *in vivo* muscle regeneration, as well as *in vitro* differentiation was slightly delayed, probably due to a transient deregulation of the pRb/MyoD pathway[100]. *Emd*$^{-/Y}$ muscle showed an excess of MyoD and its associated transcriptional components at day three of regeneration, which however failed to exert their activity on a subset of downstream targets within a usual time frame. Inappropriately activated targets of the pRb/E2F transcriptional repressor complex also indicated a defect in pRb dephosphorylation process, which lead to an increase in absolute RB protein levels. Despite the observed changes, the pRb/MyoD pathway in emerin deficient mice was effective at inducing the expression of downstream factors and mediating muscle regeneration, albeit with a slight temporal shift[100].

1.4.8 *Lmnb1*$^{-/-}$ mice

Since lamin B1 expression was shown to be essential for survival of HeLa cells *in vitro*, and the deletion of its rod domain caused nuclear structural abnormalities, Vergnes et al. decided to study the *in vivo* function of the protein by generating transgenic mice that carry an insertional mutation in *Lmnb1*[123]. The gene trap insertion resulted in the production of an mRNA fusion transcript consisting of the first five *Lmnb1* exons, encoding the N-terminal head and a truncated α-helical rod domain, followed by a βgeo reporter gene. The resulting protein lacked the NLS, the CaaX motif, as well as one of the two known phosphorylation sites. Whereas *Lmnb1*$^{+/-}$ mice were viable, homozygous lamin B1-deficient mice exhibited severe skeletal abnormalities and died only few minutes after birth due to respiratory failure. *Lmnb1*$^{+/-}$ mouse embryonic fibroblasts showed a plethora of cellular defects such as grossly misshapen nuclei, reduced replication rates, impaired differentiation, increased polyploidy and premature senescence[123].

1.4.9 *Lap2α*$^{-/-}$ mice

Cre-mediated germline deletion of α-specific exon 4 of the *Lap2* gene resulted in the generation of *Lap2α*$^{-/-}$ mice[32]. Although grossly indistinguishable from their wild type littermates, LAP2α-deficient mice exhibited higher proliferation of progenitor cells in highly regenerative tissues like skin, intestine and the hematopoietic system, as well as more efficient tissue repair after treatment with stress-inducing agents. The tightly regulated tissue homeostasis and fate decisions of progenitor cells in these systems were shown to depend on the phosphorylation status of pRb. In accordance, tissue lysates from *Lap2α*$^{-/-}$ mice showed increased pRb phosphorylation, consistent with a higher number of proliferating cells. Additionally, primary *Lap2α*$^{-/-}$ mouse fibroblasts exhibited a higher content of insoluble lamina-associated lamin A, in contrast to wild type cells which also have a significant nucleoplasmic pool, as well as delayed cell cycle arrest presumably due to impairment of contact inhibition, supporting the idea that LAP2α-lamin A complexes might be involved in the regulation of pRb activity[32].

Taken together, studies of human patients and mouse laminopathy models show that lamin proteins are involved in many nuclear processes and that the diseases caused by their mutations cannot be explained by simple straightforward hypotheses. Effects of changed nuclear mechanical properties, chromatin organization as well as transcriptional and posttranslational regulation may indiscernibly contribute to the complexity of laminopathy phenotypes. The newest studies supported the model previously proposed by Gotzmann and Foisner[13], according to which A-type lamins and LEM-domain proteins might play an important role in cell cycle regulation and differentiation of stem cells during maintenance of tissue homeostasis[32, 124, 125]. A defect in stem cell-mediated tissue repair could then explain the late onset of tissue specific symptoms in most laminopathies. Scaffidi and Misteli (2008)[125] and Espada et al. (2008)[124] demonstrated for the first time that progeria and age-related nuclear defects are directly linked to stem cell dysfunction, which might be caused by deregulation of Notch and Wnt signaling – the two major pathways governing stem cell fate. The downstream effectors of these cascades, normally sequestered at the nuclear periphery, could lose their inhibitory queues in the presence of mutated lamin proteins and therefore inappropriately exert their functions in target gene regulation. In addition, Naetar et al (2008)[32] showed that intranuclear LAP2α-lamin A complexes are involved in the tight regulation of committed-progenitor cell proliferation by their association with the pRb protein, fortifying the link between laminopathies and defects in adult stem cell-mediated tissue homeostasis.

1.5 The striated muscle story

Heart and skeletal muscle are the two tissues most frequently affected by mutations in lamin A/C (reviewed in [76]). Although numerous studies performed in the past few years made an invaluable contribution to the understanding of lamin A/C-linked pathologies, the major question of how a gene expressed in various cells of the body can specifically cause tissue-restricted disorders, still remains to be answered. In this respect, it is essential to study the function of lamin complexes within the context of tissue-specific molecular pathways.

1.5.1 Skeletal myogenesis in vertebrates

Skeletal muscles of the trunk, the limbs and partially of the head, derive from transitory embryonic structures called somites – the segments of paraxial mesoderm that form following an anterior-posterior progression on either side of the neural tube and the notochord (reviewed in [126]). During somite maturation, myogenic progenitor cells become confined to its dorso-lateral epithelial part named the dermomyotome (Figure 8). At the onset of myogenesis (E 8.0 in mouse), cells expressing the myogenic determination factors Myf5 and Mrf4 start to delaminate from the epaxial, and later mainly hypaxial edge (lip) of the dermomyotome, and move underneath it, where they rapidly differentiate into the skeletal muscle of the primary myotome (reviewed in [126]). Subsequently, in the second phase of myogenesis, the central portion of the dermomyotome gives rise to a population of progenitor cells, expressing paired box transcription factors Pax3 and Pax7. These $Pax3^+/Pax7^+$ cells remain present in all late embryonic muscle masses and, by activating the myogenic program, make a major contribution to muscle growth. At certain levels, $Pax3^+/Pax7^+$ cells cells detach and migrate away from the hypaxial dermomyotome to generate limb, diaphragm, hypoglossal and tongue muscles. Later, at E10.5, the central region of the dermomyotome loses its epithelial structure, and $Pax3^+/Pax7^+$ cells enter into the muscle mass of the myotome, providing progenitor cells for the subsequent growth of trunk muscles (reviewed in [126]).

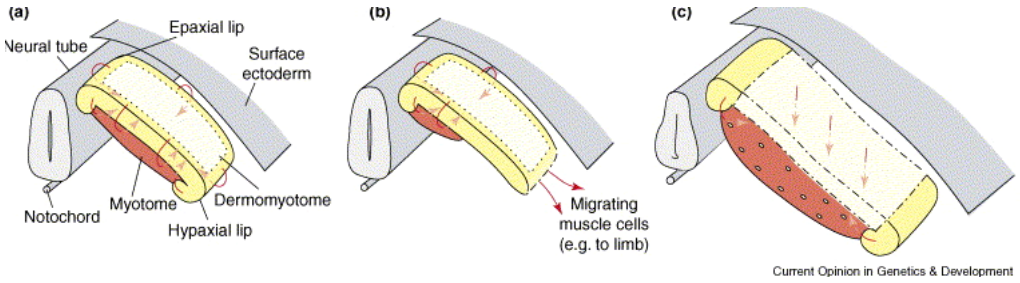

Figure 8. Skeletal myogenesis in vertebrates – dermomyotomal sources of myogenic progenitor cells. *M. Buckingham, Current Opinion in Genetics and Development, 2006.*

In addition to myogenic cells, the dermomyotome gives rise to several other mesodermal cell types including dermal, endothelial and smooth muscle cells of the dorsal aorta (reviewed in [126]).

Myogenic progenitor cells of the head derive from prechordal and anterior paraxial mesoderm cells, or from cells that migrated from anterior somites into the branchial arches. The upstream regulators of these cells include MyoR, Capsulin and the T-box factor Tbx1, which is also expressed by cells involved in heart formation (reviewed in [126]).

The process of myogenesis in the somite is orchestrated by surrounding tissues through the hedgehog (HH), Wnt, Notch, p38 MAPK, FGF, BMP, TGFβ, IGF, N-Cam and c-met signaling pathways. The HH factors secreted from the notochord and the ventral neural tube maintain the expression of myogenic genes in the dorsomedial lip of the dermomyotome – the primordial site of myogenesis (reviewed in [126, 127]). Maintenance of the epithelial structure of the dermomyotome depends on β-catenin-dependent Wnt signaling from dorsal ectoderm and the neural tube, which has also been implicated in the regulation of MyoD (Wnt7a) and Myf5 (Wnt1) activity during myogenesis through the protein kinase A-CREBP pathway[128] (Figure 9). Upon formation of the myotome and later muscle masses, endocrine TGFβ signaling affects the growth of these structures by limiting the proliferation of Pax-positive progenitor cells[129].

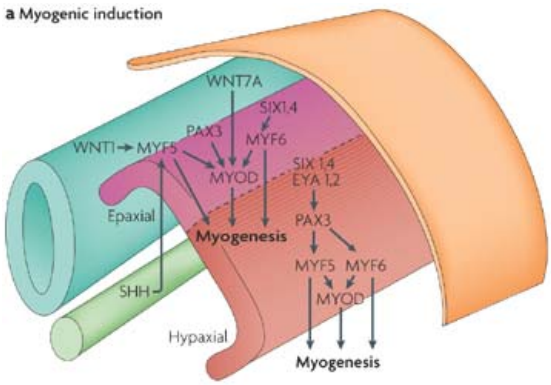

Figure 9. Signaling pathways regulating myogenic induction in the mouse. The neural tube is depicted in turquoise, the notochord in green and the dorsal ectoderm in orange. The epaxial and hypaxial parts of the dermomyotome are shown in pink and red respectively. Adapted from *R.J. Bryson-Richardson and P.D. Currie, Nature Reviews Genetics, 2008.*

During late foetal development (at approximately day E17.5), the resident hypaxial-derived Pax-positive progenitor population generates $Pax7^+$ myogenic cells, which occupy a satellite position around mature myofibers upon formation of the myotube-surrounding basal lamina (reviewed in [130]). These satellite cells account for ~30-35% of the sublaminal nuclei associated with myofibers in early postnatal mouse muscle and make the major contribution to bulk postnatal muscle growth. Adult mouse muscle possesses only 1-4% of mainly mitotically quiescent satellite cells (comprising 3-5.5% of all myofibre nuclei) which can be activated in response to external queues and either self-renew or produce myonuclei during homeostasis, hypertrophy and muscle regeneration (Figure 10) (reviewed in [131]). At present, the satellite cell pool is considered to contain a heterogeneous population of stem and committed progenitor cells, which exhibit different self-renewal and myogenic potentials, and display a range of cell surface markers such as CD34, CXCR4, β1-integrin, c-met, N-cadherin, as well as the transcriptional factor Pax7[132, 133]. The absence of a specific uniform satellite cell marker presents an additional obstacle in an effort to disclose the cellular pathways governing muscle homeostasis and regeneration.

Interestingly, a recent analysis of myofiber-associated satellite cell division suggested that the plane of cell division might be the determinant factor of daughter cell fate[132]. Satellite cells undergoing planar divisions are thought to give rise to cells with symmetric expression of Myf5, whereas apical-basal plane divisions would result in a committed progenitor cell expressing Myf5-positive and a Myf5-negative quiescent satellite cell responsible for maintenance of the stem cell pool (Figure 10).

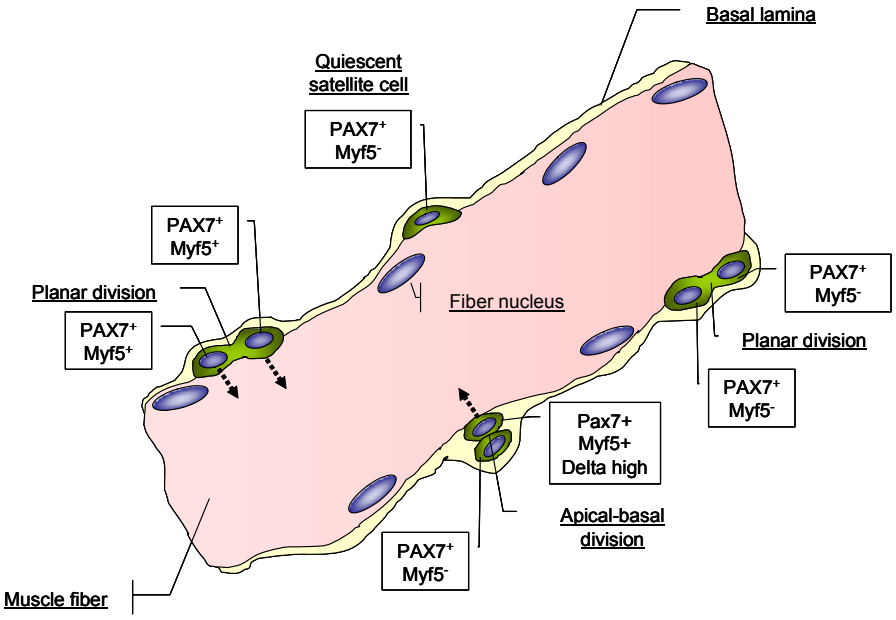

Figure 10. Shematic diagram of a skeletal myofiber with its associated satellite cells. Modified according to *R.J. Bryson-Richardson and P.D. Currie, Nature Reviews Genetics, 2008.*

Recently, the microenvironmet or the niche which modulates the function of adult stem cells, has been put into the spot light to address the issue of age-related changes in the stem cell pool (reviewed in [134]). The niche represents a dynamic environment that switches between states that support quiescence and those that contribute to the activation of stem cells in response to local and systemic influences. Muscle satellite cells reside between the myofiber and the basal lamina, which together with the microvasculature, the neural components, as well as occasionally present cells of the immune system, represent the adult muscle stem cell niche able to respond to systemic queues and modify their fate.

The myofiber association negatively effects proliferation of satellite cells in the steady state, keeping them in a quiescent mode[135]. In contrast, muscle damage causes upregulation of Delta, a transmembrane ligand that binds the Notch receptor, in the injured myofibers and induces proliferative expansion of satellite cells. Interestingly, aged muscle fibers fail to induce Delta expression, resulting in reduced proliferation of satellite cells and impaired muscle regeneration[136].

The basal lamina, composed of collagen type 4, perlecan, laminin, entactin, fibrinectin and several glycoproteins/proteoglycans, can also positively and negatively affect proliferation of satellite cells. In this regard, laminin, fibronectin and several proteoglycan receptors of inactive growth factor forms have been shown to support their proliferation. In aging muscle, the function of basal lamina and muscle regeneration are compromised due to degradation of connective tissue components and accumulation of their toxic by-products (reviewed in [137]). The reduced regeneration potential of aged muscle might also be a consequence of age-related systemic increase in Wnt signaling, which suppresses stem cell function and increases fibrogenesis in multiple tissues (reviewed in [134]).

1.5.2 Satellite cells in action

In response to external activating signals, $Pax7^+$ satellite cells initiate the expression of MyoD, the major myogenic transcription factor, and initiate the process of terminal muscle differentiation, which involves fusion of single myoblasts into multinucleated myotubes, as well as downregulation of Pax7[130] (Figure 11). MyoD, together with Myf5, myogenin and Mfr4 proteins, belongs to a family of myogenic basic helix-loop-helix (bHLH) transcription factors which form heterodimers with ubiquitously expressed bHLH-E proteins and regulate the expression of muscle specific genes by binding to a special DNA motif called the E-box (reviewed in [138]). Although expressed in undifferentiated myoblasts, MyoD, Myf5 and E proteins remain in an inactive state until the extracellular queues are interpreted as pro-differentiation signals and their post-translational modifications allow association with muscle-specific promoters and co-factors. Histone deacethylase III family member Sir2, found in a protein complex with the acethyltransferase pCAF (p300/CBP-associated factor) and MyoD in undifferentiated myoblasts, was proposed to inhibit the MyoD-specific gene activation by histone and/or pCAF/p300/MyoD deacethylation (reviewed in [138]). Another protein complex involved in the inhibition of muscle-specific regulatory regions

contains the Polycomb group protein Enhancer of zeste 2 (Ezh2), a histone lysine methyltransferase (HKMT), the transcriptional regulator YY1 and HDAC1, which all have to be removed from promoters before MyoD and SRF (Serum response factor) can initiate the differentiation process. Since Sir2 is also required for Polycomb-mediated silencing, the two pathways most probably intertwine in order to keep the cells in an undifferentiated state[138].

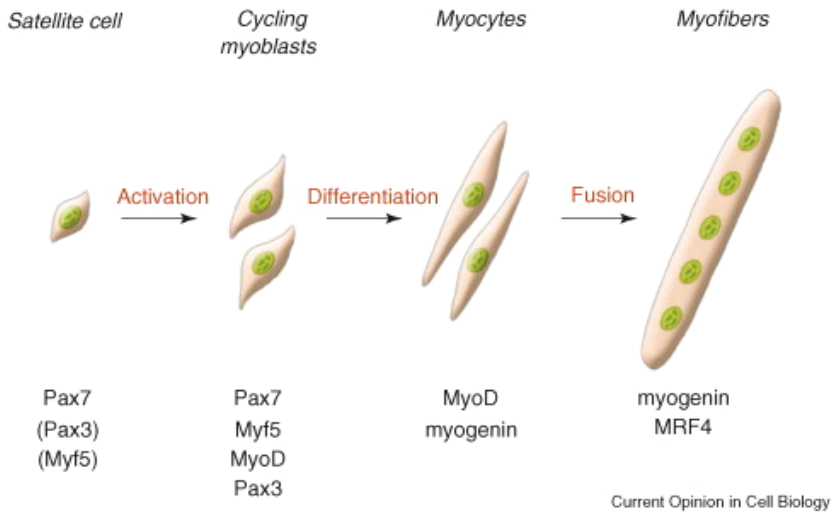

Figure 11. Schematic representation of adult myogenesis. Adapted from *F. Le Grand and M.A. Rudnicki, Current Opinion in Cell Biology, 2007.*

Once the inhibitory complexes are removed from promoters, activated MyoD recruits histone acethyletransferases (HATs), SWI/SNF chromatin-remodeling complexes, as well as polymerase II activating kinases, and promotes the expression of myogenic genes during muscle differentiation. In addition, MyoD activates pRb and p21 gene expression in an E-box independent mechanism followed by downregulation of cyclin D1, E and A. The hypophosphorylated, acethylated pRb inhibits cell cycle progression by preventing the interaction of E2F with its target genes and further upregulates and co-activates MyoD in a feed forward loop, which results in terminal cell cycle withdrawal and induction of muscle-specific transcription (reviewed in[139]). Whether MyoD and pRb are able to interact directly remains to be elucidated, but since both proteins have been found in complexes with lamin A/C, it is tempting to speculate that LAP2α-lamin A/C complexes might form the missing link between these two proteins. pRb is also essential for promoting functional cooperation between MyoD and MEF2 (Myocyte enhancer factor 2) proteins belonging to a larger evolutionary ancient MADS (MCM1, agamous, deficiens, SRF) family of transcription factors, which then act together on downstream targets such as myogenin, myosin heavy chain (MyHC) and muscle creatine kinase (MCK) and orchestrate the differentiation process[103].

Mice lacking MyoD develop normally and do not display a severe muscle phenotype, indicating that other myogenic factors like Myf5 and Mrf4 can compensate, at least in a part, for its loss during embryonic development[140]. The adult skeletal muscle of *MyoD*$^{-/-}$ mice however displays deficiency in regeneration caused by accelerated growth and delayed differentiation of myoblasts, supporting the role of MyoD in regulation of the satellite cell transcriptional program[140]. Although a full deletion of pRb causes embryonic lethality in mice due to defects in various tissues including muscle[141], a skeletal muscle-specific ablation of pRb demonstrated a role of the protein in progression through myogenic differentiation, as well as its redundancy during maintenance of terminal differentiation[142], consistent with its function in cell cycle withdrawal and MyoD-dependent gene regulation.

Interestingly, during myoblast differentiation the nucleoplasmic pool of lamin A/C becomes rearranged and antigenetically masked, without an apparent change in peripheral lamin organization[143, 144]. In addition, the expression of a mutant AD-EDMD-causing lamin A in C2C12 myoblasts promotes apoptosis and inhibits myotube formation[145], suggesting that a specific form of a functional lamin scaffold is required during muscle differentiation. What is more, a gene expression study of mouse muscle regeneration process showed an increase in *LAP2* and *LMNA* transcription at day 3.5, when a strong induction of MyoD and its downstream targets was observed, suggesting a role of these proteins in muscle-specific gene expression, as well as NE remodeling at the time of myoblast cell cycle exit[146]. The gene expression profile of EDMD patients carrying *EMD* or *LMNA* mutation analyzed in the same study, found an upregulation of the *LMNA* and *LAP2* gene products, as well as members of the CREBP/p300 acethylase pathway, suggesting disease specific perturbations of the lamin A-emerin-pRb-MyoD mechanism. An intriguing observation that the short C-terminal peptide produced during lamin A maturation might be involved

in myoblast fusion, as it resembles the yeast mating factor, adds another level to the lamin A/C functional complexity[147].

1.5.3 Transforming skeletal muscle

MyoD, myogenin and MEF2 factors not only play essential roles in muscle formation, but are also important for transformation of muscle fibers in response to external physiological signals such as innervation and endocrine/nutritional cues (reviewed in [148]). Skeletal muscle tissue is composed of muscle fibers – large syncytial cells individually surrounded by basal lamina – which present a heterogeneous population in respect to size, metabolism and contractile function. On the basis of specific myosin heavy chain isoform expression, myofibers are classified into two major groups: type I and type II (IIa, IId/x, IIb) fibers. Type I fibers (and IIa) exhibit oxidative metabolism and are also termed "slow-twitch" due to their slow contraction mode, owing to the specific activity of the ATPase associated with type I myosin. They are rich in mitochondria, have more surrounding capillaries and exhibit low velocity of shortening, as well as high resistance to fatigue. Whereas slow fibers are required for tasks involving endurance and maintenance of posture, the primarily glycolytic, fast – type II fibers, which exert quick contractions and fatigue rapidly, are involved in movements which involve strength and speed (reviewed in [148]).

Skeletal muscle is able to adapt to environmental demands and respond to physiological and pathological signals by transforming and remodeling the myofiber content. Muscle exercise causes an increase in oxidative metabolism and fast-to-slow myofiber transition, whereas muscle disuse and aging have an opposite effect. The properties of skeletal muscle fibers depend on the pattern of nerve stimulation, where low frequencies of neuron firing promote slow, and high frequencies fast muscle phenotype. The neuronal stimulation causes changes in the intracellular calcium content, which then serves as a second messenger in the signaling pathway leading to altered gene expression (reviewed in [148]).

Muscles predominantly composed of fast myofibers, like *Tibialis anterior* (TA) and *Extensor digitorum longus* (EDL), exhibit high MyoD content and *MyoD* cis regulatory regions seem to restrict the expression to IIx and IIb fibers. In accordance, *MyoD*$^{-/-}$ mice show a subtle shift in fiber content of fast muscles toward a slower type, while slow muscles tend to switch to a faster type[149]. Slow fiber containing muscles, like *Soleus*, express more myogenin, which was shown to induce oxidative enzymes in adult fast muscles in response to calcineurin (calcium-dependent phosphatase) signaling (reviewed in [150, 151]).

MEF2 contributes to establishment of slow fiber phenotype by driving oxidative, slow fiber-specific gene expression activated by calcium-dependent signaling[152] (Figure 12)[148]. Calcium/calmodulin-dependent protein kinase (CaMK), which senses the frequency of calcium oscillations and becomes activated during hypertrophic growth and endurance adaptations, phosphorylates class II HDACs thereby initiating their transport out of the nucleus. As a consequence, MEF2 is relieved of the inhibitory activity of HDAC II-recruited SUMO2 and SUMO3 enzymes and can fulfill its transcriptional function (reviewed in [138]). Skeletal muscle-specific

deletion of *Mef2c* results in a substantial reduction of slow myofibers, whereas overexpression of its super-active form promotes the slow fiber phenotype and enhances endurance exercise (reviewed in [148]).

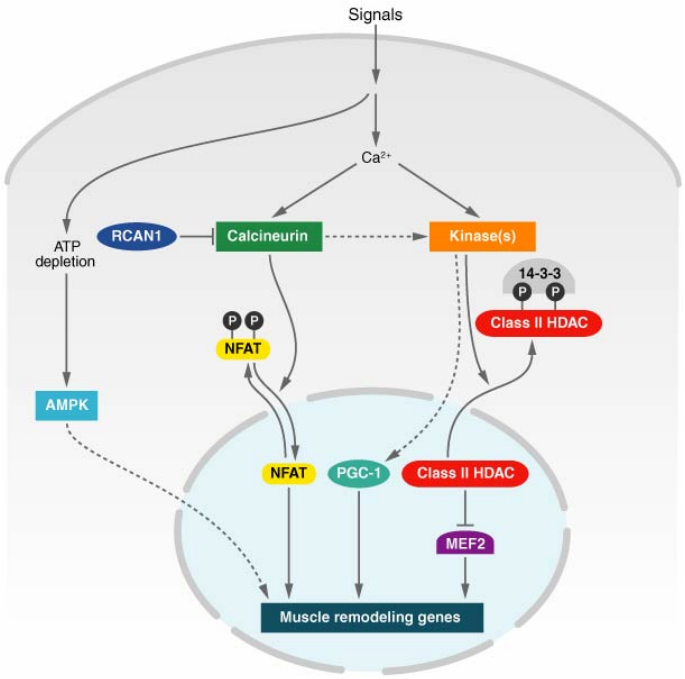

Figure 12. Signaling pathways in skeletal muscle remodelling. Adapted from *Rhonda Bassel-Duby and Eric N. Olson, Annual Review of Biochemistry, Vol. 75, 2006.*

An important partner of MEF2 in the process of fiber type switching is the nuclear factor of activated T cells (NFAT), whose translocation from the cytoplasm to the nucleus upon calcineurin-dependent dephosphorylation activates the slow – type I – muscle fiber program. In addition, another target of calcineurin signaling, the transcriptional coactivator peroxisome-proliferator-activated receptor gamma coactivator-1 (PGC-1), preferentially enriched in type I myofibers, which is considered to be a master regulator of mitochondrial gene expression activating mitochondrial biogenesis and oxidative metabolism, also activates transcription in cooperation with MEF2. PGC-1 associates with the skeletal muscle-predominant form of peroxisome proliferator-activated receptor - PPARΔ, which serves as the major transcriptional regulator of fat metabolism in adipose tissue. By activating enzymes associated with long-chain fatty-acid β-oxidation, PPARΔ in excess also causes an increase of type I fibers (reviewed in [148]).

PGC-1α also functions as Foxo coactivator, implicating the Foxo pathway in the process of fiber type switching, although the reduced number of type I fibers in *myogenin-Foxo1*$^{-/-}$ transgenic animals seemes more as a consequence of increased MyoD expression and deregulated differentiation than impaired PGC-1α transcription[153]. The O subfymily of forkhead (Fox) proteins

promotes cell survival and metabolism by regulating hormonal, nutrient and stress responses through the phosphatidylinositol 3-kinase (PI3K) mechanism. In addition to their role in terminally differentiated cells, Foxo proteins are involved in myoblast, preadipocyte and endothelial cell differentiation. The Foxo pathway was also shown to physically and functionally interact with Notch signaling to control the myogenic program by promoting corepressor clearance from the Csl factor[153]. The Notch pathway plays an important role in embryonic development and adult stem cell regulation during neural, vascular, endocrine, as well as muscle differentiation. The ligand-induced receptor cleavage causes the translocation of the Notch intracellular domain (NICD) to the nucleus and the subsequent association with the DNA-binding protein Csl, which changes its transcriptional properties from a suppressive to an activating form. The Csl targets Hairy and Enhancer of split (Hes) and Hes-related (Hey) then inhibit the MyoD protein and suppress myoblast differentiation (reviewed in [[154]]).

The slow muscle atropy found in striated muscle laminopathies[155, 156] and a specific type II fiber hypertrophy in *Lmna*^{H222P} mice[108] suggest a role of lamin A/C proteins in fiber type determination and/or age related muscle remodeling.

1.6 The developing heart

The first organ formed in a developing vertebrate embryo is the heart. Mouse cardiogenesis starts at embryonic day 6.25 with the induction of the precardiac mesoderm which will later give rise to the two distinct mesodermal heart fields in a temporally and spatially specific manner (reviewed in [156]). During mouse development, at E7.5, the cells in the anterior lateral mesodermal plate form a crescent shape corresponding to the primary or first heart field (FHF), which will form the primitive heart tube consisting of an interior layer of endocardial cells, separated by extracellular matrix from the exterior layer of myocardial cells, by day E8.0 (Figure 13) (reviewed in [157, 158]).

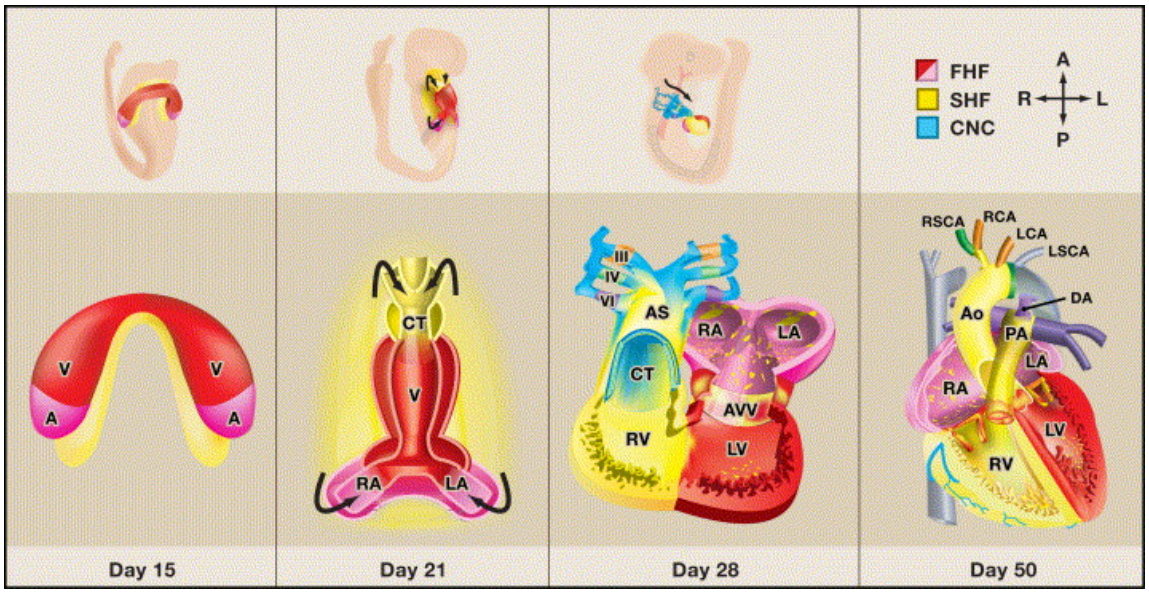

Figure 13. Schematic diagram of mammalian heart development. Oblique views of whole embryos and frontal views of cardiac precursors during human cardiac development are shown in upper and lower panels respectively. FHF – first heart field, SHF – second heart field, CNC – cardiac neural crest, V – ventricle, LV – left ventricle, LA – left atrium, RA – right atrium, AS – aortic sac, Ao – aorta, PA – pulmonary artery, RSCA – right subclavian artery, LSCA - left subclavian artery, RCA – right carotid artery, LCA – left carotid artery, DA – ductus arteriosus. Adapted from *Deepak Srivastava, Cell 126, 2006*.

Whereas the FHF differentiates at the cardiac crescent stage, differentiation of the second heart field (SHF) is relatively delayed and occurs as the second lineage migrates in, to join the cells from the first lineage which have created a scaffold for the subsequent SHF cell migration and chamber formation. During heart tube development, the SHF cells originating from the dorsal-medial aspect of the cardiogenic plate migrate into the midline and position themselves dorsal to the heart tube in the pharyngeal mesoderm. Rightward looping of the heart tube is followed by

migration of SHF cells into the large portion of the outflow tract, the future right ventricle and atria. The left ventricle, in contrast, appears mainly derived from the FHF cells (reviewed in [157]).

Migration and proliferation of both cell-lineages appear to be regulated by complex positive and negative queues of the BMP, SHH, FGF, Wnt and Notch signaling pathways (Figure 14), though the exact transcriptional cascades still remain to be elucidated. Following the rightward looping, cardiac neural crest (CNC) cells migrate from the neural folds into the outflow tract and pattern the bilaterally symmetric aortic arch arteries. Septation of the ventricles, the atria and atrioventricular valves finally results in the four-chambered mammalian heart (reviewed in [157]).

Whilst many of the central transcriptional regulators of cardiac development in the FHF, such as Nkx2.5 and GATA4, also appear in the SHF and may target its development, the regulation of SHF still calls for the expression of specific genes (reviewed in [158]). In this regard, the basic helix-loop-helix transcription factor Hand2 was found to be enriched in the mouse right ventricle and required for SHF expansion[159]. Similarly, right ventricular hypoplasia was observed in mice lacking MEF2c[160], which serves as a target of Isl1, GATA4, Foxh1 and Tbx20 in the SHF[161]. Interestingly, the LIM-homeodomain transcription factor Isl1, which is highly expressed in cells of the SHF and required for their population of the heart, also seems to be present in niches of undifferentiated cardiac progenitor cells in the postnatal heart[162, 163]. However, in contrast to skeletal muscle, which has an outstanding potential to regenerate after damage due to the presence of satellite cells, the currently highly controversial cardiac stem cells make a limited contribution to tissue repair, leaving the heart scarred.

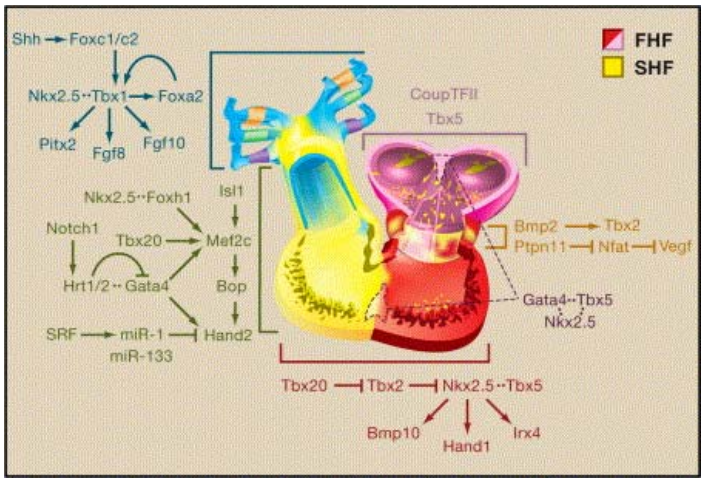

Figure 14. Pathways regulating region-specific cardiac morphogenesis. Positive signals are depicted by arrowheads and negative by bars, whereas dashed lines indicate physical interactions between factors. FHF – first heart field, SHF – second heart field. Adapted from *Deepak Srivastava, Cell, 2006.*

During the process of mouse cardiogenesis, the immature cardiomyocytes are still able to proliferate while differentiating, but soon after birth they stop cycling and arrest mainly in G0/G1 phase of the cell cycle as binucleated cells[164]. The major cell cycle regulator pRb seems to play a critical role in early heart development, directing stem cells toward a cardiac lineage through its association with a cardiomyogenic factor LEK1[165]. Rb expression in the heart exhibits a decreasing gradient from the blastocyst stage, through embryonic and neonatal heart. The other two members of the pocket protein family, p107 and p130, seem to take over some of the pRbs' activities in the late foetal and early postnatal heart respectively, since they are the predominant forms expressed in those stages[166]. Upregulation of pRb also occurs in the adult mouse heart, although the nature of these changes still remains to be elucidated[167].

A-type lamins are also expressed in the postnatal heart, but the number of positive nuclei seems to decrease with age[168]. In contrast to skeletal muscle, molecular mechanisms implicating lamins in heart development and homeostasis are only starting to be unraveled. The defects observed in *Lmna*$^{-/-}$ cardiomyocytes[99] suggest a role of lamin A/C proteins in cardiac-specific gene expression at baseline, as well as stress induced hypertrophic growth.

Mechanisms regulating hypertrophic growth in cardiomyocytes are thought to include multiple signaling cascades activated by second messengers in response to mechanical and molecular queues such as PI3, PKC, MAPK and calcineurin. These pathways then convey stress signals into hypertrophy-specific transcription, which in part mirrors gene expression fingerprint of embryonic heart development. The factors prominently involved in cardiac-specific transcription and hypertrophic stress response include GATA4, Nkx2.5 and MEF2c. The plethora of their targets comprises the early (c-fos, c-myc, c-jun, BNP and Egr-1), the intermediate (ANP, β-myosin, skeletal α-actin, AM, phospholamban) and late response genes (cardiac α-actin, CT-1, NCX, MMPs, SERCA) (reviewed in [[169]]). Since the exact upstream, as well as downstream, effectors of these pathways are currently unknown, it is tempting to hypothesize that lamin A-LAP2α complexes might influence the activity of MEF2c or other factors through the interaction with another bHLH protein equivalent to skeletal muscle-specific MyoD, such as Hand2, or through general rearrangement of the active chromatin.

1.7 The aim of the study

Since LAP2α and lamin A/C mutations have been implicated in cardiac and skeletal muscle-specific disorders, the aim of the study was to shed more light onto molecular mechanisms underlying striated muscle laminopathies. To this end, the functionality, the structural properties, as well as regeneration potential and stress response of striated muscles were analyzed in the previously generated mouse lacking LAP2α protein (Figure 15). To study the ability of the LAP2α-deficient striated muscle to recover after stress, *Lap2α*$^{-/-}$ mice were subjected to procedures causing acute and chronic tissue damage, as well as crossed with the musclular dystrophy mouse model line *Mdx*, which experiences inherent constant muscle damage, to yield compound *Lap2α*$^{-/-}$*/Mdx* mice. In order to more closely determine the time frame of the specific muscle-associated LAP2α function, two additional conditional mouse lines, which lose the protein at different stages of muscle differentiation were generated and analyzed. In the case of *Lap2α*$^{-/-}$*/Pax7-Cre*$^{+}$ mice, LAP2α protein is absent from muscle satellite and other cells expressing the transcription factor Pax7, which enables the study of its function during muscle stem cell self-renewal and proliferation. The *Lap2α*$^{-/-}$*/Mck-Cre*$^{+}$ mice, on the other hand, lose LAP2α only later in the process of muscle differentiation allowing the analysis of its function during myoblast-myotube transition.

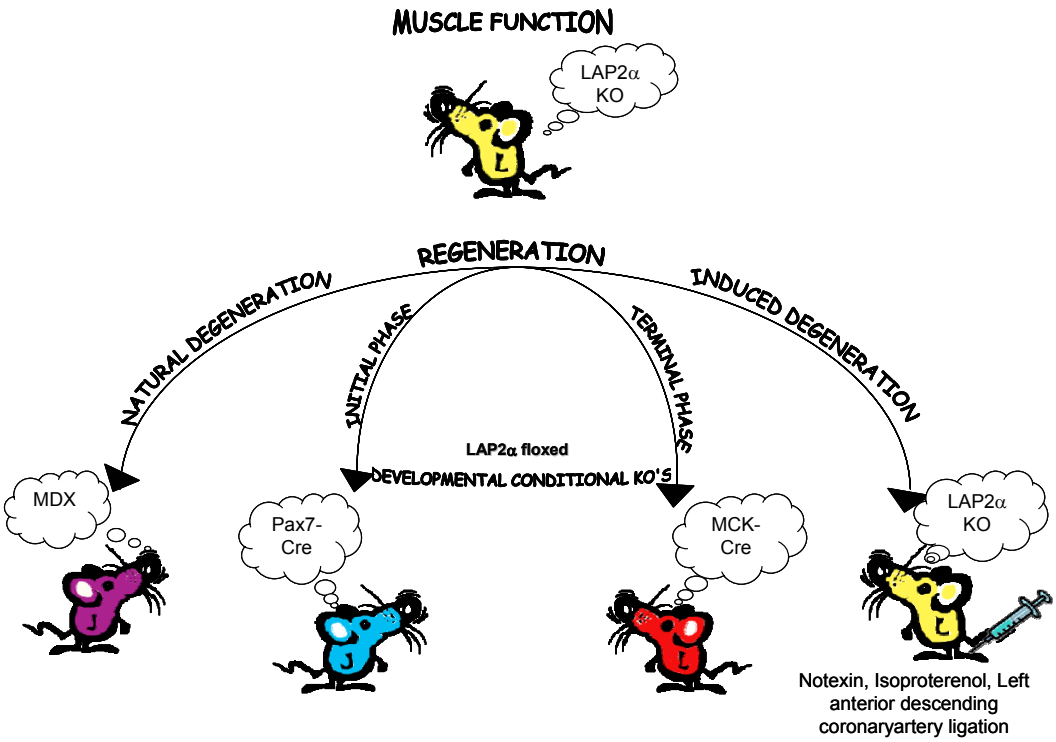

Figure 15. Schematic overview of the LAP2α-striated muscle project designed to analyze the function of the protein in the striated muscle context.

2 Materials & Methods

~Extended version of materials and methods described in the submitted manuscripts~

2.1 Mouse phenotyping

2.1.1 The SHIRPA protocol

The SHIRPA protocol is a simple first-line phenotyping screen which provides a behavioral and functional profile of genetically altered mice by observational assessment[170]. The original protocol used by the Harwell Medical Research Council was slightly modified by EUMORPHIA, a project funded by the European Commission under FP5 which developed a database of Standard Operating Procedures (SOPs) used for mouse phenotype characterization (www.eumorphia.org).

2.1.1.1 Behavior recorded in a viewing jar

A clear cylindrical viewing jar was placed upright on top of a sandpapered plastic sheet standing on a tripod (~7.5 cm high). The mouse was removed from its home cage, gripping the tail between the thumb and the forefinger, and placed into the viewing jar. Without disturbing the animal the following behaviors were recorded:

Feature	Description	Score
Body position	*Observe the mouse and identify the level of activity.*	*0 – inactive;* *1 – active;* *2 – excessive activity*
Tremor	*Make a note of whether or not the mouse appears to tremble.*	*0 – absent;* *1 – present*
Palpebral closure	*Observe the closing of the eyes.*	*0 – eyes open;* *1 – eyes closed*
Coat appearance	*Look at the mouse coat, how tidy and well groomed it is and note deviances like piloerection.*	*0 – tidy and well groomed;* *1 – irregularities*
Whiskers	*Observe whether the mouse has intact or trimmed whiskers.*	*0 – present;* *1 – absent*
Lacrimation		*0 – present;* *1 – absent*
Defecation		*0 – present;* *1 – absent*

2.1.1.2 Behavior recorded in the arena

The floor of a Perspex arena (60×37×18 cm) was marked with 15 squares (~11 × 11 cm). The mouse was transferred to the centre of the arena inside of the viewing jar, using the plastic sheet underneath the jar to constrain the mouse. The plastic sheet was then carefully removed at approximately 25 cm above the arena floor and the behavior of the animal inside of the arena was recorded:

Feature	Description of the test	Score
Transfer arousal	*Observe the immediate reaction of the mouse to the new environment and make a note whether it appears to freeze for a period longer than 5 s, freezes briefly before it begins to move, or moves immediately.*	*0 – extended freeze (over 5 s);* *1 – brief freeze followed by movement;* *2 – immediate movement*
Locomotor activity	*Start the stop watch and make a note of the total number of squares the mouse enters with all four feet in 30 s.*	
Gait	*Study the gait of the mouse and determine how fluid its movement is as well as the extent to which the pelvis is elevated during forward motion.*	*0 – fluid movement and approximately 3 mm pelvic elevation;* *1 – lack of fluidity in movement (eg. retropulsion, more than 3 mm pelvic elevation)*
Tail elevation	*During forward motion, observe the position of the tail making a note of whether it is dragging, horizontally extended or is elevated.*	*0 – dragging;* *1 – horizontal extension;* *2 – elevated/straub tail*
Touch response	*Approach the mouse from the front with a bent index finger before stroking on the back of the neck and observe the response.*	*0 – no response;* *1 – response to touch;* *2 – flees prior to touch*

2.1.1.3 Behavior recorded above the arena

The mouse was removed from the arena by gripping the tail between the thumb and the forefinger and following features were observed:

Feature	Description of the test	Score
Positional passivity	*Measure the immediate response to sequential handling of the mouse.*	*0 – struggles when held by the tail;* *1 – struggles when held by the neck;* *2 – struggles when held laid supine;* *3 – no struggle*
Skin color	*Make a note of the color gradations of the plantar surface and digits of forelimbs.*	*0 – blanched;* *1 – pink;* *2 – bright, deep red flush*
Trunk curl	*Make a note of forward curling (i.e. head to abdomen) of the mouse when held by the tail.*	*0 – absent;* *1 – present*
Limb grasping	*Make a note of the mouse grasping its limbs when held by the tail.*	*0 – absent;* *1 – present*
Pinna reflex	*Place the mouse gently on to a grid and touch the proximal part of the inner canthus lightly with the tip of a fine cotton probe, observing ear retraction.*	*0 – present;* *1 – absent*
Corneal reflex	*Whilst the mouse is on the grid, touch the cornea lightly with the tip of a fine cotton probe, observing the eye-blink response.*	*0 – present;* *1 – absent*
Evidence of biting	*Make a note of whether or not the mouse bites during the screen.*	*0 – none;* *1 – biting in response to handling*
Vocalization	*Make a note of whether or not the mouse is vocal during the screen.*	*0 – none;* *1 – vocal*
Wire maneuver	*Animal is held above the wire by tail suspension and lowered to allow the forelimbs to grip the horizontal wire. The mouse is held in extension, rotated around the horizontal and released.*	*0 – active grip with hindlegs;* *1 – difficulty to grasp with hindlegs;* *2 – unable to grasp with hindlegs;* *3 – unable to lift hindlegs, falls within seconds;* *4 – falls immediately*

2.1.2 Swim test

The laboratory sink was cleaned and filled with 20 cm depth of water at 24 – 26ºC . The mouse was removed from its home cage, carefully lowered into the water and observed for 30 s. The swimming ability was assessed in the following way:
0 – *Swims*. [Mouse body is elongated and the tail propels in a flagella-like motion].
1 – *Irregular swimming*. [Includes vertical swimming, swimming in a circle, swimming on side (left/right preference noted), swimming in an unbalanced manner (tail is raised and beat about in an unstable manner)].
2 – *Immobile floating*. [Some vestibular mutant mice, that display initial passive immobile floating, soon unbalance and display full underwater tumbling or irregular swimming, which should be reported as such].
3 – *Underwater tumbling*. [Mouse is unable to maintain a balanced body position and continuously tumbles. This represents an extremely severe behavior and the mouse must be scooped up and rescued immediately on displaying underwater tumbling].

After swimming, the mouse was carefully removed from the water, dried with paper towels and placed in a fresh cage containing dry paper towels. The cage was placed under a heat source (a red lamp) for 15 min before the mouse was returned to its home cage.

2.1.3 The voluntary wheel test

Prior to the official experiment, each mouse was allowed to adjust to the hamster-wheel placed inside a big mouse cage (3 hours/3 consecutive days). On the 4^{th} day, the mouse was returned to the wheel and its performance was measured within 3 hours (daily ride time [h], average speed in km/h, daily ride distance in km, and maximum speed in km/h). The experiment was always done at the same time during the day to avoid variations caused by different circadial activity phases of the animal.

2.1.4 The forced wheel test

In the first phase, the mouse was placed inside a motorized wheel (d = 14 cm) and its spontaneous activity – wheel turning - was recorded for 15 min. Subsequently, the wheel was set to a constant rotational speed of 0.1 – 1 round/s and the physical endurance of the mouse was assessed by measuring the time of active running. Each experiment was repeated 3 times.

2.1.5 The rotarod test

Mice were placed on the rotarod and their ability to adjust to accelerating rotational speed (0 – 60 rounds/60 s) was measured in 3 separate trials.

2.2 *In vitro* systems

2.2.1 Adult muscle fiber isolation

Adult muscle fibers were isolated according to the modified protocol described by Shefer and Yablonka-Reuveni[171]. Mice were euthanized and rinsed with 70% ethanol. The skin was cut around the ankles and pulled towards the trunk exposing the underlying muscles. The tendons were cut and, by careful pulling to avoid fiber damage, particular muscles (*Tibialis anterior* (TA), *Extensor digitorum longus* (EDL), *Soleus* (SOL), *Gastrocnemius* (GC) and *Quadriceps* (QC)) muscles were isolated. After removal of the surrounding connective tissue, muscles were collected in PBS and subsequently transferred to sterile 0.2% collagenase I/DMEM solution (3 ml/50 mg of tissue). The samples were incubated for 1.5 – 2 hours in a shaking water bath at 37ºC until single muscle fibers were loosened. In the mean time, plastic 6-cm Petri dishes were coated with 1 ml of undiluted filtered horse serum (HS) and incubated for 5 min at 37ºC. The HS was removed and the dishes, filled with 7 ml of DMEM, were subsequently stored in the incubator. Muscle digestion was stopped after 2 h by transferring the samples to DMEM-containing coated Petri dishes. The digests were then moved to fresh Petri dishes and single fibers were liberated by gentle trituration through a series of wide bore pipettes rinsed with 10%FCS/DMEM. Individual fibers were lifted with minimal residual medium and distributed into 24-well plates coated with 10% Matrigel/DMEM. Fibers were allowed to settle down for 10 min in the incubator before 500 µl of warm culture medium (20% FCS/10% HS/1% CEE/DMEM) was added to each well. Single fibers were cultured for 2-3 days until single satellite cells started to migrate off of them and proliferate. The cells were then trypsinized, washed in Hams' F-10 medium supplemented with 20% FCS, pre-plated for 2 hours on plastic dishes to get rid of the fibroblasts and finally plated on collagen-coated dishes (5 cm Petri dish incubated over night with 0.5 ml of 10% rat tail collagen/0.53% acetic acid and rinsed with PBS).

Alternatively, single fibers were either placed on glass coverslips and immediately processed for immunofluorescence, or cultured on chamber slides and stained at particular time points.

2.2.2 Muscle fiber immunofluorescence

For immunofluorescence analysis, 5 – 7 freshly isolated myofibers were placed on Dako-pen-sealed glass coverslips and fixed for 10 min in 4% para-formaldehyde. After 2×2 min washing with PBS, the samples were incubated in 50 mM NH_4Cl/PBS for 5 min, washed in PBS and blocked in 20% normal goat serum/0.5% gelatine/0.5 Triton X-100/PBS for 30 min at room temperature. Primary antibodies were diluted in PBS (eg. rat anti-mouse CD34 1:133) and applied over night at 4ºC. After washing, samples were incubated for 1 hour with matching secondary antibodies, either directly coupled to a fluorochrome or indirectly through streptavidin – biotin

association. Nuclear DNA was counterstained for 10 min with Hoechst dye diluted 1:50 000 in dH_2O and fibers were subsequently mounted in Mowiol 4-88 (*Roth*).

2.2.3 Neonatal satellite cell isolation

Neonatal satellite cells were isolated from 2-5 days old mice. Animals were sacrificed by decapitation, rinsed with 70% ethanol and de-skinned. Front and hind limbs were isolated and muscle tissue was trimmed of fat. The samples were then incubated with 0.2% collagenase I/DMEM solution (3 ml/mouse) for 1.5 hours in a shaking water bath at 37ºC. Muscle digests were transferred to a series of HS coated Petri dishes filled with DMEM and single fibers were liberated by gentle trituration. Samples were collected in 15 ml tubes filled up with DMEM and centrifuged for 3 min at 300 rpm. The pellet was washed once in PBS and re-suspended in DMEM. Undigested bulk fibers were allowed to settle down by gravity for 2-3 min before the transfer of the supernatant to new 15 ml tubes. After centrifugation at 500 rpm for 5 min, samples were re-suspended in culture medium and plated on Matrigel-coated dishes. Muscle fibers were cultured for 48-72 hours before the satellite cells were harvested and plated on collagen-coated dishes.

2.2.4 Primary mouse myoblast culture

Satellite cells were cultured on collagen coated dishes in growth medium, consisting of Hams' F-10 medium supplemented with 20% foetal calf serum/2.5 ng/ml basic FGF/50 U/ml Penicillin/ 50 µg/ml Streptomycin, in a humidified 5% CO_2 atmosphere at 37ºC. Proliferating cultures were maintained at ~ 40% density with medium changes every 2 days. For splitting, the medium was soaked off, cells washed with PBS and trypsinized for 5 min at 37ºC. Subsequently, they were collected in PBS, centrifuged at 1100 rpm (cell culture Heraeus centrifuge) for 3 min and re-suspended in growth medium. Before being plated on collagen coated dishes, the cells were pre-plated for 2-3 hours on plastic Petri dishes to get rid of the contaminating fibroblasts. Myoblast differentiation was induced by replacing the growth medium with differentiation medium (5%HS/DMEM). During the course of differentiation the medium was changed daily.

2.2.5 Cell immunofluorescence

Cultured cells were fixed in 4% paraformaldehyde/PBS for 10 min, washed in PBS and incubated for 5 min in 50 mM NH_4Cl/PBS. After washing in PBS, cells were permeabilized in 0.5%Triton/PBS for 5 min, washed again and incubated for 30 min in 0.5% gelatine/PBS blocking solution. Primary antibodies were applied for 1 h at RT diluted in PBS [anti-LAP2α 245-2 rabbit serum[23] 1:500, goat anti-lamin A/C N-18 (*Santa Cruz*) 1:100; rabbit anti-MyoD1 M-318 1:500; rabbit anti-NCL-Ki67p (*Novocastra*) 1:1000; mouse anti-embryonic myosin heavy chain F1.652 and mouse anti-myogenin F5D (*Developmental Studies Hybridoma Bank Iowa*) 1:10]. Samples were then washed in PBS and incubated with respective fluorochrome-coupled secondary antibodies for 1 h at RT (Texas Red, Cy5 (*Jackson Immuno Research*) or Alexa Fluor 488 (*Molecular Probes*)). After washing in PBS, nuclei were counterstained with Hoechst 33342 dye (1:50 000 dilution in dH_2O) for 10 min at RT and washed in dH_2O. Samples were air-dried and mounted with Mowiol.

2.2.6 Genotyping and semiquantitative PCR

Genotyping of *Lap2*$\alpha^{-/-}$, *Lap2*$\alpha^{Neo\text{-}fl/Neo\text{-}fl}$ and *Mdx* mice was done as previously described[32, 172]. In addition, the following primers were used for genotyping of Cre recombinase and Flipase expressing mice: Cre_sense CCAATTTACTGACCGTACACC; Cre_antisense TAATCGCCATCTTCCAGCAGG; Flp_sense GTGGATCGATCCTACCCCTTGCG; Flp_antisense GGTCCAACTGCAGCCCAAGCTTCC.

Primers used for semiquantitative analysis of PAX7 mRNA expression were Pax7_forw CCGTGTTTCTCATGGTTGTG and Pax7_rev GTGTTTGGCTTTCTTCTCGC[173]. PCR amplification was performed using Go Taq Green Master Mix (*Promega*) under following conditions: 95ºC 2'/58ºC 1'/72ºC 1'30''/2 $\times$ (95ºC 40''/56ºC 1'/72ºC 1')/ 28 $\times$ (95ºC 40''/54ºC 45''/72ºC 45'')/72ºC 10'/4ºC∞.

2.2.7 Sirius red collagen staining

Tissue cryo-sections were fixed in ice-cold methanol for 10 min, rinsed with PBS and incubated for 2 min in picro-sirius red solution (0.1% Sirius red F3B in saturated aqueous solution of picric acid). Samples were subsequently washed in two changes of acidified water (0.5% glacial acetic acid/H_2O), dehydrated in ethanol (3 changes) and, after clearing in xylene, mounted with Enthelan® (*Merck*).

2.2.8 *In vitro* muscle force measurement

The experiment was performed as previously described[174]. Shortly, mice were sacrificed by cervical dislocation and carefully de-skinned. Soleus and EDL muscles were exposed and their size was measured in the native position. Subsequently, cotton threads were placed on the opposing tendons near their bone-attachment sites and the entire muscles were isolated. The samples were kept in Krebs-Ringer solution (118.1 mM NaCl/3.4 mM KCl/2.5 mM $CaCl_2$/0.8 mM $MgSO_4$/1.2 mM KH_2PO_4/25.0 mM $NaHCO_3$/11.1 mM Glucose/dH_2O) during the experiment. Using the threads fixed to their tendons, muscles were suspended between 2 electrodes, respecting their native tension, and the force generated during externally-induced tetanic contraction was recorded.

2.3 *In vivo* systems

2.3.1 Acute cardiac stress

Acute cardiac stress was induced in mice by sustained infusion of β-adrenergic receptor agonist isoproterenol (*Isoproterenol hydrochloride, Sigma Aldrich*, *I 6504*) for 7 days. Mice were weighed and 15 mg/kg/day isoproterenol/0.5 mM ascorbic acid/PBS solution was prepared for each animal. Alzet® micro-osmotic pumps (model 1007D) were filled either with 100 µl of isoproterenol (ISO) or 0.5 mM ascorbic acid/PBS (sham) solutions according to manufacturers' instructions and kept in PBS for 3 hours before implantation. Mice were anaesthetized with 5% → 2% isofluorane/O_2 mixture and placed on heated pads. The inter-scapular region of the back was shaved and disinfected with 70% ethanol followed by Wundesin® (10 mg/ml polyvidone-iodide aqueous solution). A small incision was made in the skin between the scapulae and, by using a haemostat, a pocket was formed by spreading the subcutaneous connective tissue apart. The filled osmotic pump was inserted into the pocket with the flow moderator pointing away from the incision and the skin was closed with 2-3 silk (6/0) sutures. During the whole deep sleep and waking period mice were kept on heated pads with their vital functions carefully monitored. Echocardiography was performed 2 h before and 7 days after the pump implantation.

2.3.2 Ischemia-reperfusion injury model

The surgical procedure was performed as previously described[175]. Briefly, left anterior descending artery (LAD) was occluded for 30 min using a ligature made of 8-0 silk and 1 mm section of a PE-10 tube. Following 1 week of reperfusion, animals were sacrificed and hearts were harvested for histological analysis.

2.3.3 Acute skeletal muscle injury

Notexin, the venom produced by the snake *Notechis scutatus*, is a myotoxic presynaptic phospholipase A_2 which damages adult muscle fibers, but spares the satellite cells pool and is therefore used in muscle regeneration studies[176]. Acute mouse soleus muscle injury was induced in the following way:

Mice were anesthetized with isoflurane/O_2 mixture (5% starting and 2% maintenance concentration) and received 15 mg/kg piritramid analgesic injected subcutaneously. Outer sides of lower hind limbs were shaved and disinfected with Braunol® (polyvinylpyrrolidoneiodide aqueous solution). A small incision was made in the skin (~ 3 mm) and the underlying inter-muscular septum between anterior and posterior leg muscles. The soleus was exposed and 10 µl of 10 µg/ml notexin/saline solution was injected into the mid belly of the right muscle using a 30 G insulin syringe. Subsequently, the wound was closed with 7.0 nylon suture. The contra-lateral soleus

muscle served as a healthy control. Post-operative analgesia included Piritramid dissolved in drinking water (15 mg/kg body weight/15 ml water/day). Mice were sacrificed and tissue samples were taken at day 0, 2, 4, 8 and 12 to follow the muscle regeneration process.

3 Results & Discussion

3.1 Submitted manuscript I

LAP2α loss impairs heart function and stress response in mice

Ivana Gotic[1], Michael Leschnik[2], Ursula Kolm[2], Mato Markovic[2], Bernhard J. Haubner[3], Katarzyna Biadasiewicz[1], Bernhard Metzler[3], Colin L. Stewart[4] and Roland Foisner[1]*

[1]Max F. Perutz Laboratories, Department of Medical Biochemistry, Medical University of Vienna, Vienna 1030, Austria

[2]Clinic for Internal Medicine and Infectious Diseases, Department for Small Animals and Horses, Veterinary University of Vienna 1030, Austria

[3]Division of Cardiology, Medical University Innsbruck, Innsbruck 6020, Austria

[4]Institute of Medical Biology, Singapore 138648, Singapore

Short title: Impaired heart function in *Lap2α*$^{-/-}$ mice

***Correspondence to**:
Roland Foisner
Max F. Perutz Laboratories,
Medical University of Vienna, Dr. Bohr-Gasse 9/3,
A-1030 Vienna, Austria.
Email: roland.foisner@meduniwien.ac.at
Phone: +43-1-4277-61680, FAX: +43-1-4277-9616

Subject codes: [130] Animal models of human disease; [145] Genetically altered mice; [16] Myocardial cardiomyopathy disease

Abstract

Lamina-Associated Polypeptide 2α (LAP2α) is a nuclear protein in mammalian cells that associates with chromatin and interacts with a fraction of A-type lamins in the nuclear interior. Mutations in lamins and LAP2α lead to cardiac disorders in humans. To study the molecular mechanisms of the disease, we analyzed heart structure and function in recently described *Lap2α*$^{-/-}$ mice. Unlike conditional deletion of LAP2α in late embryonic striated muscle, its complete knockout caused systolic dysfunction in young mice, accompanied by higher susceptibility to fibrosis in old animals, as well as deregulation of major cardiac transcription factors GATA4 and MEF2c. Activation of compensatory pathways, including downregulation of ß-adrenergic receptor signaling, resulted in reduced responsiveness of the myocardium to chronic β-adrenergic stimulation and stalled progression of LAP2α-deficient hearts from hypertrophy towards cardiac failure. Dystrophin deficiency in an *Mdx* background resulted in a transient rescue of the *Lap2α*$^{-/-}$ phenotype. Our data suggest a novel role of LAP2α in maintenance of cardiac function under normal and stress conditions.

Keywords: Lamins, LAP2α, dilated cardiomyopathy, β-adrenergic receptors

Non-standard Abbreviations and Acronyms

ANF	Atrial Natriuretic Factor
β-AR	β-Adrenergic Receptor
BNP	Brain Natriuretic Peptide
CTGF	Connective Tissue Growth Factor
DCM	Dilated Cardiomyopathy
EF%	Ejection Fraction
EDVI	End-Diastolic Left Ventricular Volume Index
ESVI	End-Systolic Left Ventricular Volume Index
FS%	Fractional Shortening
HW/BW	Heart Weight/Body Weight
ISO	Isoproterenol
IVS	Interventricular Septum
LA	Left Atrium
LAP2α	Lamina-associated polypeptide 2α
LEM	LAP2-Emerin-MAN
LVD	Left Ventricular Diameter
LVPW	Left Ventricular Posterior Wall Thickness
MAPK	Mitogen Activated Protein Kinase
MEF2c	Myocyte Enhancer Factor
PI3-kinase	Phosphoinositide 3-kinase
SE	Standard Error
SRF	Serum Response Factor
STARS	Striated Muscle Activator of Rho Signalling
TGFβ	Transforming Growth Factor β
WT	Wild Type

Introduction

Dilated cardiomyopathy (DCM) is a primary myocardial disease characterized by dilation and impaired contraction of one or both heart ventricles. One of the genes most frequently involved in the evolution of DCM is *LMNA*, which encodes nuclear intermediate filament proteins lamin A and C[1]. Mutations in lamin A/C cause the most severe forms of DCM posing a high risk of heart failure in symptomatic patients[1]. Besides heart muscle disease, mutations in *LMNA* cause a variety of pathological conditions also in skeletal muscle, skin, nerve, bone and adipose tissue, known as laminopathies[2], emphasising the importance of the search for molecular disease mechanisms.

Recently, research on laminopathies has focused on lamin A/C-interacting proteins, whose mutations have been linked to a similar spectrum of human disorders[3]. One of the best studied lamin A/C-binding partners is lamina associated polypeptide 2α (LAP2α), an unusual splice variant of the mammalian *LAP2* gene[4]. All LAP2 proteins (α, β, γ, δ, ε, ζ) share a common chromatin-binding structural motif called the LEM (LAP2-Emerin-MAN1) domain at their N-terminus. The C-terminus of most LAP2 variants comprises a transmembrane region, which targets them to the inner nuclear membrane, where they serve mainly structural roles[5]. LAP2α lacks the common LAP2 transmembrane domain and possesses an additional chromatin-binding region at its C-terminal end, which mediates targeting to the nuclear interior[4]. In the nucleoplasm LAP2α specifically interacts with a fraction of lamin A/C proteins via its unique C-terminal tail[5, 6]. Together, LAP2α and lamin A/C influence various nuclear processes, such as epigenetic chromatin regulation, gene expression and signal transduction[7]. In particular, LAP2α-lamin A/C complexes have been found to control the balance between proliferation and differentiation of early progenitor cells in regenerative tissues by affecting the E2F/retinoblastoma pathway[8].

Interestingly, a mutation in LAP2α (c. 2068C>T, p. R690C), which lowers its binding affinity for lamin A/C *in vitro,* has also been linked to familial dilated cardiomyopathy[9]. As changes in both, LAP2α and lamin A/C, cause pathological heart conditions, we hypothesized that an intact LAP2α-lamin A/C complex may be necessary for proper cardiac function. Miss-localization or absence of one of the components would lead to disease.

Most *Lmna* transgenic mice generated so far show complex phenotypes, including various stages of heart failure[10, 11]. To see whether LAP2α is also important for normal cardiac output, we analyzed heart structure and function in previously generated *Lap2α*$^{-/-}$ mice[8]. Here we describe a new mouse model of cardiomyopathy and provide novel insights into mechanisms governing heart development and tissue homeostasis.

Materials and Methods

Mice. *Lap2α*$^{-/-}$ mice were kept on a mixed *Mus musculs* C57BL/6×129 genetic background[8]. Compound mutant *Lap2α*$^{-/-}$*Mdx* animals were obtained by crossing *Lap2α*$^{-/-}$ mice with the *Mdx* line[12]. Generation of conditional LAP2α knockout mice is described in Supplemental Figure 1. All histological and physiological analyses were done by observers blinded for the genotype as well as treatment of the animal. Mice aged 2 days were considered as newborn, 10 weeks as young and 10-12 months as old.
Mice were kept and handled in accordance with the procedures outlined in the Guide for the Care and Use of Laboratory Animals. Experiments were performed according to permissions from Austrian authorities.

Echocardiograpy. Mice were anesthetized with 5% isoflurane/O_2 and maintained on 2% mixture during the experiment. Trans-thoracic echocardiography was performed using Vivid Five/Vingmed-GE Technology/USA equipped with a 10-MHz linear transducer[13].

Gravimetric, histological and western blot analyses were performed according to standard procedures described in more detail in the online supplement. Data processing, including quantification of fibrosis in Picro-sirius red-stained samples, was done using Adobe Photoshop CS2.

Semi-quantitative and real time PCR. Total heart tissue RNA was isolated using TRIzol® reagent (Invitrogen) or RNeasy® Plus Micro Kit (Quiagen) and First Strand cDNA Synthesis Kit for RT-PCR (Roche) was used for cDNA synthesis according to manufacturers' instructions. cDNA was amplified using Go Taq Green Master Mix (Promega) in semig.-PCR and MESA GREEN qPCR MasterMix Plus for SYBR® Assay I dTTP (Eurogentec), together with MasterCycler ep realplex (Eppendorf), in quantitative PCR (qPCR) analyses. Images of ethidium bromide-stained agarose gels were documented using UVP Gel Doc-It TS Imaging System and processed by Adobe Photoshop CS2. qPCR data were normalized to endogenous HPRT levels and analyzed according to Pfaffl method[14]. The list of primers can be found in online supplement.

Isoproterenol-induced heart failure model. Mice anaesthesia and echocardiography before and after the experiment were performed as described above. Alzet mini-osmotic pumps (1007D), filled with 15mg/kg/day isoproterenol/PBS (Sigma Aldrich), were implanted according to manufacturers' instructions. 6 old male *Lap2α*$^{+/+}$ and 7 *Lap2α*$^{-/-}$ mice were infused with ISO and 2 littermate couples received only PBS (sham) for 7 days. At the end of the experiment animals were sacrificed for further analysis.

Statistical analysis. Data were analyzed either by paired Students't-test, one-way ANOVA or two-way ANOVA (followed by Boniferroni post hoc test for multiple comparisons) where appropriate

using Microsoft Excel XP. $P<0.05$ was considered significant. Data are presented as mean values ± standard error (SE) and n represents sample size.

Results

LAP2α deficient mice used in this study were generated by Cre recombinase-mediated excision of the LAP2α-specific exon 4 of the *Lap2* gene in the germline[8]. To confirm the absence of the gene product, we performed western blot, semi-quantitative PCR and immunofluorescence analysis of *Lap2α*$^{-/-}$ heart muscle tissue. LAP2α was neither detectable at mRNA, nor on protein level, while the expression, as well as localization of lamin A/C and other LAP2 isoforms were not significantly altered (Figure 1, Supplemental figure 2).

Absence of LAP2α causes ventricular systolic dysfunction in mice

The symptoms in LAP2α- and most lamin A/C-linked human cardiomyopathies appear mostly in adults[5, 9]. In mouse laminopathy models, however, heart defects develop in young animals and cause early mortality[10, 11]. As *Lap2α*$^{-/-}$ mice are grossly indistinguishable from their wild type (WT) littermates and have a normal life expectancy[8], we analyzed heart function in young, as well as old animals. Echocardiography in 10 weeks old *Lap2α*$^{-/-}$ mice revealed ventricular systolic dysfunction, characterized by significantly decreased left ventricular fractional shortening (FS%) and ejection fractions (EF%). Moreover, enlarged left atria (LA) in male LAP2α-deficient mice emphasized the defective cardiac phenotype, indicating a possible left ventricular and left atrial volume overload (Figure 2, Supplemental table 1). The FS% and EF% values remained similarly impaired in old *Lap2α*$^{-/-}$ male mice (FS of 30.39% ± 1.67 at the age of 10-12 months compared to 27.97% ± 1.38 in young animals), suggesting that the heart functional defect was not progressive. Interestingly, cardiac parameters in *Lap2α*$^{-/-}$ females appeared largely comparable to wild type at both ages (Supplemental table 1).

Old *Lap2α*$^{-/-}$ hearts are more susceptible to fibrosis

To see whether the functional heart defect in *Lap2α*$^{-/-}$ mice was accompanied by structural changes, we performed gravimetric and histological analyses. *Lap2α*$^{-/-}$ hearts had normal morphology and similar heart weight/body weight (HW/BW) indexes compared to WT littermates in newborn, young and old animals (data not shown). Furthermore, no overt histological pathologies were detectable in young *Lap2α*$^{-/-}$ mice (Figure 3A). Old *Lap2α*$^{-/-}$ hearts, however, showed high phenotypic variability in the degree of fibrosis, assessed by the extent of interstitial collagen deposition in the left ventricle. Out of 11 tested mice, 18% developed extensive subendocardial fibrosis of the left ventricle (Figure 3B and data not shown). In addition to fibrosis, one mouse presented regions of extremely thin, transparent myocardium which collapsed in the absence of internal blood pressure (Figure 3C). In contrast, wild type animals did not exhibit any signs of fibrosis at any age.

De-regulated expression of major cardiac transcription factors in LAP2α-deficient mice

In an attempt to identify molecular mechanisms leading to systolic dysfunction in *Lap2α*$^{-/-}$ mice, we analyzed the expression of several markers connected to myocardial remodelling. Two major

cardiac transcription factors, GATA4 and MEF2c, as well as their downstream targets, brain natriuretic peptide (BNP) and proteins involved in serum response factor (SRF)-mediated transcription of immediate early and muscle specific genes, Myocardin A and Striated Muscle Activator of Rho Signalling (STARS)[15-19], showed de-regulated expression patterns in *Lap2α*$^{-/-}$ mice (Figure 4A, B). Whereas MEF2c expression was repressed in newborn *Lap2α*$^{-/-}$ hearts and reached WT levels by the age of 10 weeks, GATA4, Myocardin A and STARS were down-regulated only in old hearts. In addition, consistent with the reported cooperative regulation of BNP expression by both GATA4 and MEF2c[19], BNP mRNA levels were significantly lower in LAP2α-deficient hearts compared to wild type at all ages (Figure 4A). The expression of other MEF2c and GATA4 targets, such as α- and β-myosin heavy chain and atrial natriuretic factor (*ANF)*[20] was not significantly changed in *Lap2α*$^{-/-}$ mice (data not shown). Our data show that loss of LAP2α affects the expression of GATA4 and MEF2C, as well as some of their downstream targets, which in turn may influence the expression of a plethora of genes involved in cardiovascular development and stress-induced hypertrophic growth.

Since old *Lap2α*$^{-/-}$ mice showed increased susceptibility to fibrosis, we analyzed the expression of know fibrotic markers in wild type and LAP2α-deficient hearts (Figure 4C). Interestingly, loss of LAP2α caused a downregulation of connective tissue growth factor (CTGF), an inducer of fibroblast proliferation and extracellular matrix synthesis[21], but affected only mildly the expression of its activator transforming growth factor β_2 (TGFβ_2). Altogether our data demonstrate that loss of LAP2α in mice leads to deregulated expression of genes involved in cardiac remodelling and fibrosis.

***Lap2α*$^{-/-}$ mice show a blunted response to chronic isoproterenol infusion**

GATA4 and MEF2c play important roles during cardiomyocyte hypertrophy[22, 23]. To see whether their deregulation in *Lap2α*$^{-/-}$ hearts affects the response to cardiac hypertrophic stimuli, we subjected *Lap2α*$^{-/-}$ mice to chronic infusion of the β-adrenergic agonist isoproterenol (ISO) for 7 days. To detect ISO-induced changes in heart function and structure, we performed echocardiography before and after the treatment, as well as gravimetric and histological analyses at the end of the experiment. As shown by the HW/BW indexes, ISO administration caused a similar degree of cardiac hypertrophy in *Lap2α*$^{+/+}$ and *Lap2α*$^{-/-}$ mice (Figure 5A), indicating that the hypertrophic growth response is not grossly affected by the loss of LAP2α. Similarly, the extent of subendocardial fibrosis caused by chronic ISO infusion[24] was similar in *Lap2α*$^{+/+}$ and *Lap2α*$^{-/-}$ mice (Supplemental figure 3).

In addition to hypertrophy, ISO treatment caused dilatation of left heart ventricles, as shown by echocardiography (Figure 5B, Supplemental table 2). In wild type animals, systolic and diastolic left ventricular diameters (LVD) and the corresponding ventricular volumes exhibited a significantly increase, indicating the progression from cardiac hypertrophy towards heart failure. In contrast, left ventricles of *Lap2α*$^{-/-}$ mice were already slightly enlarged at baseline and showed only a milder additional dilatation upon ISO treatment, reaching end point sizes similar to WT. HW/BW indexes and echocardiograpy parameters of sham (PBS) treated animals were not altered by the procedure

(Supplemental table 2). These data point to a blunted cardiac stress response in LAP2α-deficient mice.

FS values in treated animals were only slightly affected, showing that, in agreement with previous studies[24], chronic ISO infusion did not significantly impair left ventricular systolic function either in *Lap2α*$^{+/+}$ or *Lap2α*$^{-/-}$ mice (Figure 5B, Supplemental table 2). The preserved basal systolic function in ISO-induced cardiac hypertrophy has been associated with downregulation of β-adrenergic receptor (β-AR)-mediated inotropic responses[24]. An ISO-induced downregulation of β-AR has also been shown to cause a blunted reactivity to its subsequent re-administration[24]. Therefore, we questioned whether the reduced responsiveness of *Lap2α*$^{-/-}$ myocardium to ISO might also be a consequence of similar de-sensitization of the β-AR signalling pathway. To test this hypothesis, we analyzed the expression of β_2-AR in LAP2α-deficient and wild type mice at baseline, as well as after ISO treatment. As expected, *Lap2α*$^{-/-}$ hearts showed lower baseline expression levels of β_2-AR in young and old mice (Figure 5C). Importantly, the difference in relative β_2-AR mRNA levels in untreated LAP2α knockout versus wild type heart increased with age (Figure 5C), suggesting that the downregulation of β-AR signalling in *Lap2α*$^{-/-}$ mice is an aging-dependent phenomenon and may be a consequence of heart function impairment. ISO treatment caused an additional downregulation of β_2-AR mRNA in *Lap2α*$^{-/-}$ hearts, albeit not as extensive as in the wild type situation (~71% in WT vs. ~39% in *Lap2α*$^{-/-}$), resulting in comparable end-point expression levels in both genotypes (Figure 5C).

Development of β-AR-mediated hypertrophy is associated with the activation of the foetal cardiac transcriptional program[24], including the expression of embryonic transcription factors ANF and GATA4[25]. In accordance, ANF and GATA4 mRNA levels were upregulated in ISO-treated hearts of both *Lap2α*$^{+/+}$ and *Lap2α*$^{-/-}$ mice (Figure 5D). However, consistent with reduced ß-AR levels in old LAP2α-deficient mice, the increase in ISO-induced ANF expression was significantly lower in LAP2α-deficient myocardium than in wild type hearts. Relative GATA4 levels were also substantially lower in *Lap2α*$^{-/-}$ than in wild type hearts after ISO treatment, although the ISO-mediated increase of GATA4 expression was similar in both genotypes. Overall, these results suggest that loss of LAP2α affects cardiac-specific transcription and progression of ISO-induced hypertrophy.

Absence of dystrophin delays the onset of ventricular dysfunction in *Lap2α*$^{-/-}$/*Mdx* mice

Since baseline systolic dysfunction in *Lap2α*$^{-/-}$ mice was not progressive and did not affect their life span, we thought that the effect of LAP2α loss might be augmented in a cardiomyopathy background. Therefore, we crossed *Lap2α*$^{-/-}$ mice to *Mdx* mutants[12], which develop skeletal muscle dystrophy and DCM with advanced age due to the absence of dystrophin[26, 27].

The homozygous *Lap2α*$^{-/-}$/*Mdx* mutant animals were born according to Mendelian ratios and appeared grossly indistinguishable from their *Mdx* littermates. Unexpectedly, echocardiography in young *Lap2α*$^{-/-}$/*Mdx* mice showed normal heart function, with FS values similar to WT and *Mdx* (Figure 6, Supplemental table 3). This suggests that the absence of dystrophin can pre-sensitize the heart and turn on compensatory pathways leading to a transient rescue of the *Lap2α*$^{-/-}$

phenotype. Nevertheless, old compound mutant animals, as well as *Mdx* mice, developed similar heart function defects as *Lap2α*$^{-/-}$ mice (Figure 6, Supplemental table 1, 3).

LAP2α is dispensable in late-embryonic and adult cardiomyocytes

LAP2α is highly expressed in proliferating tissues[28, 29]. Since the vast majority of adult cardiomyocytes persists in a post-mitotic stage[30], and only low levels of LAP2α are present in nuclei throughout adult myocardium[9] (Figure 1), we thought that LAP2α may exhibit its major activity during early cardiomyocyte proliferation and myocardial growth, during which LAP2α expression is clearly detectable (Supplemental figure 4). To address this question, we generated conditional knockout mice by crossing *Lap2α*$^{Neo\text{-}fl/Neo\text{-}fl}$ (see Materials and Methods and Supplemental figure 1) animals to mice expressing Cre recombinase under the control of striated muscle-specific muscle creatine kinase (*Mck*) promoter[31]. In this system, the expression of Cre recombinase and the consequent deletion of LAP2α are turned on in heart and skeletal muscle during late stages of mouse embryonic development and striated muscle differentiation. *Lap2α*$^{Neo\text{-}fl/Neo\text{-}fl}$*/Mck-Cre*$^{+}$ mice were born at Mendelian ratios and did not demonstrate any overt phenotype. LAP2α mRNA and protein levels were significantly reduced in *Lap2α*$^{Neo\text{-}fl/Neo\text{-}fl}$*/Mck-Cre*$^{+}$ hearts, indicating an efficient recombination in the myocardium (Figure 7A). In contrast, other tissues like spleen, which do not express MCK[32], had normal levels of LAP2α (unpublished data). Echocardiography in *Lap2α*$^{Neo\text{-}fl/Neo\text{-}fl}$*/Mck-Cre*$^{+}$ mice showed normal heart function (Figure 7B, Supplemental table 4) and histological and morphometric analyses did not reveal any pathological heart phenotype (Figure 7C and data not shown). The expression levels of MEF2c and GATA4 mRNA were similar in *Lap2α*$^{Neo\text{-}fl/Neo\text{-}fl}$/*Mck-Cre*$^{+}$ and *Lap2α*$^{+/+}$/*Mck-Cre*$^{+}$ hearts (data not shown). Thus, LAP2α expression in late-embryonic and adult cardiomyocytes is dispensable for normal heart function, but may be important during earlier stages of heart development (before E13.5 when *Mck* promoter becomes active) or in non-striated muscle cells in the heart.

Discussion

In this study we describe a new mouse model of cardiomyopathy caused by the absence of LAP2α, a major binding partner of lamin A/C in the nucleoplasm[6]. Together with previous studies linking lamin A/C and the lamin-binding inner nuclear membrane proteins, emerin and nesprin to congenital heart disorders[1, 3, 9, 33], our data suggest a major role of A-type lamin complexes in normal heart function.

A mutation in the α-specific exon 4 of the human *LAP2* gene has previously been linked to familial dilated cardiomyopathy[9]. Here we show that the absence of LAP2α in mice also leads to a heart disease. Interestingly, only male *Lap2α*$^{-/-}$ mice showed a heart defect, whereas female animals exhibited normal cardiac function, implicating gender specific factors in the development of the disease. Similar gender-related phenotype variations were described in other cardiomyopathy mouse models[34], including mice carrying the H222P-*Lmna* mutation[35]. Although the exact background of this phenomenon is still unknown, gender based differences in cardiac dysfunction were linked to the activity of steroid hormones[36]. At present no data about the risk of heart failure in male versus female carriers of LAP2α mutations in humans are available.

In an attempt to disclose the molecular pathway of the disease, we analyzed the expression of factors involved in development and remodelling of the myocardium. *Lap2α*$^{-/-}$ mice showed miss-regulated expression of major heart transcription factors, MEF2C[15] and GATA4[18], as well as some of their downstream targets, at different life stages. Both GATA4 and MEF2C play essential roles in embryonic heart development and hypertrophic growth[15, 18, 22, 23]. However, while systolic dysfunction was apparent already in young *Lap2α*$^{-/-}$ mice, *Gata4* levels were decreased only in old *Lap2α*$^{-/-}$ mice, suggesting that the deregulation may be a consequence rather than the cause of the disease. Despite lower *Gata4* expression levels, *Lap2α*$^{-/-}$ hearts were able to undergo hypertrophic growth. In support of our data, mice with reduced *Gata4* levels (G4D mice) show a similar heart function defect at baseline, as well as the ability to grow under hypertrophic conditions[22]. In contrast to *Lap2α*$^{-/-}$ mice, which are at higher risk of heart fibrosis at baseline, G4D mice develop fibrosis only after pressure overload as a consequence of increased stress-induced cardiomyocyte death[22]. This discrepancy could be in part explained by differences in the origin, time course and extent of *Gata4* down-regulation in the two strains (50% reduction of GATA4 in G4D mice versus 20% in *Lap2α*$^{-/-}$ animals).

GATA4 and MEF2c synergistically activate the expression of BNP[19], a cardiac hormone involved in the regulation of blood pressure and fluid-electrolyte balance, which also plays a role in the inhibition of cardiac fibroblast proliferation and extracellular matrix production[37]. In line with GATA4 and MEF2c deregulation, we also observed a decrease in BNP levels in *Lap2α*$^{-/-}$ hearts. Interestingly, BNP-deficient mice (*Nppb*$^{-/-}$), which exhibit normal heart morphology and hypertrophic growth after ventricular pressure overload, also show higher incidence of fibrosis (~50%) in male vs. female mice at the age of 15 weeks[38].

The blunted response of LAP2α-deficient hearts to chronic isoproterenol infusion points to the existence of compensatory pathways activated in response to changes in cardiac function in

Lap2α$^{-/-}$ mice. The attenuated hypertrophic growth and lack of fibrosis observed in β-AR knockout mice after pressure overload[39] indicate that the downregulation of β-AR signalling found in *Lap2α*$^{-/-}$ hearts might be a part of this process.

The variability in the extent of fibrosis at baseline, as well as after chronic ISO infusion, might be explained by the observed de-regulated expression of pro- and anti-fibrotic factors in *Lap2α*$^{-/-}$ mice.

Since LAP2α is highly expressed in proliferating tissues and only weakly in post-mitotic tissues[9, 28, 29], such as heart muscle[30], we hypothesized that LAP2α might be required during cardiac development and/or postnatal myocardial remodelling, mediated by putative cardiac stem cells[40].Therefore, we generated conditional knockout mice which lose LAP2α during later stages of embryonic development and adult striated muscle differentiation[31]. *Lap2α*$^{Neo\text{-}fl/Neo\text{-}fl}$*/Mck-Cre*$^{+}$ mice showed normal heart function and normal levels of GATA4 and MEF2c, suggesting that the defect in complete knockout mice might arise in early embryonic development and at early stages of muscle differentiation, before *Mck* promoter becomes active, and/or it might be a consequence of LAP2α loss from heart stem- and non-striated muscle cells.

We have previously shown that LAP2α retains a sub-fraction of the nuclear lamin A/C pool inside the nucleoplasm in proliferating skin fibroblasts and intestinal cells[8]. In contrast, nucleoplasmic lamin A/C is lost in non-dividing differentiated cells[8], implicating the nucleoplasmic pool of lamin A/C in regulation of the transition from proliferating to the differentiated state. The nuclear localization of lamin A/C has also been shown to change in cardiomyocytes during aging and development from mainly nucleoplasmic to peripheral[41]. The elongated shape and different orientation of cardiomyocyte nuclei within heart tissue, however, precluded the detection of potential changes in lamin A/C localization in LAP2α-deficient tissue. In view of the lack of heart defects in muscle-specific conditional LAP2α knock out mice, there is a possibility that a potential mislocalization of lamin A/C in LAP2α-deficient cardiomyocyte precursor or non-striated muscle cells may be the primary cause of the *Lap2α*$^{-/-}$ cardiac defect. Alternatively lack of LAP2α may change the function, rather than localization of lamin A/C, such as binding to epigenetic modifiers and components of different signalling cascades[7, 42], which in turn may lead to cardiomyopathy. This model is consistent with previous reports that have linked lamin A/C-related cardiomyopathies to changes in signalling pathways, such as TGFβ, PI3-kinase and MAPK[43], which influence MEF2c and GATA4 expression during development and hypertrophic growth[44, 45] and are also affected by β-AR signalling[24].

In summary, we show that the absence of LAP2α causes a baseline ventricular systolic dysfunction in male mice and activates compensatory pathways that prevent further decline of heart function under chronic stress conditions. The origins of these defects, which could lie in impaired proliferation and/or differentiation of early embryonic cardiomyocytes, resident cardiac stem cells or non-muscle cardiac tissue, remain to be discovered.

Funding

This work was supported by grants from the Austrian Science Research Fund [grant number FWF P17871] and the EURO-Laminopathies research project of the European Commission [Contract LSHM-CT-2005-018690] to RF.

Acknowledgements

We wish to thank Ronald C. Kahn, Department of Medicine, Joslin Diabetes Center, Boston MA for kindly providing MCK Cre mice and Reginald Bittner, Medical University Vienna for *Mdx* mice.

Conflicts of interest

None.

References

1. Sylvius N, Tesson F. Lamin A/C and cardiac diseases. *Curr Opin Cardiol.* 2006;21(3):159-165.

2. Capell BC, Collins FS. Human laminopathies: nuclei gone genetically awry. *Nat Rev Genet.* 2006;7(12):940-952.

3. Worman HJ, Bonne G. "Laminopathies": a wide spectrum of human diseases. *Exp Cell Res.* 2007;313(10):2121-2133.

4. Vlcek S, Korbei B, Foisner R. Distinct functions of the unique C terminus of LAP2alpha in cell proliferation and nuclear assembly. *J Biol Chem.* 2002;277(21):18898-18907.

5. Schirmer EC, Foisner R. Proteins that associate with lamins: many faces, many functions. *Exp Cell Res.* 2007;313(10):2167-2179.

6. Dechat T, Korbei B, Vaughan OA, Vlcek S, Hutchison CJ, Foisner R. Lamina-associated polypeptide 2alpha binds intranuclear A-type lamins. *J Cell Sci.* 2000;113 Pt 19:3473-3484.

7. Gruenbaum Y, Margalit A, Goldman RD, Shumaker DK, Wilson KL. The nuclear lamina comes of age. *Nat Rev Mol Cell Biol.* 2005;6(1):21-31.

8. Naetar N KB, Kozlov S, Kerenyi MA, Dorner D, Kral I, Gotic I, Fuchs P, Cohen T, Bittner R, Stewart CL, Foisner R. Loss of nucleoplasmic LAP2alpha-lamin A complexes causes erythroid and epidermal progenitor hyperproliferation. *Nature Cell Biology.* 2008.

9. Taylor MR, Slavov D, Gajewski A, Vlcek S, Ku L, Fain PR, Carniel E, Di Lenarda A, Sinagra G, Boucek MM, Cavanaugh J, Graw SL, Ruegg P, Feiger J, Zhu X, Ferguson DA, Bristow MR, Gotzmann J, Foisner R, Mestroni L. Thymopoietin (lamina-associated polypeptide 2) gene mutation associated with dilated cardiomyopathy. *Hum Mutat.* 2005;26(6):566-574.

10. Nikolova V, Leimena C, McMahon AC, Tan JC, Chandar S, Jogia D, Kesteven SH, Michalicek J, Otway R, Verheyen F, Rainer S, Stewart CL, Martin D, Feneley MP, Fatkin D. Defects in nuclear structure and function promote dilated cardiomyopathy in lamin A/C-deficient mice. *J Clin Invest.* 2004;113(3):357-369.

11. Stewart CL, Kozlov S, Fong LG, Young SG. Mouse models of the laminopathies. *Exp Cell Res.* 2007;313(10):2144-2156.

12. Bulfield G, Siller WG, Wight PA, Moore KJ. X chromosome-linked muscular dystrophy (mdx) in the mouse. *Proc Natl Acad Sci U S A.* 1984;81(4):1189-1192.

13. Kuba K, Zhang L, Imai Y, Arab S, Chen M, Maekawa Y, Leschnik M, Leibbrandt A, Markovic M, Schwaighofer J, Beetz N, Musialek R, Neely GG, Komnenovic V, Kolm U, Metzler B, Ricci R, Hara H, Meixner A, Nghiem M, Chen X, Dawood F, Wong KM, Sarao R, Cukerman E, Kimura A, Hein L, Thalhammer J, Liu PP, Penninger JM. Impaired heart contractility in Apelin gene-deficient mice associated with aging and pressure overload. *Circ Res.* 2007;101(4):e32-42.

14. Pfaffl MW. A new mathematical model for relative quantification in real-time RT-PCR. *Nucleic Acids Res.* 2001;29(9):e45.

15. Black BL. Transcriptional pathways in second heart field development. *Semin Cell Dev Biol.* 2007;18(1):67-76.

16. Kuwahara K, Teg Pipes GC, McAnally J, Richardson JA, Hill JA, Bassel-Duby R, Olson EN. Modulation of adverse cardiac remodeling by STARS, a mediator of MEF2 signaling and SRF activity. *J Clin Invest.* 2007;117(5):1324-1334.

17. Pipes GC, Creemers EE, Olson EN. The myocardin family of transcriptional coactivators: versatile regulators of cell growth, migration, and myogenesis. *Genes Dev.* 2006;20(12):1545-1556.

18. Xin M, Davis CA, Molkentin JD, Lien CL, Duncan SA, Richardson JA, Olson EN. A threshold of GATA4 and GATA6 expression is required for cardiovascular development. *Proc Natl Acad Sci U S A.* 2006;103(30):11189-11194.

19. Morin S, Charron F, Robitaille L, Nemer M. GATA-dependent recruitment of MEF2 proteins to target promoters. *Embo J.* 2000;19(9):2046-2055.

20. Pikkarainen S, Tokola H, Kerkela R, Ruskoaho H. GATA transcription factors in the developing and adult heart. *Cardiovasc Res.* 2004;63(2):196-207.

21. Chen MM, Lam A, Abraham JA, Schreiner GF, Joly AH. CTGF expression is induced by TGF- beta in cardiac fibroblasts and cardiac myocytes: a potential role in heart fibrosis. *J Mol Cell Cardiol.* 2000;32(10):1805-1819.

22. Bisping E, Ikeda S, Kong SW, Tarnavski O, Bodyak N, McMullen JR, Rajagopal S, Son JK, Ma Q, Springer Z, Kang PM, Izumo S, Pu WT. Gata4 is required for maintenance of postnatal cardiac function and protection from pressure overload-induced heart failure. *Proc Natl Acad Sci U S A.* 2006;103(39):14471-14476.

23. van Oort RJ, van Rooij E, Bourajjaj M, Schimmel J, Jansen MA, van der Nagel R, Doevendans PA, Schneider MD, van Echteld CJ, De Windt LJ. MEF2 activates a genetic program promoting chamber dilation and contractile dysfunction in calcineurin-induced heart failure. *Circulation.* 2006;114(4):298-308.

24. Osadchii OE. Cardiac hypertrophy induced by sustained beta-adrenoreceptor activation: pathophysiological aspects. *Heart Fail Rev.* 2007;12(1):66-86.

25. Pikkarainen S, Tokola H, Majalahti-Palviainen T, Kerkela R, Hautala N, Bhalla SS, Charron F, Nemer M, Vuolteenaho O, Ruskoaho H. GATA-4 is a nuclear mediator of mechanical stretch-activated hypertrophic program. *J Biol Chem.* 2003;278(26):23807-23816.

26. Quinlan JG, Hahn HS, Wong BL, Lorenz JN, Wenisch AS, Levin LS. Evolution of the mdx mouse cardiomyopathy: physiological and morphological findings. *Neuromuscul Disord.* 2004;14(8-9):491-496.

27. Sicinski P, Geng Y, Ryder-Cook AS, Barnard EA, Darlison MG, Barnard PJ. The molecular basis of muscular dystrophy in the mdx mouse: a point mutation. *Science.* 1989;244(4912):1578-1580.

28. Parise P, Finocchiaro G, Masciadri B, Quarto M, Francois S, Mancuso F, Muller H. Lap2alpha expression is controlled by E2F and deregulated in various human tumors. *Cell Cycle.* 2006;5(12):1331-1341.

29. Ishijima Y, Toda T, Matsushita H, Yoshida M, Kimura N. Expression of thymopoietin beta/lamina-associated polypeptide 2 (TP beta/LAP2) and its family proteins as revealed by specific antibody induced against recombinant human thymopoietin. *Biochem Biophys Res Commun.* 1996;226(2):431-438.

30. MacLellan WR, Schneider MD. Genetic dissection of cardiac growth control pathways. *Annu Rev Physiol.* 2000;62:289-319.

31. Bruning JC, Michael MD, Winnay JN, Hayashi T, Horsch D, Accili D, Goodyear LJ, Kahn CR. A muscle-specific insulin receptor knockout exhibits features of the metabolic syndrome of NIDDM without altering glucose tolerance. *Mol Cell.* 1998;2(5):559-569.

32. Lyons GE, Muhlebach S, Moser A, Masood R, Paterson BM, Buckingham ME, Perriard JC. Developmental regulation of creatine kinase gene expression by myogenic factors in embryonic mouse and chick skeletal muscle. *Development.* 1991;113(3):1017-1029.

33. Zhang Q, Bethmann C, Worth NF, Davies JD, Wasner C, Feuer A, Ragnauth CD, Yi Q, Mellad JA, Warren DT, Wheeler MA, Ellis JA, Skepper JN, Vorgerd M, Schlotter-Weigel B, Weissberg PL, Roberts RG, Wehnert M, Shanahan CM. Nesprin-1 and -2 are involved in the pathogenesis of Emery Dreifuss muscular dystrophy and are critical for nuclear envelope integrity. *Hum Mol Genet.* 2007;16(23):2816-2833.

34. Du XJ. Gender modulates cardiac phenotype development in genetically modified mice. *Cardiovasc Res.* 2004;63(3):510-519.

35. Arimura T, Helbling-Leclerc A, Massart C, Varnous S, Niel F, Lacene E, Fromes Y, Toussaint M, Mura AM, Keller DI, Amthor H, Isnard R, Malissen M, Schwartz K, Bonne G. Mouse model carrying H222P-Lmna mutation develops muscular dystrophy and dilated cardiomyopathy similar to human striated muscle laminopathies. *Hum Mol Genet.* 2005;14(1):155-169.

36. Murphy E, Steenbergen C. Gender-based differences in mechanisms of protection in myocardial ischemia-reperfusion injury. *Cardiovasc Res.* 2007;75(3):478-486.

37. Kapoun AM, Liang F, O'Young G, Damm DL, Quon D, White RT, Munson K, Lam A, Schreiner GF, Protter AA. B-type natriuretic peptide exerts broad functional opposition to transforming growth factor-beta in primary human cardiac fibroblasts: fibrosis, myofibroblast conversion, proliferation, and inflammation. *Circ Res.* 2004;94(4):453-461.

38. Tamura N, Ogawa Y, Chusho H, Nakamura K, Nakao K, Suda M, Kasahara M, Hashimoto R, Katsuura G, Mukoyama M, Itoh H, Saito Y, Tanaka I, Otani H, Katsuki M. Cardiac fibrosis in mice lacking brain natriuretic peptide. *Proc Natl Acad Sci U S A.* 2000;97(8):4239-4244.

39. Kiriazis H, Wang K, Xu Q, Gao XM, Ming Z, Su Y, Moore XL, Lambert G, Gibbs ME, Dart AM, Du XJ. Knockout of beta(1)- and beta(2)-adrenoceptors attenuates pressure overload-induced cardiac hypertrophy and fibrosis. *Br J Pharmacol.* 2008;153(4):684-692.

40. Segers VF, Lee RT. Stem-cell therapy for cardiac disease. *Nature.* 2008;451(7181):937-942.

41. Afilalo J, Sebag IA, Chalifour LE, Rivas D, Akter R, Sharma K, Duque G. Age-related changes in lamin A/C expression in cardiomyocytes. *Am J Physiol Heart Circ Physiol.* 2007;293(3):H1451-1456.

42. Dechat T, Pfleghaar K, Sengupta K, Shimi T, Shumaker DK, Solimando L, Goldman RD. Nuclear lamins: major factors in the structural organization and function of the nucleus and chromatin. *Genes Dev.* 2008;22(7):832-853.

43. Marmiroli S, Bertacchini J, Beretti F, Cenni V, Guida M, De Pol A, Maraldi NM, Lattanzi G. A-type lamins and signaling: The PI 3-kinase/Akt pathway moves forward. *J Cell Physiol.* 2009.

44. Kerkela R, Pikkarainen S, Majalahti-Palviainen T, Tokola H, Ruskoaho H. Distinct roles of mitogen-activated protein kinase pathways in GATA-4 transcription factor-mediated regulation of B-type natriuretic peptide gene. *J Biol Chem.* 2002;277(16):13752-13760.

45. Potthoff MJ, Olson EN. MEF2: a central regulator of diverse developmental programs. *Development.* 2007;134(23):4131-4140.

Figure legends

Figure 1. LAP2α is absent from heart muscle tissue of *Lap2α*$^{-/-}$ mice. **A)** Immunofluorescence analysis of *Lap2α*$^{+/+}$ and *Lap2α*$^{-/-}$ heart tissue. **B)** LAP2α mRNA and protein are absent from heart muscle tissue of *Lap2α*$^{-/-}$ mice, while the expression of lamin A/C and alternative LAP2 splice variants remains unaltered. (Western blot and semiq.-RT-PCR analyses. Samples were normalized for endogenous γ-tubulin and GAPDH content respectively).

Figure 2. Loss of LAP2α impairs heart function in mice. Echocardiography data show left ventricular systolic dysfunction in young (10 weeks) and old male *Lap2α*$^{-/-}$ mice (10-12 months). (FS – fractional shortening; LA – left atrium diameter, *p<0.05 ANOVA, values are means ± SE).

Figure 3. Old *Lap2α*$^{-/-}$ hearts are more susceptible to fibrosis. **A)** Young *Lap2α*$^{-/-}$ myocardium is histologically indistinguishable from the wild type, whereas **B)** 18% of the old *Lap2α*$^{-/-}$ hearts shows disperse fibrotic foci (upper panels haematoxylin & eosin, lower panels Picro-sirius red stained heart sections). **C)** Thinning of the old *Lap2α*$^{-/-}$ myocardium – arrows mark the transparent fibrotic regions of the heart.

Figure 4. Deregulated expression of major cardiac transcription factors in LAP2α-deficient mice. **A)** MEF2c and GATA4, as well as their downstream targets BNP and Myocardin A (MYOCA), are downregulated on mRNA level at specific stages in *Lap2α*$^{-/-}$ mice. **B)** STARS mRNA levels are lower only in old LAP2α-deficient hearts. **C)** Old *Lap2α*$^{-/-}$ mice exhibit a decrease in CTGF expression and normal TGFβ$_2$ mRNA content. qPCR and semiq.-PCR analyses of heart tissue. n = 4 – 5 littermate pairs of each age. Samples were normalized for endogenous HPRT mRNA levels in qPCR according to Pfaffl method[14], and GAPDH in semiq-PCR. Each knockout (KO) sample was compared to its respective wild type (WT) littermate sample. Data are presented as average WT/KO expression ratios ± SE. *p<0.05, ANOVA.

Figure 5. *Lap2α*$^{-/-}$ mice show a blunted response to chronic isoproterenol infusion. **A)** *Lap2α*$^{+/+}$ and *Lap2α*$^{-/-}$ exhibit a similar increase in heart weight/body weight (HW/BW) index after 7 days of ISO treatment. (*p<0.05 ANOVA). **B)** Echocardiography reveals the absence of significant left ventricular chamber dilatation in *Lap2α*$^{-/-}$ mice and a preserved basal systolic function in both genotypes. (LVDd/s – left ventricular diameter in diastole/systole; ESVI – end-systolic left ventricular volume; EDVI – end-diastolic left ventricular volume). Data were analysed using Students' paired t-test (comparisons within one genotype before and after the treatment), one way-ANOVA (comparisons between the two genotypes). (a) p<0.05, (b) p = 0.05. **C)** Relative baseline mRNA levels of β$_2$-AR are lower in *Lap2α*$^{-/-}$ hearts compared to wild type, whereas ISO treatment causes its downregulation in both genotypes. **D)** ISO-induced increase in expression of foetal and pro-fibrotic genes is diminished in the absence of LAP2α. (qPCR analyses of heart tissue, n = 5 ISO-treated + 4 – 5 untreated littermate pairs of each age; ANOVA, p<0.05 (c) WT vs. KO of the

respective age (mean ± SE), (d) WT baseline vs. WT ISO-treated and (e) KO baseline vs. KO ISO-treated animals).

Figure 6. Absence of dystrophin delays the onset of ventricular dysfunction in *Lap2α*$^{-/-}$*/Mdx* mice. FS values in young *Lap2α*$^{-/-}$*/Mdx* mice are higher compared to *Lap2α*$^{-/-}$ animals, whereas old mice of both genotypes show similar systolic dysfunction (ANOVA; $p<0.05$ for (a) WT vs. KO, (b) WT vs. *Mdx* and (c) WT vs. *Lap2α*$^{-/-}$*/Mdx* mice).

Figure 7. LAP2α is dispensable in late-embryonic and adult cardiomyocytes. **A)** Reduced LAP2α mRNA and protein levels in *Lap2α*$^{Neo\text{-}fl/Neo\text{-}fl}$*/Mck-Cre*$^{+}$ vs. *Lap2α*$^{+/+}$*/Mck-Cre*$^{+}$ heart tissue (samples were normalized to GAPDH in semiq PCR and to γ-tubulin in western blot analysis). **B)** Normal FS values in young *Lap2α*$^{Neo\text{-}fl/Neo\text{-}fl}$*/Mck-Cre*$^{+}$ mice ($p>0.05$, ANOVA). **C)** Normal heart structure in conditional knockout mice.

Figure 1

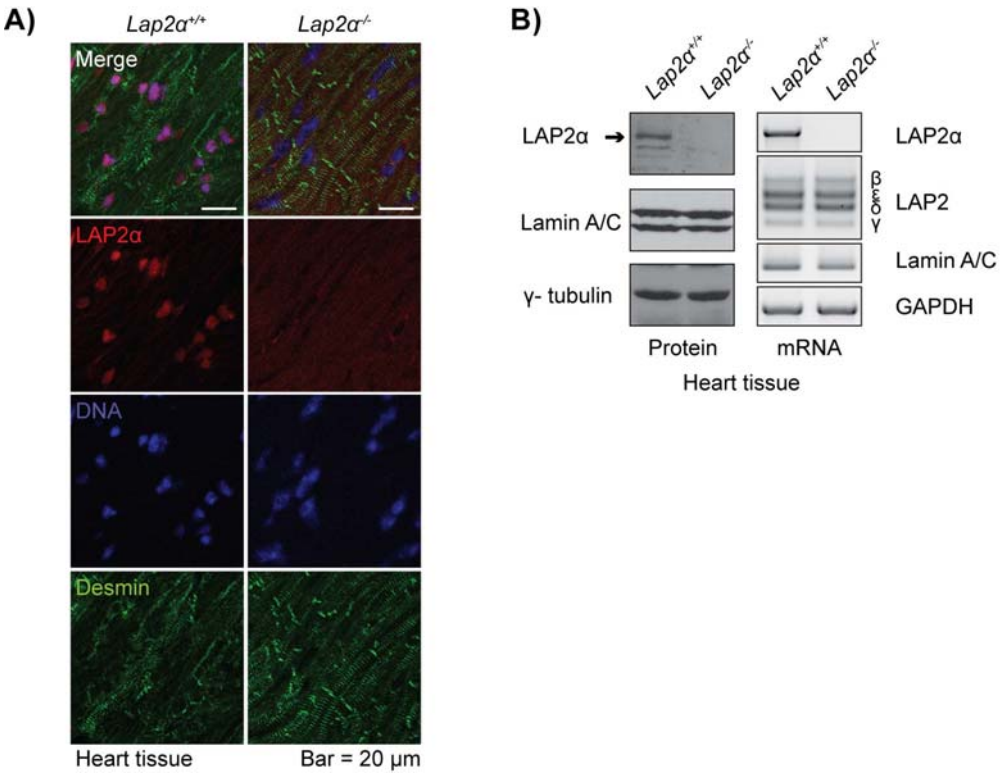
A)
Lap2α+/+
Lap2α-/-
Merge
LAP2α
DNA
Desmin
Heart tissue
Bar = 20 µm
B)
Lap2α+/+
Lap2α-/-
Lap2α+/+
Lap2α-/-
LAP2α
Lamin A/C
γ- tubulin
LAP2α
β
ε
δ
γ
LAP2
Lamin A/C
GAPDH
Protein
mRNA
Heart tissue

Figure 2

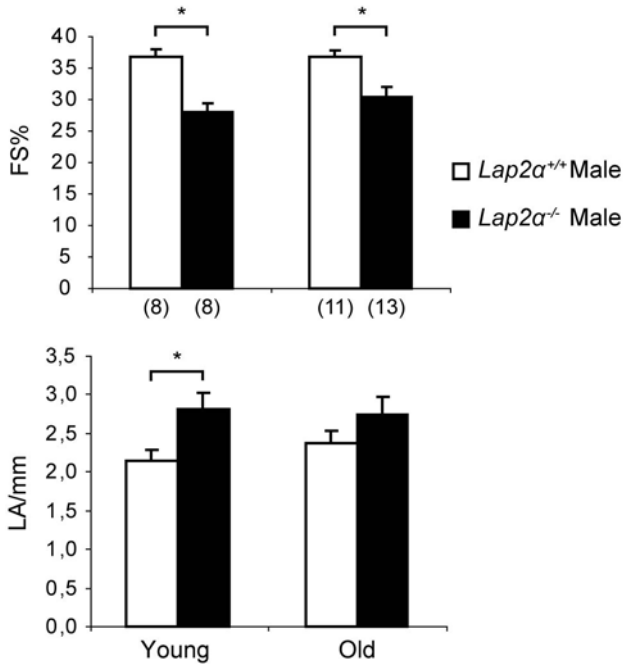
FS%
40
35
30
25
20
15
10
5
0
*
*
(8) (8) (11) (13)
Lap2α+/+ Male
Lap2α-/- Male
LA/mm
3,5
3,0
2,5
2,0
1,5
1,0
0,5
0,0
*
Young
Old

Figure 3

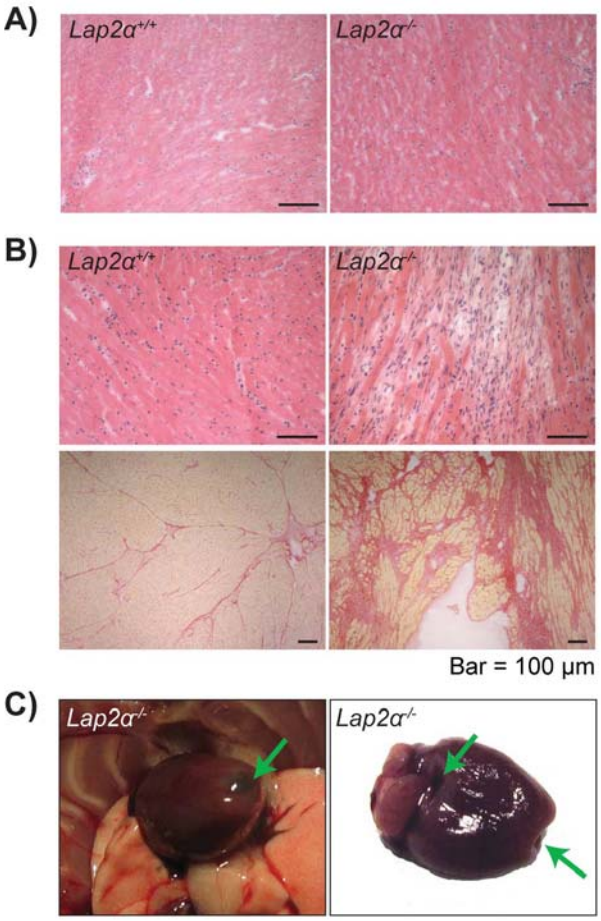

Figure 4

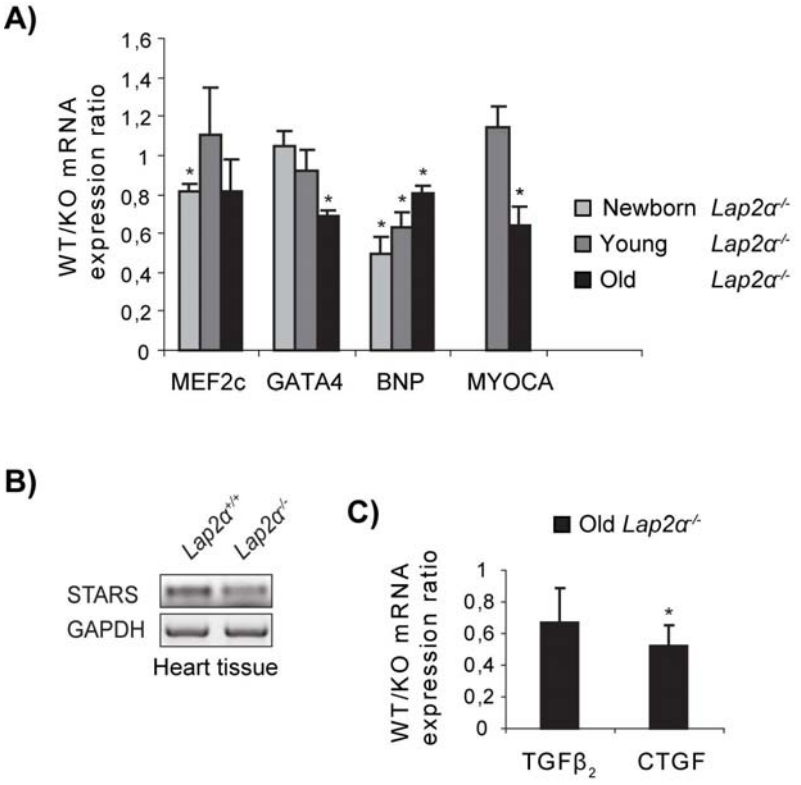
A)
WT/KO mRNA expression ratio
1,6
1,4
1,2
1
0,8
0,6
0,4
0,2
0
MEF2c
GATA4
BNP
MYOCA
Newborn Lap2α-/-
Young Lap2α-/-
Old Lap2α-/-
B)
Lap2α+/+
Lap2α-/-
STARS
GAPDH
Heart tissue
C)
Old Lap2α-/-
WT/KO mRNA expression ratio
1
0,8
0,6
0,4
0,2
0
TGFβ2
CTGF

Figure 5

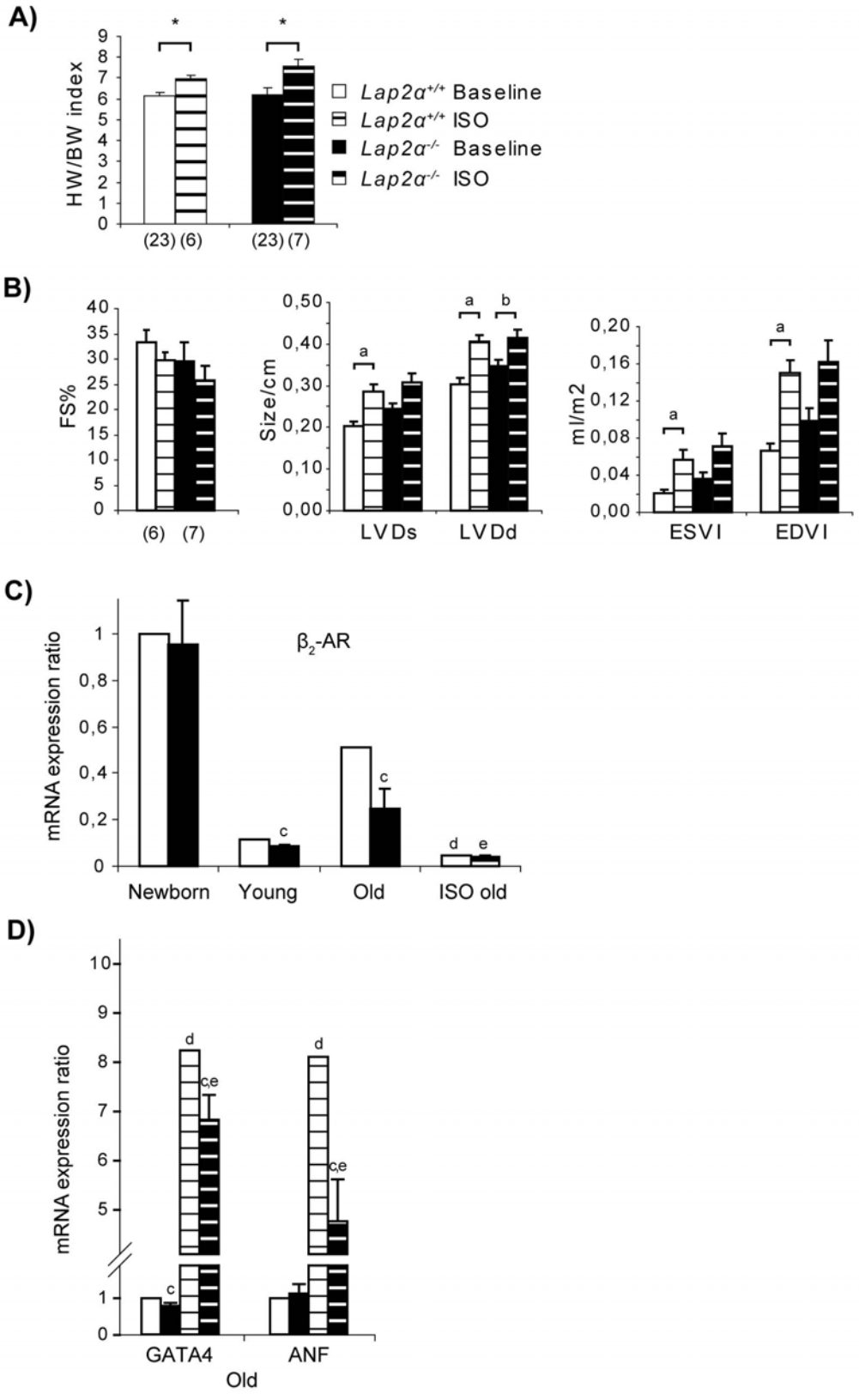
A)
HW/BW index
Lap2α+/+ Baseline
Lap2α+/+ ISO
Lap2α-/- Baseline
Lap2α-/- ISO
(23) (6)
(23) (7)
B)
FS%
(6) (7)
Size/cm
LVDs
LVDd
ml/m2
ESVI
EDVI
C)
mRNA expression ratio
β2-AR
Newborn
Young
Old
ISO old
D)
mRNA expression ratio
GATA4
ANF
Old

Figure 6

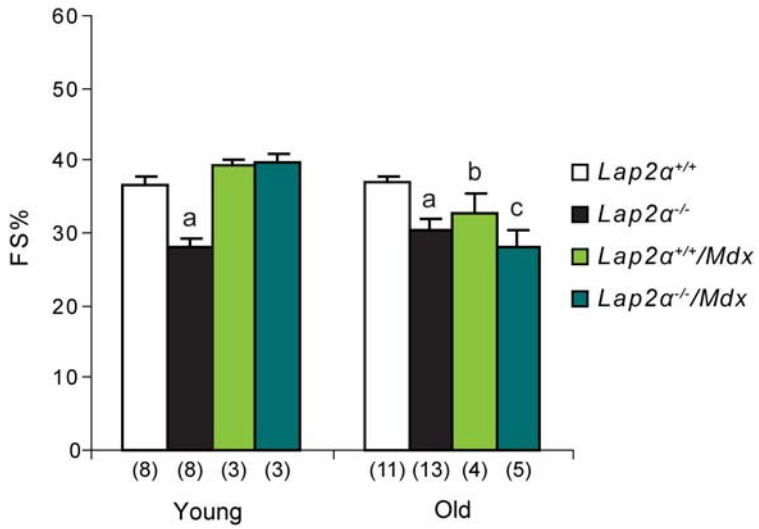
60
50
40
30
20
10
0
FS%
a
a
b
c
(8) (8) (3) (3)
(11) (13) (4) (5)
Young
Old
Lap2α+/+
Lap2α-/-
Lap2α+/+/Mdx
Lap2α-/-/Mdx

Figure 7

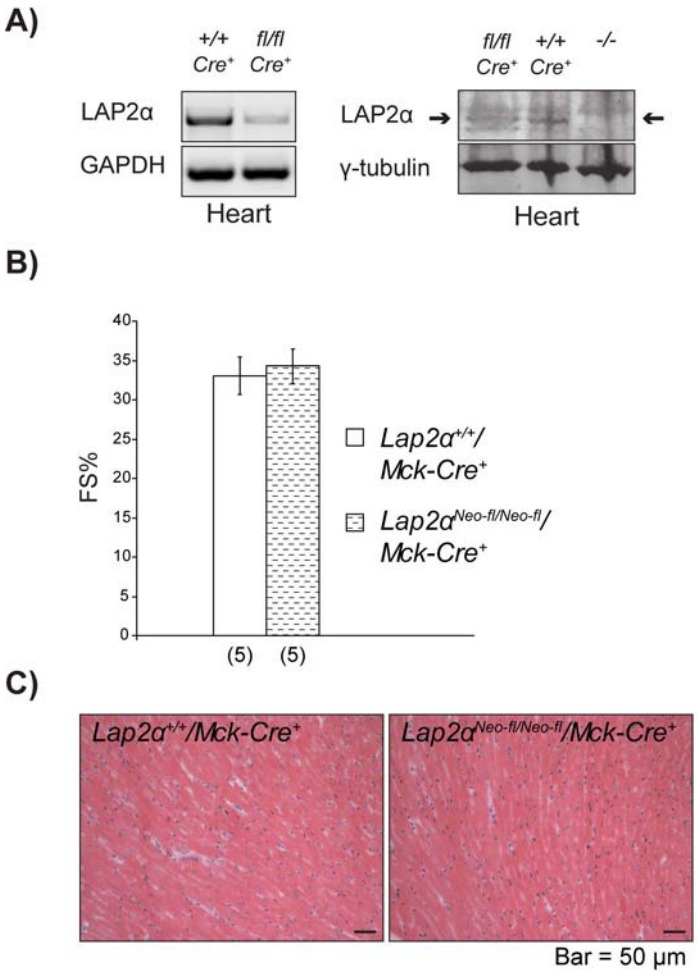
A)
+/+ Cre+
fl/fl Cre+
LAP2α
GAPDH
Heart
fl/fl Cre+
+/+ Cre+
-/-
LAP2α
γ-tubulin
Heart
B)
FS%
40
35
30
25
20
15
10
5
0
(5)
(5)
Lap2α+/+/ Mck-Cre+
Lap2αNeo-fl/Neo-fl/ Mck-Cre+
C)
Lap2α+/+/Mck-Cre+
Lap2αNeo-fl/Neo-fl/Mck-Cre+
Bar = 50 µm

Supplemental Figure 1

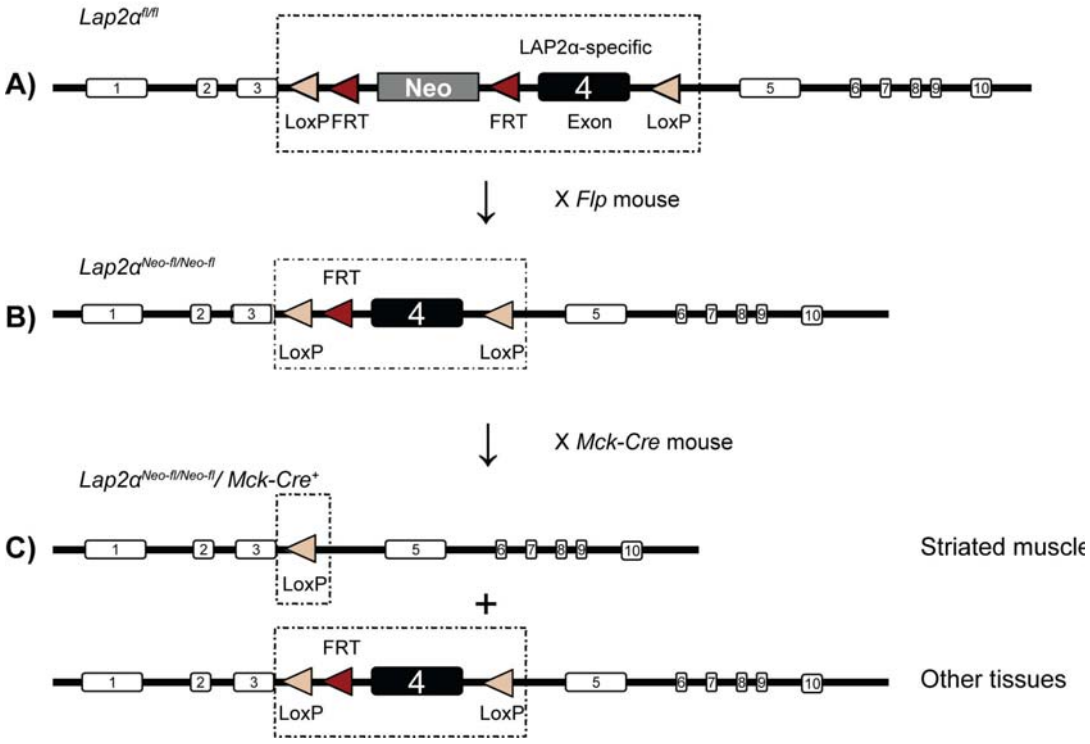

Supplemental Figure 2

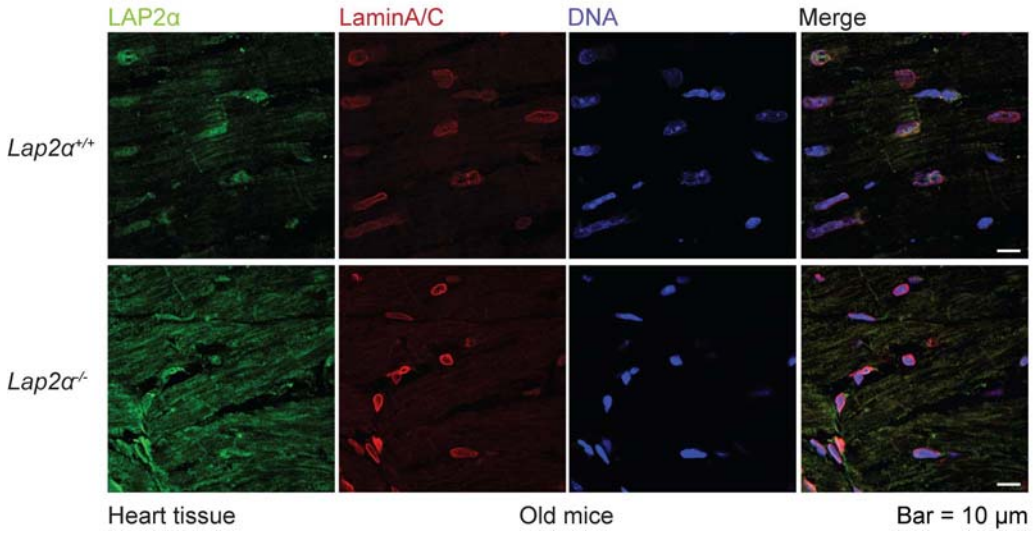

Supplemental Figure 3

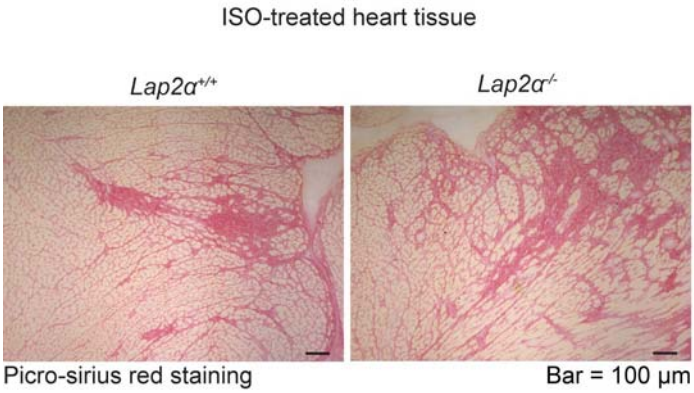

Supplemental Figure 4

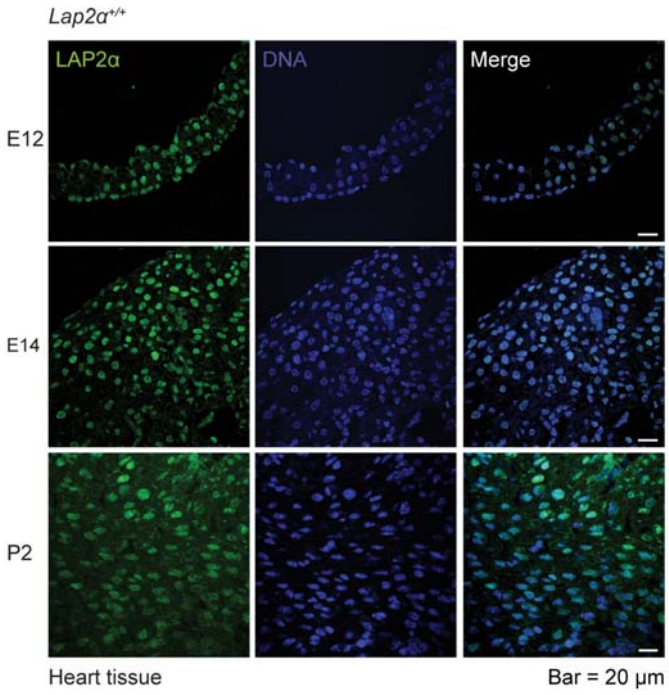

Supplemental Legends

Supplemental figure 1. Generation of *Lap2α*$^{Neo\text{-}fl/Neo\text{-}fl}$*/Mck-Cre*$^{+}$ mice.
A) Crossing *Lap2α*$^{fl/fl}$mice[1] to *Flp*-deleter mice[2] resulted in removal of the Neomycine resistance cassette from the transgenic *Lap2* locus in all tissues. **B)** The newly generated *Lap2α*$^{Neo\text{-}fl/Neo\text{-}fl}$ strain was interbred to *Mck-Cre* transgenic line[3] to create striated muscle-specific *Lap2α*$^{-/-}$ mice lacking the α-specific exon 4 of the *Lap2* gene only in tissues expressing MCK (*Lap2α*$^{Neo\text{-}fl/Neo\text{-}fl}$*/Mck-Cre*$^{+}$) **C)**.

Supplemental figure 2. Lamin A/C localization in *Lap2α*$^{-/-}$ heart cells appears normal. (Immunofluorescence analysis of old heart tissue).

Supplemental figure 3. ISO-treatment causes subendocardial fibrosis in both *Lap2α*$^{-/-}$ and wild type mice. (Picro-sirius stained heart sections).

Supplemental figure 4. LAP2α is highly expressed in developing cardiac tissue.
Immunofluorescence analysis of heart tissue sections at embryonic day 12 and 14 (E12 and E14) and postnatal day 2 (P2).

Supplemental table 1. Echocardiography reveals impaired heart function in male *Lap2α*$^{-/-}$ mice.

Young mice (10 weeks)

	Lap2α$^{+/+}$ M	*Lap2α*$^{-/-}$ M	*Lap2α*$^{+/+}$ F	*Lap2α*$^{-/-}$ F
n	8	8	4	4
Heart rate/ bpm	410.63 ± 15.76	410.25 ± 21.72	380.00 ± 17.80	387.50 ± 12.50
FS %	**36.72** ± 1.23	**27.97** ± 1.38*	**37.22** ± 0.81	**36.49** ± 1.44
LVDd/cm	0.36 ± 0.01	0.35 ± 0.03	0.34 ± 0.02	0.33 ± 0.01
LVDs/cm	0.23 ± 0.01	0.25 ± 0.02	0.22 ± 0.01	0.21 ± 0.01
LVPWd/mm	0.85 ± 0.06	0.82 ± 0.10	0.74 ± 0.07	0.72 ± 0.03
LVPWs/mm	1.43 ± 0.08	1.23 ± 0.07	1.26 ± 0.09	1.16 ± 0.05
IVSd/mm	0.91 ± 0.04	0.81 ± 0.04	0.79 ± 0.06	0.73 ± 0.02
IVSs/mm	1.26 ± 0.07	1.17 ± 0.09	1.11 ± 0.11	0.96 ± 0.06
LA/mm	2.14 ± 0.15	2.82 ± 0.21*	2.70 ± 0.34	2.56 ± 0.07
ESVI ml/m2	0.04 ± 0.00	0.05 ± 0.01	0.03 ± 0.01	0.03 ± 0.01
EDVI ml/m2	0.14 ± 0.01	0.14 ± 0.03	0.14 ± 0.02	0.12 ± 0.01
EF %	73.18 ± 0.02	61.00 ± 0.02*	74.01 ± 0.96	73.08 ± 1.72

Old mice (10-12 months)

	Lap2α$^{+/+}$ M	*Lap2α*$^{-/-}$ M	*Lap2α*$^{+/+}$ F	*Lap2α*$^{-/-}$ F
n	11	13	4	5
Heart rate/ bpm	418.91 ± 15.80	428.31 ± 10.31	430.00 ± 14.63	408.00 ± 35.28
FS %	**36.88** ± 0.86	**30.39** ± 1.67*	**33.00** ± 3.41	**37.83** ± 3.94
LVDd/cm	0.36 ± 0.02	0.38 ± 0.01	0.36 ± 0.01	0.39 ± 0.03
LVDs/cm	0.23 ± 0.01	0.26 ± 0.01	0.23 ± 0.02	0.24 ± 0.03
LVPWd/mm	0.91 ± 0.05	0.92 ± 0.06	0.71 ± 0.03	0.77 ± 0.04
LVPWs/mm	1.48 ± 0.07	1.41 ± 0.07	1.33 ± 0.11	1.23 ± 0.17
IVSd/mm	0.91 ± 0.03	0.92 ± 0.04	0.84 ± 0.02	0.75 ± 0.07*
IVSs/mm	1.30 ± 0.07	1.28 ± 0.07	1.16 ± 0.06	1.01 ± 0.07
LA/mm	2.37 ± 0.16	2.75 ± 0.23	2.40 ± 0.29	2.13 ± 0.22
ESVI ml/m2	0.04 ± 0.01	0.05 ± 0.01	0.03 ± 0.00	0.04 ± 0.01
EDVI ml/m2	0.13 ± 0.01	0.13 ± 0.02	0.13 ± 0.01	0.16 ± 0.00
EF %	73.43 ± 0.01	64.65 ± 0.03*	73.66 ± 2.06	73.78 ± 4.45

*p<0.05 ANOVA, values are represented as ± standard error (SE). M – male; F – female; n = number of mice; bpm – beats per minute; FS% – fractional shortening; LVDd/s – left ventricular diameter in diastole/systole; LVPWd/s left ventricular posterior wall thickness in diastole/systole; IVSd/s – interventricular septum thickness in diastole/systole, LA – left atrium diameter; ESVI – end-systolic left ventricular volume index; EDVI – end-diastolic left ventricular volume index; EF% – ejection fraction.

Supplemental table 2. *Lap2α*$^{-/-}$ mice show a blunted response to chronic isoproterenol infusion. Echocardiography parameters recorded before and after ISO-infusion.

Isoproterenol

	***Lap2α*$^{+/+}$ M**	***Lap2α*$^{-/-}$M**	***Lap2α*$^{+/+}$ M**	***Lap2α*$^{-/-}$M**
Old mice (10 months)	**Before**		**Isoproterenol**	
n	6	7	6	7
Heart rate/ bpm	489.50 ± 26.27	452.57 ± 10.16	507.17 ± 36.33	532.29 ± 14.55**
FS %	**33.44** ± 2.37	**29.77** ± 1.61	**29.63** ± 3.70	**25.84** ± 2.94
LVDd/cm	0.30 ± 0.01	0.35 ± 0.02	0.41 ± 0.01**	0.41 ± 0.02
LVDs/cm	0.20 ± 0.01	0.24 ± 0.01	0.29 ± 0.02**	0.31 ± 0.02
LVPWd/mm	1.14 ± 0.09	1.05 ± 0.06	1.00 ± 0.05	1.06 ± 0.10
LVPWs/mm	1.60 ± 0.08	1.51 ± 0.03	1.42 ± 0.10	1.41 ± 0.09
IVSd/mm	1.07 ± 0.04	0.96 ± 0.05	0.89 ± 0.07	1.02 ± 0.10
IVSs/mm	1.50 ± 0.07	1.40 ± 0.04	1.31 ± 0.08	1.45 ± 0.11
LA/mm	3.02 ± 0.31	3.05 ± 0.38	3.44 ± 0.31	3.81 ± 0.39
ESVI ml/m2	0.02 ± 0.00	0.04 ± 0.01	0.06 ± 0.01**	0.07 ± 0.01
EDVI ml/m2	0.07 ± 0.01	0.10 ± 0.01	0.15 ± 0.01**	0.16 ± 0.02
EF %	68.82 ± 3.28	63.69 ± 2.43	62.21 ± 6.00	56.52 ± 5.00

Sham (PBS)

	***Lap2α*$^{+/+}$ M**	***Lap2α*$^{-/-}$M**	***Lap2α*$^{+/+}$ M**	***Lap2α*$^{-/-}$M**
	Before		**PBS**	
n	2	2	2	2
Heart rate/ bpm	465.00 ± 55.00	500.00 ± 40.00	445.00 ± 15.00	477.50 ± 37.50
FS %	**34.64** ± 4.49	**34.07** ± 0.29	**33.44** ± 3.01	**32.70** ± 1.93
LVDd/cm	0.31 ± 0.01	0.31 ± 0.02	0.30 ± 0.00	0.34 ± 0.00
LVDs/cm	0.20 ± 0.02	0.21 ± 0.01	0.20 ± 0.01	0.23 ± 0.01
LVPWd/mm	0.97 ± 0.00	1.07 ± 0.09	1.06 ± 0.09	1.14 ± 0.17
LVPWs/mm	1.17 ± 0.20	1.37 ± 0.04	1.38 ± 0.05	1.43 ± 0.13
IVSd/mm	1.01 ± 0.30	1.17 ± 0.01	1.05 ± 0.05	1.11 ± 0.07
IVSs/mm	1.33 ± 0.23	1.72 ± 0.03	1.42 ± 0.07	1.72 ± 0.16
LA/mm	2.40 ± 0.00	1.87 ± 0.40	2.35 ± 0.35	2.15 ± 0.20
ESVI ml/m2	0.02 ± 0.01	0.02 ± 0.00	0.02 ± 0.00	0.03 ± 0.00
EDVI ml/m2	0.06 ± 0.01	0.06 ± 0.01	0.06 ± 0.00	0.08 ± 0.00
EF %	70.54 ± 5.89	70.17 ± 0.33	69.21 ± 4.05	68.15 ± 2.65

Data were analysed using Students' paired t-test (comparisons within one genotype before and after the treatment) and ANOVA (comparisons between the two genotypes and multiple comparisons), followed by Boniferroni adjustment where applicable. **p<0.05 Students' paired t-test; mean values ± SE are shown.

Supplemental table 3. Echocardiography parameters – *Lap2α$^{-/-}$/Mdx* mice.

	Lap2α$^{+/+}$/Mdx	*Lap2α$^{-/-}$/Mdx*	*Lap2α$^{+/+}$/Mdx*	*Lap2α$^{-/-}$/Mdx*
	Young (10 weeks)		**Old (10-12 months)**	
n	3	3	4	5
Heart rate/ bpm	400.00 ± 0.00	413.33 ± 17.64	442.50 ± 63.03	404.00 ± 26.94
FS %	**39.51** ± 0.43*	**39.58** ± 1.46*	**31.22** ± 2.74**	**28.24** ± 2.21**
LVDd/cm	0.37 ± 0.03	0.38 ± 0.02	0.42 ± 0.01	0.41 ± 0.01
LVDs/cm	0.22 ± 0.01	0.23 ± 0.02	0.29 ± 0.02	0.30 ± 0.01
LVPWd/mm	0.58 ± 0.08	0.70 ± 0.11	0.73 ± 0.07	0.70 ± 0.04
LVPWs/mm	1.15 ± 0.09	1.28 ± 0.11	1.17 ± 0.07	1.03 ± 0.10
IVSd/mm	0.75 ± 0.04	0.71 ± 0.02	0.91 ± 0.10	0.87 ± 0.07
IVSs/mm	1.10 ± 0.13	1.10 ± 0.09	1.11 ± 0.11	1.08 ± 0.06
LA/mm	2.16 ± 0.16	2.50 ± 0.07	3.43 ± 0.14	3.27 ± 0.18
ESVI ml/m2	0.03 ± 0.01	0.03 ± 0.01	0.06 ± 0.01	0.06 ± 0.01
EDVI ml/m2	0.14 ± 0.03	0.15 ± 0.02	0.16 ± 0.01	0.15 ± 0.01
EF %	76.63 ± 0.43	76.62 ± 1.70	65.45 ± 3.97	61.05 ± 3.64

*p<0.05, ANOVA, *Lap2α$^{-/-}$* vs *Lap2α$^{+/+}$/Mdx* and *Lap2α$^{-/-}$/Mdx* young mice.

**p<0.05, ANOVA, *Lap2α$^{+/+}$* vs *Lap2α$^{+/+}$/Mdx* and *Lap2α$^{-/-}$/Mdx* old mice.

Supplemental table 4. Echocardiography parameters – *Lap2α*$^{Neo\text{-}fl/Neo\text{-}fl}$*/Mck-Cre*$^{+}$ mice.

	Lap2α$^{+/+}$*/Mck-Cre*$^{+}$	*Lap2α*$^{Neo\text{-}fl/Neo\text{-}fl/}$*Mck-Cre*$^{+}$
Young (10 weeks)		
n	5	5
Heart rate/ bpm	360.00 ± 7.07	378.00 ± 18.81
FS %	**32.54** ± 1.01	**33.88** ± 1.42
LVDd/cm	0.39 ± 0.01	0.38 ± 0.01
LVDs/cm	0.26 ± 0.01	0.25 ± 0.01
LVPWd/mm	0.72 ± 0.05	0.72 ± 0.02
LVPWs/mm	1.22 ± 0.08	1.28 ± 0.07
IVSd/mm	0.79 ± 0.02	0.84 ± 0.05
IVSs/mm	1.05 ± 0.09	1.06 ± 0.07
LA/mm	2.38 ± 0.13	2.35 ± 0.19
ESVI ml/m2	0.05 ± 0.00	0.04 ± 0.01
EDVI ml/m2	0.14 ± 0.01	0.13 ± 0.01
EF %	67.78 ± 1.38	69.55 ± 1.97

Supplemental table 5. Primer sequences used for quantitative and semi-quantitative PCR.

Name/Target	Sequence	Tm ºC	Source
Adrb2_forward	TCTGTGCCTTCGCAGGTCTT	59,4	4
Adrb2_reverse	GTCCGTTCTGCCGTTGCTA	58,8	
ANF_forward	CGGTGTCCAACACAGATCTG	59,4	5
ANF_reverse	TCTCTCGAGGTGGGTTGAC	58,8	
mBNP_forward	CTGCTGGAGCTGATAAGAGA	57,3	6
mBNP_reverse	TGCCCAAAGCAGCTTGAGAT	57,3	
Cre2_forward	CGAACGCACTGATTTCGA	56,7	7
Cre2_reverse	GGCAACACCATTTTTTCTGAC	55,9	
Ctgf_forward	TGTGTGACGAGCCCAAGGA	58,8	8
Ctgf_reverse	TTGGGTCTGGGCCAAATGT	56,7	
GAPDH-hm1	CATCACCATCTTCCAGGAGCGA	62,1	9
GAPDH-hm2	CCTGCTTCACCACCTTCTTGAT	60,3	
GATA4b_forward	CACTATGGGCACAGCAGCTCC	63,7	10
GATA4b_reverse	TTGGAGCTGGCCTGCGATGTC	63,7	
Hprt_forward	TGATTAGCGATGATGAACCAGG	58,4	11
Hprt_reverse	CTTTCATGACATCTCGAGCAAG	60,3	
LAP2com_hm1	GTGGGAACAACCAGGAAGCTATATGA	63,2	1
LAP2ar_hm1	AGAGTGCTAAGTCCAACTGCTGAT	61,0	
LAP2br_hm1	CTCCCACTTCAGCTCTTGTCAATG	62,7	
mLamAC1091f	CATCAAGCTGGCCCTGGACATGGA	67,9	1
mLamAC1549r	TGCGCCTTCCACACCAAGTCAGTA	66,3	
MEF2C-RT2-1	GTATGTCTCCTGGTGTAACA	55,3	12
MEF2C-RT2-2	GGATATCCTCCCATTCCTTG	57,3	
MCK_forward	GAGATCTTCAAGAAGGCTGGTCA	60,6	13
MCK_reverse	GAGATGTCGAACACGGCG	58,2	
MyocardinA_forward	TCACTGTGTGGAGTCCTCAGGTC	64,2	14
MyocardinA_reverse	TGGCATCGGCTGGCATTT	58,8	
STARS_forward	GGCTCCTGCCAGGATCAAAC	61,4	NM_175456.4
STARS_reverse	TAGCCCTCGTCTCCCTTGTG	61,4	
TGFβ_forward	AGCGCTACATCGATAGCAAG	57,3	8
TGFβ_reverse	TCCTGTCTTTGTGGTGAAGC	57,3	

Supplemental References

1. Naetar N KB, Kozlov S, Kerenyi MA, Dorner D, Kral I, Gotic I, Fuchs P, Cohen T, Bittner R, Stewart CL, Foisner R. Loss of nucleoplasmic LAP2alpha-lamin A complexes causes erythroid and epidermal progenitor hyperproliferation. *Nature Cell Biology.* 2008.

2. Dymecki SM. Flp recombinase promotes site-specific DNA recombination in embryonic stem cells and transgenic mice. *Proc Natl Acad Sci U S A.* 1996;93(12):6191-6196.

3. Bruning JC, Michael MD, Winnay JN, Hayashi T, Horsch D, Accili D, Goodyear LJ, Kahn CR. A muscle-specific insulin receptor knockout exhibits features of the metabolic syndrome of NIDDM without altering glucose tolerance. *Mol Cell.* 1998;2(5):559-569.

4. Parker GE, Pederson BA, Obayashi M, Schroeder JM, Harris RA, Roach PJ. Gene expression profiling of mice with genetically modified muscle glycogen content. *Biochem J.* 2006;395(1):137-145.

5. Lou DY, Dominguez I, Toselli P, Landesman-Bollag E, O'Brien C, Seldin DC. The alpha catalytic subunit of protein kinase CK2 is required for mouse embryonic development. *Mol Cell Biol.* 2008;28(1):131-139.

6. Ellmers LJ, Knowles JW, Kim HS, Smithies O, Maeda N, Cameron VA. Ventricular expression of natriuretic peptides in Npr1(-/-) mice with cardiac hypertrophy and fibrosis. *Am J Physiol Heart Circ Physiol.* 2002;283(2):H707-714.

7. Mo L, Cheng J, Lee EY, Sun TT, Wu XR. Gene deletion in urothelium by specific expression of Cre recombinase. *Am J Physiol Renal Physiol.* 2005;289(3):F562-568.

8. Bisping E, Ikeda S, Kong SW, Tarnavski O, Bodyak N, McMullen JR, Rajagopal S, Son JK, Ma Q, Springer Z, Kang PM, Izumo S, Pu WT. Gata4 is required for maintenance of postnatal cardiac function and protection from pressure overload-induced heart failure. *Proc Natl Acad Sci U S A.* 2006;103(39):14471-14476.

9. Vlcek S, Foisner R, Wilson KL. Lco1 is a novel widely expressed lamin-binding protein in the nuclear interior. *Exp Cell Res.* 2004;298(2):499-511.

10. Xu C, Liguori G, Adamson ED, Persico MG. Specific arrest of cardiogenesis in cultured embryonic stem cells lacking Cripto-1. *Dev Biol.* 1998;196(2):237-247.

11. Kerenyi MA, Grebien F, Gehart H, Schifrer M, Artaker M, Kovacic B, Beug H, Moriggl R, Mullner EW. Stat 5 regulates cellular iron uptake of erythroid cells via IRP-2 and TfR-1. *Blood.* 2008.

12. Azmi S, Ozog A, Taneja R. Sharp-1/DEC2 inhibits skeletal muscle differentiation through repression of myogenic transcription factors. *J Biol Chem.* 2004;279(50):52643-52652.

13. Porter JD, Merriam AP, Gong B, Kasturi S, Zhou X, Hauser KF, Andrade FH, Cheng G. Postnatal suppression of myomesin, muscle creatine kinase and the M-line in rat extraocular muscle. *J Exp Biol.* 2003;206(Pt 17):3101-3112.

14. Ueyama T, Kasahara H, Ishiwata T, Nie Q, Izumo S. Myocardin expression is regulated by Nkx2.5, and its function is required for cardiomyogenesis. *Mol Cell Biol.* 2003;23(24):9222-9232.

3.2 Submitted manuscript II

Loss of LAP2α Delays Satellite Cell Differentiation and Affects Postnatal Fibre Type Determination

Ivana Gotic[1], Wolfgang M. Schmidt[3], Katarzyna Biadasiewicz[1], Michael Leschnik[2], Rita Spilka[1], Juliane Braun[1], Colin L. Stewart[4] and Roland Foisner[1]*

[1]Department of Medical Biochemistry, Max F. Perutz Laboratories, Medical University of Vienna, Vienna, Austria

[2]Department for Small Animals and Horses, Clinic for Internal Medicine and Infectious Diseases, Veterinary University of Vienna, Vienna, Austria

[3]Neuromuscular Research Department, Center of Anatomy and Cell Biology, Medical University of Vienna, Vienna, Austria

[4]Institute of Medical Biology, Singapore, Singapore

Running title: Functions of LAP2α in skeletal muscle

***Correspondence to**:
Roland Foisner
Max F. Perutz Laboratories,
Department of Medical Biochemistry
Medical University of Vienna,
Dr. Bohr-Gasse 9/3,
A-1030 Vienna, Austria
Email: roland.foisner@meduniwien.ac.at
Phone: +43-1-4277-61680, FAX: +43-1-4277-9616

Abstract

Lamina-associated polypeptide 2α (LAP2α) is a nucleoplasmic protein implicated in cell cycle regulation through its interaction with A-type lamins and the retinoblastoma protein (pRb). Mutations in lamin A/C and LAP2α cause late onset striated muscle diseases, but the molecular mechanisms are poorly understood. To study the role of LAP2α in skeletal muscle function and postnatal tissue homeostasis, we generated complete and muscle-specific LAP2α knockout mice. While overall muscle morphology, function and regeneration were not detectably affected, the myofibre-associated muscle stem cell pool was increased in LAP2α-deficient mice. At molecular level, the absence of LAP2α preserved the stem cell-like phenotype of primary myoblasts and delayed their *in vitro* differentiation. In addition, loss of LAP2α shifted the myofibre type ratios of adult slow muscles towards fast fibre types. Muscle-specific ablation of LAP2α affected early stages of myoblast differentiation, as well as fibre type determination, but did not change fibre-associated stem cell numbers. Our data demonstrate multiple and distinct functions of LAP2α in muscle stem cell maintenance, early phases of myogenic differentiation and muscle remodelling.

Keywords: Lamin / LAP2α / Muscle fibre type / Regeneration /Satellite cells

List of Abbreviations

BMP4	Bone Morphogenetic Protein 4
CSM4B	CD45$^-$Sca1$^-$Mac1$^-$CXCR4$^+$$\beta_1$-integrin$^+$
EDL	Extensor Digitorum Longus
EDMD	Emery Dreifuss Muscular Dystrophy
GAPDH	Glycerinaldehyde-3-phosphate-Dehydrogenase
GO	Gene Ontology
H & E	Haematoxylin and Eosin
HPRT	Hypoxanthine-Guanine Phosphoribosyl Transferase
IGF	Insulin-like Growth Factor
LAP2	Lamina Associated Polypeptide
LEM	LAP2-Emerin-MAN1
MAPK	Mitogen-activated Protein Kinase
MCK	Muscle Creatine Kinase
MEF2c	Myocyte Enhacner Factor
MFPL	Max F. Perutz Laboratories
MyHC	Myosin Heavy Chain
PDGF	Platelet-derived Growth Factor Receptor
qPCR	Quantitative PCR
Rb	Retinoblastoma protein
SE	Standard Error
SHH	Sonic Hedgehog
TA	Tibialis Anterior

Introduction

Muscular dystrophies are clinically and genetically heterogeneous disorders characterized by progressive muscle wasting and weakness. The most prominent genes involved in their development encode structural components of the sarcolemma, the cytoskeleton and the extracellular matrix (1). In the past decade, a group of idiopatic muscular dystrophies has been linked to mutations in nuclear envelope proteins, including lamin A/C and some of its binding partners. Lamins form a supporting framework for the nucleus and regulate various cellular processes such as DNA replication, transcription and signal transduction (2).

The onset of pathological symptoms in most lamin A/C-associated striated muscle disorders, such as Emery-Dreifuss and Limb-girdle muscular dystrophy 1B, occurs in early adulthood (2), pointing to a defect in stem-cell mediated adult tissue homeostasis and damage repair (3). Adult stem cells in muscle are represented by a heterogeneous population of quiescent, autonomously myogenic, cells in a satellite position between the myofibre and the basal lamina (4). The maintenance and self-renewal of these, so called, satellite cells depends on the expression of a member of the paired box transcription factor family, Pax7, which antagonizes the activity of the major myogenic regulatory factor MyoD and keeps the cells in an undifferentiated state (5).

Lamina-associated polypeptide 2α (LAP2α) is a lamin A/C binding protein that has been implicated in the regulation of proliferation and differentiation of adult tissue progenitor cells (6). LAP2α is a mammal-specific non-membrane-associated isoform of the vertebrate *LAP2* gene (7), which localizes to the nucleoplasm and interacts with chromatin through its LAP2-common N-terminal LEM (LAP2-emerin-MAN1) domain and a unique C-terminal α-specific region (8, 9). The C-terminus of LAP2α also binds a distinct fraction of lamin A/C inside the nucleus and regulates cell cycle progression by affecting retinoblastoma (Rb)-mediated E2F-dependent transcription (6, 10). Interestingly, a mutation in LAP2α affecting its lamin A/C interaction has also been linked to a pathological heart condition (11), symptomatically similar to lamin A/C-linked cardiomyopathies (2), pointing to a common disease mechanism of these two proteins.

Taking into account the potential impairment of muscle homeostasis and tissue regeneration in striated muscle disorders linked to mutations in lamin A/C and LAP2α, we analyzed the functional properties of the satellite cell pool in the recently described *Lap2α*$^{-/-}$ mice. Here we demonstrate that lack of LAP2α preserves the stem cell phenotype of satellite cells and delays their differentiation and has an additional role in muscle fiber type remodelling.

Results

Absence of LAP2α in mice causes an increase in the muscle satellite cell pool

Deletion of the α-specific *Lap2* exon 4 in mice (6) resulted in complete ablation of LAP2α protein in skeletal muscle, without affecting the expression of other LAP2 isoforms. In addition, loss of LAP2α did not markedly alter the expression or localization of its major binding partner lamin A/C in muscle tissue (Supplemental Figure 1a; 1b). *Lap2α*$^{-/-}$ mice showed no overt dystrophic muscle phenotype at histological level under normal conditions within 19 months after birth (Supplemental Figure 2) (6). Based on our previous findings, demonstrating a role of LAP2α in proliferation of adult tissue stem/progenitor cells (6), we hypothesized that the activity and maintenance of the satellite cell pool, which normally expresses LAP2α (Figure 1a), might be affected in LAP2α-deficient muscle tissue. To identify the putative self-renewing stem cell population in adult muscle, we used a combination of cell surface markers (CD45, Sca1, Mac1 and CXCR4, β_1-integrin), whose absence or presence, respectively, defines the majority of autonomously myogenic cells (>90% Pax7$^+$) within the myofibre-associated satellite cell compartment (12). Fluorescence-activated cell sorting (FACS) analysis of enzymatically digested skeletal muscle tissue revealed a ~43% increase in the CD45$^-$Sca1$^-$Mac1$^-$CXCR4$^+\beta_1$-integrin$^+$ (CSM4B) satellite cell pool within the fibre-associated CD45$^-$Sca1$^-$Mac1$^-$ cell population in young (aged 10 weeks) *Lap2α*$^{-/-}$ mice compared to their wild type (WT) littermates (Figure 1b), pointing to a defect in the regulation of the stem cell pool. In WT mice, CSM4B cell numbers gradually decreased during aging, reaching 65% and 46% of the level in young muscle after 6 (defined as adult) and 19 (defined as old) months respectively. Interestingly, the increase in the CSM4B satellite cell population in young *Lap2α*$^{-/-}$ vs. WT mice was completely lost by the age of 6 months, suggesting that the initial increase in CSM4B cell numbers might be a consequence of their accelerated proliferation and/or delayed myogenic commitment during early postnatal muscle growth.

Activated *Lap2α*$^{-/-}$ satellite cells retain a stem cell-like phenotype *in vitro*

To identify genes and molecular pathways directly or indirectly affected by the loss of LAP2α in skeletal muscle, we performed genome-wide microarray (GeneChip) analyses and compared global gene expression profiles of primary *Lap2α*$^{+/+}$ and *Lap2α*$^{-/-}$ neonatal myoblasts, representing activated satellite cell progeny. Surprisingly, the differential gene expression profile revealed that only a small number of genes, other than *Lap2*, was affected by the *Lap2α* knockout: a total of 124 probe sets corresponding to 98 well-annotated genes, showed altered expression, with the majority (~66%) being downregulated. (Figure 2, Supplemental Table 1). Interestingly, among the few genes whose expression was enhanced in the absence of LAP2α, we found genes encoding proteins involved in stem cell renewal, early stages of muscle differentiation and tissue development/regeneration, such as Pax7 (13), Myf5 (14) syndecan 4 (*Sdc4*) (15), netrin 4 (*Ntn4*) (16) and the Notch signaling target Hey1 (17) (Table 1). In addition, components of several signaling cascades, such as BMP4, SHH, IGF, PDGF and MAPK, which influence muscle development and homeostasis (18, 19), were downregulated in *Lap2α*$^{-/-}$ cells (Table 1).

Furthermore, LAP2α-deficient cells exhibited downregulation of several extracellular matrix proteins (Table 1), consistent with the observed looser attachment of the knockout cells to the surface of the culture dish (data not shown). The decreased expression of genes encoding extracellular matrix components, accompanied by the upregulation of stem cell genes, indicates a preservation of a stem cell-like phenotype of activated *Lap2α*$^{-/-}$ satellite cells, which favour self-renewal as opposed to skeletal muscle commitment, potentially explaining the increase in CSM4B cell numbers observed *in vivo*.

Lap2α$^{-/-}$ myoblasts exhibit delayed differentiation

To test whether the upregulated expression of stem cell determinants in proliferating *Lap2α*$^{-/-}$ myoblasts causes a concomitant defect in their differentiation towards myotubes, we compared the *in vitro* differentiation potentials of LAP2α-deficient and WT primary myoblasts (Figure 3). As previously reported (20), protein and mRNA levels of LAP2α in wild type cells peaked at the onset of myoblast differentiation and declined at later stages (Figure 3a, b upper panels). Loss of LAP2α did not substantially affect the expression of lamin A/C at protein level in primary myoblasts, although a slight temporal upregulation of the mRNA transcript was observed during initial stages of their differentiation (Figure 3a; 3b). Consistent with the microarray data, Pax7 was upregulated in proliferating *Lap2α*$^{-/-}$ myoblasts compared to WT cells at both mRNA and protein level (Figure 3a and data not shown). Interestingly, loss of LAP2α caused a decrease in protein levels of the major myogenic differentiation factor MyoD (Figure 3a middle panels), while the mRNA levels of both MyoD and its related myogenic regulatory factor Myf5 were upregulated, indicating a compensatory mechanism in response to reduced MyoD protein levels (Figure 3b, middle panels). In line with the downregulation of MyoD protein, LAP2α-deficient cells also showed delayed expression of MyoD target genes and co-factors, such as desmin and myocyte enhancer factor 2c (MEF2c), which specify early phases of myoblast differentiation. Similarly, the expression of the late stage differentiation marker myosin heavy chain (MyHC) (5, 21) was reduced in LAP2α-deficient myoblasts (Figure 3a; 3b lower panels). Still, *Lap2α*$^{-/-}$ myoblasts were able to differentiate *in vitro* into MyHC-containing myotubes (Figure 3c), albeit in a slightly delayed manner. The transient rise in LAP2α and lamin A/C expression, within the first 3 days of *in vitro* differentiation in WT myoblasts, and the delayed expression of muscle-specific markers in LAP2α-deficient cells, point to a role of LAP2α in early stages of myoblast differentiation. These data are consistent with the proposed function of LAP2α and lamin A/C in controlling the balance between proliferation and differentiation of progenitor cells in adult tissues (6).

Loss of LAP2α does not affect *in vivo* muscle regeneration in mice

As proliferation of activated satellite cells and differentiation of their progeny represent the hallmarks of muscle regeneration, we wondered whether the observed delay in *in vitro* differentiation of LAP2α-deficient myoblasts would also affect tissue repair *in vivo.* Taking into account the observed age-related differences in CSM4B satellite cell numbers, we tested the ability of young, as well as old, *Lap2α*$^{-/-}$ muscle to regenerate after notexin-induced acute injury. Within

the first 4 days after injury, the muscle resident myogenic stem cells generated a population of proliferating myoblasts, which differentiated and fused into myofibres expressing the embryonic form of MyHC (EMyHC), in both, WT and *Lap2α*$^{-/-}$ mice (Figure 4a, right panels). During myofibre maturation, EMyHC was replaced by adult myosin isoforms and muscle integrity was restored by day 12 in both – WT and *Lap2α*$^{-/-}$ mice (Figure 4). To evaluate the efficiency of muscle regeneration in our system more precisely, we measured the size of the newly formed EMyHC^{+} myofibres within the damaged region at day 4 and calculated the corresponding fibrotic indexes (for details see Materials and Methods). Although muscle regeneration (lower fibrotic indexes) appeared better in young versus old *Lap2α*$^{-/-}$ animals, there were only subtle, statistically non-significant differences between WT and *Lap2α*$^{-/-}$ age-matched mice (Figure 4b). Thus, the increased satellite cell pool of young *Lap2α*$^{-/-}$ mice was not able to enhance muscle regeneration, probably due to a delay in myogenic differentiation, leading to a net effect of zero.

In order to test whether muscle regeneration would be affected in *Lap2α*$^{-/-}$ mice under conditions of constant muscle damage, we crossed *Lap2α*$^{-/-}$ mice with the Duchenne muscular dystrophy mouse model line *Mdx* (22). Chronic muscle damage in *Mdx* mutants, caused by the absence of the sarcolemma-linked protein dystrophin, evokes repetitive satellite cell activation and tissue repair (22). *Lap2α*$^{-/-}$*/Mdx* mutant mice appeared indistinguishable from their *Mdx* littermates and presented signs of muscle damage and hypertrophy starting at the age of 3 weeks (data not shown), as described for the *Mdx* mice (22), suggesting that LAP2α loss does not significantly affect muscle regeneration *in vivo*.

Absence of LAP2α promotes fast fibre phenotype in predominantly slow muscles

Muscle is a highly dynamic tissue able to modify its metabolic and contractile properties according to physiological needs. On the basis of specific MyHC isoform expression, size and metabolic profile, skeletal muscle fibres are classified into two major groups: the thinner, type I or slow-twitch fibres, which exhibit low velocity of shortening and are required for maintenance of posture and muscle endurance, and thicker, fast or type II (IIa, IIx/d, IIb) fibres which exert quick contractions and are engaged in movements requiring strength and speed (23). MyoD and MEF-2c transcription factors orchestrate the transformation of mature muscle fibres in response to physiological signals, such as enervation and endocrine/nutritional cues. Whereas, high levels of active MyoD are found in muscles predominantly composed of fast myofibres, the slow muscle phenotype seems to depend on MEF2c, among other factors (23). Since MyoD and MEF2c showed aberrant expression patterns during *in vitro* differentiation of LAP2α-deficient myoblasts, we predicted that the tightly regulated process of muscle remodelling might be affected in *Lap2α*$^{-/-}$ mice. To test this hypothesis we analyzed fibre type composition of predominantly fast (Tibialis anterior – TA) and slow (soleus) muscles in WT and *Lap2α*$^{-/-}$ mice by immunohistochemistry (Figure 5a). Interestingly, whereas myofibre type and size distributions of *Lap2α*$^{-/-}$ TA muscle were similar to WT (data not shown), the soleus muscle of adult *Lap2α*$^{-/-}$ mice exhibited a shift towards the fast fibre phenotype (from 53% type I + 47% type II $\rightarrow$ 44% type I + 56% type II fibres) (Figure 5a; 5b) without a significant change in the myofibre cross-sectional area (Figure 5c). However, the change in fibre type composition of

particular slow muscles did not affect muscle strength and general fitness of *Lap2α*$^{-/-}$ mice at measurable level. Their performance in various tests assessing muscle and lower motor neuronal function, such as locomotor activity, wire manoeuvre, forced and voluntary wheel, rotarod and swim test, included in the SHIRPA mouse phenotypic assessment protocol (24), were similar to that of their WT littermates (data not shown).

Muscle-specific ablation of LAP2α reveals functions during early myoblast differentiation and muscle transformation distinguishable from those in stem cell maintenance

In order to determine the stage of muscle differentiation during which LAP2α exerts its specific functions *in vivo* and to test the possible contribution of defects in other tissues to the observed muscle phenotype in full LAP2α knockout mice, we generated conditional, striated muscle-specific LAP2α-deficient animals. By using the previously described *Mck-Cre*$^{+}$ line (25), which expresses Cre recombinase under the control of late muscle-specific promoter *Mck* (muscle creatine kinase), we generated mice that lose LAP2α expression during later stages of muscle differentiation (unpublished data). As expected, proliferating myoblasts and non-muscle tissues such as spleen, which do not express MCK and Cre recombinase, exhibited WT levels of LAP2α (Figure 6a), whereas differentiated muscle tissue of *Lap2α*$^{Neo\text{-}fl/Neo\text{-}fl}$*/Mck-Cre*$^{+}$ mice expressed only low levels of LAP2α (Figure 6a). Similar to complete LAP2α knockout animals, *Lap2α*$^{Neo\text{-}fl/Neo\text{-}fl}$*/Mck-Cre*$^{+}$ mice did not exhibit an overt skeletal muscle defect (Supplemental Figure 3). Consistent with the sustained LAP2α expression in *Lap2α*$^{Neo\text{-}fl/Neo\text{-}fl}$*/Mck-Cre*$^{+}$ satellite cell progeny, *Lap2α*$^{Neo\text{-}fl/Neo\text{-}fl}$*/Mck-Cre*$^{+}$ mice had similar CSM4B cell numbers as their WT Cre recombinase-expressing littermates at all ages (Figure 6b), supporting the hypothesis that loss of LAP2α expression in satellite cells or in other non-muscle cells (e.g. stem cell niches) causes the muscle stem cell phenotype in complete LAP2α knockout animals.

Interestingly, *in vitro* differentiation of *Lap2α*$^{Neo\text{-}fl/Neo\text{-}fl}$*/Mck-Cre*$^{+}$ primary myoblasts revealed a temporary lag at day 3 (Figure 6c, d), coinciding with the activation of the *Mck* promoter and induction of Cre recombinase. Compared to WT cultures, which predominantly contained myotubes at day 3, differentiating *Lap2α*$^{Neo\text{-}fl/Neo\text{-}fl}$*/Mck-Cre*$^{+}$ cultures had a higher number of single non-fused myoblasts and exhibited lower level of MyHC mRNA (Figure 6c, 6d). Since LAP2α expression was highest at day 3 of WT myoblast differentiation (Figure 6d, Figure 3b), we concluded that the *in vitro* differentiation defects in *Lap2α*$^{Neo\text{-}fl/Neo\text{-}fl}$*/Mck-Cre*$^{+}$ cells are a direct consequence of their inability to upregulate LAP2α. These data confirm the role of LAP2α during early myogenic differentiation. Interestingly, the delay in *in vitro* differentiation was more extensive in *Lap2α*$^{Neo\text{-}fl/Neo\text{-}fl}$*/Mck-Cre*$^{+}$ than in *Lap2α*$^{-/-}$ myoblasts (compare Figures 3c, 6c). This discrepancy may be explained by the activation of compensatory mechanisms in response to loss of LAP2α during development of complete LAP2α knockout animals.

Like in complete *Lap2α*$^{-/-}$ animals, the muscle-specific downregulation of LAP2α in *Lap2α*$^{Neo\text{-}fl/Neo\text{-}fl}$*/Mck-Cre*$^{+}$ mice affected the process of skeletal muscle transformation. While the number of fibres reactive with anti-type I antibodies in soleus muscle was similar in wild type and conditional LAP2α knockout mice, significantly fewer type I negative fibres reacted with anti-type II (a and x/d)

antibody in *Lap2α*$^{Neo\text{-}fl/Neo\text{-}fl}$*/Mck-Cre*$^{+}$ muscles (Figure 6e). Since these type II negative fibres were also negative for IIb myosin heavy chain, we concluded that they represent an intermediate type, pointing towards a defect in fibre type determination in LAP2α-deficient muscle.

Overall these results suggest that the role of LAP2α in myoblast differentiation and fibre type determination is distinct and independent of its role in stem cell maintenance.

Discussion

Laminopathies are complex human disorders caused by mutations in lamins and their interacting proteins (2). Recently, we and others provided evidence for the, so called “stem cell disease model”, explaining the late onset of particular laminopathic disorders by defective cell cycle regulation and differentiation of stem cells during maintenance of tissue homeostasis (6, 26, 27).

In this study, we demonstrate that the absence of LAP2α affects the maintenance of satellite cells – the putative stem cells in adult muscle. The *Lap2α*$^{-/-}$ stem cell phenotype described here, including increased number of CSM4B cells within the myofibre-associated satellite cell population of young LAP2α-deficient mice and their normalization during aging, as well as upregulated expression of stem cell determinants and delayed differentiation of primary *Lap2α*$^{-/-}$ myoblasts, points to a defect in proliferation and/or myogenic commitment of muscle stem cells in *Lap2α*$^{-/-}$ mice during early postnatal growth. The specific contributions of these two processes are hard to discriminate, as the effect of delayed differentiation of an increased pool of stem cells may have a zero net effect, potentially explaining the absence of an overt muscle phenotype in young *Lap2α*$^{-/-}$ mice. The grossly unaffected muscle regeneration after acute injury in young *Lap2α*$^{-/-}$ mice might be explained by the same phenomenon. Interestingly, although *Lmna*$^{-/-}$ mice develop muscular dystrophy and die by the age of 8 weeks, their skeletal muscle regeneration also seems to be unaffected (28).

As for the molecular cause of the stem cell phenotype in *Lap2α*$^{-/-}$ mice, our study suggests a role of LAP2α in the regulation of MyoD-dependent muscle-specific transcription during the transition from proliferation to early differentiation states. Interestingly, a similar phenotype – higher number of satellite cells, whose progeny displays an accelerated growth rate and delayed terminal differentiation – has been reported in MyoD-deficient mice (29). A temporal impairment of MyoD activity, as observed in *Lap2α*$^{-/-}$ mice, may not cause serious regeneration defects under physiological conditions, as opposed to complete loss of MyoD (30), presumably due to the upregulation of other compensating myogenic transcription factors, such as Myf5 (31). Although neither MyoD nor Myf5 can fully substitute for the complete loss of the other protein during adult muscle regeneration (14, 32), the slight upregulation of Myf5 in proliferating *Lap2α*$^{-/-}$ myoblasts may be sufficient to overcome the defects caused by MyoD downregulation.

Striated muscle laminopathies and muscle regeneration in mice bearing mutations in lamin A/C and in another lamin-binding protein, emerin, show a disruption of the Rb-MyoD transcriptional pathway (28, 33). Since MyoD was found in protein complexes containing lamin A/C (33), and primary *Lmna*$^{-/-}$ (33) and *Lap2α*$^{-/-}$ myoblasts show reduced MyoD protein levels, it is tempting to speculate that LAP2α-lamin A/C complexes might serve as scaffolding proteins or regulators of MyoD and its co-activator Rb during initial phases of muscle differentiation. The slightly increased expression of the respective binding partner during *in vitro* differentiation of *Lmna*$^{-/-}$ (28) or *Lap2α*$^{-/-}$ primary myoblasts points to a compensatory effect of the two interacting proteins during muscle differentiation.

In addition to its role in satellite cell regulation, our studies reveal an additional function of LAP2α in muscle physiology, namely in adult myofibre type-specification. Skeletal muscle is able to adapt to environmental demands and respond to physiological and pathological signals by changing the myofibre properties of challenged muscles (23). Whereas exercise causes an increase in oxidative metabolism and fast-to-slow myofibre transitions, muscle disuse and aging have an opposite effect (23). Here we report a subtle shift in the fibre type distribution of adult *Lap2α*$^{-/-}$ mice towards faster phenotypes. In view of similar effects described in MyoD- and MEF2c-deficient mice (34, 35), fibre type switching in *Lap2α*$^{-/-}$ mice might be a consequence of deregulated expression of major myogenic transcription factors involved in muscle transformation. As *Lap2α*$^{-/-}$ animals did not exhibit any behavioural defects or altered physical performance, muscle disuse as a major reason for the observed changes in fibre type composition is rather unlikely. Intriguingly, however, the *Lap2α*$^{-/-}$ myofibre phenotype could also be a sign of accelerated muscle aging, which is particularly appealing in view of the reported involvement of A-type lamins in age related changes (36). In support of our data, type II fibre hypertrophy found in *Lmna*^{H222P} mice (37) and slow muscle atrophy in some human striated muscle laminopathies (38), point to a role of lamins and their interaction partners in adult muscle remodelling.

The properties of skeletal myofibres also depend on the pattern of nerve stimulation, where low frequencies of neuron firing promote slow, and high frequencies fast muscle phenotype by affecting the calcium/calmodulin signaling pathway (23). However, the observed shift towards faster fibre types in the soleus muscle of conditional *Lap2α*$^{Neo\text{-}fl/Neo\text{-}fl}$*/Mck-Cre*$^{+}$ mice, which show normal LAP2α expression in non-muscle tissues, rules out a defective neuronal stimulation as the primary cause of fibre type switching in complete LAP2α knockout animals.

In conclusion, our study implicates LAP2α in the regulation of multiple distinct events in skeletal muscle – maintenance and differentiation of satellite cells and their progeny, and adult fibre type switching and postnatal remodelling of slow muscles.

Materials and methods

Mouse lines

In this study we used *Lap2α*$^{-/-}$ (6), *Lap2α*$^{-/-}$*/Mdx* and *Lap2α*$^{Neo\text{-}fl/Neo\text{-}fl}$*/Mck-Cre*$^{+}$ (I. Gotic, manuscript in preparation) mouse lines. Animals were categorized according to their age as young (10 weeks) adult (6-8 months) and old (16-19 months). All experiments were performed according to permissions from Austrian authorities (BMBWK-66-009/0130-BrGT/2006). Mice were maintained and handled following the procedures outlined in the Guide for the Care and Use of Laboratory Animals. Data acquisition was done by observers blinded for the genotype of the animal.

Immunofluorescence and histochemistry

3.7% formaldehyde/1% methanol-fixed tissue cryo-sections were washed in PBS and incubated for 30 min in blocking solution containing 20% normal goat serum/0.5% gelatine/0.5% TritonX-100/PBS. Primary antibodies were diluted in PBS and applied overnight at 4ºC. Sections were then washed in PBS and incubated with respective fluorochrome-coupled secondary antibodies for 1 h at RT. After washing in PBS, nuclei were counterstained with Hoechst 33342/dH_2O for 10 min at RT and washed in dH_2O. Samples were air-dried and mounted with Mowiol 4-88 (Sigma-Aldrich, Milwaukee, WI, USA).

Cultured cells were fixed in 4% paraformaldehyde/PBS for 10 min, washed in PBS and incubated for 5 min in 50 mM NH_4Cl/PBS. After washing in PBS, cells were permeabilized in 0.5%Triton/PBS for 5 min, washed again and incubated for 30 min in 0.5% gelatine/PBS blocking solution. Primary antibodies were applied for 1 h at RT, diluted in PBS. Samples were subsequently treated as described above. The list of primary antibodies used in these studies can be found in Supplemental Table 2. Appropriate secondary antibodies were coupled to either Texas Red, Cy5 (Jackson ImmunoResearch, West Grove, PA, USA) or Alexa Fluor 488 (Molecular Probes, Eugene, OR, USA) fluorochromes.

For immunohistochemistry, incubation with primary antibodies was followed by washing in PBS and 30 min application of biotinylated secondary antibodies. Consequently, samples were washed in PBS, incubated with Elite ABC Reagent (Vectastain Elite ABC Kit, Vector Laboratories, Burligame, CA, USA) for 20 min at RT and washed with dH_2O. Finally, DAB detection solution (DAB substrate kit for peroxidase from Vector Laboratories) was applied for 5 min and samples were mounted in Mowiol after washing in dH_2O.

Haematoxylin and eosin (H & E) staining was done according to standard protocol. Fluorescence images were acquired on a Axiovert 200M microscope, equipped with LSM 510 META confocal laser-scanning unit, using LSM imaging software (Zeiss, Jena, Germany). Data were processed by Zeiss LSM Image Browser and Adobe Photoshop CS2.

Bright field images were acquired using Axio Imager.M1 equipped with AxioCam MRc5 camera and AxioVision Rel. 4.6 software (Zeiss). Data were processed in Adobe Photoshop CS2 and figures were created in Adobe Illustrator CS2.

Western blot

Frozen tissue samples were homogenized in modified RIPA buffer (150 mM NaCl/50 mM Tris-HCl pH 7.4/1 mM EDTA/1 mM PMSF/1 × Protease Inhibitor Cocktail Complete® EDTA free (Roche, Basel, Switzerland) using Precellys 24 homogenizer (PeqLab Biotechnology, Erlangen, Germany) and incubated for 2 h at 4ºC with 1% TritonX-100/ 0.1% SDS. Lysates were centrifuged at 15 000 *g* for 1 min, diluted in protein sample buffer and cooked for 5 min at 96ºC.

Cells were lysed directly in the culture dish using standard protein sample buffer and cooked for 5 min 96ºC. SDS-PAGE and immunoblotting of cell lysates and homogenized frozen tissue samples was performed according to standard protocols, using antibodies listed in Supplemental table 2.

Semi-quantitative and quantitative real time PCR

Total RNA was isolated from muscle tissue and cultured cells using TRIzol® reagent (Invitrogen, Carlsbad, CA, USA) or RNeasy® Plus Micro Kit (Quiagen, Hilden, Germany). cDNA was synthesized by First Strand cDNA Synthesis Kit for RT-PCR (Roche) according to manufacturers' instructions and specific sequences were subsequently amplified using either Go Taq Green Master Mix (Promega, Madison, WI, USA) for semi-quantitative PCR or MESA GREEN qPCR MasterMix Plus for SYBR Assay I TTP (Eurogentec, Liege, Belgium) for quantitative PCR, and primers listed in Supplemental Table 3. Data were documented using UVP Gel Doc-It TS Imaging System and Mastercycler® ep realplex (Eppendorf, Hamburg, Germany) respectively and processed by Adobe Photoshop CS2 or Microsoft Excel XP. Endogenous levels of either *GAPDH* (semi-qPCR) or *Hprt* (qPCR) were used for data normalization according to Pfaffl method (39).

Flow cytometry

Myofibre-associated cells were isolated from mouse front and hind limb muscles (EDL, TA, quadriceps, gastrocnemius, soleus, and triceps brachii) according to the two-step enzymatic digestion protocol (12) and stained on ice for 30 min in 2% FCS/ PBS containing anti-CD45, anti-Sca1, anti-Mac1, anti-CXCR4 and anti-β-integrin antibody cocktail. A list of used antibodies and their suppliers can be found in the Supplemental Table 2. The number of $CD45^-Sca1^-Mac1^-CXCR4^+\beta_1\text{-intergin}^+$ cells within the parent $CD45^-Sca1^-Mac1^-$ population of the particular sample was determined using FASCAria equipped with DIVA acquisition software (BD Biosciences, San Jose, CA, USA).

Primary myoblast isolation

For primary myoblast culture, de-skinned front and hind limbs of neonatal mice (2 days old) were isolated and incubated for 1.5 hours in 0.2% collagenase I (Gibco)/DMEM solution at 37ºC. Single muscle fibres were released by gentle trituration, collected in fresh DMEM and spun at 15 *g* for 3 min. The pellets were subsequently washed twice in PBS (2 × 3 min at 15 *g*) and re-suspended in DMEM to allow fibre aggregates to settle down by gravity for 1 min. Single fibres remaining in the supernatant were pelleted (5 min at 50 *g*), collected in plating medium (20%FCS / 10% horse serum / 1% chicken embryo extract / DMEM / 50 U/ml Penicillin / 50 µg/ml Streptomycin) and

plated on Matrigel™ (BD Bioscience) coated dishes. 48 hours later outgrowing cells were collected in proliferation medium (20% FCS / 2.5 ng/ml basic FGF / Hams' F-10 / Pen-Strep), pre-plated on plastic Petri dishes for 2 hours to get rid of the contaminating fibroblasts and transferred to collagen coated dishes. Cells were maintained in a humidified atmosphere containing 5% CO_2 at 37ºC. To induce muscle differentiation, proliferation medium was substituted by DMEM containing 5% horse serum containing penicillin and streptomycin.

GeneChip expression analysis

Primary myoblasts were isolated from three independent *Lap2α*$^{+/+}$ and *Lap2α*$^{-/-}$ littermate couples and expanded in culture for one week. Total RNA from proliferating cells was isolated with TRIzol reagent (Invitrogen) according to manufacturers' instructions and quality-tested on Agilent 2100 Bioanalyzer using RNA 6000 Nano chips (Agilent Technologies, Santa Clara, CA, USA). All kits and equipment in the subsequent steps were purchased from Affymetrix (Santa Clara, CA, USA). Double-stranded cDNA and the complementary cRNA were synthesized with GeneChip Expression 3' Amplification One-Cycle Target Labelling Kit following protocols provided in the kit. GeneChip Hybridization, Wash, and Stain Kit as well as Fluidics 450 Station were used for hybridization of high quality cRNA samples to Mouse Genome 430 2.0 Arrays for 16 h at 45 ºC with constant rotation at 60 rpm. Scanning of the chips and quality control parameter assessment were done using GeneChip 3000 Scanner and Affymetrix GCOS software respectively. Microarray data were deposited in the public ArrayExpress repository (http://www.ebi.ac.uk/microarray-as/ae/; accession number E-MEXP-2200).

GeneChip data analysis and statistical procedures

Data were analyzed using Bioconductor 2.01 (http://www.bioconductor.org) and R 2.7.0 software (40). Raw cell files were used for quantile normalization and generation of probe set signal intensities applying *gcrma* algorithm (41). *Gcrma* metrics was used for gene expression quantification. After exclusion of probe sets with low expression values (signal log2< 5 in >50 % of all arrays), statistical analysis was done on 18713 probe sets using the "CyberT" *t*-test based on Bayesian standard deviation estimation as previously described (42). For the final list of genes differentially expressed between *Lap2α*$^{+/+}$ and *Lap2α*$^{-/-}$ myoblasts, a nominal significance level of $P < 0.05$ (Bayes *t*-test) was used. Probe set annotations, biological information of genes and gene ontology data were retrieved from the NetAffx Analysis Center (43). All probe set information provided in this paper is as of March 23 2009.

Muscle injury

Induction and maintenance of anaesthesia during the procedure was achieved by administration of 5% and 2% isoflurane/O_2 mixture, respectively. For analgesia, 15 mg/kg body weight of piritramid was injected subcutaneously before surgery and added to the drinking water during the regeneration phase (1μg/g of body weight/ml/day). The right soleus was surgically exposed and 10 μl of 0.74 mM notexin solution (*Notechis scutatus scutatus*; Latoxan, Valence, France) was injected

into the mid belly of the muscle. The contra-lateral muscle served as uninjured control during the regeneration process. Mice were sacrificed at day 0, 2, 4, 8 and 12 days after injury and the efficiency of regeneration was assessed by histology and immunofluorescence. The size of total damaged area and the corresponding embryonic $MyHC^+$ positive fibres were measured on five transverse muscle sections of each mouse obtained from fixed positions in the soleus mid belly using AxioVision Rel. 4.5 software. Fibrotic index was calculated according to the equation FI = (1-(total $EMyHC^+$ fibre area/total damaged area)) × 100%.

Statistical analysis

Data were analyzed either by ANOVA (followed by Boniferroni post hoc test for multiple comparisons), or paired Students't-test where appropriate using Microsoft Excel XP. $P<0.05$ was considered significant. Data are presented as mean ± standard error (SE) and n represents the sample size.

Supplementary information is available at Cell Death and Differentiation website

Acknowledgements

The authors would like to thank Thomas Sauer (MFPL) for performing FACS analysis, Josef Gotzmann, PhD (MFPL), Nana Naetar, PhD (MFPL) and Reginald Bittner, MD (Center of Anatomy & Cell Biology, Medical University Vienna) for scientific discussions.

The *Mck-Cre*$^{+}$ mouse line used in this study was kindly provided by Ronald C. Kahn, Department of Medicine, Joslin Diabetes Center, Boston MA and *Mdx* mice were a generous gift of Reginald Bittner, Medical University Vienna.

The monoclonal antibodies used in the study, developed by Helen M. Blau, Atsushi Kawakami, Woodring E. Wright and Donald A. Fischman were obtained from the Developmental Studies Hybridoma Bank developed under the auspices of the NICHD and maintained by the University of Iowa, Department of Biological Sciences, Iowa City, IA 52242.

Funding

This work was supported by grants from the Austrian Science Research Fund [grant number FWF P17871] and the EURO-Laminopathies research project of the European Commission [Contract LSHM-CT-2005-018690] to RF. The funders had no role in study design, data collection and analysis, decision to publish, or preparation of the manuscript.

Author contributions: IG and RF conceived and designed the experiments. IG, WMS, KB, ML, JB and RS performed the analyses. IG, WMS and RF analyzed the data and wrote the paper. CLS critically reviewed the manuscript.

Competing Interest

None.

References

1. Jaalouk DE, Lammerding J Mechanotransduction gone awry. Nat Rev Mol Cell Biol. 2009; 10: 63-73
2. Worman HJ, Bonne G "Laminopathies": a wide spectrum of human diseases. Exp Cell Res. 2007; 313: 2121-2133
3. Gotzmann J, Foisner R A-type lamin complexes and regenerative potential: a step towards understanding laminopathic diseases? Histochem Cell Biol. 2006; 125: 33-41
4. Peault B, Rudnicki M, Torrente Y, Cossu G, Tremblay JP, Partridge T, et al Stem and progenitor cells in skeletal muscle development, maintenance, and therapy. Mol Ther. 2007; 15: 867-877
5. Sartorelli V, Caretti G Mechanisms underlying the transcriptional regulation of skeletal myogenesis. Curr Opin Genet Dev. 2005; 15: 528-535
6. Naetar N, Korbei B, Kozlov S, Kerenyi MA, Dorner D, Kral R, et al Loss of nucleoplasmic LAP2alpha-lamin A complexes causes erythroid and epidermal progenitor hyperproliferation. Nat Cell Biol. 2008; 10: 1341-1348
7. Berger R, Theodor L, Shoham J, Gokkel E, Brok-Simoni F, Avraham KB, et al The characterization and localization of the mouse thymopoietin/lamina-associated polypeptide 2 gene and its alternatively spliced products. Genome Res. 1996; 6: 361-370
8. Vlcek S, Korbei B, Foisner R Distinct functions of the unique C terminus of LAP2alpha in cell proliferation and nuclear assembly. J Biol Chem. 2002; 277: 18898-18907
9. Bradley CM, Jones S, Huang Y, Suzuki Y, Kvaratskhelia M, Hickman AB, et al Structural basis for dimerization of LAP2alpha, a component of the nuclear lamina. Structure. 2007; 15: 643-653
10. Dorner D, Vlcek S, Foeger N, Gajewski A, Makolm C, Gotzmann J, et al Lamina-associated polypeptide 2alpha regulates cell cycle progression and differentiation via the retinoblastoma-E2F pathway. J Cell Biol. 2006; 173: 83-93
11. Taylor MR, Slavov D, Gajewski A, Vlcek S, Ku L, Fain PR, et al Thymopoietin (lamina-associated polypeptide 2) gene mutation associated with dilated cardiomyopathy. Hum Mutat. 2005; 26: 566-574
12. Cerletti M, Jurga S, Witczak CA, Hirshman MF, Shadrach JL, Goodyear LJ, et al Highly efficient, functional engraftment of skeletal muscle stem cells in dystrophic muscles. Cell. 2008; 134: 37-47
13. Le Grand F, Rudnicki MA Skeletal muscle satellite cells and adult myogenesis. Curr Opin Cell Biol. 2007; 19: 628-633
14. Gayraud-Morel B, Chretien F, Flamant P, Gomes D, Zammit PS, Tajbakhsh S A role for the myogenic determination gene Myf5 in adult regenerative myogenesis. Dev Biol. 2007; 312: 13-28

15. Cornelison DD, Filla MS, Stanley HM, Rapraeger AC, Olwin BB Syndecan-3 and syndecan-4 specifically mark skeletal muscle satellite cells and are implicated in satellite cell maintenance and muscle regeneration. Dev Biol. 2001; 239: 79-94
16. Staquicini FI, Dias-Neto E, Li J, Snyder EY, Sidman RL, Pasqualini R, et al Discovery of a functional protein complex of netrin-4, laminin gamma1 chain, and integrin alpha6beta1 in mouse neural stem cells. Proc Natl Acad Sci U S A. 2009; 106: 2903-2908
17. Fischer A, Gessler M Delta-Notch--and then? Protein interactions and proposed modes of repression by Hes and Hey bHLH factors. Nucleic Acids Res. 2007; 35: 4583-4596
18. Bryson-Richardson RJ, Currie PD The genetics of vertebrate myogenesis. Nat Rev Genet. 2008; 9: 632-646
19. Buckingham M Myogenic progenitor cells and skeletal myogenesis in vertebrates. Curr Opin Genet Dev. 2006; 16: 525-532
20. Capanni C, Del Coco R, Squarzoni S, Columbaro M, Mattioli E, Camozzi D, et al Prelamin A is involved in early steps of muscle differentiation. Exp Cell Res. 2008; 314: 3628-3637
21. Li H, Capetanaki Y Regulation of the mouse desmin gene: transactivated by MyoD, myogenin, MRF4 and Myf5. Nucleic Acids Res. 1993; 21: 335-343
22. Stedman HH, Sweeney HL, Shrager JB, Maguire HC, Panettieri RA, Petrof B, et al The mdx mouse diaphragm reproduces the degenerative changes of Duchenne muscular dystrophy. Nature. 1991; 352: 536-539
23. Bassel-Duby R, Olson EN Signaling pathways in skeletal muscle remodeling. Annu Rev Biochem. 2006; 75: 19-37
24. Rafael JA, Nitta Y, Peters J, Davies KE Testing of SHIRPA, a mouse phenotypic assessment protocol, on Dmd(mdx) and Dmd(mdx3cv) dystrophin-deficient mice. Mamm Genome. 2000; 11: 725-728
25. Bruning JC, Michael MD, Winnay JN, Hayashi T, Horsch D, Accili D, et al A muscle-specific insulin receptor knockout exhibits features of the metabolic syndrome of NIDDM without altering glucose tolerance. Mol Cell. 1998; 2: 559-569
26. Espada J, Varela I, Flores I, Ugalde AP, Cadinanos J, Pendas AM, et al Nuclear envelope defects cause stem cell dysfunction in premature-aging mice. J Cell Biol. 2008; 181: 27-35
27. Scaffidi P, Misteli T Lamin A-dependent misregulation of adult stem cells associated with accelerated ageing. Nat Cell Biol. 2008; 10: 452-459
28. Melcon G, Kozlov S, Cutler DA, Sullivan T, Hernandez L, Zhao P, et al Loss of emerin at the nuclear envelope disrupts the Rb1/E2F and MyoD pathways during muscle regeneration. Hum Mol Genet. 2006; 15: 637-651
29. Asakura A, Hirai H, Kablar B, Morita S, Ishibashi J, Piras BA, et al Increased survival of muscle stem cells lacking the MyoD gene after transplantation into regenerating skeletal muscle. Proc Natl Acad Sci U S A. 2007; 104: 16552-16557
30. Megeney LA, Kablar B, Garrett K, Anderson JE, Rudnicki MA MyoD is required for myogenic stem cell function in adult skeletal muscle. Genes Dev. 1996; 10: 1173-1183

31. Rudnicki MA, Braun T, Hinuma S, Jaenisch R Inactivation of MyoD in mice leads to up-regulation of the myogenic HLH gene Myf-5 and results in apparently normal muscle development. Cell. 1992; 71: 383-390
32. White JD, Scaffidi A, Davies M, McGeachie J, Rudnicki MA, Grounds MD Myotube formation is delayed but not prevented in MyoD-deficient skeletal muscle: studies in regenerating whole muscle grafts of adult mice. J Histochem Cytochem. 2000; 48: 1531-1544
33. Bakay M, Wang Z, Melcon G, Schiltz L, Xuan J, Zhao P, et al Nuclear envelope dystrophies show a transcriptional fingerprint suggesting disruption of Rb-MyoD pathways in muscle regeneration. Brain. 2006; 129: 996-1013
34. Hughes SM, Koishi K, Rudnicki M, Maggs AM MyoD protein is differentially accumulated in fast and slow skeletal muscle fibres and required for normal fibre type balance in rodents. Mech Dev. 1997; 61: 151-163
35. Potthoff MJ, Wu H, Arnold MA, Shelton JM, Backs J, McAnally J, et al Histone deacetylase degradation and MEF2 activation promote the formation of slow-twitch myofibers. J Clin Invest. 2007; 117: 2459-2467
36. Meshorer E, Gruenbaum Y Gone with the Wnt/Notch: stem cells in laminopathies, progeria, and aging. J Cell Biol. 2008; 181: 9-13
37. Arimura T, Helbling-Leclerc A, Massart C, Varnous S, Niel F, Lacene E, et al Mouse model carrying H222P-Lmna mutation develops muscular dystrophy and dilated cardiomyopathy similar to human striated muscle laminopathies. Hum Mol Genet. 2005; 14: 155-169
38. Mittelbronn M, Hanisch F, Gleichmann M, Stotter M, Korinthenberg R, Wehnert M, et al Myofiber degeneration in autosomal dominant Emery-Dreifuss muscular dystrophy (ADEDMD) (LGMD1B). Brain Pathol. 2006; 16: 266-272
39. Pfaffl MW A new mathematical model for relative quantification in real-time RT-PCR. Nucleic Acids Res. 2001; 29: e45
40. Gentleman RC, Carey VJ, Bates DM, Bolstad B, Dettling M, Dudoit S, et al Bioconductor: open software development for computational biology and bioinformatics. Genome Biol. 2004; 5: R80
41. Wu Z, Irizarry RA, R. G, F. M-M, F. S A model-based background adjustment for oligonucleotide expression arrays. Journal of the American Statistical Association. 2004; 99: 909-917
42. Baldi P, Long AD A Bayesian framework for the analysis of microarray expression data: regularized t -test and statistical inferences of gene changes. Bioinformatics. 2001; 17: 509-519
43. Liu G, Loraine AE, Shigeta R, Cline M, Cheng J, Valmeekam V, et al NetAffx: Affymetrix probesets and annotations. Nucleic Acids Res. 2003; 31: 82-86

Titles and legends to figures

Figure 1 Absence of LAP2α in mice causes deregulation of the muscle stem cell pool. (**a**) Immunostainig of isolated satellite cells reveals LAP2α expression in Pax7-positive cells (bar = 20 µm). (**b**) Flow cytometric analysis of skeletal muscle tissue shows an increase in the number of myofibre-associated $CD45^-Sca1^-Mac1^-$ and $CXCR4^+\beta_1$-$integrin^+$ (CSM4B) cells within the parent $CD45^-Mac1^-Sca1^-$ satellite cell population in young *Lap2α*$^{-/-}$ mice (aged 10 weeks) compared to their wild type (WT) littermates (n = 5 WT + 6 knockout mice). The number of CSM4B satellite cells in *Lap2α*$^{-/-}$ skeletal muscle levels down to WT values by the age of 6 months (adult mice) and continues to decrease with age at a rate similar to the WT (n = 5 littermate pairs of each age, $p<0.05$ ANOVA for (a) WT young vs. KO young, (b) WT young vs. WT old, (c) KO young vs. KO adult and old; bars represent standard error (SE)).

Figure 2 Loss of LAP2α in primary myoblasts predominantly causes downregulation of genes. Volcano plot of genes differentially expressed in proliferating *Lap2α*$^{-/-}$ and WT primary myoblasts shows that only a small number of genes other than *Lap2* itself is affected by the loss of LAP2α.

Figure 3 *Lap2α*$^{-/-}$ myoblasts exhibit delayed differentiation. Protein (**a**) and mRNA (**b**) analyses of sequentially expressed differentiation markers in LAP2α-deficient cells show delayed myoblast differentiation. The increase in Pax7 and decrease in MyoD protein levels (upper panels) are followed by the diminished expression of MyoD target genes and myogenic interaction partners such as MEF2c, desmin and myosin heavy chain (MyHC), as well as upregulation of the alternative basic myogenic factor Myf5 (lower panels). In contrast, the expression level of lamin A/C, the major binding partner of LAP2α, is not altered (upper panels). (**c**) Although *Lap2α*$^{-/-}$ myoblasts were able to differentiate into myotubes (left panels; bright field images, bar = 100 µm), immunostaining of differentiating myoblasts shows a slight delay in the expression of myosin heavy chain (right panels; confocal images, bar = 20 µm). Data were normalized to endogenous levels of actin in Western blot, and the housekeeping gene *Hprt* (Hypoxanthine-Guanine Phosphoribosyl Transferase) according to the Pfaffl method (39) in quantitative PCR analyses. WT mRNA levels at different time points were compared to the Day0 stage and each knockout sample was normalized to its corresponding WT time point (error bars represent SE of the WT/KO ratio, *$p<0.05$ ANOVA). Means of 3-4 independent experiments are shown.

Figure 4 *Lap2α*$^{-/-}$ mice exhibit normal skeletal muscle regeneration**.** (**a**) H & E staining (Haematoxylin and eosin; left panels) and immunofluorescence analysis of notexin-injured LAP2α-deficient skeletal muscle, using embryonic MyHC (EMyHC – red) antibody (right panels), showing normal *in vivo* muscle regeneration in *Lap2α*$^{-/-}$ mice (bar = 20 µm). (**b**) The efficiency of muscle regeneration quantified at day 4 post injury by measuring the size of embryonic MyHC-containing myofibres within the damaged region and calculating the corresponding fibrotic indexes (n = 4

littermate pairs of each age; p<0.05 ANOVA for (a) young vs. old knockout mice, bars represent SE).

Figure 5 Absence of LAP2α in mice promotes fast myofibre phenotype in predominantly slow muscles. Soleus muscle of *Lap2α*$^{-/-}$ mice, (**a**) immunostained with anti-slow MyHC antibody (type I – depicted in brown, bar = 50 μm), reveals a myofibre shift towards faster phenotypes (**b**), without a change in fibre size distribution (**c**) (n = 8 littermate pairs, *p<0.05, ANOVA, bars represent SE).

Figure 6 LAP2α is required during initial phases of myoblast differentiation as well as adult muscle remodelling. (**a**) Semi-quantitative PCR analysis of cell and tissue lysates showing a downregulation of LAP2α in the presence of MCK and Cre recombinase, which, in contrast to adult skeletal muscle, are not expressed in proliferating myoblasts and non-muscle tissues such as spleen. (Samples were normalized to endogenous levels of GAPDH). (**b**) CD45$^-$Sca1$^-$Mac1$^-$ CXCR4$^+$β$_1$-integrin$^+$ (CSM4B) muscle fibre-associated satellite cell numbers in *Lap2α*$^{Neo\text{-}fl/Neo\text{-}fl}$*/Mck-Cre*$^+$ mice are similar to WT at all ages. (FACS analysis of whole muscle digests, n = 5 littermate pairs of each age; p<0.05 ANOVA for (a) young vs. old *Lap2α*$^{Neo\text{-}fl/Neo\text{-}fl}$*/Mck-Cre*$^+$ mice, bars represent SE). (**c**) Bright field images of *Lap2α*$^{Neo\text{-}fl/Neo\text{-}fl}$*/Mck-Cre*$^+$ myoblasts showing a lag at day 3 of the *in vitro* muscle differentiation (bar = 100 μm). (**d**) As a consequence of *Mck* promoter activation and Cre recombinase expression, LAP2α mRNA levels do not increase during differentiation in *Lap2α*$^{Neo\text{-}fl/Neo\text{-}fl}$*/Mck-Cre*$^+$ myoblasts, causing a delay in the expression of MyHC. Due to high variability in Cre recombinase expression and the consecutive substantial variation in LAP2α levels, which hindered the statistical analysis of qPCR data, representative images from 3 separate experiments are shown. Data were analyzed as described in Figure 3. (**e**) Quantification of muscle tissue sections immunostained with anti-type I and anti-type II (a + x/d) MyHC-specific antibodies showing a myofibre shift towards an intermediate (type I and type II (a, x/d) negative) phenotype in *Lap2α*$^{Neo\text{-}fl/Neo\text{-}fl}$*/Mck-Cre*$^+$ soleus muscle. (n = 3 littermate pairs, *p<0.05, paired Students' t-test, bars represent SE).

Table 1 Changes in gene expression associated with LAP2α loss in primary mouse myoblasts – selected GO-enriched microarray candidates.

Category	Gene Symbol	Probe Set ID	Name/GO-annotation	Fold change	p value (BayesT)	Validation
Nuclear structure						
	Tmpo (α isoform)	1428976_at	lamina-associated polypeptide 2a	-203.53	0.00004	[1]RT/qRT/Ab
		1421237_at		-12.53	0.0004	[1]RT/qRT/Ab
	Tmpo (β, γ, δ, ε)	1426349_s_at	lamina-associated polypeptide	1.80	0.003	-
		1452036_a_at		1.60	0.004	-
	Lmna	1425472_a_at	lamin A	-1.50	0.01	-
	Syne1	1421545_a_at	synaptic nuclear envelope 1	-2.00	0.01	-
Muscle stem cell determinants						
	Myf5	1420757_at	myogenic factor 5	1.70	0.04	[1]RT/qRT
	Pax7	1444596_at	paired box gene 7	1.60	0.05	[1]RT/qRT
	Sdc4	1448793_a_at	syndecan 4	3.10	0.0006	-
Cell signaling pathways						
	Pdgfra	1421917_at	*PDGF signaling*	-1.60	0.006	-
		1438946_at	marker for paraxial mesoderm derived ES cells with muscle regeneration potential	-1.50	0.03	-
	Gja1	1415801_at	gap junction protein, alpha 1;connexin protein family	-1.50	0.009	
	Grem1	1425357_a_at	gremlin 1; *sonic hedgehog signaling;BMP4 signaling*	-1.80	0.01	-
	Prrx1	1425526_a_at	paired related homeobox 1 *FGF, sonic hedgehog signaling*	-1.60	0.02	-
	Hey1	1415999_at	hairy/enhancer-of-split related with YRPW motif 1; *Notch signaling*	1.80	0.03	[1]RT
	Igf2r	1424112_at	insulin-like growth factor 2 receptor	-1.50	0.03	-
	Map3k2	1438719_at	mitogen-activated protein kinase kinase kinase 2	-1.50	0.04	-
Extracellular matrix						
	Capg	1450355_a_at	capping protein (actin filament), gelsolin-like	-1.40	0.02	-
	Coch	1423285_at	coagulation factor C homolog (*Limulus polyphemus*)	-9.00	0.04	-
	Col12a1	1434411_at	collagen, type XII, alpha 1	-1.70	0.02	-
		1427391_a_at		-1.80	0.03	-
	Col5a1	1416740_at	collagen, type V, alpha 1	-1.30	0.04	-
	Ntn4	1450512_at	netrin 4	-8.40	0.01	-
	Pcolce	1448433_a_at	procollagen C-endopeptidase enhancer protein	-1.60	0.01	-
		1437165_a_at		-1.20	0.04	-
	Smoc2	1415935_at	SPARC related modular calcium binding 2	-3.80	0.05	-
	Timp2	1454677_at	tissue inhibitor of metalloproteinase 2	-1.30	0.02	-

[1]RT (semi-quantitative reverse transcriptase PCR), qRT (quantitative reverse transcriptase PCR), Ab (western blot and/or immunofluorescence).

Figure 1

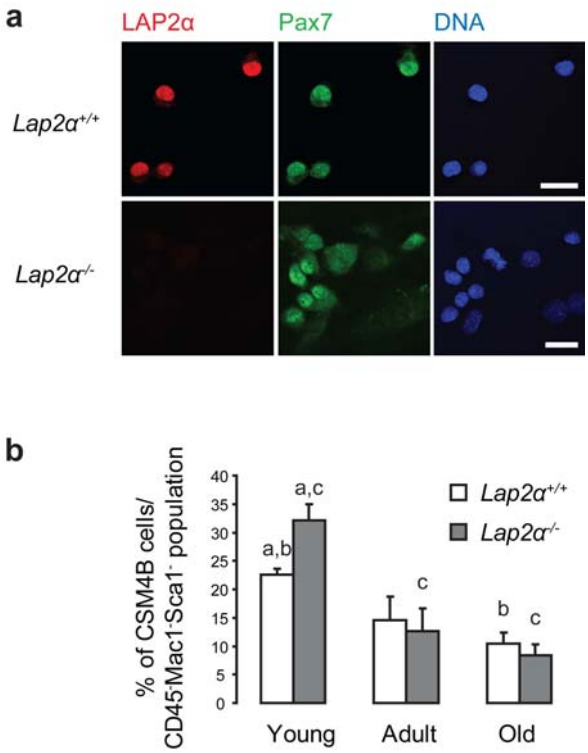
a
LAP2α
Pax7
DNA
Lap2α+/+
Lap2α-/-
b
% of CSM4B cells/ CD45-Mac1-Sca1- population
40
35
30
25
20
15
10
5
0
a,c
a,b
c
b
c
Lap2α+/+
Lap2α-/-
Young
Adult
Old

Figure 2

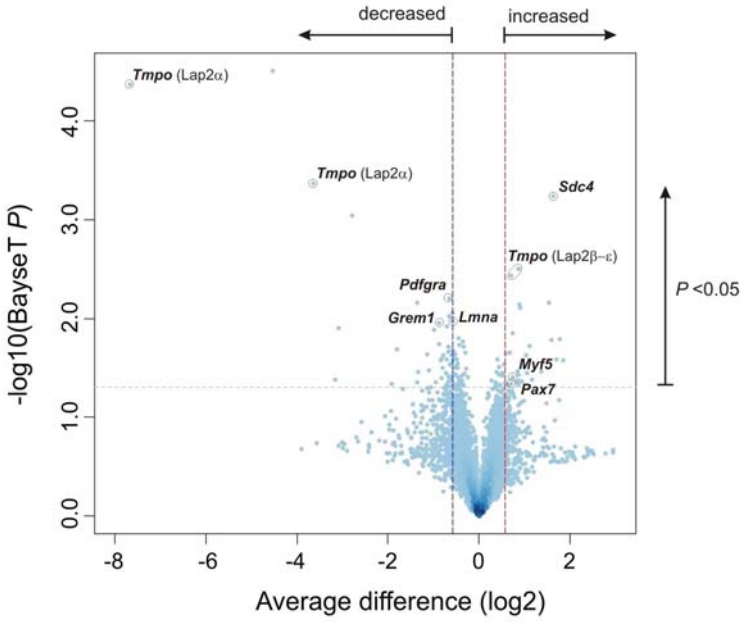
decreased
increased
Tmpo (Lap2α)
Tmpo (Lap2α)
Sdc4
Tmpo (Lap2β–ε)
Pdfgra
Grem1
Lmna
Myf5
Pax7
P <0.05
-log10(BayseT P)
0.0
1.0
2.0
3.0
4.0
-8
-6
-4
-2
0
2
Average difference (log2)

Figure 3

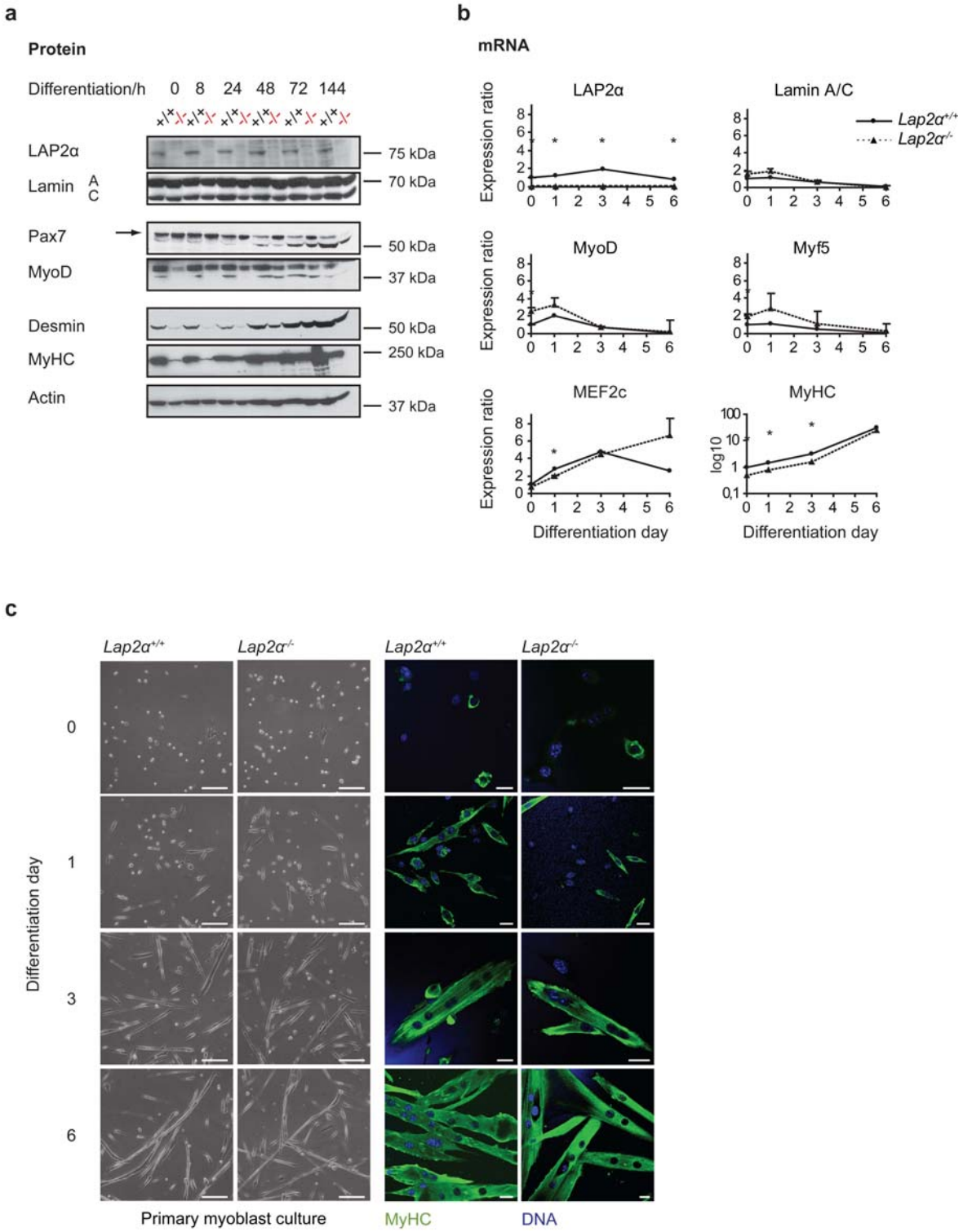
a
Protein
Differentiation/h 0 8 24 48 72 144
LAP2α
Lamin A C
Pax7
MyoD
Desmin
MyHC
Actin
75 kDa
70 kDa
50 kDa
37 kDa
50 kDa
250 kDa
37 kDa
b
mRNA
LAP2α
Lamin A/C
MyoD
Myf5
MEF2c
MyHC
Expression ratio
log10
Lap2α+/+
Lap2α-/-
Differentiation day
c
Lap2α+/+
Lap2α-/-
Differentiation day
0
1
3
6
Primary myoblast culture
MyHC
DNA

Figure 4

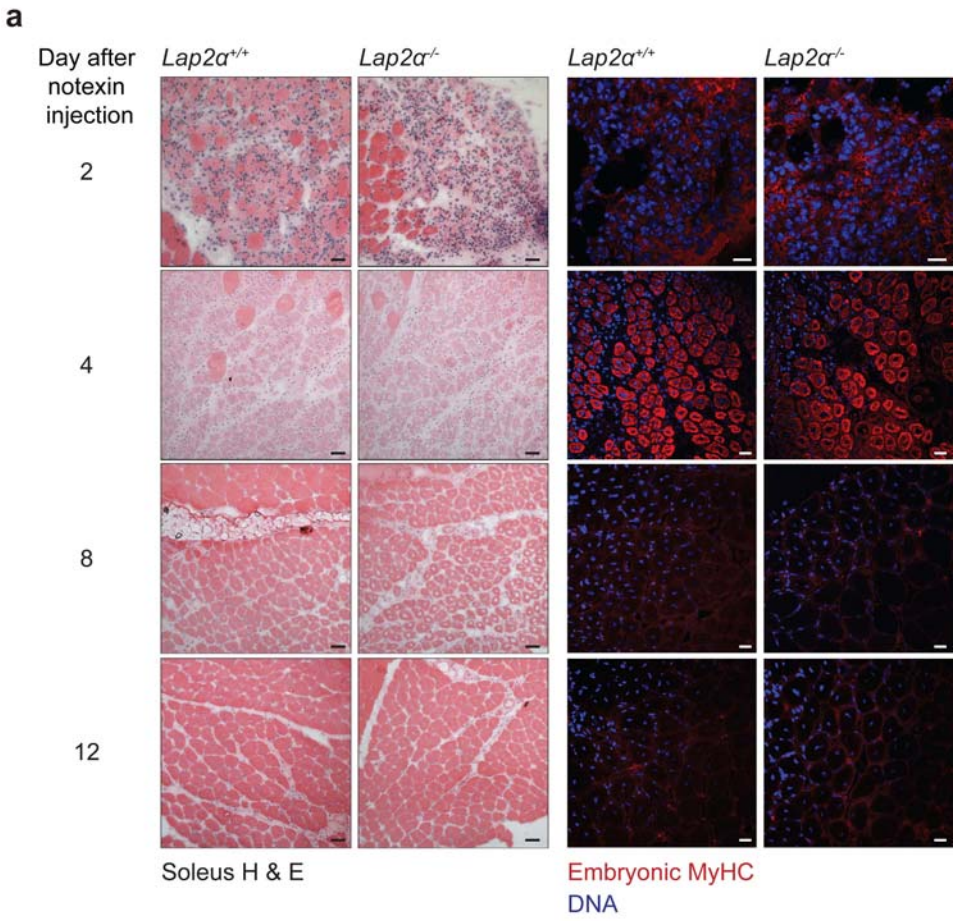
a
Day after notexin injection
Lap2α+/+
Lap2α-/-
Lap2α+/+
Lap2α-/-
2
4
8
12
Soleus H & E
Embryonic MyHC
DNA
b
Fibrotic index/%
100
80
60
40
20
0
a
a
Young
Old
Lap2α+/+
Lap2α-/-

Figure 5

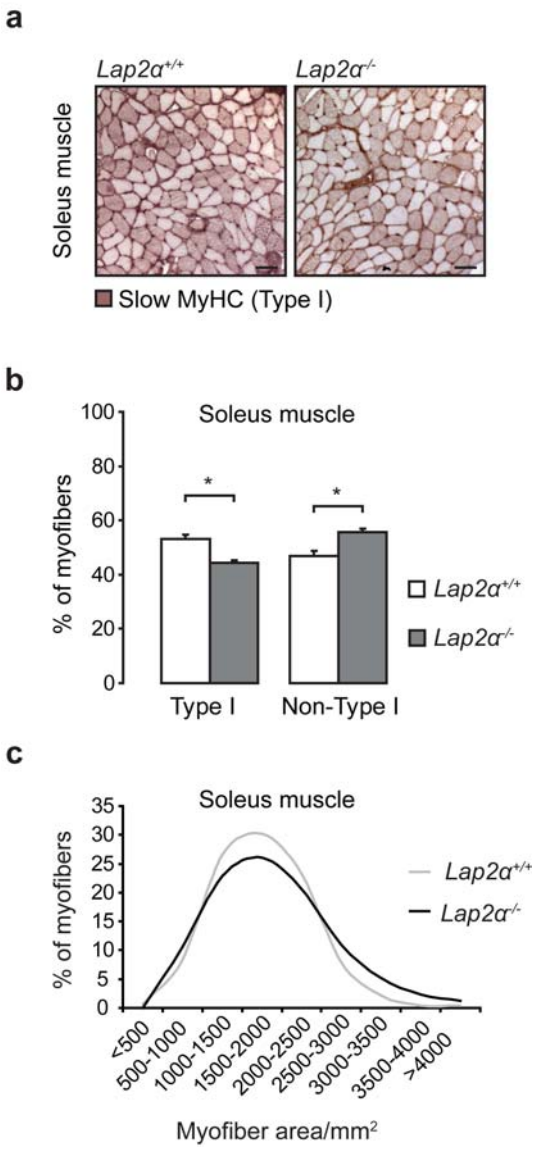
a
Lap2α+/+
Lap2α-/-
Soleus muscle
Slow MyHC (Type I)
b
Soleus muscle
% of myofibers
100
80
60
40
20
0
*
*
Lap2α+/+
Lap2α-/-
Type I
Non-Type I
c
Soleus muscle
% of myofibers
35
30
25
20
15
10
5
0
Lap2α+/+
Lap2α-/-
<500
500-1000
1000-1500
1500-2000
2000-2500
2500-3000
3000-3500
3500-4000
>4000
Myofiber area/mm2

Figure 6

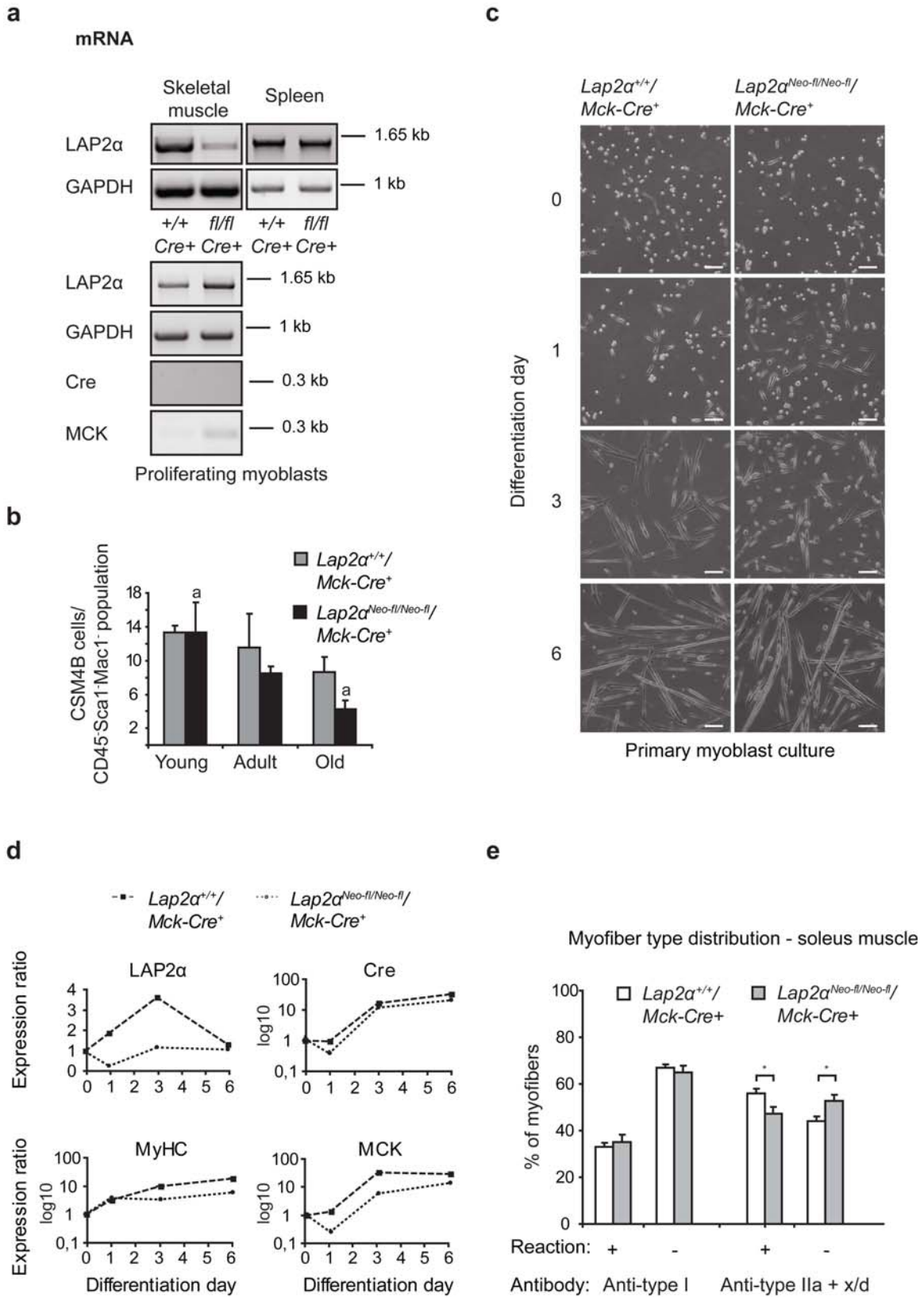
a
mRNA
Skeletal muscle
Spleen
LAP2α
GAPDH
1.65 kb
1 kb
+/+ Cre+
fl/fl Cre+
+/+ Cre+
fl/fl Cre+
LAP2α
GAPDH
Cre
MCK
1.65 kb
1 kb
0.3 kb
0.3 kb
Proliferating myoblasts
b
CSM4B cells/ CD45-Sca1-Mac1- population
Lap2α+/+/ Mck-Cre+
Lap2αNeo-fl/Neo-fl/ Mck-Cre+
Young
Adult
Old
c
Lap2α+/+/ Mck-Cre+
Lap2αNeo-fl/Neo-fl/ Mck-Cre+
Differentiation day
Primary myoblast culture
d
Lap2α+/+/ Mck-Cre+
Lap2αNeo-fl/Neo-fl/ Mck-Cre+
LAP2α
Cre
MyHC
MCK
Expression ratio
log10
Differentiation day
e
Myofiber type distribution - soleus muscle
Lap2α+/+/ Mck-Cre+
Lap2αNeo-fl/Neo-fl/ Mck-Cre+
% of myofibers
Reaction:
Antibody:
Anti-type I
Anti-type IIa + x/d

Supplemental Figure 1

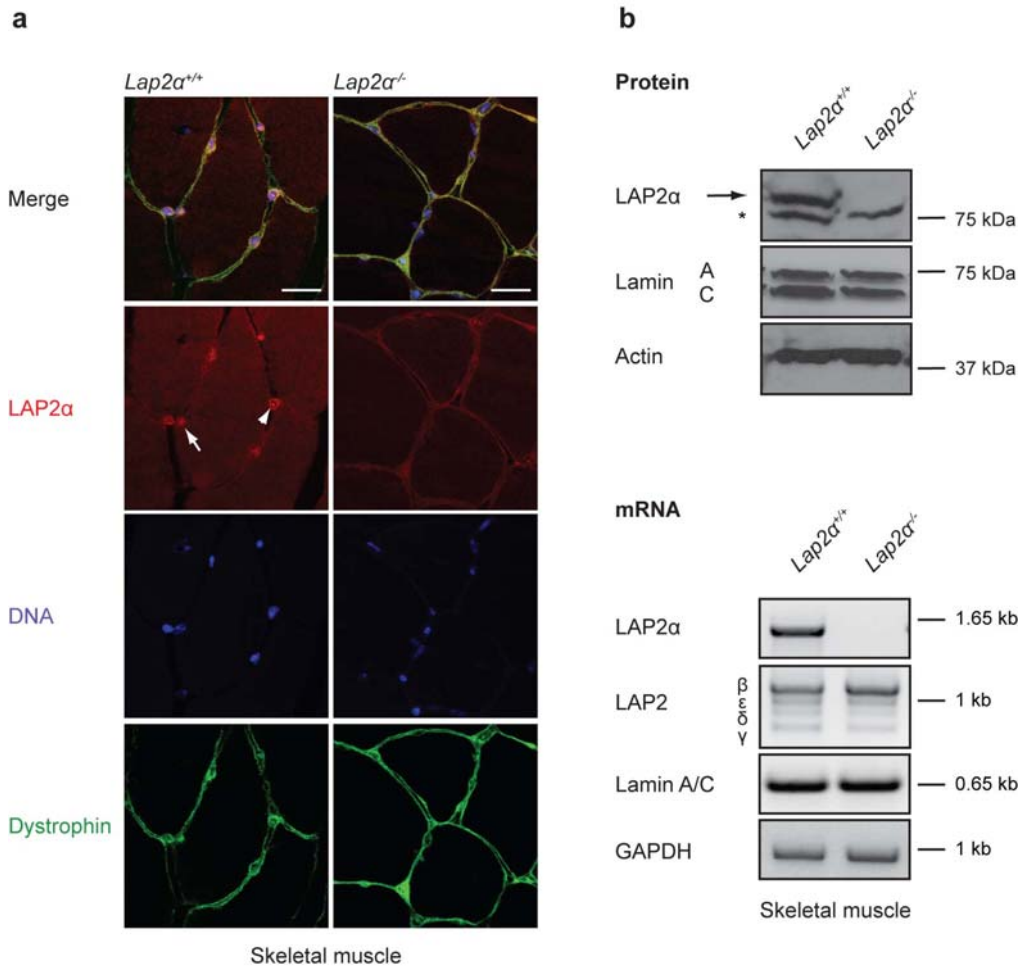

Supplemental Figure 2

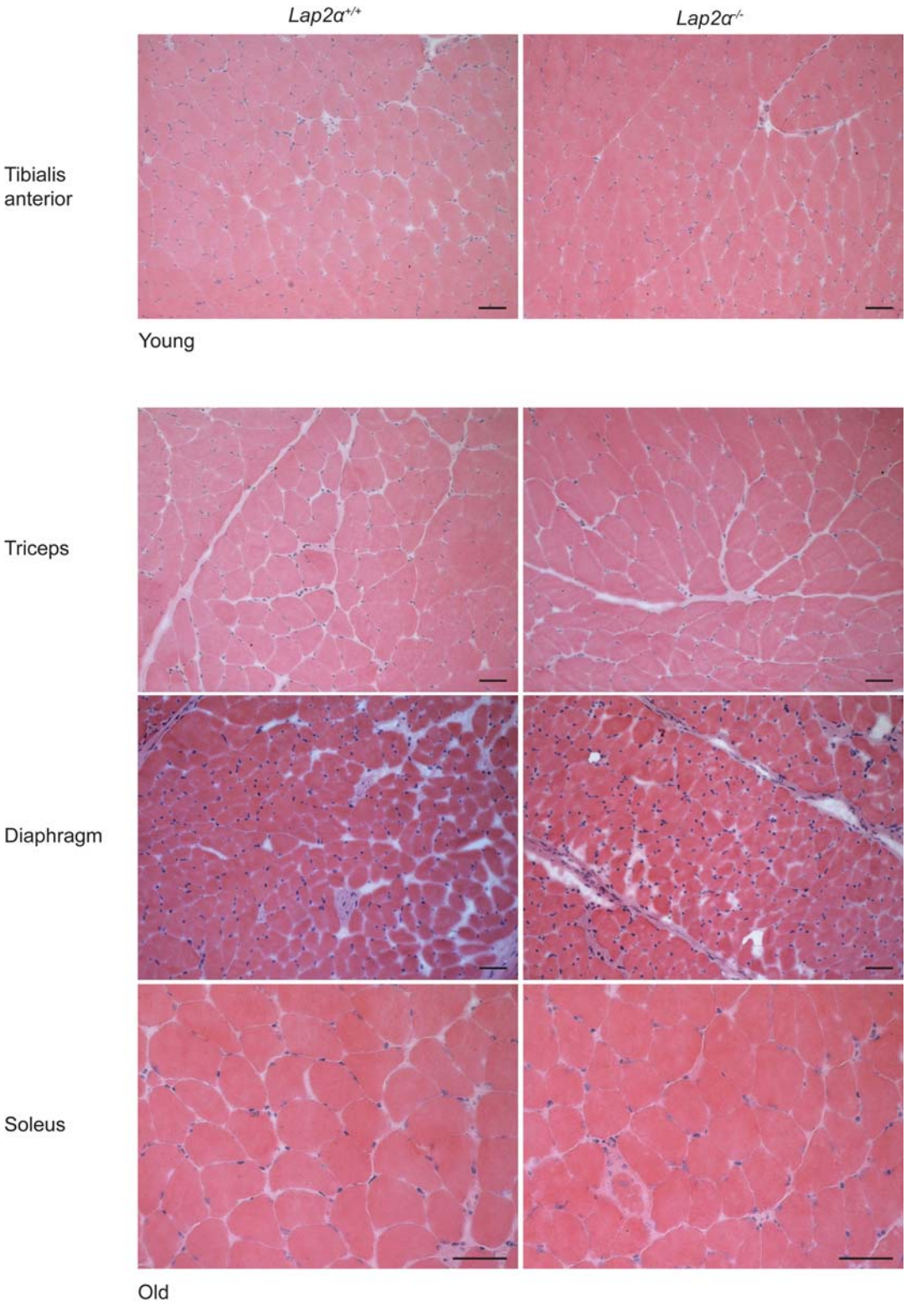

Supplemental Figure 3

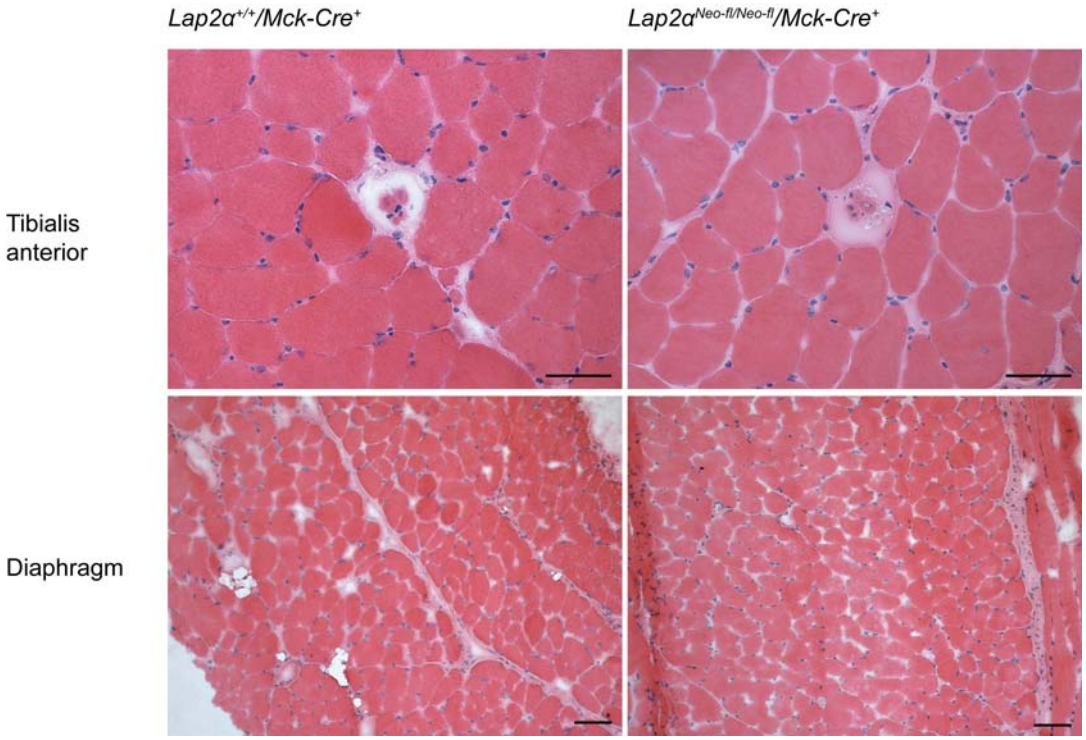

Titles and Legends to Supplemental Figures

Supplemental Figure 1 Skeletal muscle tissue of *Lap2α*$^{-/-}$ mice does not express the α-specific *Lap2* isoform. (**a**) LAP2α is present in nuclei of postmitotic *Lap2α*$^{+/+}$ skeletal myofibres (arrow) and muscle interstitial cells (arrow head) and absent from muscle tissue of *Lap2α*$^{-/-}$ mice, as shown by immunostaining of transverse muscle sections (bar = 20 µm). (**b**) Western blot (upper panels) and semi-quantitative RT-PCR (lower panels) analyses of skeletal muscle tissue from *Lap2α*$^{+/+}$ and *Lap2α*$^{-/-}$ mice. Samples were normalized for endogenous levels of actin and GAPDH (Glycerinaldehyde-3-phosphate-Dehydrogenase), respectively. (* unspecific band appearing in striated muscle tissue lysates)

Supplemental Figure 2 Absence of dystrophic changes in *Lap2α*$^{-/-}$ skeletal muscle. H & E stained transverse muscle sections of young (TA, upper panel) and old mice (lower panels), show no overt dystrophic muscle phenotype (bar = 50 µm).

Supplemental Figure 3 *Lap2α*$^{Neo\text{-}fl/Neo\text{-}fl}$*/Mck-Cre*$^{+}$ mice do not exhibit an overt skeletal muscle phenotype. H & E stained skeletal muscle sections (bar = 50 µm).

Supplemental Table 1 Changes in gene expression induced by LAP2α loss in primary mouse myoblasts.

Symbol	Probe Set ID	Name	Fold change	*p* value (Bayes T)
---	1446130_at	---	-23,17241	3,09969E-05
Tmpo	1428976_at	thymopoietin	-203,5333	4,28991E-05
Tmpo	1421237_at	thymopoietin	-12,53333	0,000430283
Sdc4	1448793_a_at	syndecan 4	3,0819672	0,000572144
---	1439794_at	---	-6,9375	0,000901098
Tmpo	1426349_s_at	thymopoietin	1,8228782	0,003130126
Tmpo	1452036_a_at	thymopoietin	1,6117424	0,003680447
Pdgfra	1421917_at	platelet derived growth factor receptor, alpha polypeptide	-1,566667	0,006293655
---	1427086_at	---	-2,580524	0,006892995
---	1456973_at	---	2,9019608	0,006956688
Afap1l1	1454727_at	actin filament associated protein 1-like 1	1,853229	0,00713412
Frmd4b	1438169_a_at	FERM domain containing 4B	1,8588469	0,007759323
Gja1	1415801_at	gap junction protein alpha 1	-1,497354	0,008821696
Oaf	1424086_at	OAF homolog (Drosophila)	-1,585968	0,009516138
Lmna	1425472_a_at	lamin A	-1,504692	0,010691108
Grem1	1425357_a_at	gremlin 1	-1,838122	0,011203551
Pcolce	1448433_a_at	procollagen C-endopeptidase enhancer protein	-1,639439	0,012095208
Ntn4	1450512_at	netrin 4	-8,434783	0,012615054
Syne1	1421545_a_at	synaptic nuclear envelope 1	-1,992063	0,01294275
Pcdhb22	1418941_at	protocadherin beta 22	1,6638655	0,014020096
Bnip3	1422470_at	BCL2/adenovirus E1B interacting protein 3	-1,366605	0,015836859
2900001G08Rik	1430642_at	RIKEN cDNA 2900001G08 gene	3,3953488	0,01630495
---	1457483_at	---	3	0,016374156
Timp2	1454677_at	tissue inhibitor of metalloproteinase 2	-1,27914	0,017249749
Etv3	1418635_at	ets variant gene 3	-1,846667	0,018160353
Capg	1450355_a_at	capping protein (actin filament), gelsolin-like	-1,355938	0,018483491
Zfp40	1435984_at	Zinc finger protein 40	2,1372549	0,019103413
Tpi1	1415918_a_at	triosephosphate isomerase 1	-1,274766	0,019205485
Pcdh19	1444422_at	protocadherin 19	-1,59	0,019473094
Slit3	1452296_at	slit homolog 3 (Drosophila)	-3,504425	0,020602275
Hcfc1r1	1428406_s_at	host cell factor C1 regulator 1 (XPO1-dependent)	-1,493255	0,020736075
Cd248	1417439_at	CD248 antigen, endosialin	-1,472763	0,021241652
Prrx1	1425526_a_at	paired related homeobox 1	-1,602878	0,021633046
---	1441391_at	---	1,5963303	0,021979351
S100a4	1424542_at	S100 calcium binding protein A4	-1,228758	0,022304232

Symbol	Probe Set ID	Name	Fold change	*p* value (Bayes T)
1200009F10Rik	1429219_at	RIKEN cDNA 1200009F10 gene	1,494311	0,022626502
Cspg4	1450944_at	chondroitin sulfate proteoglycan 4	-2,21223	0,022911152
Lrp1	1448655_at	low density lipoprotein receptor-related protein 1	-1,443643	0,023053676
Jmjd3	1456610_at	jumonji domain containing 3	-1,476582	0,023305136
Frmd4b	1452123_s_at	FERM domain containing 4B	2,0530035	0,023471035
Serinc3	1434548_at	serine incorporator 3	-1,52346	0,023654625
Col12a1	1434411_at	collagen, type XII, alpha 1	-1,729354	0,023728149
Pdgfra	1438946_at	platelet derived growth factor receptor, alpha polypeptide	-1,47644	0,025216721
P4ha2	1417149_at	procollagen-proline, 2-oxoglutarate 4-dioxygenase (proline 4-hydroxylase), alpha II polypeptide	-1,453503	0,025242593
Col12a1	1427391_a_at	collagen, type XII, alpha 1	-1,772575	0,025592569
Ly6a	1417185_at	lymphocyte antigen 6 complex, locus A	-1,476317	0,025609628
Pcdh19	1455145_at	protocadherin 19	-1,402029	0,025699572
Pnrc2	1416187_s_at	proline-rich nuclear receptor coactivator 2	1,3205503	0,026027527
Tmem19	1443049_at	Transmembrane protein 19	3,2537313	0,026073708
Vasn	1427894_at	vasorin	-1,646499	0,02616581
---	1442019_at	---	3,6050955	0,026234459
Grb14	1417673_at	growth factor receptor bound protein 14	-1,784638	0,026623827
Igf2r	1424112_at	insulin-like growth factor 2 receptor	-1,488342	0,026914393
Mtdh	1455129_at	Metadherin	-1,377947	0,028602452
Txnip	1415996_at	thioredoxin interacting protein	1,4662872	0,029118375
Plod1	1416289_at	procollagen-lysine, 2-oxoglutarate 5-dioxygenase 1	-1,549333	0,029432255
---	1437199_at	---	-1,407169	0,030006526
Sfrs2ip	1452885_at	splicing factor, arginine/serine-rich 2, interacting protein	-1,486278	0,030832934
Alkbh8	1429521_at	alkB, alkylation repair homolog 8 (E. coli)	1,347355	0,030918852
Tspo	1416695_at	translocator protein	-1,460777	0,031121271
Arid5b /// LOC100044968	1420973_at	AT rich interactive domain 5B (MRF1-like) /// similar to modulator recognition factor 2	-1,752381	0,03151538
Aebp1	1450637_a_at	AE binding protein 1	-1,387579	0,031556012
Fstl1	1448259_at	follistatin-like 1	-1,423422	0,031817203
S100a10	1416762_at	S100 calcium binding protein A10 (calpactin)	-1,211698	0,032123314
Slc5a3	1440227_at	solute carrier family 5 (inositol transporters), member 3	-2,156198	0,03330394

Symbol	Probe Set ID	Name	Fold change	*p* value (Bayes T)
Atp10d	1436544_at	ATPase, class V, type 10D	2,5753425	0,034497037
Hey1	1415999_at	hairy/enhancer-of-split related with YRPW motif 1	1,8009479	0,034497872
Klhl24	1429351_at	kelch-like 24 (Drosophila)	1,306374	0,034671495
2900019G14Rik	1457800_at	RIKEN cDNA 2900019G14 gene	-2,524272	0,034836324
D0H4S114	1436736_x_at	DNA segment, human D4S114	2,0648929	0,035438816
EG545124 /// ENSMUSG00000051559 /// Tdg	1448462_at	predicted gene, EG545124 /// predicted gene, ENSMUSG00000051559 /// thymine DNA glycosylase	1,4324324	0,035734189
Loxl3	1418269_at	lysyl oxidase-like 3	-1,659309	0,03588936
Pi4k2a	1433462_a_at	phosphatidylinositol 4-kinase type 2 alpha	-1,473389	0,036452501
Pcolce	1437165_a_at	procollagen C-endopeptidase enhancer protein	-1,246584	0,036583601
Krit1	1448701_a_at	KRIT1, ankyrin repeat containing	1,3596713	0,037041671
2900024C23Rik	1429503_at	RIKEN cDNA 2900024C23 gene	-1,429896	0,037047549
Irak1	1448668_a_at	interleukin-1 receptor-associated kinase 1	-1,493166	0,037288555
---	1443057_at	---	1,8113208	0,037340928
Map3k2	1438719_at	mitogen-activated protein kinase kinase kinase 2	-1,451499	0,037709723
Col5a1	1416740_at	collagen, type V, alpha 1	-1,296137	0,037850513
Cramp1l	1456042_s_at	Crm, cramped-like (Drosophila)	1,4296081	0,037983815
Nrk	1450079_at	Nik related kinase	-1,603004	0,038746284
Tia1	1416812_at	cytotoxic granule-associated RNA binding protein 1	1,6711864	0,039197992
Ldha	1419737_a_at	lactate dehydrogenase A	-1,181132	0,039207225
Myf5	1420757_at	myogenic factor 5	1,6626263	0,03962744
Hyou1	1423290_at	hypoxia up-regulated 1	-1,771626	0,039723743
Cd99l2	1456746_a_at	CD99 antigen-like 2	-1,371672	0,040017481
Kif1b	1423995_at	kinesin family member 1B	-1,540179	0,040453898
Coch	1423285_at	coagulation factor C homolog (Limulus polyphemus)	-8,955224	0,041289639
LOC100047339	1431004_at	similar to lysyl oxidase-like 2	2,2330189	0,041731884
Glrx3	1456244_x_at	glutaredoxin 3	1,2024408	0,042128606
Elmo2	1436011_at	engulfment and cell motility 2, ced-12 homolog (C. elegans)	-1,5625	0,042219333
Gda	1435748_at	guanine deaminase	1,8252427	0,042557721
Ly6e	1453304_s_at	lymphocyte antigen 6 complex, locus E	-1,296086	0,042567597
Aebp1	1422514_at	AE binding protein 1	-1,51675	0,042636078
Lpar1	1448606_at	lysophosphatidic acid receptor 1	-1,295117	0,042835961

Symbol	Probe Set ID	Name	Fold change	*p* value (Bayes T)
Pfkl	1439148_a_at	phosphofructokinase, liver, B-type	-1,354676	0,043091608
---	1436003_at	---	1,9101796	0,043245586
Sema3c	1429348_at	sema domain, immunoglobulin domain (Ig), short basic domain, secreted, (semaphorin) 3C	-1,588801	0,043433807
Mgst3	1448300_at	microsomal glutathione S-transferase 3	-2,567987	0,044223481
Ivns1abp	1450084_s_at	influenza virus NS1A binding protein	1,2882159	0,044241755
Mtss1	1424826_s_at	metastasis suppressor 1	1,7671756	0,044290716
Prkcdbp	1423771_at	protein kinase C, delta binding protein	-1,937415	0,044299028
Eya1	1457424_at	eyes absent 1 homolog (Drosophila)	1,4739677	0,045147903
Pfkp	1416069_at	phosphofructokinase, platelet	-1,470732	0,045244371
Smoc2	1415935_at	SPARC related modular calcium binding 2	-3,754991	0,045590637
Plec1	1434610_at	plectin 1	-1,34142	0,045747803
Npepps	1417385_at	aminopeptidase puromycin sensitive	-1,392113	0,046026998
Efemp2	1417018_at	epidermal growth factor-containing fibulin-like extracellular matrix protein 2	-1,276237	0,046256814
Pax7	1444596_at	paired box gene 7	1,6151515	0,046331877
---	1444126_at	---	1,5492958	0,04662409
Srpx2	1427919_at	sushi-repeat-containing protein, X-linked 2	1,80937	0,046676924
Kif5b	1418429_at	kinesin family member 5B	1,2824014	0,046715423
Qk	1417073_a_at	quaking	1,3626325	0,04701093
Tmem45a	1422587_at	transmembrane protein 45a	-1,647303	0,0471142
Rbpj	1454896_at	recombination signal binding protein for immunoglobulin kappa J region	-1,270696	0,048120778
Ptprf	1420841_at	protein tyrosine phosphatase, receptor type, F	-1,651934	0,048309123
Gulp1	1453771_at	GULP, engulfment adaptor PTB domain containing 1	-1,412827	0,04869051
Pcdh19	1437360_at	protocadherin 19	-1,548319	0,04900889
Eml1 /// LOC634102	1428321_at	echinoderm microtubule associated protein like 1 /// similar to echinoderm microtubule associated protein like 1	-1,588972	0,049105018
Gadd45a	1449519_at	growth arrest and DNA-damage-inducible 45 alpha	1,2864275	0,049190869
Sned1	1435603_at	sushi, nidogen and EGF-like domains 1	-2,103226	0,049537552
Stk4	1436015_s_at	serine/threonine kinase 4	1,2966867	0,049738307
Pdk1	1423748_at	pyruvate dehydrogenase kinase, isoenzyme 1	-1,451245	0,049963932

Supplemental Table 2 Primary antibodies used in the study.

Name	Clone	Source	Assay	Dilution
			IF	1:500
Anti-LAP2α serum	245-2	(1)	WB	1:1000
Anti-lamin A/C (N-18)	sc-6215	Santa Cruz	WB	1:200
Anti-actin	A-2066	Sigma	WB	1:200
Anti-dystrophin	MANDRA1	Sigma	IF	1:500
Anti-myosin heavy chain (MyHC)	MF20-s	Developmental Studies Hybridoma Bank	WB/IF	1:10
Anti-MyoD1 (M-318)	sc-760	Santa Cruz Biotech.	WB	1:500
anti-PAX7	PAX7-s	Developmental Studies Hybridoma Bank	WB	1:10
Anti-desmin	RD301	Abcam	WB	1:100
Anti-myogenin	F5D-s	Developmental Studies Hybridoma Bank	WB	1:10
Anti-fast MyHC (type IIa+IIx/d)	A4.74-s	Developmental Studies Hybridoma Bank	IF	1:10
Anti-slow MyHC (type I)	A4.840-c	Developmental Studies Hybridoma Bank	IF	1:100
Anti-embryonic MyHC	F1.652	Developmental Studies Hybridoma Bank	IF	1:10
FITC Anti-mouse CXCR4 (CD 184)	2B11	BD Pharmingen	FACS	1:50
PE Anti-mouse integrin β1 (CD 29) conjugate	eBioHMb1-1	eBioscience	FACS	1:40
APC Anti-mouse CD 45 (Ly-5 LCA)	30-F11	eBioscience	FACS	1:333
APC Anti-mouse Mac-1a (CD11b, Integrin αM)	M1/70	eBioscience	FACS	1:333
PerCP-Cy5.5 Anti-mouse Sca-1 (Ly-6A/E)	D7	eBioscience	FACS	1:150

Supplemental Table 3 Primer sequences used for quantitative and semi-quantitative PCR.

Name/Target	Sequence	Tm ºC	Source
QLAP2aII-forward	AGCAGGGAACTGAATCGAGA	57,3	
QLAP2aII-reverse	GCACCAGAGGGAGTAGATGC	61,4	NM_011605
LAP2com_hm1	GTGGGAACAACCAGGAAGCTATATGA	63,2	
LAP2br_hm1	CTCCCACTTCAGCTCTTGTCAATG	62,7	(2)
GAPDH-hm1	CATCACCATCTTCCAGGAGCGA	62,1	
GAPDH-hm2	CCTGCTTCACCACCTTCTTGAT	60,3	NM_008084
mLamAC1091f	CATCAAGCTGGCCCTGGACATGGA	67,9	
mLamAC1549r	TGCGCCTTCCACACCAAGTCAGTA	66,3	(2)
MyoD-forw-A	GCAGGCTCTGCTGCGCGACC	67,6	
MyoD-rev-A	TGCAGTCGATCTCTCAAAGCACC	62,4	(3)
Mfy5-forw	ACCAAGCTTTCGAGACGCTCAAGAG	64,6	
Mfy5-rev	AGATGCTGTCAAAGCTGCTGTTCT	61,0	[3]
MEF2C-RT2-1	GTATGTCTCCTGGTGTAACA	55,3	
MEF2C-RT2-2	GGATATCCTCCCATTCCTTG	57,3	(4)
MyHC2b_forward	ACAAGCTGCGGGTGAAGAGC	61,4	
MyHC2b_reverse	CAGGACAGTGACAAAGAACG	57,3	(5)
MCK_forward	GAGATCTTCAAGAAGGCTGGTCA	60,6	
MCK_reverse	GAGATGTCGAACACGGCG	58,2	(6)
Cre2_forward	CGAACGCACTGATTTCGA	56,7	
Cre2_reverse	GGCAACACCATTTTTTCTGAC	55,9	(7)
Hprt_forw	TGATTAGCGATGATGAACCAGG	58,4	
Hprt_rev	CTTTCATGACATCTCGAGCAAG	60,3	(2)

Supplemental references

1. Vlcek S, Korbei B, Foisner R. Distinct functions of the unique C terminus of LAP2alpha in cell proliferation and nuclear assembly. *J Biol Chem* 2002 May 24; **277** (21)**:** 18898-18907.
2. Naetar N, Korbei B, Kozlov S, Kerenyi MA, Dorner D, Kral R*, et al.* Loss of nucleoplasmic LAP2alpha-lamin A complexes causes erythroid and epidermal progenitor hyperproliferation. *Nat Cell Biol* 2008 Nov; **10** (11)**:** 1341-1348.
3. Yan Z, Choi S, Liu X, Zhang M, Schageman JJ, Lee SY*, et al.* Highly coordinated gene regulation in mouse skeletal muscle regeneration. *J Biol Chem* 2003 Mar 7; **278** (10)**:** 8826-8836.
4. Azmi S, Ozog A, Taneja R. Sharp-1/DEC2 inhibits skeletal muscle differentiation through repression of myogenic transcription factors. *J Biol Chem* 2004 Dec 10; **279** (50)**:** 52643-52652.
5. Usami A, Abe S, Ide Y. Myosin heavy chain isoforms of the murine masseter muscle during pre- and post-natal development. *Anat Histol Embryol* 2003 Aug; **32** (4)**:** 244-248.
6. Porter JD, Merriam AP, Gong B, Kasturi S, Zhou X, Hauser KF*, et al.* Postnatal suppression of myomesin, muscle creatine kinase and the M-line in rat extraocular muscle. *J Exp Biol* 2003 Sep; **206** (Pt 17)**:** 3101-3112.
7. Mo L, Cheng J, Lee EY, Sun TT, Wu XR. Gene deletion in urothelium by specific expression of Cre recombinase. *Am J Physiol Renal Physiol* 2005 Sep; **289** (3)**:** F562-568.

3.3 „Data not shown“ in the submitted manuscripts

3.3.1 Phenotypic analysis of *Lap2α*$^{-/-}$ mice

Lap2α$^{-/-}$ mice were generated by Cre-mediated excision of the α-specific exon 4 of the *Lap2* gene in the germline[32]. The new LAP2α-deficient mouse line was crossed back for 11 generations into the C57/B6 mouse background and analyzed on physiological, histological as well as molecular level.

3.3.1.1 Physical & behavioural profile of *Lap2α*$^{-/-}$ mice

Crosses between mice heterozygous for the α-specific deletion in the *Lap2* locus resulted in live born progeny with Mendellian genotypic distribution. All genotypic variants had comparable body weight values at birth and thrived at a similar rate until weaning age (21 days) (Figure 16). *Lap2α*$^{-/-}$ mice continued to grow normally and, at the age of 2.5 – 3 months (young), as well as 16 – 19 months (old), weighted as much as their wild type littermates (Figure 17). Average life spans of all animals were >2 years.

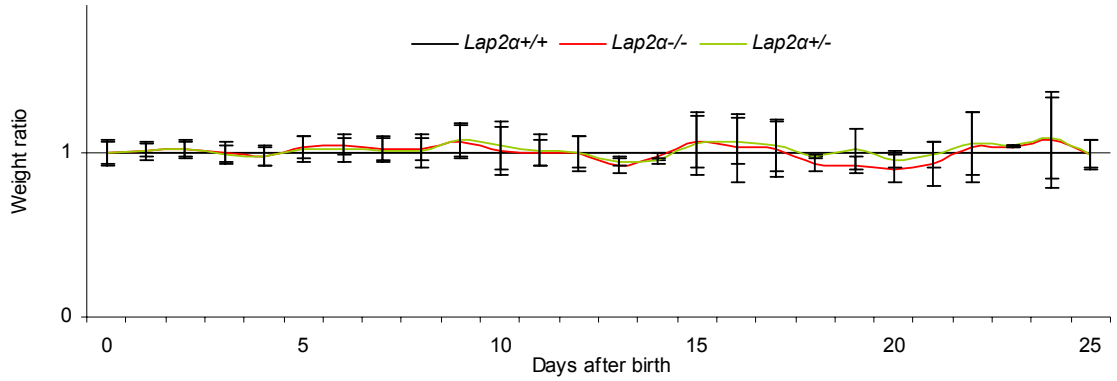

Figure 16. Heterozygous (*Lap2α*$^{+/-}$) and homozygous (*Lap2α*$^{-/-}$) LAP2α knockout mice exhibit normal postnatal growth. The average weight of *Lap2α*$^{+/-}$ as well as *Lap2α*$^{-/-}$ mice was normalized to the average weight of their wild type (*Lap2α*$^{+/+}$) littermates at the particular time point and presented as mean weight ratio. [n = 13 litters (28 wild type, 22 KO and 56 heterozygous mice). Mean values ± 95% confidence intervals (CI) are shown].

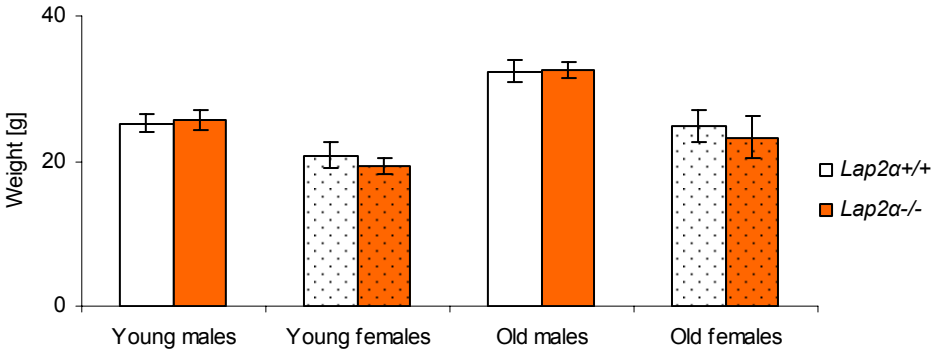

Figure 17. *Lap2α*$^{-/-}$ mice have normal body weight. (Young mice – n = 16 male and 12 female littermate pairs aged 2.5 – 3 months; old mice – n = 31 male and 4 female littermate pairs aged 16 – 19 months. p> 0.05, ANOVA; values are means ± 95% CI).

The physical appearance and behavioral profile of *Lap2α*$^{-/-}$ and *Lap2α*$^{+/-}$ mice did not substantially differ from the wild type, as assessed by the SHIRPA[170] mouse phenotyping protocol. LAP2α-deficient mice had well groomed fur and whiskers, as well as normal skin color. Their body position, reflexes, transfer arousal, gait and tail elevation were indistinguishable from those of their wild type (WT) littermates. As shown in Figure 18, the locomotor activity of *Lap2α*$^{-/-}$ and *Lap2α*$^{+/-}$ mice was also similar to the WT.

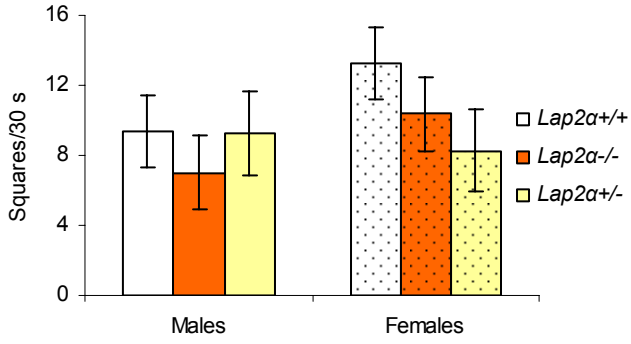

Figure 18. Absence of LAP2α does not affect locomotor activity in mice. Animals were placed inside a grid floor arena and the total number of squares (122 cm^2) simultaneously touched by all four feet in 30 seconds was recorded. (n = 14 *Lap2α*$^{+/+}$, 13 *Lap2α*$^{-/-}$ and 6 *Lap2α*$^{+/-}$ male and 7 *Lap2α*$^{+/+}$, 7 *Lap2α*$^{-/-}$ and 3 *Lap2α*$^{+/-}$ female old mice; p> 0.05, ANOVA followed by Boniferroni adjustment; values are means ± 95%).

3.3.1.2 Heart muscle tissue analysis

3.3.1.2.1 Histological and gravimetric analyses of LAP2α-deficient hearts

Since a mutation in LAP2α was linked to dilated cardiomyopathy in human[28], it was interesting to see whether loss of LAP2α would have a similar effect on structural and functional properties of the heart muscle in mice. Indeed, echocardiographic analyses in *Lap2α*$^{-/-}$ mice revealed a gender-specific impairment of heart function, characterized by depression of left ventricular fractional shortening (FS%) and enlargement of left atria in male animals. Female *Lap2α*$^{-/-}$ mice, however, exhibited normal heart function (I. Gotic, submitted manuscript I). Although a slight increase in the left ventricular diameter was recorded in male *Lap2α*$^{-/-}$ mice during echocardiography (I. Gotic, submitted manuscript I), there were no statistically significant differences in the heart weight between LAP2α-deficient and wild type animals, irrespective of age or gender (Figure 19).

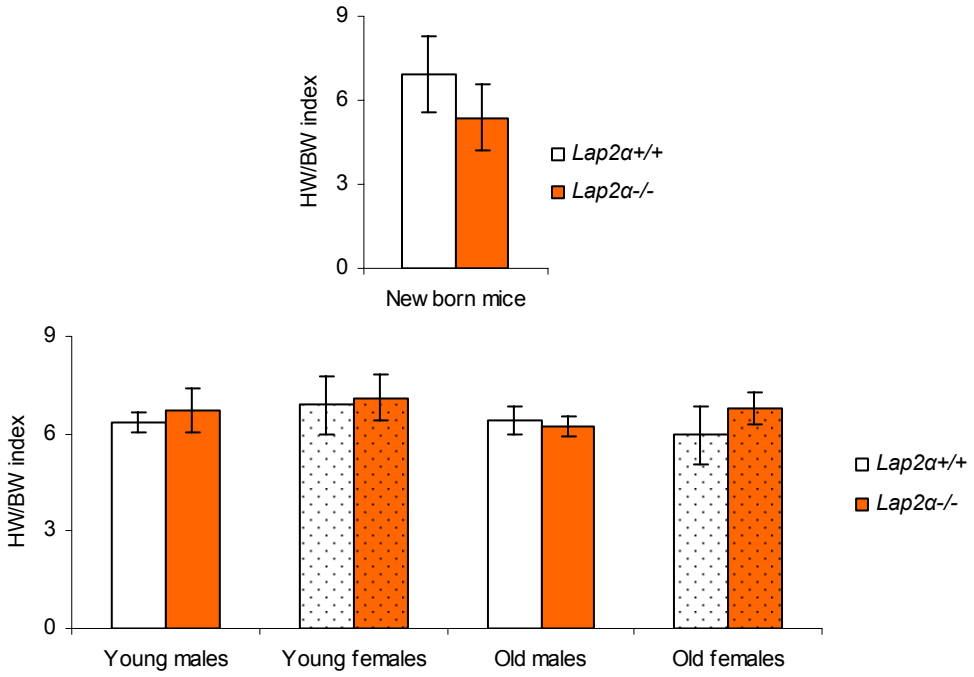

Figure 19. *Lap2α*$^{-/-}$ mice show normal heart weight. Heart weight (mg) was normalized to the body weight (g) of the animal and presented as HW/BW index. (Newborn mice – n = 9 *Lap2α*$^{+/+}$ and 10 *Lap2α*$^{-/-}$ mice; young – n = 17 male and 10 female littermate pairs; old – n = 24 male and 4 female littermate pairs; p>0.05 ANOVA, values are means ± 95% CI).

At histological level, LAP2α-deficient hearts did not show any overt pathological changes in young mice. Old *Lap2α*$^{-/-}$ mice, however, exhibited high phenotypic variability in the extent of cardiac fibrosis. Whereas the majority (72%) of males had normal levels (WT) of myocardial collagen deposits (Figure 20), 18% of them showed extensive fibrosis of the heart tissue (I Gotic, submitted manuscript I).

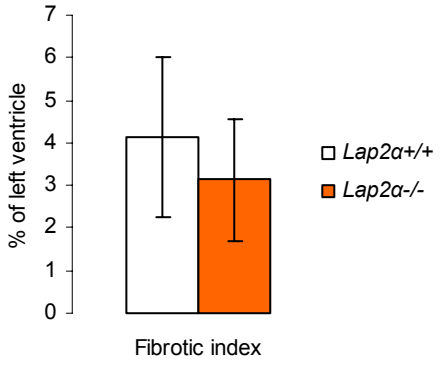

Figure 20. Cardiac fibrotic indexes in the majority of LAP2α-deficient mice are comparable to wild type. Cases with severe fibrosis (18%) are not included in the calculation to avoid high variations between WT and KO values. n = 9 *Lap2α*$^{+/+}$ and 8 *Lap2α*$^{-/-}$ mice aged >12 months, p>0.05, ANOVA, values are means ± 95% CI).

3.3.1.2.2 *Molecular analysis of Lap2α$^{-/-}$ heart muscle tissue*

To elucidate molecular mechanisms leading to systolic dysfunction in LAP2α-deficient mice, I analyzed the expression of key cardiac transcription factors and their heart muscle-specific targets, which play major roles in embryonic development, postnatal tissue homeostasis and remodeling of the myocardium. Semi-quantitative and quantitative reverse transcription (RT)-PCR analyses of *Lap2α$^{-/-}$* heart muscle tissue showed an age-dependent decrease in the expression of MEF2c and GATA4, the two transcription factors essential for cardiac development and postnatal myocardial remodeling[158, 160, 177-179]. Consequently, some of their downstream targets, such as brain natriuretic peptide (BNP)[180, 181], Myocardin A[182] and striated muscle activator of Rho-signaling (STARS)[183] were down-regulated in LAP2α-deficient hearts, compared to wild type (I. Gotic, submitted manuscript I). On the other hand, targets like desmin[184], α- and β-myosin heavy chain[185], as well as atrial natriuretic factor (ANF)[186], which show de-regulated expression in various other cardiomyopathy backgrounds[187-190], were not affected by the loss of LAP2α (Figure 21).

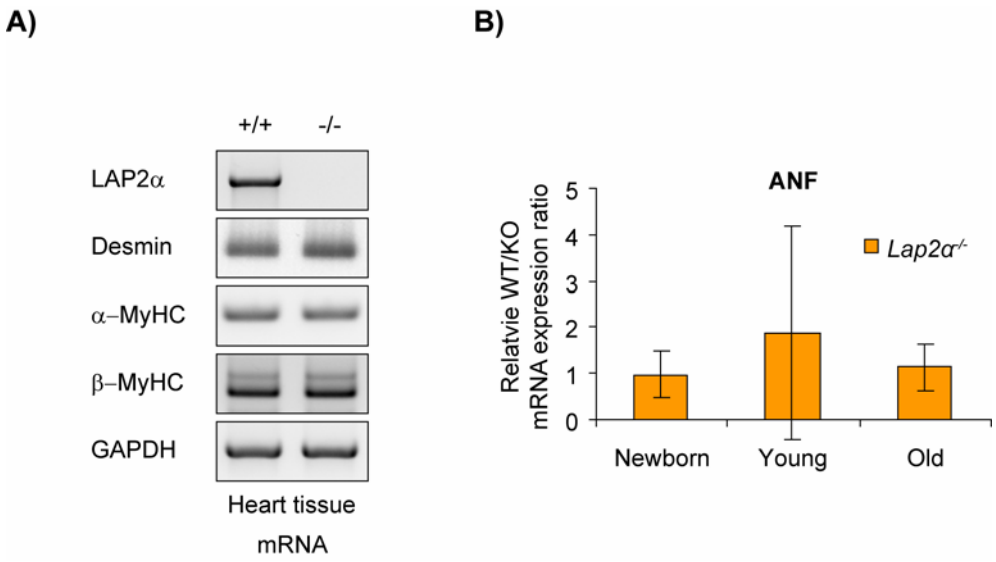

Figure 21. The expression of distinct MEF2c and GATA4 downstream targets is not affected by the loss of LAP2α in heart muscle tissue. Semi-quantitative A) and quantitative B) RT-PCR analysis of total heart lysates. (MyHC = myosin heavy chain; GAPDH = Glycerinaldehyde-3-phosphate-Dehydrogenase. Representative images of 5 separate experiments are shown in panel A). Panel B) shows mean values ± 95% CI of n = 2 – 4 littermate pairs of each age; p>0.05, ANOVA).

3.3.1.2.3 *LAP2α-deficient hearts under stress*

As the functional defect in *Lap2α*$^{-/-}$ mice was not progressing with age under normal conditions, I questioned whether the pathological phenotype would be augmented under chronic cardiac stress. Thus, I crossed *Lap2α*$^{-/-}$ mice with *Mdx* mutants[191], which develop DCM later in life[192]. The evolution of DCM in *Mdx* mice has been linked to increased mechanical fragility of the myocardium caused by the absence of a sarcolemmal structural protein dystrophin[193]. Interestingly, loss of dystrophin caused a transient rescue of the *Lap2α*$^{-/-}$ heart phenotype, as young *Lap2α*$^{-/-}$*/Mdx* mice exhibited normal cardiac structure and function, similar to their *Mdx* littermates. However, by the age of 10-12 months, both *Lap2α*$^{-/-}$*/Mdx* mice developed left ventricular systolic dysfunction and their FS% values leveled with those of the old *Lap2α*$^{-/-}$ and *Mdx* mice (I. Gotic, submitted manuscript I).

Sarcolemmal instability evokes cardiomyocyte necrosis and accumulation of fibrous tissue in old *Mdx* mice[193]. Similarly, old *Lap2α*$^{-/-}$*/Mdx* mice exhibited widespread fibrosis of heart muscle tissue (Figure 22).

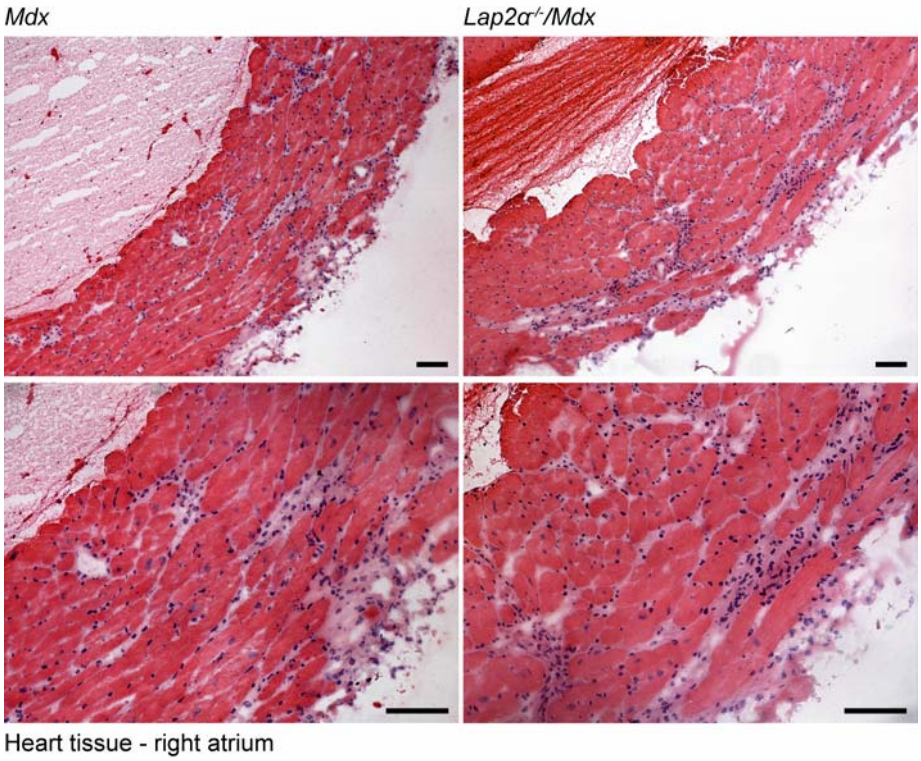

Figure 22. Old *Lap2α*$^{-/-}$*/Mdx* and *Mdx* mice exhibit heart fibrosis. (H&E-stained transverse heart sections; white arrows mark the fibrotic areas; representative images of 5 separate experiments are shown; bar = 100 μm).

3.3.1.2.4 Conditional deletion of LAP2α in cardiomyocytes

To see whether *Lap2α*$^{-/-}$ heart phenotype was a direct consequence of LAP2α loss in mature cardiomyocytes, or indirectly caused by defects in cardiac progenitors and/or other non-striated muscle tissues, I generated striated muscle-specific conditional knockout mice. By crossing transgenic mice carrying the *Lap2* exon 4 flanked by *loxP* sites[32], with mice expressing Cre recombinase under the control of muscle creatine kinase (MCK) promoter[194], I obtained animals that lose LAP2α during later stages of heart development and cardiomyocyte differentiation (I. Gotic, submitted manuscript I).

Since *Lap2α*$^{Neo\text{-}fl/Neo\text{-}fl}$*/Mck-Cre*$^{+}$ exhibited normal heart structure and function, as well as wild type cardiac transcription profiles (Figure 23., I. Gotic, submitted manuscript I), I concluded that LAP2α might exert its function either earlier in the embryonic development, or in non-striated muscle cells of the heart. One way to test this hypothesis, would be to cross *Lap2α*$^{-/-}$ animals with transgenics expressing Cre recombinase under the control of an early cardiomyocyte-specific promoter, such as Nkx2.5[195].

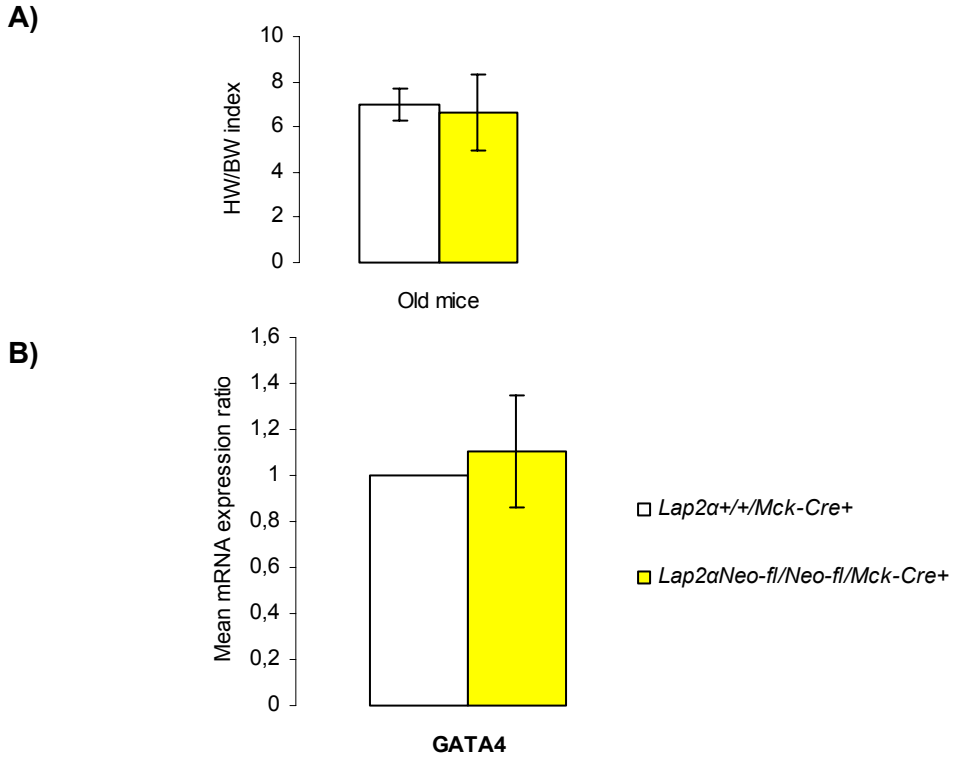

Figure 23. *Lap2α*$^{Neo\text{-}fl/Neo\text{-}fl}$*/Mck-Cre*$^{+}$ mice have normal HW/BW indexes (A) and express wild type levels of GATA4 (B). (qPCR analysis, n = 3 littermate pairs, each floxed sample was compared to its respective WT littermate sample, values are mean floxed/WT expression ratios ± 95% CI, p>0.05, ANOVA).

3.3.1.3 Skeletal muscle analysis

As mutations in lamin A/C and their interaction partners also cause skeletal muscle defects[76], I wondered if the structure and function of skeletal muscle tissue would be affected by the loss of LAP2α in mice. *Lap2α*$^{-/-}$ mice did not exhibit an overt pathological skeletal muscle phenotype at any age under normal conditions (I. Gotic, submitted manuscript II). Since most striated muscle laminopathies manifest only with advanced age, recent studies proposed a model according to which, the impaired function of adult stem cells would play a key role in the development of the disease[13, 32, 124, 125]. Therefore, I analyzed the functional properties of LAP2α-deficient muscle satellite cells in *in vivo* and *in vitro* systems.

3.3.1.3.1 Lap2α$^{-/-}$ *stem cell properties*

Consistent with the increase in their erytropoietic progenitor cell population[32], young *Lap2α*$^{-/-}$ mice showed a higher content of adult skeletal muscle satellite cells (I. Gotic, submitted manuscript II). However, LAP2α-deficient satellite cell progeny exhibited a delay in myogenic differentiation *in vitro*, characterized by stalled expression of muscle-specific genes and slightly belated myoblast fusion (Figure 24 – 26, I. Gotic, submitted manuscript II).

LAP2α-deficient mouse primary fibroblasts and intestinal cells showed a loss of the nucleoplasmic lamin A/C pool[32]. In contrast, *in vitro* cultured *Lap2α*$^{-/-}$ myoblasts, which represent activated satellite cell progeny[196], had seemingly similar distributions of peripheral and intranuclear lamin A/C as wild type cells (Figure 26). However, as rearrangement of the nuclear lamina and the re-localization of the nucleoplasmic lamin A/C fraction to the periphery represent the hallmarks of muscle differentiation[144], the effects of LAP2α loss on lamin A/C pool could be masked by changes caused by improper differentiation.

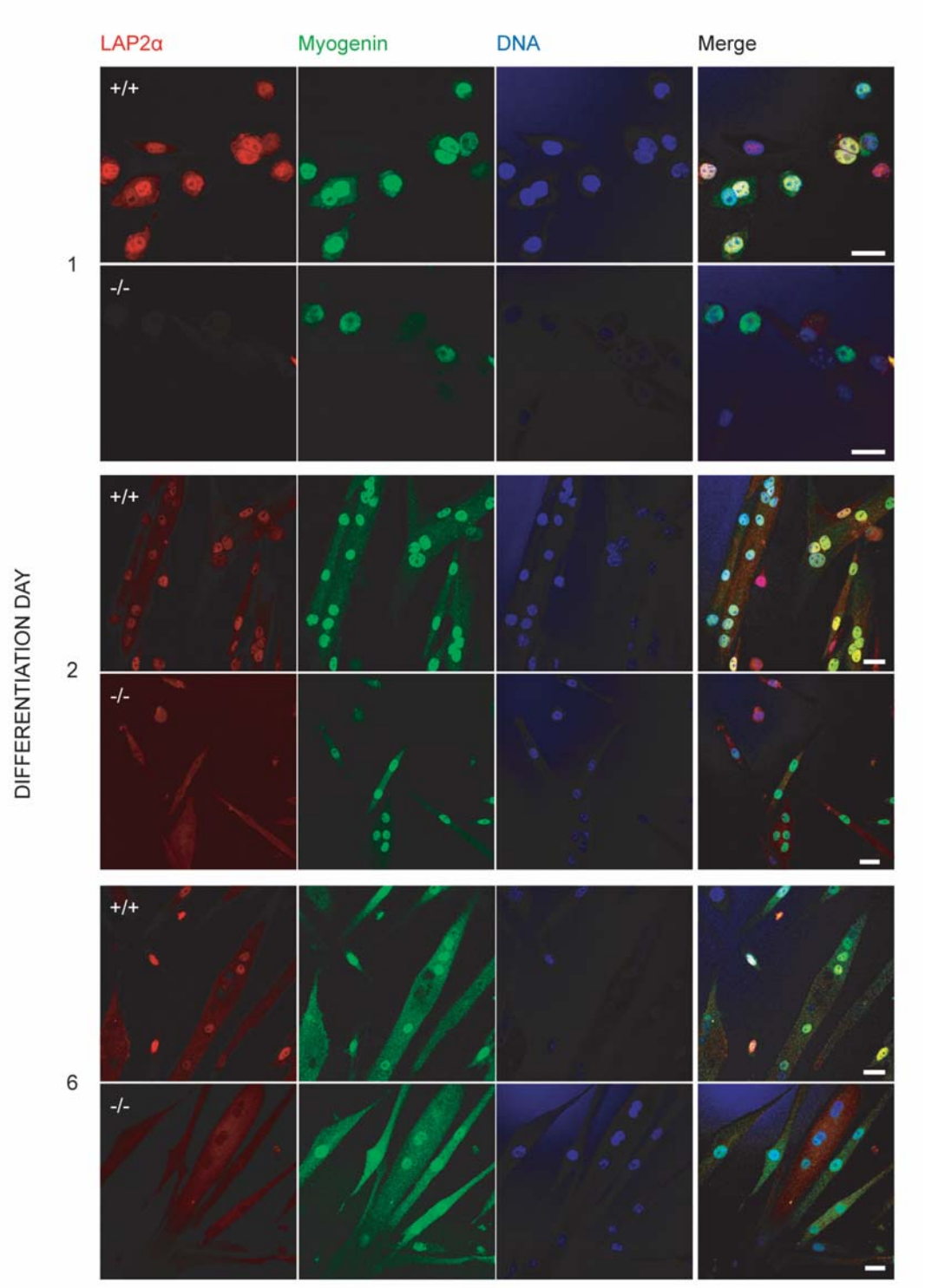

Figure 24. LAP2α-deficient myoblasts show slightly delayed fusion and expression of early muscle-specific differentiation factor myogenin. (Immunostained primary mouse myoblasts, bar = 20 μm).

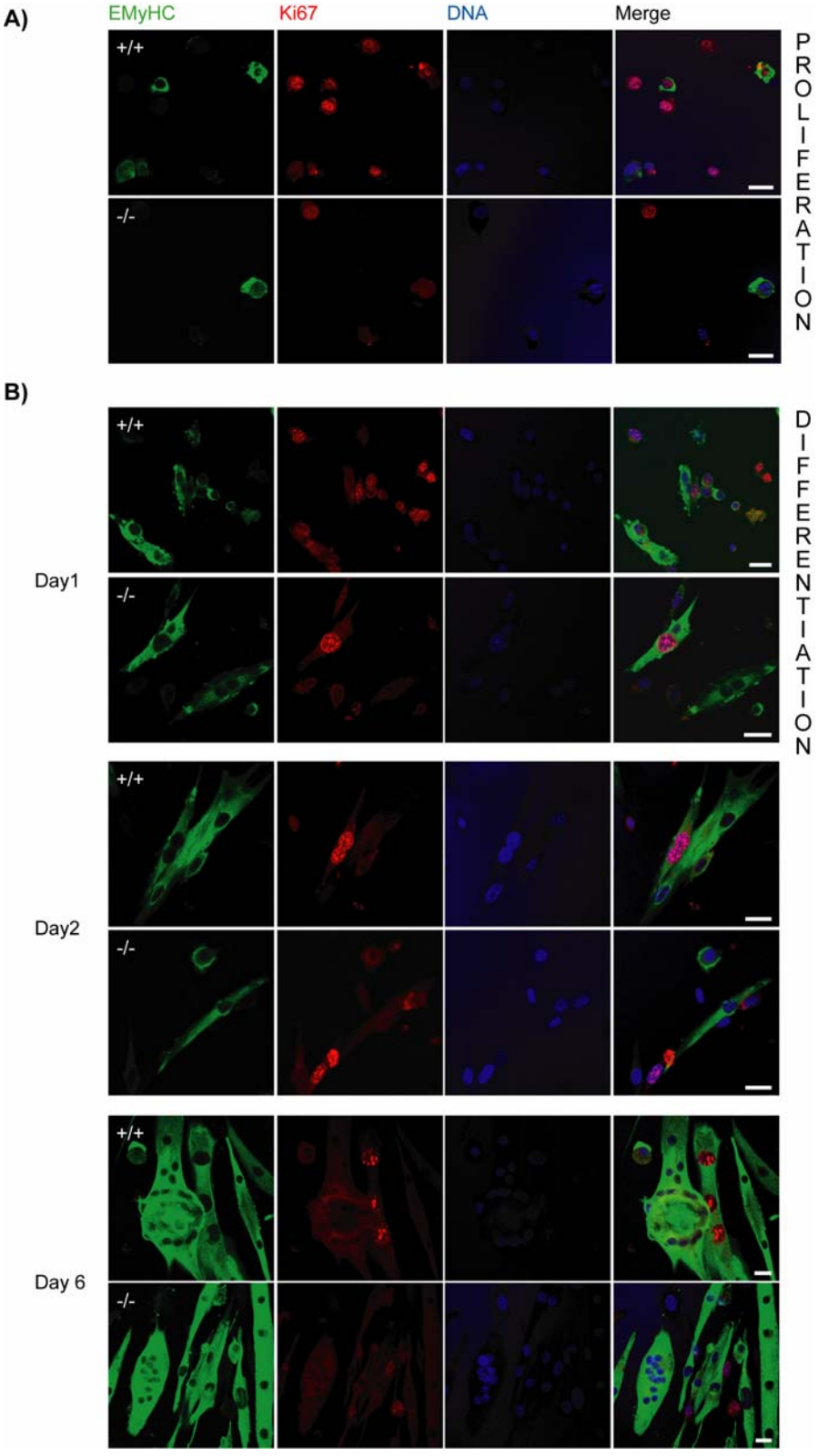

Figure 25. The delay in differentiation does not affect the expression of proliferation marker Ki67 in LAP2α-deficient cells. (Immunofluorescence stained primary mouse myoblasts, EMyHC – embryonic heavy chain, bar = 20 μm).

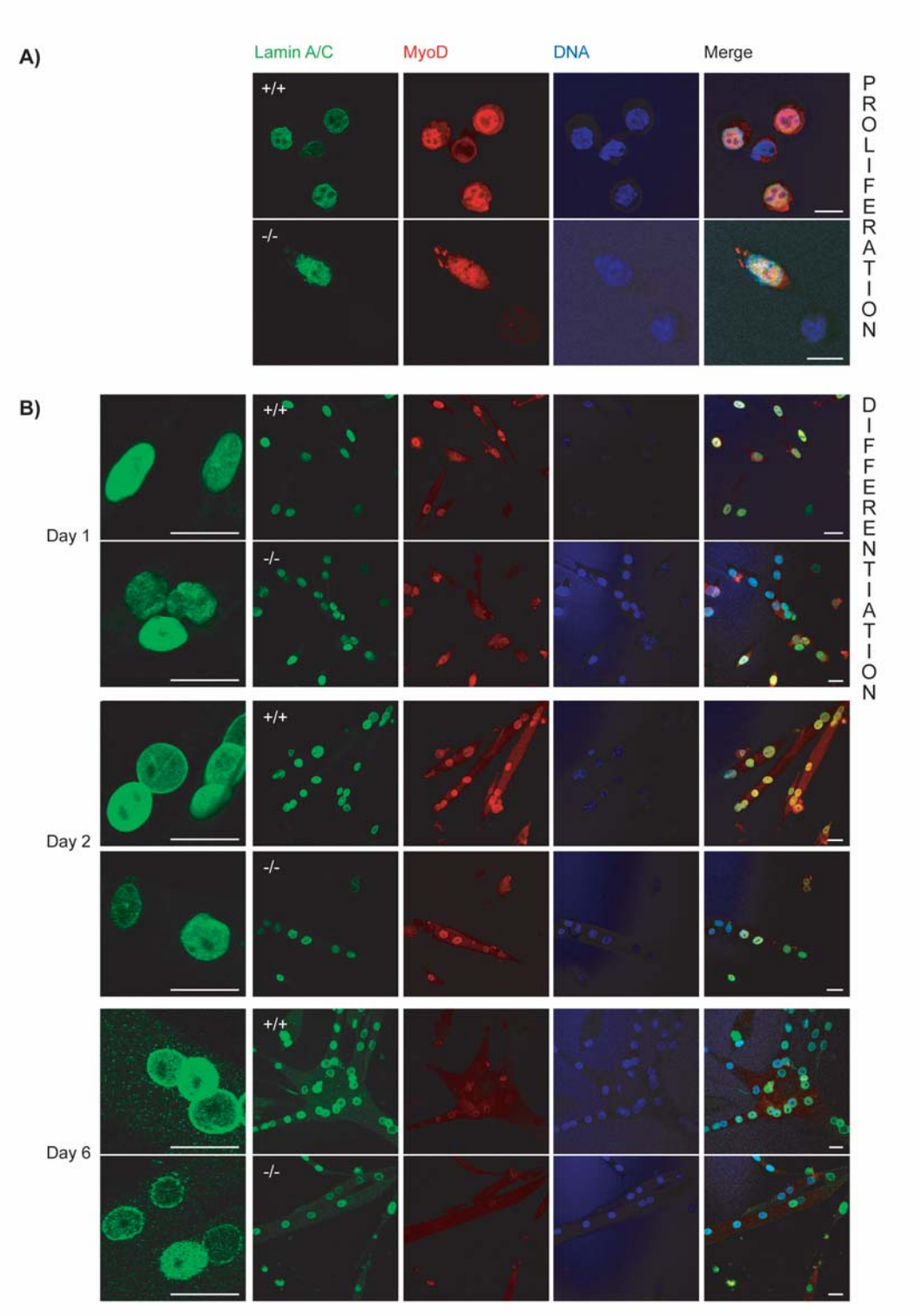

Figure 26. Loss of LAP2α does not substantially affect lamin A/C localization in differentiating myoblasts. Re-localization of the intranuclear lamin A/C pool coincides with the downregulation of the early myogenic factor MyoD. (Immunofluorescence stained primary mouse myoblasts, bar = 20 μm).

3.3.1.3.2 *Muscle transformation*

Myogenic factors MyoD, myogenin and MEF2c, which showed delayed expression patterns during *in vitro* differentiation of *Lap2α*$^{-/-}$ myoblasts, also play important roles in the process of muscle fiber transformation, driving the expression of fast (MyoD) or slow (myogenin, MEF2c) fiber type-specific genes (reviewed in [148]). As loss of LAP2α did not largely impinge on the steady-state mRNA levels of these factors, either in predominantly slow (Soleus) or fast (Extensor digitorum longus – EDL) muscle tissue (Figure 27), I wondered whether even a subtle change in their expression dynamics would have an impact on the tightly regulated process of fiber type specification. Therefore, I analyzed fiber size and type distribution patterns in predominantly slow and fast muscles of *Lap2α*$^{-/-}$ mice, represented by soleus and Tibialis anterior (TA) muscle respectively. Whereas the absence of LAP2α in mouse soleus muscle caused a slight shift towards faster fiber types, without affecting fiber size (I. Gotic, submitted manuscript II), myofibers type and size distributions in *Lap2α*$^{-/-}$ TA muscles were similar to wild type (Figure 28).

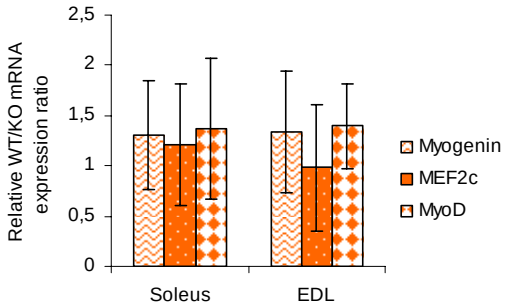

Figure 28. Steady-state mRNA levels of major myogenic transcription factors in *Lap2α*$^{-/-}$ muscle tissue are normal. (EDL – Extensor digitorum longus; qPCR analysis, n = 3 – 5 littermate pairs, p>0.05, ANOVA, values are means ± 95% CI)

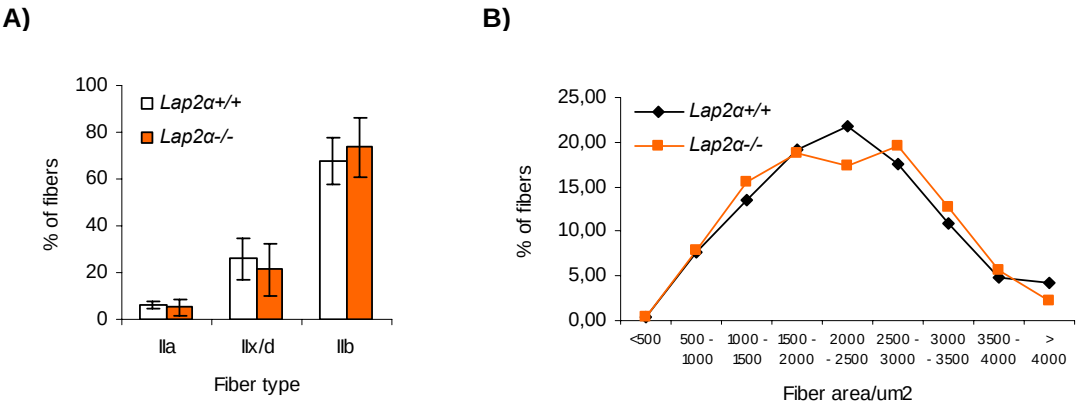

Figure 27. Absence of LAP2α does not affect myofiber type and size distribution in mouse TA muscle. Fiber type **(A)** and size **(B)** distribution was analyzed on transverse sections of TA muscle stained with antibodies specific for fast type IIa and IIx/d myosin heavy chain. (n >1000 fibers/mouse in 3 – 4 littermate pairs; p>0.05, ANOVA; mean values ± 95% CI are shown).

Different muscle fiber types have distinct metabolic and contractile properties. Whereas fast myofibers exert quick contractions and fatigue rapidly, slow muscle fibers exhibit low velocity of shortening and high resistance to fatigue (reviewed in [[148]]). In order to see if the shift in myofiber type ratio in soleus muscle was affecting the physical performance and fitness of *Lap2α*$^{-/-}$ mice, I subjected the animals to a battery of muscle strength tests, such as voluntary wheel, forced wheel, rotarod, swim and wire test. In all tasks *Lap2α*$^{-/-}$ mice scored similar to their wild type littermates (Figure 29 and data not shown). This suggests that a slight change in the contractile profile of one muscle type does not significantly alter the physical performance of the whole organism.

A)

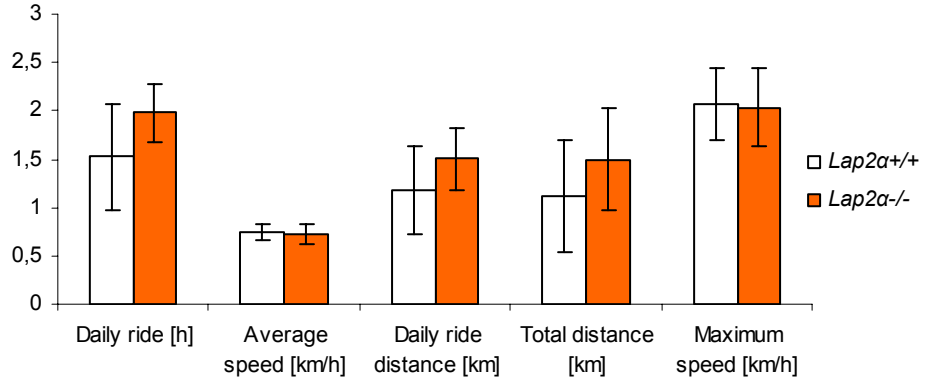

B)

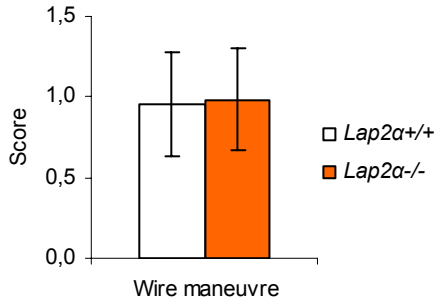

Figure 29. General fitness and muscle strength of *Lap2α*$^{-/-}$ mice is similar to wild type. Performance of *Lap2α*$^{+/+}$ and *Lap2α*$^{-/-}$ mice in voluntary wheel **A)** and wire test **B)**. [n = 8 littermate pairs in A) and 29 pairs in B); p>0.05, ANOVA; mean values ± 95% CI are shown].

3.3.1.3.3 Muscle regeneration

Seeing that skeletal muscle of *Lap2*$\alpha^{-/-}$ mice was not significantly affected by the absence of LAP2α at baseline, I analyzed its potential to regenerate after acute and chronic stress.

Muscle regeneration is mediated by satellite cells, a population of putative adult muscle stem cells, which are able to generate myogenic progeny that will differentiate into adult myofibers, as well as self-renew[131]. To see whether the increase in stem cell numbers in young *Lap2*$\alpha^{-/-}$ mice, as well as their delayed differentiation *in vitro*, would have an effect on muscle regeneration in young and old animals *in vivo*, I subjected the mice to acute and chronic muscle injury.

3.3.1.3.3.1 Acute muscle injury

To induce acute muscle damage, I injected notexin, a potent myotoxin from *Notecis scutatus* snake venom[176], into the right soleus muscle and followed the regeneration process during the subsequent 12 days. Histological analysis of damaged muscles showed that skeletal muscle of young and old *Lap2*$\alpha^{-/-}$ mice was able to regenerate at a rate similar to the wild type (I. Gotic, submitted manuscript II). The activated satellite cells gave rise to desmin/EMyHC positive proliferating myoblasts which fused and formed new muscle fibers within the first 4 days after notexin injection (Figure 30; I. Gotic, submitted manuscript II). At day 12 of regeneration, the damaged muscle tissue was fully restored.

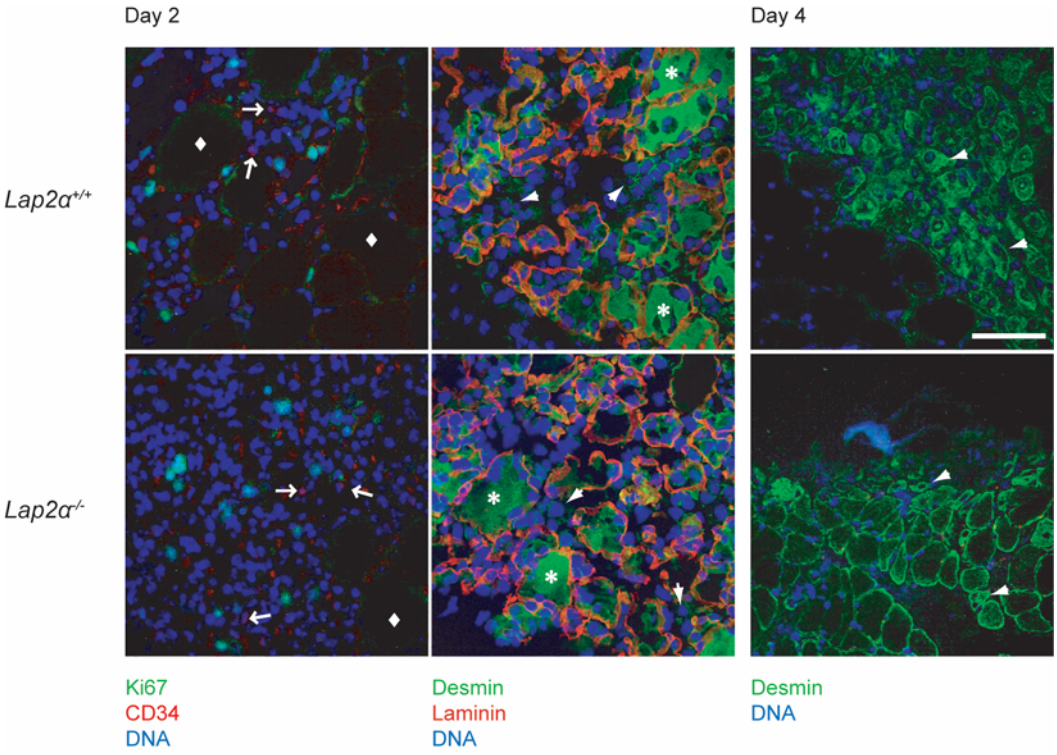

Figure 30. *Lap2α*$^{-/-}$ mice show efficient muscle regeneration. At day 2 after notexin injection a low percentage of cells within the regenerating region stains positive for proliferation marker Ki67 (left panels, green) and satellite cell marker CD34 (left panels, arrows; diamonds mark undamaged fibers). The majority of single nuclei belongs to desmin positive myoblasts (middle panels, arrowheads) which fuse into new myofibers by day 4 (right panels, arrowheads). Degenerating old fibers surrounded by laminin (middle panels, red) also show a strong immunological reaction with anti-desmin antibody (asterisk). (Immunostained cryo-sections, bar = 50 μm).

3.3.1.3.3.2 Chronic muscle injury

Chronic muscle degeneration and regeneration represent the hallmarks of the Duchene muscular dystrophy mouse model *Mdx*[191, 197]. The absence of dystrophin – a structural component of the myofiber sarcolemma – due to a nonsense point mutation, causes increased fragility of muscle fibers and damage upon mechanical stress. However, the degenerated muscle tissue is continuously repaired owing to the existence of resident adult muscle stem cells. Therefore, to study the long term effects of LAP2α loss on muscle regeneration, I crossed *Lap2α*$^{-/-}$ mice into the dystrophic background of the *Mdx* mouse.

Although *Lap2α*$^{+/-}$*/Mdx* mice exhibited decreased fertility and higher postnatal mortality of all progeny, *Lap2α*$^{-/-}$*/Mdx* mice were born according to Mendellian ratios and appeared indistinguishable from their wild type and *Mdx* littermates at birth. The double mutants grew at a similar rate as *Mdx* mice until the age of 3 weeks (Figure 31), when both genotypes started to show signs of muscular dystrophy. As a consequence of repetitive muscle de- and re-generation, *Lap2α*$^{-/-}$*/Mdx* mice as well as *Mdx* mice, exhibited muscle hypertrophy and reduced fitness as assessed by SHIRPA protocol[170] (Figure 32 and data not shown). Nonetheless, absence of LAP2α did not have a major effect on muscle regeneration in *Mdx* background, as double mutant mice presented a similar behavioral, physiological and histological phenotype as their *Mdx* littermates (Figure 33 and data not shown).

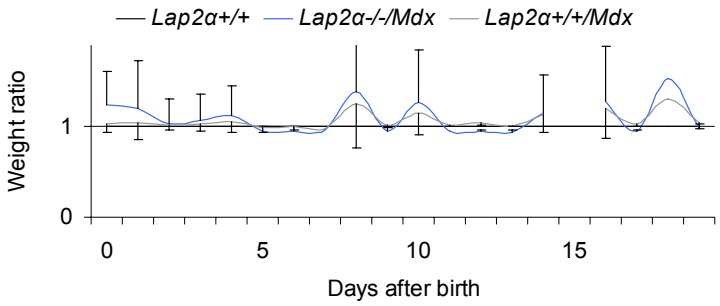

Figure 31. Newborn *Lap2α*$^{-/-}$*/Mdx* and *Mdx* mice grow normally. The average weight of *Lap2α*$^{-/-}$*/Mdx* as well as *Lap2α*$^{+/+}$*/Mdx* mice was normalized to the average weight of their wild type (*Lap2α*$^{+/+}$) littermates at the particular time point and presented as weight ratio. (n = 5 litters (6 wild type, 6 double mutant and 9 *Mdx* mice, mean values ± 95% CI are shown.)

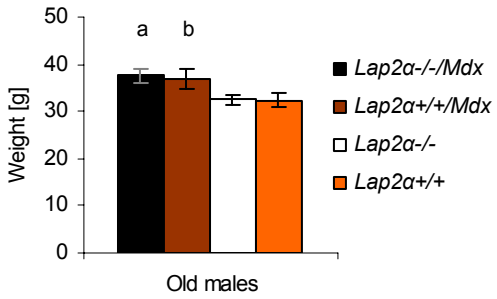

Figure 32. Old *Lap2α$^{-/-}$/Mdx* and *Mdx* mice have increased body weight due to muscle hypertrophy. (n = 17 *Lap2α$^{-/-}$/Mdx* + 7 *Mdx* + 31 *Lap2α$^{+/+}$* + 32 *Lap2α$^{-/-}$* mice, p<0.05 for (a) *Lap2α$^{-/-}$/Mdx* vs. *Lap2α$^{+/+}$* and (b) *Mdx* vs. *Lap2α$^{+/+}$*; ANOVA followed by Boniferroni adjustment, mean values ± 95% CI are shown).

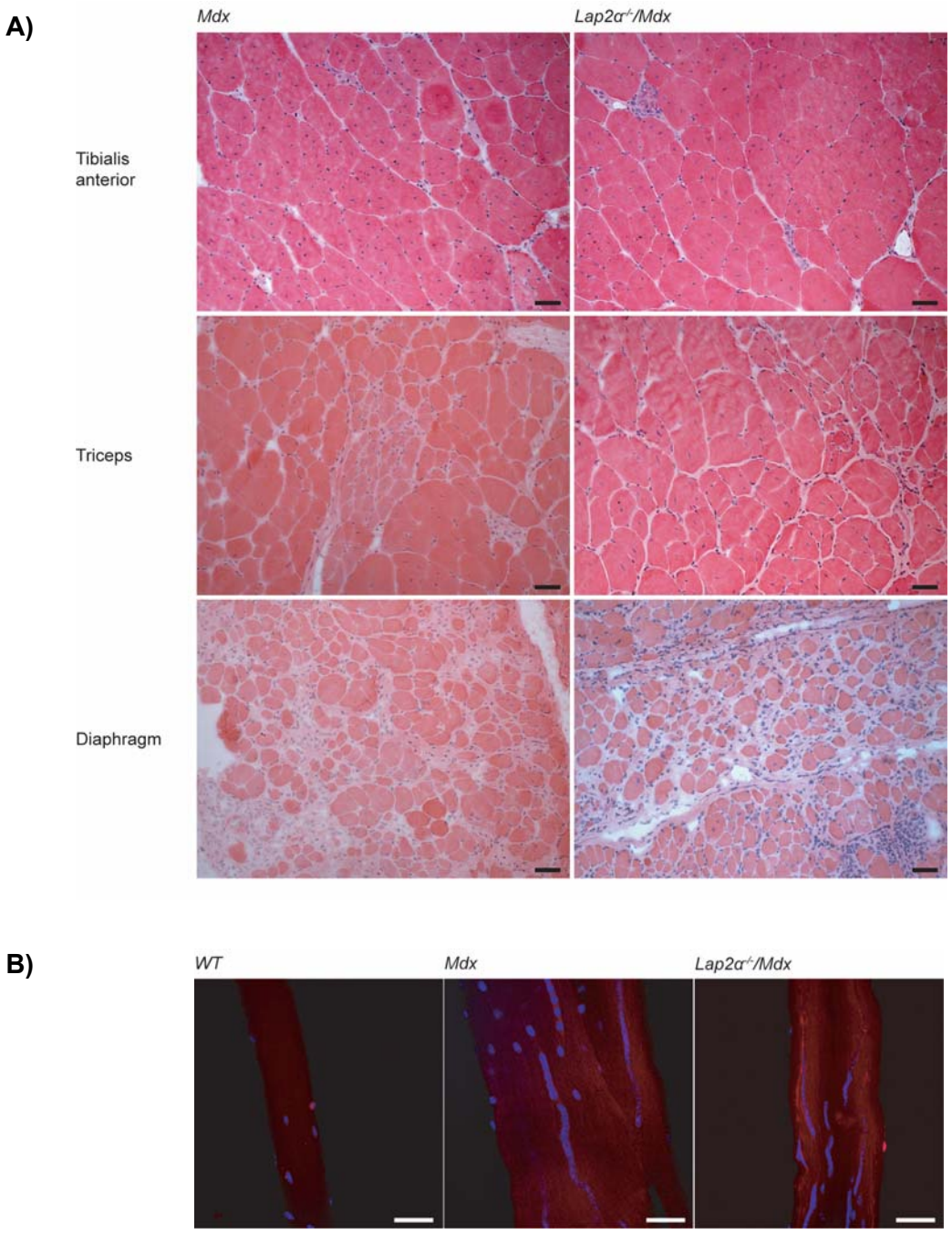

Figure 33. Skeletal muscle of *Mdx* and *Lap2α*$^{-/-}$*/Mdx* mice shows signs of muscular dystrophy. A) Hypertrophic myofibers of irregular shape, fibrosis, fiber branching and size alterations, foci of inflammation, degeneration and regeneration, all characterize dystrophic mouse muscle. (Haematoxylin & eosin stained tissue cryo-sections. Bar = 50 μm). **B)** Myonuclei of hypertrophic *Mdx* and *Lap2α*$^{-/-}$*/Mdx* fibers are stacked into multiple chains distributed throughout the fiber interior, compared to singly positioned nuclei that lie under the sarcolema of WT fibers. (Immunostaining of adult myofibers: CD34 red, DNA blue; bar = 50 μm).

Absence of LAP2α did not substantially affect the size of the *Mdx* satellite cell pool, as *Lap2α*$^{-/-}$*/Mdx* mice showed similar CD45^{-}Sca1^{-}Mac1^{-}CXCR4^{+}β$_1$-integrin^{+} (CSM4B)-satellite cell numbers as their *Mdx* littermates (Figure 34). However, as a consequence of fiber damage, constant satellite cell activation, proliferation and differentiation of their progeny might have masked the initial effect of LAP2α loss on the satellite cell population. In general, the CSM4B satellite cell pool was enlarged in *Mdx* mice, compared to wild type animals (Figure 34). Interestingly, a recent study reported a decrease in the CSM4B cell content in *Mdx* mice already at the age of 8 weeks[198]. What is more, total CSM4B cell numbers in young *Mdx* mice in the previous study were lower than the numbers found in my studies in old animals, which does not conform to the accepted model of aging-related loss of stem cells [136, 199]. The discrepancy between the data presented here and the results of the aforementioned study may be explained by several means. Apart from potentially different genetic background of *Mdx* mice and experimental conditions used for CSM4B quantification in these two studies, the differences in satellite cell numbers might also reflect different regeneration/degeneration states of the animals. Thus, if old *Mdx* mice were sacrificed at the beginning of a massive regeneration phase, their satellite cell numbers might have been higher than those in young mice experiencing muscle fiber growth at the end of the regeneration process. Unfortunatelly, the same study did not show CSM4B cell numbers in old *Mdx* mice to confirm their decrease during natural aging.

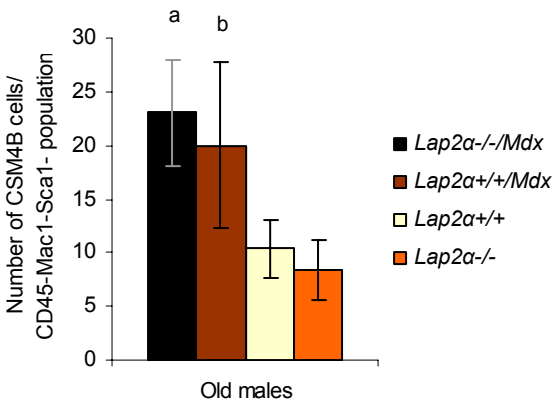

Figure 34. Loss of LAP2α does not substantially affect the size of the *Mdx* CSM4B satellite cell pool. (CSM4B – CD45^{-}Sca1^{-}Mac1^{-}CXCR4^{+}β$_1$-integrin^{+}; n = 3 *Lap2α*$^{-/-}$*/Mdx* + 3 *Mdx* + 5 *Lap2α*$^{+/+}$ + 4 *Lap2α*$^{-/-}$ mice; p<0.05 (a) *Lap2α*$^{-/-}$*/Mdx* vs. *Lap2α*$^{+/+}$; p = 0.049 for (b) *Mdx* vs. *Lap2α*$^{+/+}$; ANOVA followed by Boniferroni adjustment, mean values ± 95% CI are shown).

3.3.2 Mice with a conditional deletion of LAP2α

In order to specify the phase of muscle differentiation during which LAP2α exerts its function more closely, I made use of the existing muscle-specific Cre recombinase-expressing lines and generated conditional LAP2α knockout mice.

As already mentioned, by crossing *Lap2α*$^{Neo\text{-}fl/Neo\text{-}fl}$ and *Mck-Cre* lines[32, 194], I obtained transgenic mice that lose LAP2α during later phases of striated muscle differentiation, when *Mck* promoter becomes active[200]. Similar to complete *Lap2α*$^{-/-}$ mice, *Lap2α*$^{Neo\text{-}fl/Neo\text{-}fl}$*/Mck-Cre*$^{+}$ animals grew normally and did not show an overt skeletal muscle phenotype (Figure 35; I. Gotic, submitted manuscript II). However, I observed delayed *in vitro* differentiation of primary myoblasts isolated from *Lap2α*$^{Neo\text{-}fl/Neo\text{-}fl}$*/Mck-Cre*$^{+}$ mice, confirming the role of LAP2α at the onset of myogenic differentiation. In addition, the change in myofiber type ratios observed in soleus muscles, as well as the normal fiber type distribution in TA muscle, of *Lap2α*$^{-/-}$ mice was also phenocopied in *Lap2α*$^{Neo\text{-}fl/Neo\text{-}fl}$*/Mck-Cre*$^{+}$ animals (I. Gotic, submitted manuscript II & data not shown).

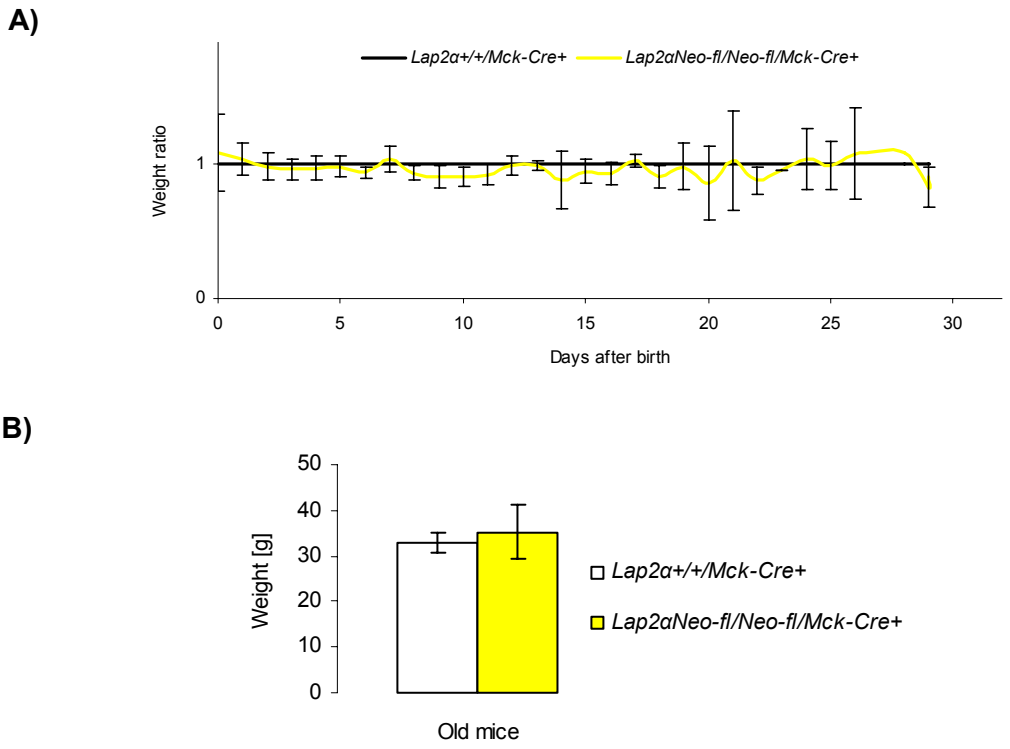

Figure 35. Newborn (A) and old (B) *Lap2α*$^{Neo\text{-}fl/Neo\text{-}fl}$*/Mck-Cre*$^{+}$ mice have normal body weight. A) The average weight of *Lap2α*$^{Neo\text{-}fl/Neo\text{-}fl}$*/McK-Cre*$^{+}$ mice was normalized to the average weight of their wild type *Mck-Cre*$^{+}$ littermates at the particular time point and presented as weight ratio. [**A)** n = 8 *Mck-Cre*$^{+}$ *litters* (11 wild type and 12 *Lap2α*$^{Neo\text{-}fl/Neo\text{-}fl}$ mice). **B)** n = 3 littermate *Lap2α*$^{Neo\text{-}fl/Neo\text{-}fl}$*/Mck-Cre*$^{+}$ and *Lap2α*$^{+/+}$*/Mck-Cre*$^{+}$ pairs; p> 0.05, ANOVA; values are means ± 95% CI].

3.4 Unpublished data

3.4.1 *Lap2α*$^{-/-}$ hearts under chronic stress

Since heart function in *Lap2α*$^{-/-}$ mice was not deteriorating further with age under normal conditions, I decided to test the ability of the LAP2α-deficient myocardium to cope with acute stress. To this end, as part of a collaboration project, I subjected the mice to ischemia-reperfusion injury, modeling myocardial infarction[175]. In this experimental set up, coronary ischemia was induced in mice by ligating the left anterior descending coronary artery (LAD) for 30 minutes. After one week of reperfusion, the extent of damage imposed upon the tissue was assessed by histological analysis. As shown in Figure 36, both – wild type and *Lap2α*$^{-/-}$ mice showed a great variability in the size of the damaged myocardium, precluding any conclusion about the effect of LAP2α loss on this process at present. Due to the nature of the experimental set up and the high variability in the system, further experiments on a larger cohort of animals would be necessary to yield a reliable result. However, the response of the LAP2α-deficient myocardium to ischemia-induced hypoxic conditions is especially interesting, as transgenic mice lacking one of its binding partners – the heat shock protein Hsp70[34] – show cardiac contractile dysfunction after *ex vivo* ischemia/reperfusion-induced heart stress, together with baseline left ventricular hypertrophy[201]. On the other hand, overexpression of this stress induced protein confers protection against simulated ischemia and metabolic stress[202].

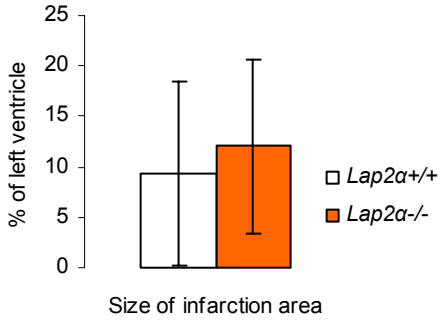

Figure 36. *Lap2α*$^{+/+}$ and *Lap2α*$^{-/-}$ mice show high variability in the extent of myocardial damage after ischemia/reperfusion-induced injury. The size of myocardial infarction area was measured on 5 × 5 µm transverse sections taken at fixed positions starting from 1 mm below the ligature. (n = 4 *Lap2α*$^{+/+}$ and 6 *Lap2α*$^{-/-}$mice, p>0.05, ANOVA, values are means ± 95% CI).

3.4.2 Contractile properties of LAP2α-deficient skeletal muscle – the *in vitro* study

As the change in myofiber type composition of *Lap2α*$^{-/-}$ soleus muscles was too subtle to substantially affect the general physical performance of LAP2α-deficient mice, I decided to test the functional output of single isolated muscles. In a collaborative study, the force produced by isolated soleus (exhibiting slow to fast myofiber shift in *Lap2α*$^{-/-}$ mice) and Extensor digitorum longus (EDL – composed of predominantly fast myofibers) muscles was measured in an *in vitro* system[174]. Although the average maximum force generated by both – soleus and EDL – LAP2α-deficient muscles was lower than in the wild type case, and muscle fatigue induced by tetanic stimulation was faster in *Lap2α*$^{-/-}$ soleus muscle (Figure 37), the high variability in the experimental set up prevented a final conclusion about the effects of LAP2α loss on the muscle force production. Since the present study could not even confirm the previously reported deleterious effects of dystrophin deficiency on muscle force generated by the respective *Mdx* muscles used as a positive control[198], the primary cause of recorded variability is more likely the sub-optimal experimental procedure than the biological variation. Therefore, the effects of LAP2α loss on muscle force production in an *Mdx* mouse background could also not be evaluated at this instance. To overcome the problem of high experimental variability, further development of the technique and a larger group of animals would be required.

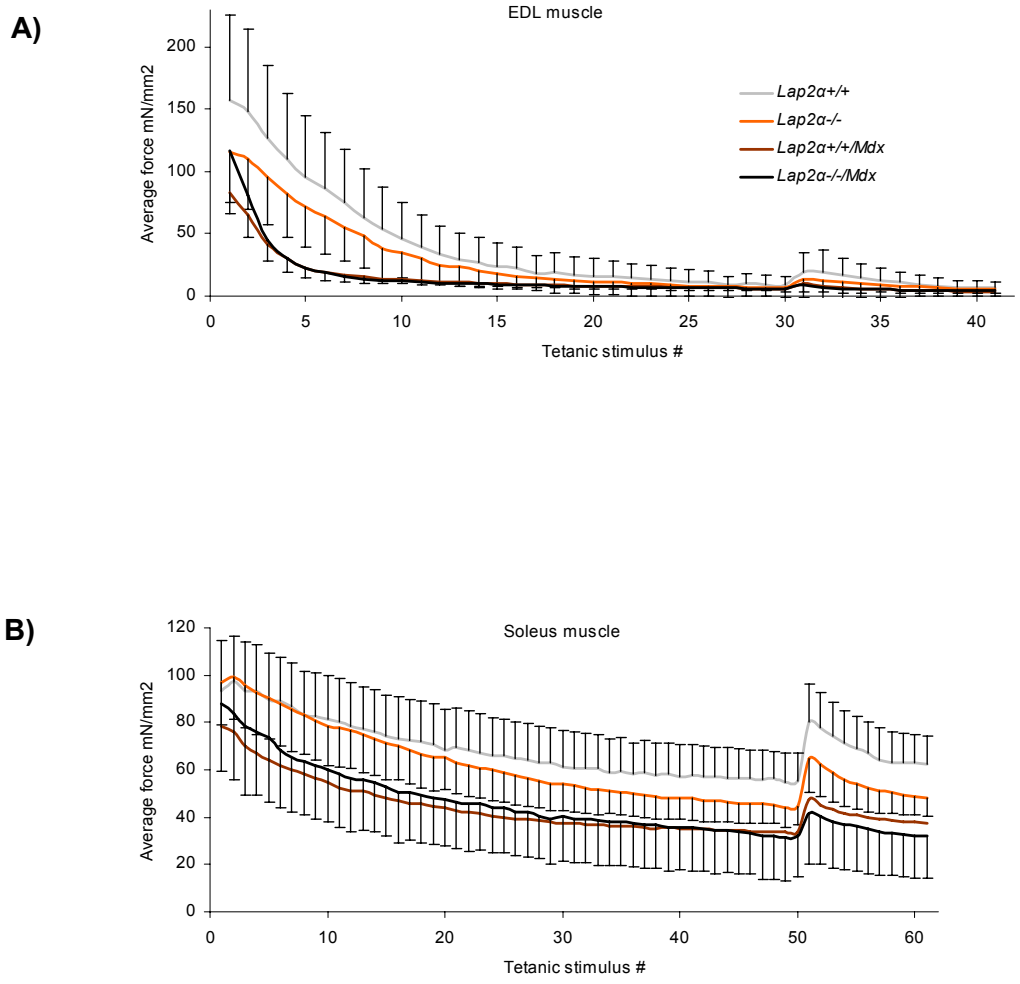

Figure 37. Muscle force generated during *in vitro* tetanic stimulation of mouse Extensor digitorum longus (EDL) (A) and soleus (B) muscle. (n = 4 littermate mice of each genotype; mean values ± 95% CI are shown).

3.4.3 Phenotypic analysis of *Lap2α*$^{Neo\text{-}fl/Neo\text{-}fl}$*/Pax7-Cre*$^{+}$ mice

The increase in the satellite cell pool of complete *Lap2α*$^{-/-}$ mice might be a consequence of intrinsic stem cell-specific defects and/or systemic changes caused by the absence of LAP2α in other non-muscle cells and tissues. To be able to discern between these two phenomena, I generated transgenic mice in which the Cre recombinase-mediated deletion of the α-specific LAP2 exon 4 occurs at early phases of muscle development and stem cell specification – in cells expressing the paired box transcription factor PAX7[203]. Similar to complete *Lap2α*$^{-/-}$ mice, *Lap2α*$^{Neo\text{-}fl/Neo\text{-}fl}$*/Pax7-Cre*$^{+}$ animals were born according to Mendellian ratios and thrived normally after birth (Figure 38). In addition, like *Lap2α*$^{-/-}$ and conditional late muscle-specific *Lap2α*$^{Neo\text{-}fl/Neo\text{-}fl}$*/Mck-Cre*$^{+}$ animals, *Lap2α*$^{Neo\text{-}fl/Neo\text{-}fl}$*/Pax7-Cre*$^{+}$ mice did not exhibit any overt pathological changes of striated muscle tissue at histological level (Figure 39).

A)

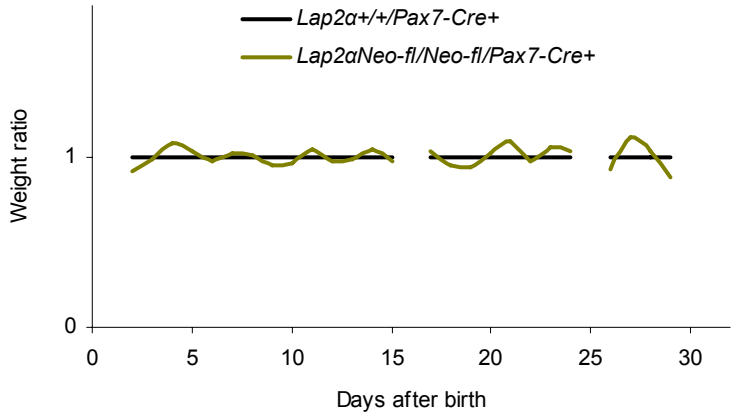

B)

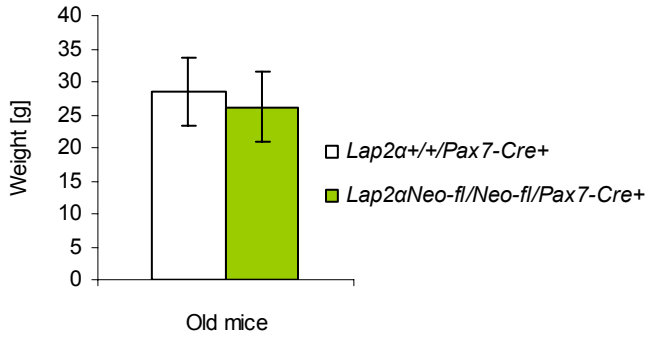

Figure 38. Newborn (A) and old (B) *Lap2α*$^{Neo\text{-}fl/Neo\text{-}fl}$*/Pax7-Cre*$^{+}$ mice have normal body weight. A) The average weight of *Lap2α*$^{Neo\text{-}fl/Neo\text{-}fl}$*/Pax7-Cre*$^{+}$ mice was normalized to the average weight of their wild type *Pax7-Cre*$^{+}$ littermates at the particular time point and presented as weight ratio. (n = 5 *Pax7-Cre*$^{+}$ litters (10 wild type and 8 *Lap2α*$^{Neo\text{-}fl/Neo\text{-}fl}$ mice). **B)** n = 5 littermate *Lap2α*$^{Neo\text{-}fl/Neo\text{-}fl}$*/Pax7-Cre*$^{+}$ and *Lap2α*$^{+/+}$*/Pax7-Cre*$^{+}$ pairs; p> 0.05, ANOVA; values are means ± 95% CI.

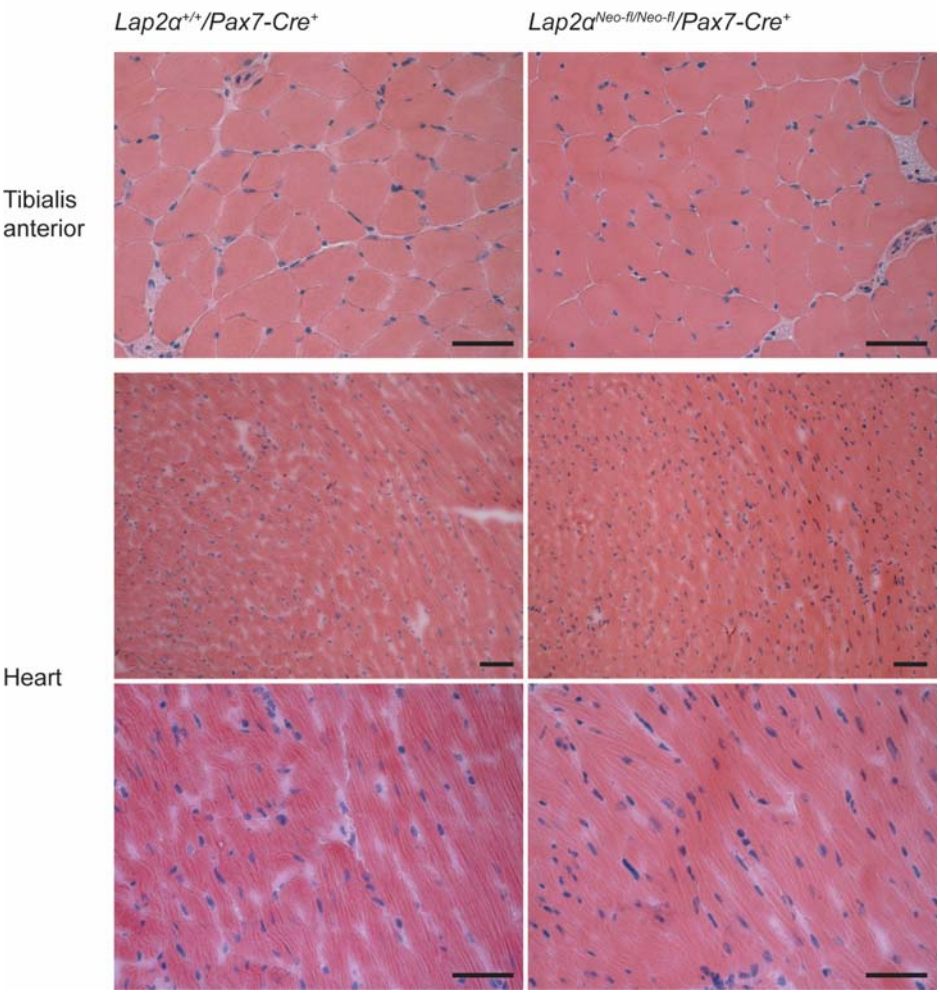

Figure 39. Absence of dystrophic features in *Lap2α*$^{Neo\text{-}fl/Neo\text{-}fl}$*/Pax7-Cre*$^{+}$ striated muscle. (H&E stained TA (upper panels) and heart (lower panels) cryo-sections. Bar =50 μm).

Fluorescence-activated cell sorting (FACS) analysis of myofiber-associated satellite cells showed a slight increase in the CSM4B cell content in *Lap2α*$^{Neo\text{-}fl/Neo\text{-}fl}$*/Pax7-Cre*$^{+}$ mice compared to wild type *Pax7-Cre*$^{+}$ animals at all ages (Figure 40 & 41). However, *Lap2α*$^{Neo\text{-}fl/Neo\text{-}fl}$*/Pax7-Cre*$^{+}$ mice did not fully reconstitute the stem cell phenotype of complete *Lap2α*$^{-/-}$ animals, as due to high variation, the difference between *Lap2α*$^{Neo\text{-}fl/Neo\text{-}fl}$*/Pax7-Cre*$^{+}$ and *Lap2α*$^{+/+}$*/Pax7-Cre*$^{+}$ CSM4B cell numbers was not statistically significant. Interestingly, all *Pax7-Cre*$^{+}$ mice showed a lower content of CSM4B satellite cells in their skeletal muscle tissue, compared to *Lap2α*$^{+/+}$ animals with predominantly C57/B6 background and *Mck-Cre*$^{+}$ mice of mixed *Mus musculus* genetic background (I. Gotic, submitted manuscript II), indicating a potential defect in the maintenance of the muscle stem cell pool. What is more, CSM4B cell numbers in both *Lap2α*$^{+/+}$ and *Lap2α*$^{Neo\text{-}fl/Neo\text{-}fl}$ *Pax7-Cre*$^{+}$ mice did not exhibit the age-related decline observed in other mouse lines reported in this and other previously published studies[136, 199].

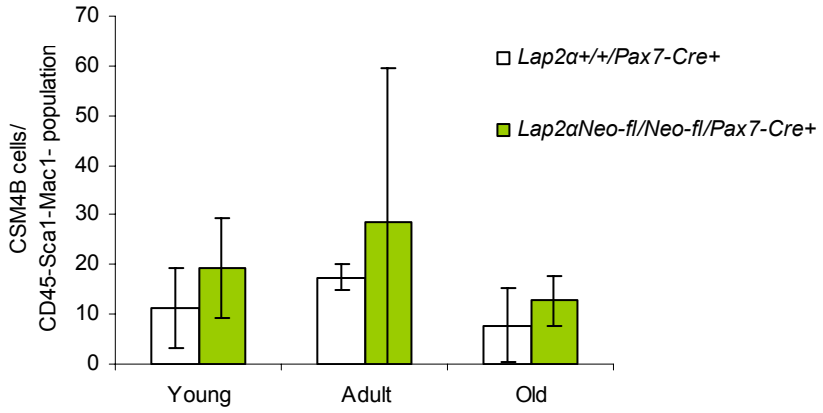

Figure 40. *Lap2α*$^{+/+}$*/Pax7-Cre*$^{+}$ and *Lap2α*$^{Neo\text{-}fl/Neo\text{-}fl}$ *Pax7-Cre*$^{+}$ mice show a deregulation of the CSM4B myofiber-associated satellite cell pool. (young – n = 5 WT + 7 floxed mice, adult – n = 2 WT + 2 floxed mice; old – n = 4 WT + 6 floxed mice; p>0.05, ANOVA, values are means ± 95% CI).

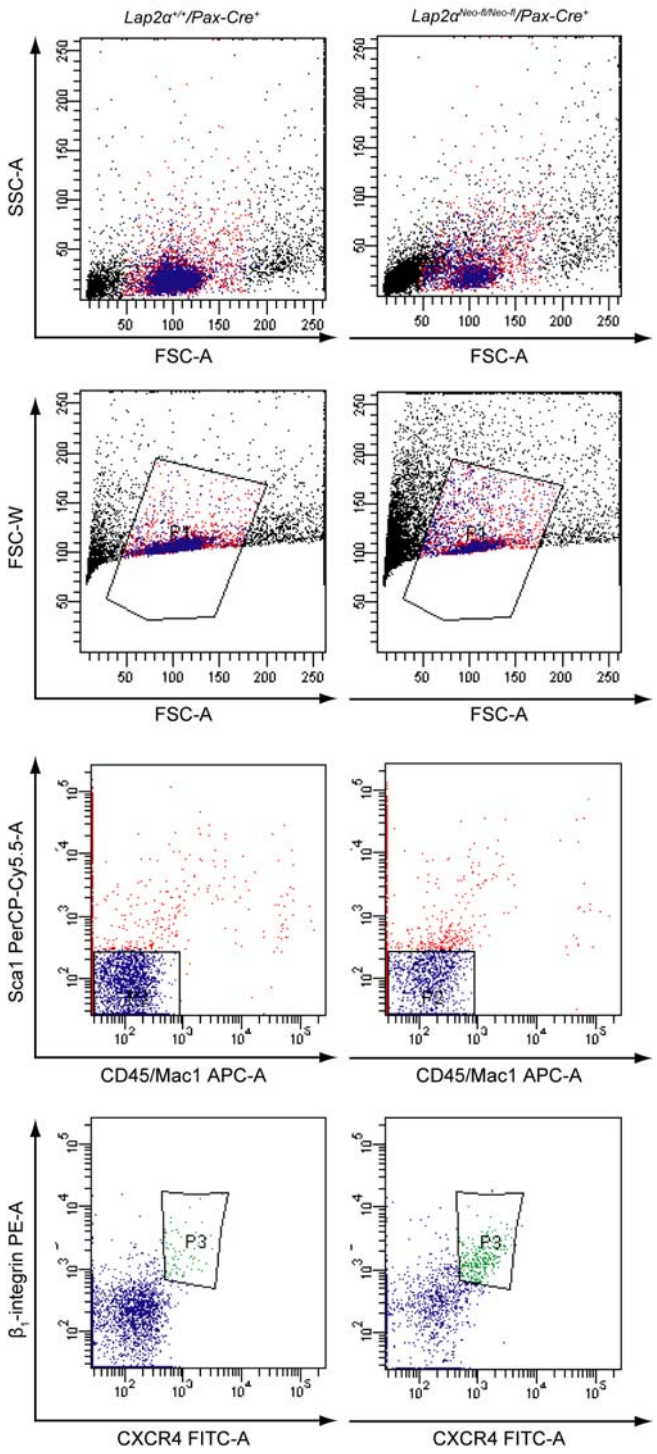

Figure 41. Fluorescence-activated cell sorting analysis of myofiber-associated satellite cells reveals a slight increase in the CSM4B cell population in *Lap2α*$^{Neo\text{-}fl/Neo\text{-}fl}$ *Pax7-Cre*$^{+}$ mice. Cells were analyzed for their size, complexity and the expression of specific surface markers. Frame P1 represents the parent population selected for cell surface analysis. Every subsequent image in descending order represents further analysis of the parent gated population. (Representative images of 5 independent experiments are shown. FSC – Forward Scatter (related to cell size); SSC – Side Scatter (a measure of cell granularity); APC, FITC, PE, PerCP-Cy5.5 – fluorochromes coupled to cell surface-specific antibodies).

The huge variability in the FACS data from *Pax7-Cre*$^{+}$ mice might be a consequence of incomplete deletion of the LAP2 exon 4 in PAX7^{+} satellite cells and, therefore, in skeletal muscle tissue, resulting in high variability in LAP2α protein levels in *Lap2α*$^{Neo\text{-}fl/Neo\text{-}fl}$*/Pax7-Cre*$^{+}$ animals. As shown in Figure 42, in some *Lap2α*$^{Neo\text{-}fl/Neo\text{-}fl}$*/Pax7-Cre*$^{+}$ mice, skeletal muscle LAP2α mRNA levels were significantly lower than in the wild type tissue, whereas in other animals they were similar to wild type, suggesting that the Cre recombinase did not exert its activity in all mice. As the bulk postnatal muscle growth depends on the activity of PAX7^{+} stem cells (reviewed in [126]), most myofiber nuclei should be negative for LAP2α. Even myonuclei that originated from other PAX7-negative cells should lose LAP2α, as Cre recombinase is small enough to diffuse inside the myofiber syncytium. Although the activity of the *Pax7* promoter, and therefore the expression of Cre recombinase, is downregulated during initial phases of muscle differentiation, a low level of PAX7 expression still persists during myoblast fusion (reviewed in [130]), which should enable the Cre-mediated excision of LAP2 exon 4 in all myofiber nuclei. The remaining low levels of LAP2α mRNA in those *Lap2α*$^{Neo\text{-}fl/Neo\text{-}fl}$*/Pax7-Cre*$^{+}$ muscles which went through Cre-mediated LAP2α ablation might have originated from other non-muscle PAX7-negative cells present in the tissue.

The *Pax7-Cre*$^{+}$ mouse line was generated by site-specific insertion of the *Cre* cassette into the 3' UTR of the endogenous *Pax7* gene (Pax7$^{tm1(cre)Mrc}$)[203]. Although the initial study claimed that this insertion did not affect the expression of the endogenous protein, the effects of this genetic manipulation on the specification and maintenance of PAX7^{+} satellite cells were not studied in detail. Since PAX7 is essential for satellite cell survival and >90% of CSM4B cells expresses this protein[198], the deregulation of the *Pax7-Cre*$^{+}$ CSM4B satellite cell pool observed in *Pax7-Cre*$^{+}$ mice, might also be a consequence of the genetic manipulation in the *Pax7* locus. The effect of LAP2α loss in *Pax7-Cre*$^{+}$ CSM4B cells might thus be masked by impaired biological function of endogenous PAX7.

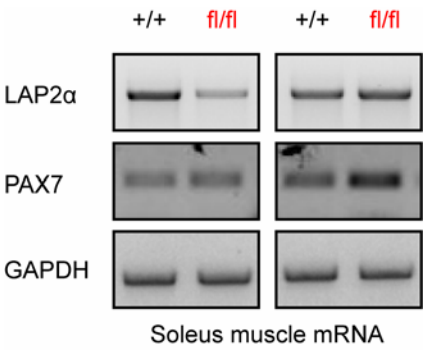

Figure 42. Muscle tissue of *Lap2α*$^{Neo\text{-}fl/Neo\text{-}fl}$*/Pax7-Cre*$^{+}$ mice shows incomplete downregulation of LAP2α expression. (+/+ → *Lap2α*$^{+/+}$*/Pax7-Cre*$^{+}$; fl/fl → *Lap2α*$^{Neo\text{-}fl/Neo\text{-}fl}$*/Pax7-Cre*$^{+}$. Representative images of semiq-PCR analysis in 3 independent littermate couples. Data were normalized to endogenous levels of GAPDH).

Consistent with the *in vivo* results which showed an overall decrease in CSM4B cell population in *Pax7-Cre*$^{+}$ muscles, primary myoblasts isolated from *Lap2*$\alpha^{Neo\text{-}fl/Neo\text{-}fl}$*/Pax7-Cre*$^{+}$, as well as *Lap2*$\alpha^{+/+}$*/Pax7-Cre*$^{+}$ transgenic mice, died after the induction of differentiation (removal of basic fibroblast growth factor and 20% foetal calf serum $\rightarrow$ 5% horse serum substitution). As shown in Figure 43, *Pax7-Cre*$^{+}$ myoblasts initiated the differentiation process, but the majority of newly formed myotubes, as well as single cells, died by day 5 of differentiation. At this point, however it is not possible to distinguish whether these cells died due to cell-intrinsic defects or require special *in vitro* culturing conditions. Presumably, if the cell-intrinsic defects were as extensive *in vivo*, the mice would probably show signs of retarded postnatal growth, as observed in *Pax7*$^{-/-}$ mice, which lose their stem cell pool after birth due to apoptosis[204, 205]. Still, a reduced number of satellite cells, as observed in *Pax7-Cre*$^{+}$ mice, may be sufficient to rescue the phenotype of *Pax7*$^{-/-}$ animals.

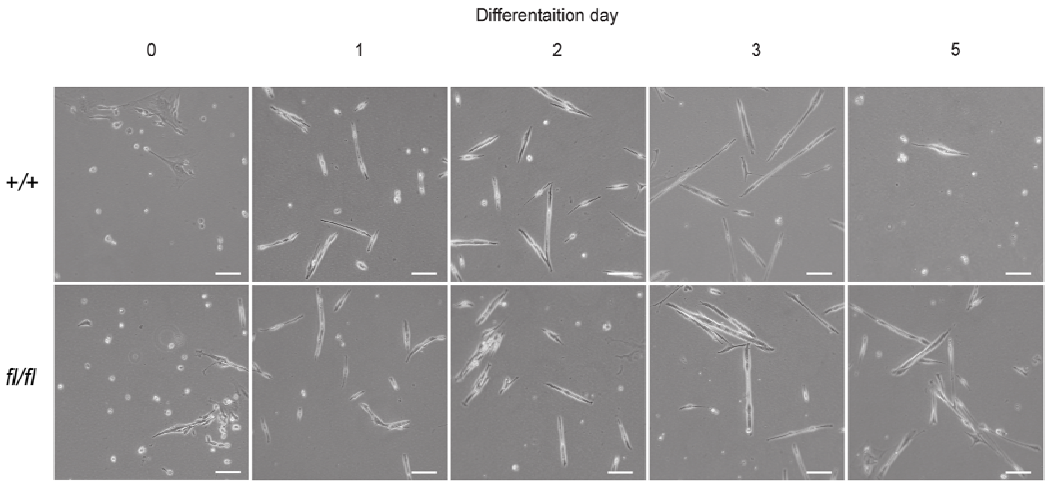

Figure 43. *Pax7-Cre*$^{+}$ primary myoblasts die after the induction of differentiation. Both *Lap2*$\alpha^{+/+}$*/Pax7-Cre*$^{+}$ *(+/+) and Lap2*$\alpha^{Neo\text{-}fl/Neo\text{-}fl}$*/Pax7-Cre*$^{+}$ *(fl/fl)* myoblasts are able to differentiate into myotubes, but the majority of cells dies by day 5 of differentiation. (Representative bright field images of 5 independent experiments, bar = 50 μm).

The death of *Pax7-Cre*$^{+}$ cells prevented the analysis of their muscle-specific gene expression patterns. However, as shown in Figure 44, the expression of LAP2α in *Lap2α*$^{+/+}$*/Pax7-Cre*$^{+}$ myoblasts followed the standard differentiation curve described above for the other LAP2α lines. *Lap2α*$^{Neo\text{-}fl/Neo\text{-}fl}$*/Pax7-Cre*$^{+}$ cells used in this study showed an efficient ablation of LAP2α already in proliferating satellite cells progeny.

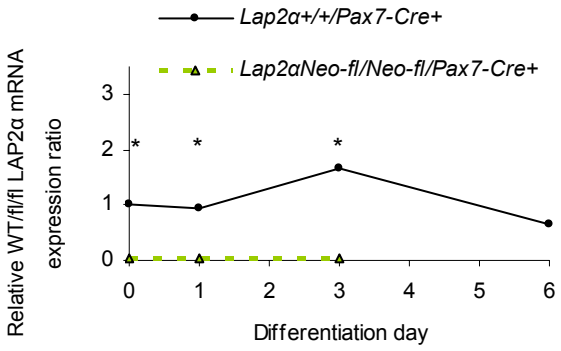

Figure 44. *Lap2α*$^{Neo\text{-}fl/Neo\text{-}fl}$*/Pax7-Cre*$^{+}$ cells show efficient deletion of LAP2α. (qPCR analyses of primary myoblast cultures; n = 3 separate experiments; *p<0.05 for *Lap2α*$^{+/+}$*/Pax7-Cre*$^{+}$ vs. *Lap2α*$^{Neo\text{-}fl/Neo\text{-}fl}$*/Pax7-Cre*$^{+}$ samples, ANOVA; each wild type sample was compared to its respective Day 0 value and each floxed sample to its respective wild type littermate sample at the particular time point).

Histological analysis of soleus and TA muscles in *Pax7-Cre*$^{+}$ mice revealed a general shift in soleus myofiber type ratios towards faster types (57% of slow fibers in C57/B6 background → 30% in *Pax7-Cre*$^{+}$ animals), specific for the *Pax7-Cre*$^{+}$ transgenic line and irrespective of LAP2α presence (Figure 45). This phenomenon might originate from a specific genetic constitution of the mouse line used for the generation of *Pax7-Cre*$^{+}$ mice, as it was shown that various laboratory mice exhibit substantial differences in muscle fiber type composition[206]. Conversely, the shift in myofiber type ratios might also reflect a general deficiency in muscle tissue homeostasis caused by defects in PAX7-expressing cells. Interestingly, similar changes in the fiber type distribution characterize muscle aging and disuse.

A)

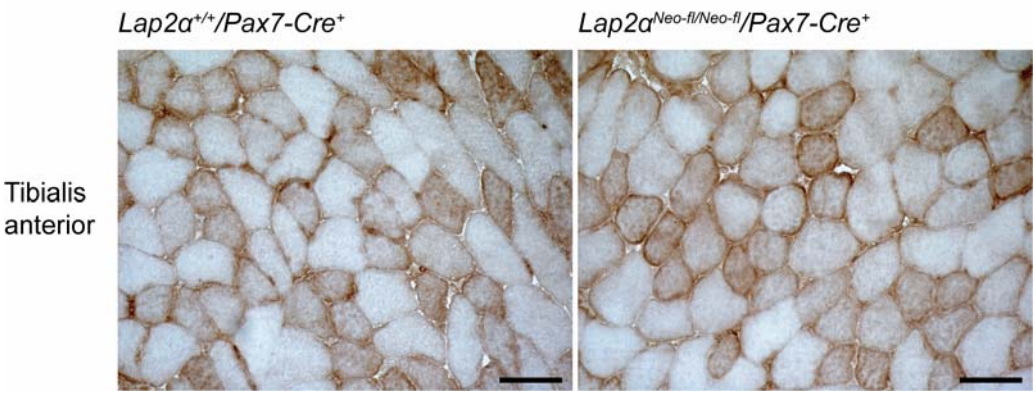

B)

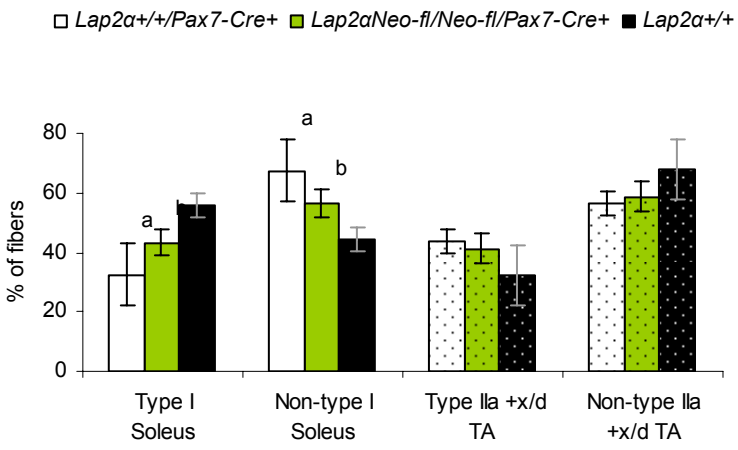

Figure 45. *Lap2α*$^{+/+}$*/Pax7-Cre*$^{+}$ and *Lap2α*$^{Neo\text{-}fl/Neo\text{-}fl}$*/Pax7-Cre*$^{+}$ soleus muscles show a shift in myofiber ratios towards faster types. A) Immunohistochemical analysis of TA (upper panels) muscle stained with antibodies specific for fast (Type IIa+x/d) myosin heavy chain. Bar = 50 μm. **B)** Quantification of specific myofiber types. (n = 3 *Pax7-Cre*$^{+}$ littermate pairs and 5 *Lap2α*$^{+/+}$ mice; p<0.05 for (a) *Lap2α*$^{+/+}$ vs. *Lap2α*$^{+/+}$*/Pax7-Cre*$^{+}$ mice and (b) *Lap2α*$^{+/+}$ vs. *Lap2α*$^{Neo\text{-}fl/Neo\text{-}fl}$*/Pax7-Cre*$^{+}$ mice; ANOVA followed by Boniferroni adjustment; values are means ± 95% CI).

In conclusion, the conditional muscle-specific *Pax7-Cre*$^{+}$ LAP2α knockout mice did not allow the analysis of LAP2α function during early phases of muscle stem cell specification and establishment of satellite cell population, due to intrinsic defects of the *Pax7-Cre*$^{+}$ line. To overcome this problem, an alternative *Pax7-Cre*$^{+}$ transgenic line could be used in future studies[207]. Still, since PAX7 is also expressed in developing central neural system and the neural crest, and plays an important role in maintenance of adult neural cells[208], the contribution of defects in other tissues to the skeletal muscle phenotype could not be excluded this way.

Therefore, until an exclusive muscle-specific stem cell marker has been identified, alternative approaches could be used to elucidate LAP2α functions in stem cell maintenance. In particular, studies of mice in which the endogenous stem cell pool has been replaced by satellite cells with a specific LAP2α knockdown might give more conclusive answers. However, the loss of myogenic potential during *in vitro* culture of satellite cells and their complex re-administration into the native niche after isolation (reviewed in [[133]]), present serious pitfalls of such an approach.

3.5 Related co-authored publication

nature cell biology

Loss of nucleoplasmic LAP2α–lamin A complexes causes erythroid and epidermal progenitor hyperproliferation

Nana Naetar[1,6], Barbara Korbei[1,6], Serguei Kozlov[2], Marc A. Kerenyi[1,3], Daniela Dorner[1], Rosana Kral[1], Ivana Gotic[1], Peter Fuchs[1], Tatiana V. Cohen[2], Reginald Bittner[4], Colin L. Stewart[2,5] and Roland Foisner[1,7]

Lamina-associated polypeptide (LAP) 2α is a chromatin-associated protein that binds A-type lamins[1,2]. Mutations in both LAP2α and A-type lamins are linked to human diseases called laminopathies[3], but the molecular mechanisms are poorly understood. The A-type lamin–LAP2α complex interacts with and regulates retinoblastoma protein (pRb)[4,5], but the significance of this interaction *in vivo* is unknown. Here we address the function of the A-type lamin–LAP2α complex with the use of LAP2α-deficient mice. We show that LAP2α loss causes relocalization of nucleoplasmic A-type lamins to the nuclear envelope and impairs pRb function. This causes inefficient cell-cycle arrest in dense fibroblast cultures and hyperproliferation of epidermal and erythroid progenitor cells *in vivo*, leading to tissue hyperplasia. Our results support a disease-relevant model[6] in which LAP2α defines A-type lamin localization in the nucleoplasm, which in turn affects pRb-mediated regulation of progenitor cell proliferation and differentiation in highly regenerative tissues.

LAP2α is one of six LAP2 isoforms[7]; it belongs to the LEM (LAP–Emerin–MAN1) protein family characterized by a structural motif (LEM domain) that mediates binding to the chromatin protein Barrier to Autointegration Factor[2]. Most LAP2 isoforms and other LEM-domain proteins are integral proteins of the inner nuclear membrane and bind to the peripheral nuclear lamin network[2], which organizes chromatin and regulates gene expression[1]. In contrast, LAP2α localizes to the nucleoplasm, where it interacts with A-type lamins[8] and the cell-cycle regulator and tumour-suppressor protein retinoblastoma (pRb), and affects E2F–pRb-dependent gene expression[4]. Unlike B-type lamins, A-type lamins are expressed at later stages of development and their mutation causes a variety of diseases, including striated muscle diseases, lipodystrophy and Hutchinson–Gilford progeria[3]. A mutation in LAP2α that impairs binding to A-type lamins also causes dilated cardiomyopathy[9]. We hypothesized that A-type lamin–LAP2α complexes may control proliferation and differentiation of adult stem or progenitor cells through the pRb pathway and that a deregulation of this function in patients may impair stem cell activity and tissue homeostasis[6]. To test the role of LAP2α in pRb-regulated progenitor cell proliferation *in vivo*, we generated a *Lap2α* knockout mouse and analysed regenerative tissues, whose homeostasis is known to depend on pRb. The LAP2α-specific exon 4 in the *Lap2* gene (also known as thymopoietin, *Tmpo*) was flanked by loxP sites, and mice were crossed with Cre-recombinase-expressing mice[10] (Supplementary Information, Fig. S2). *Lap2α* messenger RNA and LAP2α protein were absent in postnatal primary fibroblasts and tissue extracts of LAP2α-deficient mice, whereas the expression of other LAP2 isoforms was not significantly affected (Supplementary Information, Fig. S2d–g). Immunofluorescence microscopy with LAP2 isoform-specific and pan-LAP2 antibodies revealed unchanged localization of the LAP2β isoform at the nuclear periphery and loss of LAP2α in the nuclear interior in *Lap2α*$^{-/-}$ fibroblasts (Supplementary Information, Fig. S2f).

Although the expression of A-type lamins was unchanged in LAP2α-deficient primary fibroblasts at the mRNA and protein level (Fig. 1c and Supplementary Information, Fig. S2g), localization of A-type lamins was affected. In wild-type fibroblasts, which were synchronized in G1 phase to avoid cell-cycle-dependent effects, A-type lamins were found at the nuclear periphery and throughout the nucleoplasm. In *Lap2α*$^{-/-}$ fibroblasts, staining of nucleoplasmic A-type lamins was greatly decreased (Fig. 1a). Intensity profiles of A-type lamin staining along a central axis through nuclei revealed a decrease in nucleoplasmic lamin in LAP2α-deficient cells (Fig. 1b). In addition, histograms depicting the number of cells with a given ratio of nucleoplasmic over rim staining intensities showed a shift in A-type lamin localization from the nucleoplasm in wild-type cells to the nuclear periphery in LAP2α-deficient cells (Fig. 1b). Furthermore,

[1]Max F. Perutz Laboratories, Medical University of Vienna and University of Vienna, Dr. Bohr-Gasse 9, A-1030 Vienna, Austria. [2]Advanced BioScience Laboratories, Basic Research Program, National Cancer Institute, Frederick Cancer Research and Development Center, Maryland 21702, USA. [3]Institute of Molecular Pathology, Vienna Biocenter, Dr. Bohr-Gasse 7, A-1030 Vienna, Austria. [4]Neuromuscular Research Center, Center for Anatomy and Cell Biology, Medical University of Vienna, Schwarzspanierstr. 17, A-1090 Vienna, Austria. [5]Present address: Institute of Medical Biology, 8A Biomedical Grove no. 06-40, Immunos, Singapore 138648.
[6]These authors contributed equally to this work.
[7]Correspondence should be addressed to R.F. (roland.foisner@meduniwien.ac.at).

Received 30 June 2008; accepted 1 September 2008; published online 12 October 2008; DOI: 10.1038/ncb1793

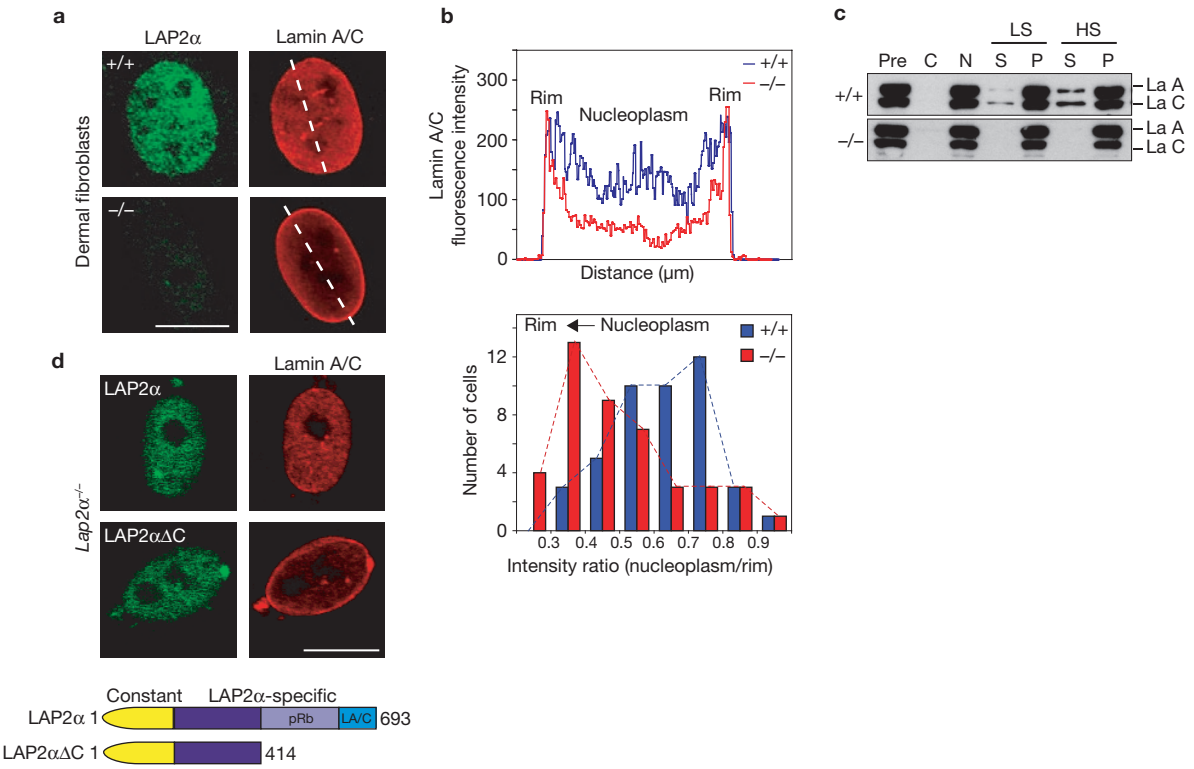

Figure 1 *Lap2α*$^{-/-}$ fibroblasts have reduced nucleoplasmic lamin A/C levels. (**a**) Immunofluorescence of aphidicolin-arrested wild-type (+/+) or *Lap2α* knockout (–/–) fibroblasts stained with antiserum against LAP2α and antibody against lamins A and C. Confocal images are shown. Scale bar, 10 μm. (**b**) Upper panel: fluorescence intensity of lamin A/C staining was determined along the axis shown as a dashed line in **a**, and plotted as a graph. Lower panel: ratios of nucleoplasmic to peripheral mean A-type lamin fluorescence intensity were calculated for 40 *Lap2α* knockout (–/–) and wild-type (+/+) fibroblasts and plotted in a histogram. (**c**) Total cell lysates (pre) or cytoplasmic (C) and nuclear (N) fractions, or soluble (S) and insoluble pellet (P) fractions after extraction of nuclei with low-salt (LS) or high-salt (HS) buffer were analysed by immunoblotting with antibodies against lamins A and C (La A and La C, respectively). (**d**) *Lap2α*$^{-/-}$ fibroblasts were transiently transfected with GFP-tagged full-length LAP2α or a LAP2α mutant lacking the pRb-binding and lamin-binding domain (LAP2αΔC) and processed for immunofluorescence microscopy 24 h after transfection with an antibody against lamins A and C. Confocal images are shown. Scale bar, 10 μm.

in wild-type fibroblasts extraction of nuclei at high salt concentrations solubilized a small fraction of lamins A and C (probably the nucleoplasmic pool), whereas lamins A and C from *Lap2α*$^{-/-}$ cells were completely insoluble (Fig. 1c). These data suggest that nucleoplasmic A-type lamins translocated to the peripheral lamina in *Lap2α*$^{-/-}$ cells. To examine the direct role of LAP2α in nucleoplasmic A-type lamin localization, we expressed full-length LAP2α or truncated LAP2α lacking its lamin binding domain (LAP2αΔC) in *Lap2α*$^{-/-}$ fibroblasts. Unlike the truncated protein, full-length LAP2α rescued the nucleoplasmic localization of lamins A and C (Fig. 1d). Thus, localization of A-type lamins in the nuclear interior is mediated by LAP2α and requires the lamin-binding domain of LAP2α.

We showed previously that nucleoplasmic LAP2α and A-type lamins affect the transition of cells between cycling and arrested states by repressing E2F–pRb-dependent promoter activity[4,5]. To test whether a loss of LAP2α and the accompanied decrease in nucleoplasmic A-type lamins disturbed pRb-mediated cell-cycle control, we followed contact-mediated cell-cycle arrest in primary mouse fibroblasts. *Lap2α*$^{-/-}$ fibroblasts reached a density about 1.5-fold that of control cells before cell-cycle arrest (Fig. 2a). This effect was probably caused by impaired contact inhibition, indicated by the more than twofold increase in the cell proliferation marker protein proliferating-cell nuclear antigen (PCNA) in dense *Lap2α*$^{-/-}$ versus control cultures (Fig. 2b), and was not caused by differences in cell size (Supplementary Information, Fig. S3b) or apoptotic rates (Fig. 2c). Several observations linked the cell-cycle phenotype to a deregulation of the pRb pathway. First, whereas total levels of pocket proteins pRb and p107 were unchanged, hyperphosphorylated pRb was upregulated up to twofold in dense *Lap2α*$^{-/-}$ versus control primary fibroblasts (Fig. 2b) and in immortalized *Lap2α*$^{-/-}$ lines (Supplementary Information, Fig. S3a). Second, mRNA levels of the E2F target genes *cyclin E1*, *PCNA* and *E2F1* were increased up to 50% in growth-arrested *Lap2α*$^{-/-}$ versus wild-type cells (Fig. 2d). Third, and in contrast, protein levels of the cyclin-dependent kinase inhibitors p16 and p27, which regulate pRb phosphorylation and cell-cycle arrest, were unchanged (Fig. 2b). Thus, loss of LAP2α in fibroblasts is accompanied by a p16- and p27-independent deregulation of pRb, leading to delayed contact-mediated cell-cycle arrest.

To test whether pRb deregulation is a direct cause of LAP2α loss, we expressed full-length LAP2α or a LAP2α mutant lacking the pRb-binding and lamin-binding domain (LAP2αΔC; see Fig. 1d), or green fluorescent protein (GFP) as a control in *Lap2α*$^{-/-}$ or wild-type cells, and analysed cell-cycle progression by the incorporation of bromodeoxyuridine (BrdU) (Fig. 2e). BrdU incorporation rates were increased in untransfected and GFP-transfected *Lap2α*$^{-/-}$ compared with wild-type cells. Re-expression of full-length LAP2α in knockout cells rescued the phenotype and decreased BrdU incorporation to wild-type levels (Fig. 2e). In contrast, expression of LAP2αΔC had no significant effect.

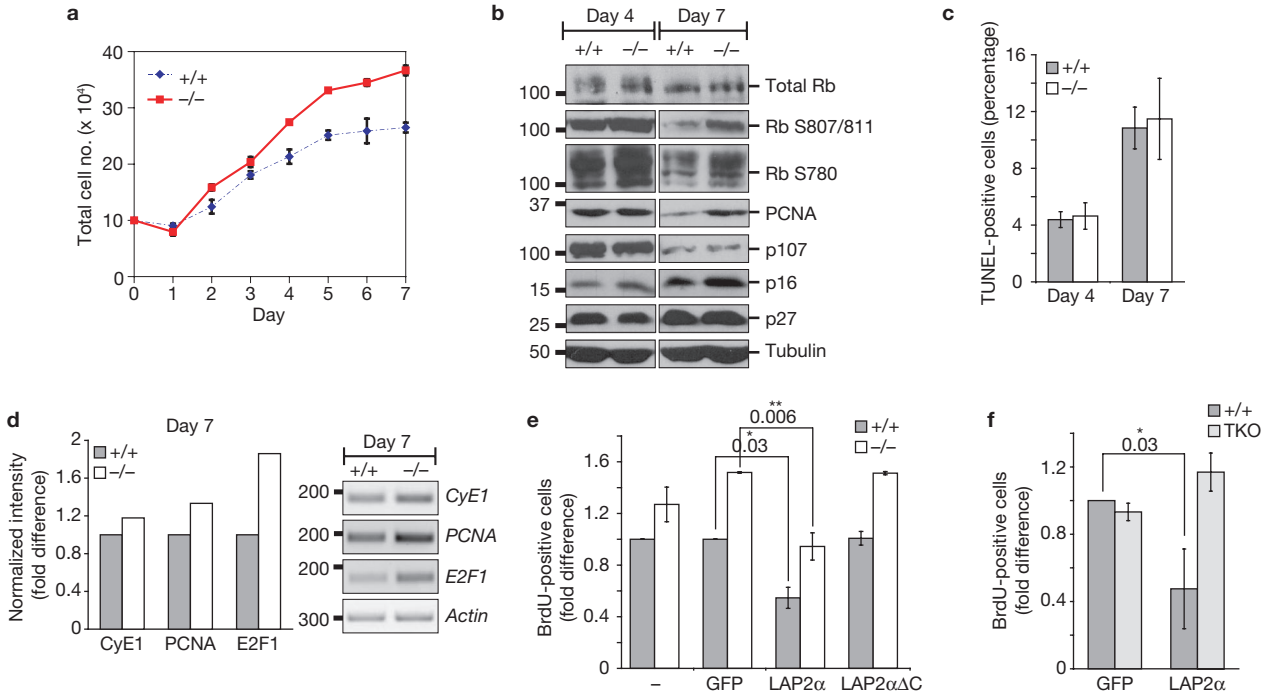

Figure 2 Loss of LAP2α in fibroblasts impairs cell-cycle arrest. (**a**) Primary postnatal *Lap2α*$^{+/+}$ and *Lap2α*$^{-/-}$ fibroblasts were seeded at equal densities. Cell numbers were determined daily and plotted against cultivation time. Values are means ± s.d. for four biological replicates. (**b**, **d**) Cells were lysed at the indicated time points and analysed by immunoblotting with antibodies against the indicated antigens (**b**) or mRNA was isolated and analysed by RT–PCR for expression of *cyclin E1* (*CyE1*), *PCNA*, *E2F1* and *actin* mRNA as control (**d**). An agarose gel of PCR fragments and quantification of band intensities normalized to actin mRNA levels are shown. Knockout values are depicted as fold difference from wild-type. (**c**) Apoptosis was quantified at the indicated time points with a TUNEL assay. (**e**, **f**) Primary *Lap2α*$^{-/-}$ (–/–) and wild-type (+/+) fibroblasts (**e**) or immortalized wild-type and *p130*$^{-/-}$ *p107*$^{-/-}$ *Rb*$^{-/-}$ triple knockout fibroblasts (TKO) (**f**) were transiently transfected with GFP-tagged full-length LAP2α, LAP2αΔC or GFP alone as indicated, and processed for BrdU incorporation assays 24 h after transfection. BrdU-positive transfected cells were counted and plotted in a bar graph. Values are shown as fold difference from GFP-transfected wild-type cells. Untransfected cultures (–) were included in the analysis as a control. Means ± s.e.m. for three independent experiments are shown in **c**, **e** and **f**. *P* values are indicated as follows: two asterisks, highly significant; asterisk, significant. Numbers in **b** indicate the molecular masses of marker proteins in kDa. Numbers in **d** denote corresponding marker bands and their length in base pairs. Uncropped images of blots in **b** are shown in Supplementary Information, Fig. S7.

Unlike with LAP2αΔC and GFP, expression of full-length LAP2α also impaired cell-cycle progression in wild-type cells. Thus, the cell-cycle phenotype observed in *Lap2α*$^{-/-}$ cells is directly linked to the absence of LAP2α and to the loss of binding of LAP2α to pRb and A-type lamins. Accordingly, the expression of full-length LAP2α in triple knockout cells lacking pocket proteins p107, p130 and pRb (ref. 11) had no effect on cell-cycle progression (Fig. 2f).

Next we tested the phenotypes of LAP2α loss at the organismal level. As LAP2α-deficient mice were viable and indistinguishable from their wild-type littermates, we investigated regenerative tissues immunohistochemically, most of which were previously shown to require pRb function for proper homeostasis. Muscle and liver from 2-month-old animals did not reveal an overt phenotype (Supplementary Information, Fig. S4a). In addition, heart, which is affected in patients with a *LAP2α* mutation, was unaffected histologically. In contrast, we detected a phenotype in paw epidermis of *Lap2α*$^{-/-}$ mice. The thickness of the epidermis (basal to granular cell layers) was increased by about 20% in *Lap2α*$^{-/-}$ versus wild-type tissue (Fig. 3a). This phenotype was most pronounced in the thickest regions of the plantar paw epidermis but was undetectable in the thin epidermis of the paw dorsum and the back skin. Because the plantar epidermis is exposed to mechanical stress, causing epidermal thickening and a high proliferative index, we reasoned that the observed phenotype might be linked to mechanical-stress-induced high turnover of the epidermis. Immunostaining revealed a prominent expression of LAP2α in nuclei of the basal cell layer and neighbouring suprabasal cells (Fig. 3b). Intriguingly, the number of Ki67-positive, proliferating cells, was increased up to twofold (in plantar epidermis) in *Lap2α*$^{-/-}$ versus control tissue (Fig. 3b). The hyperproliferation phenotype was linked to a deregulation of the pRb pathway, because pRb phosphorylation was increased in *Lap2α* knockout versus wild-type tissue (Supplementary Information, Fig. S5a). Phosphorylation of pRb was similarly increased in back skin, suggesting that pRb phosphorylation is not indirectly caused by the hyperproliferation of cells but is a direct consequence of LAP2α loss. We also tested transit amplifier cells in hair follicles and detected the highest expression of LAP2α in the Ki67-positive, proliferative matrix cells at the hair base, but neither their number nor localization was visibly affected in *Lap2α*$^{-/-}$ mice (data not shown). However, an upregulation of proliferating transit amplifier cells was observed in large and small intestine, yielding extended crypt lengths in large intestine (Supplementary Information, Fig. S4b). Thus, the effect of LAP2α loss on progenitor cells is most pronounced in highly regenerative regions of interfollicular epidermis, but it also occurs in other regenerative tissues.

Because proliferation and differentiation of the epidermal transit amplifier cells are closely linked, we tested the expression of epithelial differentiation markers by immunostaining. The layers expressing keratin 5, a basal cell marker, were significantly expanded in *Lap2α*$^{-/-}$

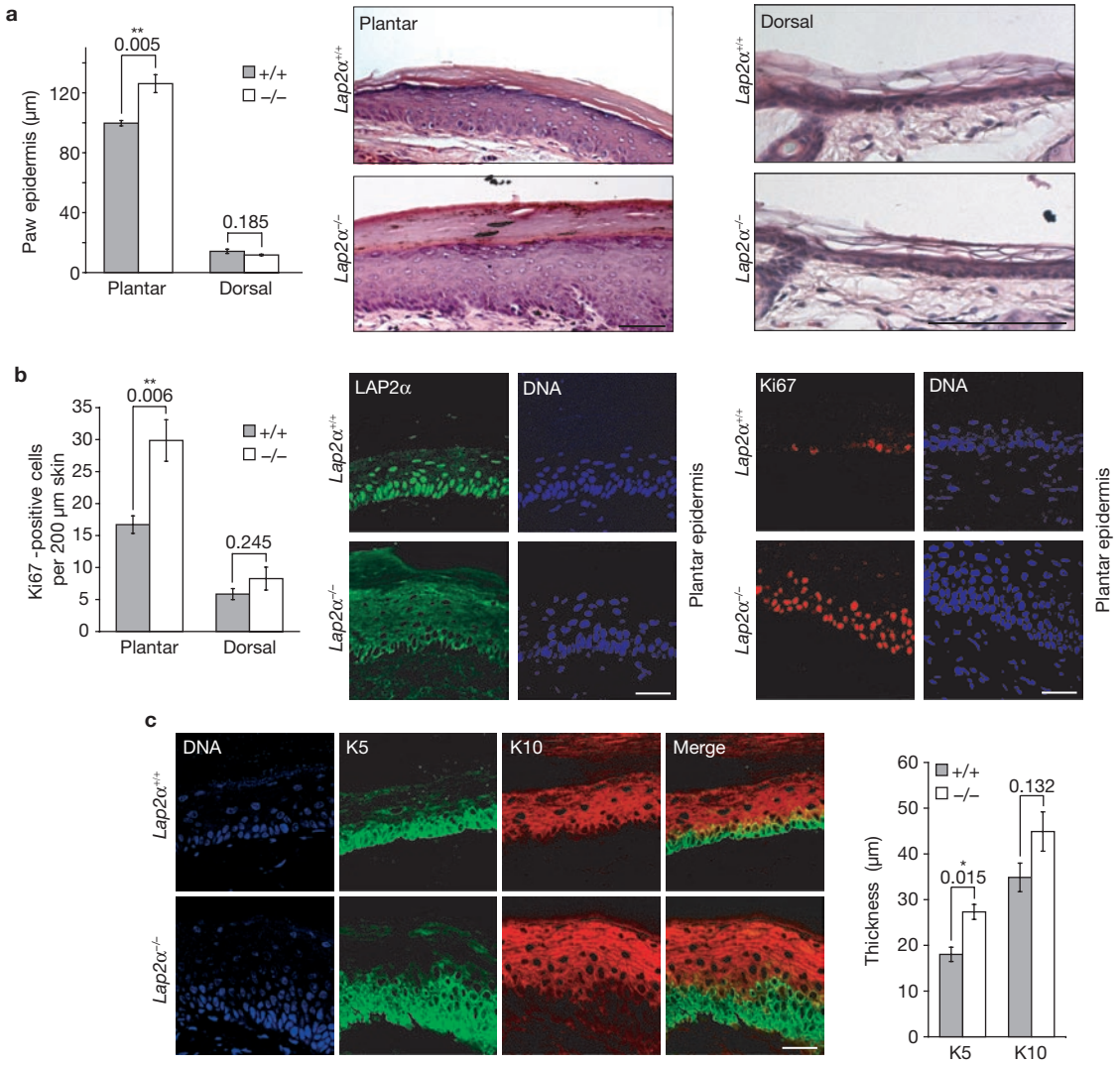

Figure 3 LAP2α-deficient paw epidermis contains a higher number of proliferating progenitor cells causing epidermal hyperplasia. (**a**) Right: haematoxylin/eosin-stained paraffin sections of epidermis from different paw regions (plantar or dorsal paw epidermis) of eight-week-old *Lap2α*$^{+/+}$ and *Lap2α*$^{-/-}$ mice. Scale bar, 50 μm. Left: the thickness of the different epidermal regions (excluding stratum corneum) was quantified using Axiovision imaging software and plotted in a bar graph ($n = 4$). (**b**, **c**) Paraffin sections of paw epidermis were analysed by immunofluorescence microscopy with antibodies against the indicated antigens. DNA was stained with Hoechst. Confocal images are shown. Scale bar, 50 μm. (**b**) Ki67-positive cells from paw epidermis were counted, normalized to skin length and plotted in a bar graph ($n = 7$). (**c**) The thickness of the K5-expressing and K10-expressing layer was quantified with LSM imaging software and plotted in a bar graph ($n = 3$). Results are shown as means ± s.e.m. *P* values are indicated as follows: two asterisks, highly significant; asterisk, significant.

tissue, as well as layers expressing keratin 10, a marker of suprabasal differentiated cells (Fig. 3c). Keratin-10-positive layers were negative for proliferation marker Ki67, and the expression and localization of the epidermal proteins plectin, desmoplakin and involucrin were unaffected in *Lap2α*$^{-/-}$ mice (Supplementary Information, Fig. S5b, c). Thus, *Lap2α*$^{-/-}$ transit amplifier cells hyperproliferate but differentiate normally and do not differentiate prematurely before exit from the cell cycle.

To test whether hyperproliferation of progenitor cells in LAP2α-deficient epidermis is accompanied by a delocalization of A-type lamins, we stained epidermal tissue sections for lamins A and C and Ki67. In wild-type tissue, a weak nucleoplasmic lamin staining was detectable in 70% of proliferating, Ki67-positive keratinocytes (Fig. 4a, arrows), whereas the staining was strongly reduced in non-proliferating, Ki67-negative cells (arrowheads). In contrast, 80% of proliferating LAP2α-deficient transit amplifier cells were negative for nucleoplasmic lamins. Thus, LAP2α loss is tightly linked to lower levels of nucleoplasmic lamins A and C in the context of an intact tissue.

If the LAP2α-loss-mediated delocalization of lamins A and C and the hyperproliferation of progenitor cells are functionally linked, one would expect a similar phenotype in A-type lamin-deficient tissues. Indeed, we found a subtle, but statistically significant, increase in Ki67-positive transit amplifier cells in the paw epidermis of *Lmna*$^{-/-}$ mice, causing a mild tissue hyperplasia (Fig. 4b). Thus, the absence of A-type lamins partly phenocopies the effects seen in LAP2α-deficient tissues and supports a common role for A-type lamin–LAP2α complexes in pRb-mediated cell-cycle control.

Our data indicate a dependence of the LAP2α loss phenotype on regenerative activity. We therefore tested the haematopoietic system,

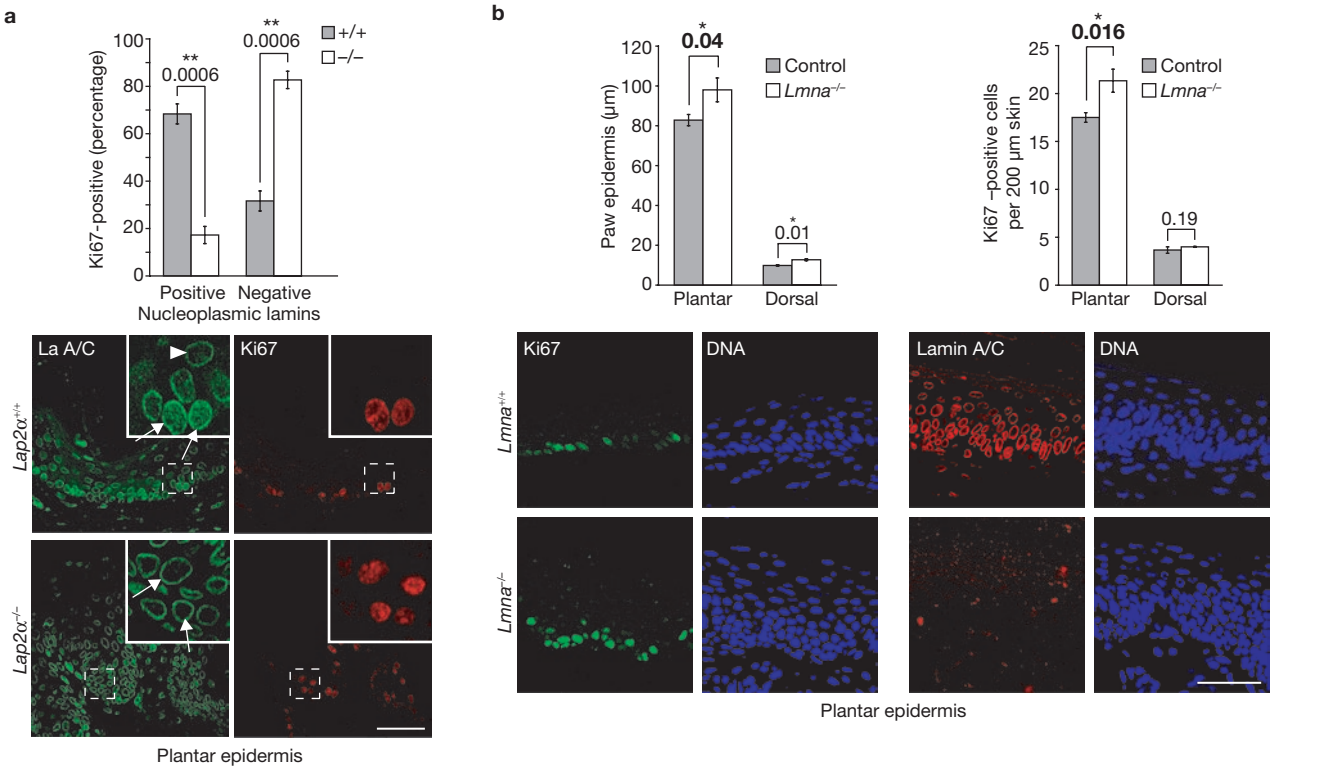

Figure 4 Loss of nucleoplasmic lamins A and C is linked to epidermal hyperproliferation. (**a**, **b**) Paraffin sections of paw epidermis from *Lap2α*$^{-/-}$ (**a**) or *Lmna*$^{-/-}$ (**b**) mice and wild-type controls were analysed by immunofluorescence microscopy with antibodies against Ki67 and lamins A and C. Confocal images are shown. Scale bar, 50 μm. Rectangles in **a** mark the regions shown as insets. Arrows indicate Ki67-positive cells; arrowheads indicate Ki67-negative cells. (**a**) The percentages of Ki67-positive cells either positive or negative for nucleoplasmic lamin A/C staining in *Lap2α* knockout (–/–) and wild-type (+/+) paw epidermis are shown ($n = 4$). (**b**) Left: the thickness of the different epidermal regions (excluding stratum corneum) in the paw (plantar or dorsal epidermis) of *Lmna*$^{-/-}$ (–/–) or *Lmna*$^{+/-}$ and *Lmna*$^{+/+}$ (Control) mice was quantified with Axiovision imaging software and plotted in a bar graph ($n = 3$). Right: Ki67-positive cells were counted, normalized to skin length and the results are shown in a bar graph ($n = 3$). Results are shown as means ± s.e.m. *P* values are indicated as follows: bold, one-tailed; two asterisks, highly significant; asterisk, significant.

which has a high regenerative capacity and expresses LAP2α at high level (Supplementary Information, Fig. S6a). Because flow cytometry revealed no alterations in lineage-marker-negative Sca-1/c-Kit-positive cells (LSK cells, comprising haematopoietic stem cells and primitive multipotent progenitors) in the bone marrow of *Lap2α*$^{-/-}$ versus control mice (Supplementary Information, Fig. S6b), we tested erythropoiesis, which requires pRb (refs 12, 13). Four cell populations (R1–R4; Fig. 5a) with different expression levels of cell-surface markers Ter119 and CD71 (Ter119^{med}CD71^{high}, Ter119^{high}CD71^{high}, Ter119^{high}CD71^{med} and Ter119^{high} CD71^{low}) represent consecutive stages of erythroid differentiation[14]. Flow cytometry revealed an up to fourfold increase in erythroid progenitors (R1 and R2) in spleens from *Lap2α*$^{-/-}$ versus control mice and a more subtle, but significant, increase in bone marrow erythroid progenitors (Fig. 5a). The number of mature erythroid cells (R3 and R4) was barely affected, indicating that *LAP2α*-null erythroblasts can differentiate. Spleen size and architecture were not affected (Supplementary Information, Fig. S4a). Haematocrit levels, reflecting erythrocyte numbers in peripheral blood, were slightly but significantly increased in *Lap2α*$^{-/-}$ (56.5 ± 0.8% (s.e.m); $n = 8$) versus wild-type littermates (52.8 ± 1.0% (s.e.m.); $n = 9$; $P = 0.014$). Thus, the increase in progenitor cell numbers leads to a net increase in mature erythrocytes in peripheral blood. To investigate the cell-cycle phenotype of early erythroblasts, we analysed lysates of Ter119-positive spleen cells by immunoblotting: *Lap2α*$^{-/-}$ lysates had increased levels of the proliferation markers PCNA and phospho-pRb in comparison with wild-type samples (Fig. 5b), whereas the apoptotic marker poly(ADP-ribose) polymerase (PARP) p85 fragment was unchanged. Thus, the increase of early erythroblasts in *Lap2α*$^{-/-}$ mice is caused by inefficient exit from the cell cycle and a deregulated pRb pathway rather than by decreased apoptosis.

Because the skin phenotype was most pronounced in stressed tissue, we tested how *Lap2α*$^{-/-}$ mice responded to severe erythroid stress, caused by phenylhydrazine (PHZ)-induced haemolysis. Three days after PHZ injection, spleen size was increased fourfold compared with mock-treated animals, and haematocrit values were decreased from about 50% to about 30%. Flow cytometry of spleen cells from PHZ-treated mice revealed a significant increase in all erythroid cell types in both *Lap2α*$^{-/-}$ and control littermates, reflecting the response to haemolytic stress. However, erythroid progenitor cells in PHZ-treated *Lap2α*$^{-/-}$ spleens were significantly increased in comparison with those in the PHZ-treated controls (Fig. 5d). Haematocrit levels were rescued to almost the pre-treatment levels within seven days after treatment, but red blood cell levels recovered more efficiently in *Lap2α*$^{-/-}$ versus wild-type littermates within the first five days (Fig. 5c).

It has previously been suggested that pRb loss may affect erythropoiesis indirectly by inhibiting the differentiation of macrophages, which provide the niche for erythropoiesis[15]. However, LAP2α-deficient bone marrow cells readily differentiated into macrophages *in vitro*, and,

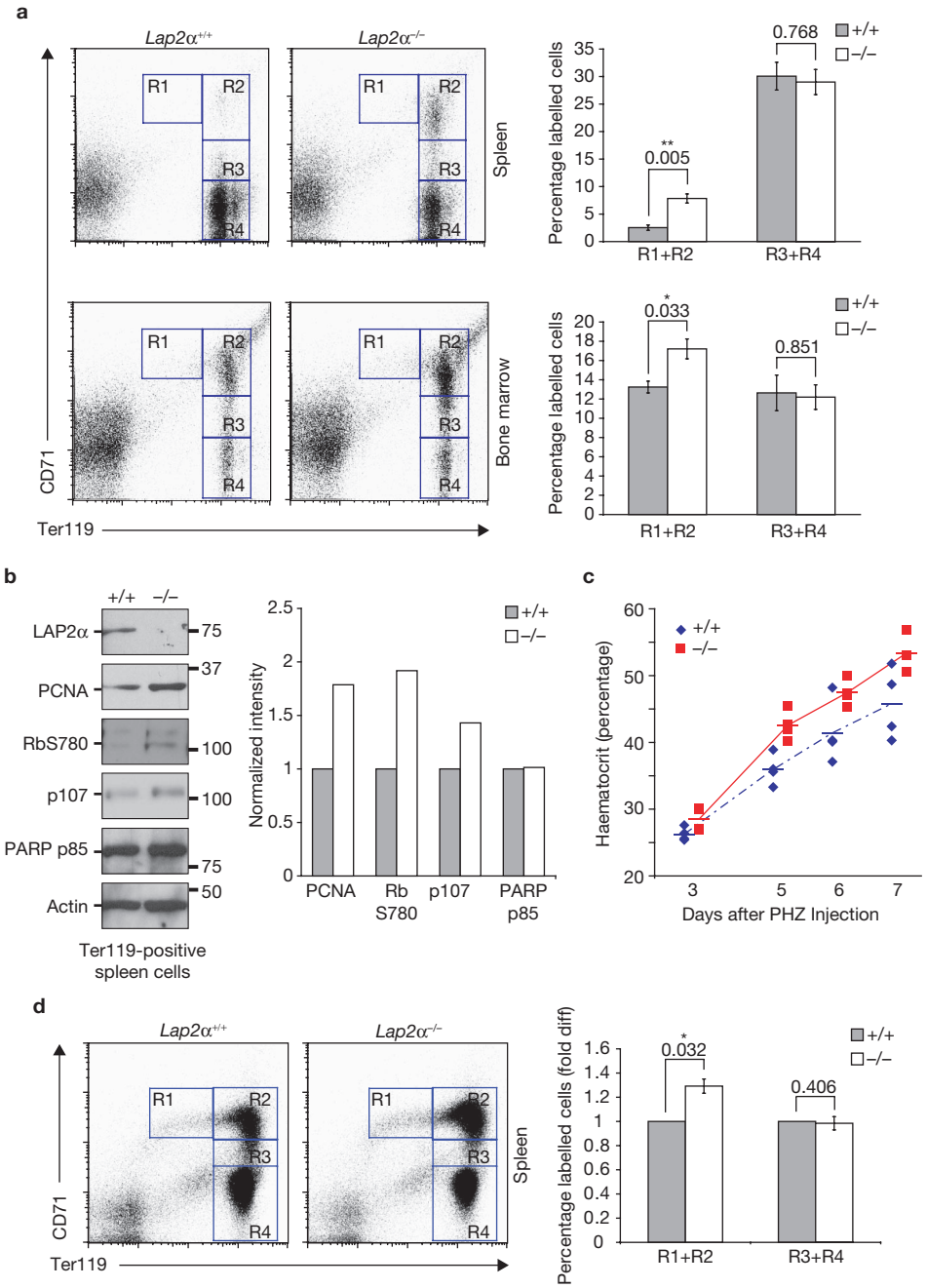

Figure 5 Absence of LAP2α leads to elevated levels of erythroid progenitors. (**a**) Representative flow cytometric profiles of spleen or bone marrow cells from eight-week-old wild-type (+/+) or *Lap2α* knockout (–/–) mice. Cells were labelled with antibodies against Ter119 and CD71. Regions 1–4 (R1–R4) represent four erythroid maturation stages. Bar graphs show the percentage of labelled erythroid progenitors (R1 and R2) and mature erythroid cells (R3 and R4) in spleen and bone marrow. Results are shown as means ± s.e.m. ($n = 3$). (**b**) Ter119$^+$ spleen cells obtained by magnetic cell sorting from *Lap2α* knockout and wild-type control mice were lysed and processed for immunoblotting with antibodies against the indicated antigens. Numbers indicate the molecular masses of marker proteins in kDa. Quantifications of band intensities normalized to actin levels are shown on the right. Knockout values are depicted as fold difference from the wild-type. (**c**, **d**) *Lap2α*$^{-/-}$ mice (–/–) and wild-type littermate controls (+/+) were injected with PHZ; after two days, spleen cells were analysed by flow cytometry with antibodies against Ter119 and CD71 (**d**). Regions 1–4 are as in **a**. The bar graph shows values of *Lap2α*$^{-/-}$ mice and wild-type littermates. Knockout values are depicted as fold difference from the wild-type. Results are shown as means ± s.e.m. ($n = 3$). (**c**) Haematocrit levels in peripheral blood from *LAP2α* knockout (–/–) and wild-type (+/+) mice were determined over a time course of seven days after PHZ injection at day 0 and day 1. Horizontal lines indicate mean values ($n = 4$). *P* values are indicated as follows: two asterisks, highly significant; asterisk, significant. Uncropped images of blots in **b** are shown in Supplementary Information, Fig. S7.

unlike pRb-deficient macrophages[15], showed normal expression of the late macrophage differentiation markers CSF-1R (colony stimulating factor-1 receptor), SR-A (scavenger receptor A) and Cd11b (data not shown). We therefore concluded that the effects of LAP2α are intrinsic to erythroblasts and are not caused indirectly by affecting the niche of erythroid progenitors.

Taken together, our results reveal two major functions of LAP2α *in vivo*. First, it is required for localizing a subfraction of A-type lamins in the nuclear interior (Supplementary Information, Fig. S1). The existence of a nucleoplasmic pool of lamin A, as opposed to the stable lamina-forming pool at the nuclear periphery, has been described before[16], but the molecular mechanisms of lamin A targeting were unclear. Our hypothesis is consistent with earlier findings showing that the loss of nucleoplasmic A-type lamins during myoblast differentiation *in vitro*[17] and on entering senescence[5] is linked to a downregulation or loss of LAP2α. Second, our study provides strong evidence for a function of the nucleoplasmic, LAP2α-associated A-type lamins in regulating early progenitor cell proliferation in regenerative tissues *in vivo*. Several observations indicate a role of A-type lamin–LAP2α complexes in the pRb pathway: first, pRb was deregulated (hyperphosphorylated) and E2F–pRb target genes were upregulated in LAP2α-deficient cells on contact-inhibition-mediated growth arrest and in affected tissues; second, the effects of LAP2α on cell-cycle progression depend on its pRb-binding and lamin-binding domains and on the presence of pocket proteins; and third, the set of tissues affected in *Lap2α*$^{-/-}$ mice was similar to that in pRb-deficient animals. LAP2α and pRb[18] are dispensable for self-renewal of lin^{-}Sca-1^{+}c-Kit^{high} haematopoietic cells, but they affect the cell-cycle exit of early erythroid progenitors during erythropoiesis[12,13]. LAP2α-deficient and pRb-deficient epidermis[19] and intestine[20] show an impaired balance between proliferation and differentiation of transit amplifier cells. However, LAP2α-linked phenotypes are milder than those caused by pRb deficiency, because pRb is not absent from *Lap2α*$^{-/-}$ cells but functionally impaired, and LAP2α deficiency may affect only a subset of pRb functions. Although at present we do not have any experimental evidence for an interaction of LAP2α with the closest relatives of pRb, namely p107 and p130, we cannot completely rule out possible effects of LAP2α on other pocket proteins.

Loss of p16, which may also cause hyperphosphorylation of pRb, could have consequences similar to those of LAP2α loss in mice. Indeed, hyperproliferation of haematopoietic[21] and neural stem cells[22] and of pancreatic island cells[23] was described in aged p16-deficient mice. The different cell types affected in LAP2α-deficient and p16-deficient mice may be explained by the different expression profiles of these proteins.

Our data suggest that LAP2α-mediated targeting of A-type lamins to the nucleoplasm regulates pRb activity in early progenitor cells to maintain a proper balance between proliferation and differentiation (Supplementary Information, Fig. S1). Whereas multipotent stem cells (for example haematopoietic stem cells), which express little LAP2α and no lamin A/C (refs 24, 25), are not affected by LAP2α loss, this mechanism may be highly relevant for stem-cell-derived, lineage-committed progenitors, which start to express lamin A/C and have high levels of LAP2α. We consider our findings to be highly relevant for laminopathic diseases in humans[3], suggesting that mutations in *LMNA* or *LAP2* may impair early progenitor cells in tissue regeneration[6]. This hypothesis is supported by recent studies showing impaired function of adult stem cells on expression of progeria-linked lamin variants[26–28]. □

METHODS

Targeted disruption of the *Lap2α* gene. To generate LAP2α-isoform-deficient mice, we made a targeting construct allowing conditional deletion of the LAP2α-specific exon 4 in the mouse *Lap2* gene on chromosome 10, which encodes six isoforms[7]. The targeting vector contained a neomycin resistance cassette, flanked by *flipase recognition target* recombination sites, upstream of exon 4, as well as Cre-recombinase-specific *loxP* sites at the 5′ end of the *neo* gene and the 3′ end of exon 4 (Supplementary Information, Fig. S2a). The targeting construct comprised a 6.5-kilobase (kb) 5′ homologous region including exons 2 and 3, and a 3.2-kb 3′ homologous region including exon 5, derived from genomic *Lap2*-containing bacterial artificial chromosome (BAC) clones from Genome Systems (*Lap2*-genomic 22427). It also contained a diphtheria toxin gene after the 3′ homology arm as a negative selection marker for random insertion. For cloning of the targeting construct, see Supplementary Information. The targeting construct was introduced into embryonic stem cells, and clones were tested for homologous recombination by Southern blot analyses (Supplementary Information, Fig. S2c). Heterozygous clones were used for blastocyst injection, and chimaeric offspring were derived with subsequent germline transmission of the floxed allele. Heterozygotes were intercrossed to obtain viable homozygous offspring, which were crossed with transgenic mice ubiquitously expressing the Cre recombinase[10]. Homozygous *Lap2α* knockout mice were further crossed with wild-type C57BL/6 mice to remove the Cre recombinase gene. Mice were maintained in accordance with the procedures outlined in the Guide for the Care and Use of Laboratory Animals. Animal experiments were performed in accordance with permission from the Austrian authorities and under National Institutes of Health guidelines. Adult mice were analysed between 3 and 12 weeks after birth. PHZ (Sigma-Aldrich, St Louis, MO, USA) was dissolved in PBS and injected intraperitoneally at 60 mg kg^{-1}. Haematocrit was determined from tail-vein blood with the Vet animal blood count (Scil Animal Care). Genotyping of mice was performed as described in Supplementary Information.

Isolation and analyses of primary fibroblasts. Primary fibroblasts were isolated one to three days postnatally from back skin as described[29]. Cells were cultivated in high-glucose DMEM medium, 10% fetal calf serum, 50 U ml^{-1} penicillin, 50 μg ml^{-1} streptomycin and 0.2 μM L-glutamine (all from Invitrogen, Carlsbad, CA, USA) at 37 °C and 5% CO_2. Experiments were performed between passages 1 and 3. For analysis of cell growth, 10^5 cells were seeded on six-well plates and cell numbers and cell volume were determined daily with a CASY counter Model TTC (Schärfe System, Reutlingen, Germany). For transfection experiments, modified pEGFP-C1 (Clontech Laboratories, Palo Alto, CA, USA) encoding full-length LAP2α (amino-acid residues 1–693, derived from pTD15 (ref. 30)) or a LAP2α deletion mutant (residues 1–414, derived from pSV12 (ref. 30)) with amino-terminal GFP tags, or empty pEGFP-C1 were transiently transfected into primary skin fibroblasts with Lipofectamine LTX (Invitrogen). Labelling with BrdU was performed with the 5-bromo-2′-deoxyuridine labelling and detection kit I (Roche, Mannheim, Germany). Apoptosis was analysed by TdT-mediated dUTP nick end labelling (TUNEL) reaction, using the *in situ* cell death detection kit/TMR red (Roche). Positive cells were analysed with an Axiovert 200M microscope (Zeiss, Jena, Germany).

For subcellular fractionation[31], isolated nuclei were resuspended in 500 μl of hypotonic buffer per 10^7 cells (10 mM HEPES pH 7.4, 10 mM NaCl, 5 mM $MgCl_2$, 1 mM EGTA, 1 mM dithiothreitol, and protease inhibitor cocktail from Roche) and 8.5% sucrose. Suspensions were mixed with NaCl to 50 or 200 mM, and soluble and insoluble fractions were separated by centrifugation for 30 min at 16,000*g* at 4 °C, and analysed by immunoblotting. SDS–PAGE and immunoblotting were performed as described[31].

Reverse transcription (RT–) PCR. Poly(A)$^+$ mRNAs were isolated and reverse transcribed as described[4]. Complementary DNAs were normalized to actin expression levels. PCR amplification was performed with GoTaq Green Master Mix (Promega, Madison, WI, USA) using primers specific for mouse LAP2α, LAP2, lamin A/C, PCNA, cyclin E and E2F1. For primer sequences see Supplementary Information. Ethidium bromide-stained bands on agarose gels were quantified with Adobe Photoshop version 8.0.

Haematoxylin/eosin staining and immunofluorescence microscopy. Tissues were dipped into prechilled 2-methylbutane and snap-frozen in liquid nitrogen. Cryosections were obtained with the Cryostat HM500 OM at −23 °C. Alternatively, tissues were fixed in 4% formaldehyde (Rotifix; Roth, Karlsruhe, Germany), dehydrated, embedded in paraffin and sectioned with a Leica RM 2155 microtome. Staining with haematoxylin/eosin was performed using the tissue-processing system Pat Histo ASS-1.

For immunofluorescence microscopy, cryosections were fixed in 3.7% formaldehyde (Merck) in PBS. Paraffin sections were rehydrated and incubated for 60 min in citrate buffer (1.8 mM citric acid solution, 8.2 mM sodium citrate) at

100 °C. Sections were incubated for 30 min in 0.1% Triton X-100 in PBS, blocked with goat serum (Vectastain; Vector Labs, Burlingame, CA, USA), and incubated with antibodies and Hoechst dye as described[32]. Immunofluorescence microscopy of cells was performed as described[32]. Where indicated, fibroblasts were synchronized in G1 by the addition of 5 μg ml^{-1} aphidicolin (Sigma-Aldrich) overnight before staining. Fluorescence intensity measurement was performed with LSM Imaging software (Zeiss). To determine the intensity ratio of nucleoplasm to rim, nucleoplasmic and peripheral intensity values were determined along a nuclear axis and averaged (ratio = average intensity of nucleoplasm/average intensity of rim).

Fluorescence-activated cell sorting (FACS) and magnetic-activated cell sorting (MACS). Spleen and bone marrow were squashed through a 70-μm cell strainer, washed with PBS, centrifuged and resuspended in 1–2 ml of PBS/0.2% BSA. Of this suspension, 50 μl was mixed with Fc block (CD16/CD32, BD Biosciences, Franklin Lakes, NJ, USA) and stained with primary antibodies for 30 min on ice. Samples were washed, resuspended in PBS/0.2% BSA and analysed with the BD FACSCalibur system. Data were quantified with FlowJo software (Tree Star). For MACS, 2×10^7 spleen cells were stained with phycoerythrin (PE)-labelled Ter119 antibody (BD Biosciences) for 30 min on ice, washed, resuspended in PBS/0.2% BSA and incubated with anti-PE MicroBeads (Miltenyi Biotec, Auburn, CA, USA). Cells were resuspended in PBS/0.2% BSA and Ter119-positive cells were collected with the autoMACS separator (Miltenyi Biotec).

Antibodies. The following antibodies were used: monoclonal antibodies against LAP2 and LAP2β (ref. 31), lamin A/C (1E4, a gift from Frank McKeon)[33], p27 (F8; Santa Cruz Biotechnology, Santa Cruz, CA, USA), cytokeratin 10 (MAB3230, Chemicon, Temecula, USA), desmoplakins 1 and 2 (Progen Biotechnik, Heidelberg, Germany), total Rb (G3-245; BD Biosciences) and PCNA (BD Biosciences); and polyclonal antibodies against LAP2α (ref. 32), lamin A/C (N18; Santa Cruz Biotechnology), Ki67 (Novocastra Laboratories, Newcastle, UK), p16 (M156; Santa Cruz Biotechnology), p107 (C18; Santa Cruz), cytokeratin 5 (AF138; Covance, Berkeley, CA, USA), plectin (provided by Gerhard Wiche), involucrin (Covance), RbS780 and RbS807/811 (Cell Signaling Technologies, Beverly, MA, USA), anti-PARP p85 fragment (Promega) and actin (A-2066; Sigma-Aldrich). For FACS analyses we used biotin-labelled anti-CD71, PE-labelled anti-Ter119, PE-labelled anti-c-Kit, fluorescein isothiocyanate-labelled anti-Sca-1 and biotin-labelled lineage cocktail (all from BD Biosciences).

Statistical analyses. Statistical analyses were performed with Microsoft Office Excel 2003. Student's *t*-test was used to calculate *P* values (two-tailed unless stated otherwise, α level 0.05). Percentages were converted to arcsin values before statistical analysis.

Note: Supplementary Information is available on the Nature Cell Biology website.

ACKNOWLEDGEMENTS

We thank W. Müller for the Cre-deleter mouse strain, Larry Gerace for the genomic BAC clone, T. Jacks for triple knockout mouse embryonic fibroblasts, P. Luvalle for providing paws from lamin A/C-deficient mice, K. Biadasiewicz for expert technical assistance, and H. Beug and E. W. Müllner for helpful discussions. This study was supported by grants from the Austrian Science Research Fund (FWF P17871) and the EURO-Laminopathies research project of the European Commission (contract LSHM-CT-2005-018690) to R.F. and a postdoctoral fellowship from L'Oreal/UNESCO/ÖADW/BMWF to N.N.

AUTHOR CONTRIBUTIONS

N.N., B.K., P.F., C.L.S. and R.F. planned the project; N.N., B.K., S.K., M.A.K., D.D., R.K., I.G. and T.C. performed the experiments; N.N., B.K., M.A.K., D.D., R.B. and R.F. analysed the data; N.N., B.K., C.L.S. and R.F. wrote the manuscript.

COMPETING FINANCIAL INTERESTS

The authors declare no competing financial interests.

Published online at http://www.nature.com/naturecellbiology/
Reprints and permissions information is available online at http://npg.nature.com/reprintsandpermissions/

1. Dechat, T. *et al.* Nuclear lamins: major factors in the structural organization and function of the nucleus and chromatin. *Genes Dev.* **22,** 832–853 (2008).
2. Schirmer, E. C. & Foisner, R. Proteins that associate with lamins: many faces, many functions. *Exp. Cell Res.* **313,** 2167–2179 (2007).
3. Capell, B. C. & Collins, F. S. Human laminopathies: nuclei gone genetically awry. *Nature Rev. Genet.* **7,** 940–952 (2006).
4. Dorner, D. *et al.* Lamina-associated polypeptide 2α regulates cell cycle progression and differentiation via the retinoblastoma–E2F pathway. *J. Cell Biol.* **173,** 83–93 (2006).
5. Pekovic, V. *et al.* Nucleoplasmic LAP2α–lamin A complexes are required to maintain a proliferative state in human fibroblasts. *J. Cell Biol.* **176,** 163–172 (2007).
6. Gotzmann, J. & Foisner, R. A-type lamin complexes and regenerative potential: a step towards understanding laminopathic diseases? *Histochem. Cell Biol.* **125,** 33–41 (2006).
7. Berger, R. *et al.* The characterization and localization of the mouse thymopoietin/lamina-associated polypeptide 2 gene and its alternatively spliced products. *Genome Res.* **6,** 361–370 (1996).
8. Dechat, T. *et al.* Lamina-associated polypeptide 2α binds intranuclear A-type lamins. *J. Cell Sci.* **19,** 3473–3484 (2000).
9. Taylor, M. R. *et al.* Thymopoietin (lamina-associated polypeptide 2) gene mutation associated with dilated cardiomyopathy. *Hum. Mutat.* **26,** 566–574 (2005).
10. Schwenk, F., Baron, U. & Rajewsky, K. A cre-transgenic mouse strain for the ubiquitous deletion of loxP-flanked gene segments including deletion in germ cells. *Nucleic Acids Res.* **23,** 5080–5081 (1995).
11. Sage, J. *et al.* Targeted disruption of the three Rb-related genes leads to loss of G_1 control and immortalization. *Genes Dev.* **14,** 3037–3050 (2000).
12. Sankaran, V. G., Orkin, S. H. & Walkley, C. R. Rb intrinsically promotes erythropoiesis by coupling cell cycle exit with mitochondrial biogenesis. *Genes Dev.* **22,** 463–475 (2008).
13. Spike, B. T. *et al.* The Rb tumor suppressor is required for stress erythropoiesis. *EMBO J.* **23,** 4319–4329 (2004).
14. Socolovsky, M. *et al.* Ineffective erythropoiesis in $Stat5a^{-/-}5b^{-/-}$ mice due to decreased survival of early erythroblasts. *Blood* **98,** 3261–3273 (2001).
15. Iavarone, A. *et al.* Retinoblastoma promotes definitive erythropoiesis by repressing Id2 in fetal liver macrophages. *Nature* **432,** 1040–1045 (2004).
16. Moir, R. D., Yoon, M., Khuon, S. & Goldman, R. D. Nuclear lamins A and B1: different pathways of assembly during nuclear envelope formation in living cells. *J. Cell Biol.* **151,** 1155–1168 (2000).
17. Markiewicz, E., Ledran, M. & Hutchison, C. J. Remodelling of the nuclear lamina and nucleoskeleton is required for skeletal muscle differentiation in vitro. *J. Cell Sci.* **118,** 409–420 (2005).
18. Walkley, C. R. & Orkin, S. H. Rb is dispensable for self-renewal and multilineage differentiation of adult hematopoietic stem cells. *Proc. Natl Acad. Sci. USA* **103,** 9057–9062 (2006).
19. Ruiz, S. *et al.* Unique and overlapping functions of pRb and p107 in the control of proliferation and differentiation in epidermis. *Development* **131,** 2737–2748 (2004).
20. Haigis, K., Sage, J., Glickman, J., Shafer, S. & Jacks, T. The related retinoblastoma (pRb) and p130 proteins cooperate to regulate homeostasis in the intestinal epithelium. *J. Biol. Chem.* **281,** 638–647 (2006).
21. Janzen, V. *et al.* Stem-cell ageing modified by the cyclin-dependent kinase inhibitor $p16^{INK4a}$. *Nature* **443,** 421–426 (2006).
22. Molofsky, A. V. *et al.* Increasing $p16^{INK4a}$ expression decreases forebrain progenitors and neurogenesis during ageing. *Nature* **443,** 448–452 (2006).
23. Krishnamurthy, J. *et al.* $p16^{INK4a}$ induces an age-dependent decline in islet regenerative potential. *Nature* **443,** 453–457 (2006).
24. Constantinescu, D., Gray, H. L., Sammak, P. J., Schatten, G. P. & Csoka, A. B. Lamin A/C expression is a marker of mouse and human embryonic stem cell differentiation. *Stem Cells* **24,** 177–185 (2006).
25. Pajerowski, J. D., Dahl, K. N., Zhong, F. L., Sammak, P. J. & Discher, D. E. Physical plasticity of the nucleus in stem cell differentiation. *Proc. Natl Acad. Sci. USA* **104,** 15619–15624 (2007).
26. Espada, J. *et al.* Nuclear envelope defects cause stem cell dysfunction in premature-aging mice. *J. Cell Biol.* **181,** 27–35 (2008).
27. Sagelius, H. *et al.* Targeted transgenic expression of the mutation causing Hutchinson–Gilford progeria syndrome leads to proliferative and degenerative epidermal disease. *J. Cell. Sci.* **121,** 969–978 (2008).
28. Scaffidi, P. & Misteli, T. Lamin A-dependent misregulation of adult stem cells associated with accelerated ageing. *Nature Cell Biol.* **10,** 452–459 (2008).
29. Andra, K., Nikolic, B., Stocher, M., Drenckhahn, D. & Wiche, G. Not just scaffolding: plectin regulates actin dynamics in cultured cells. *Genes Dev.* **12,** 3442–3451 (1998).
30. Vlcek, S., Just, H., Dechat, T. & Foisner, R. Functional diversity of LAP2α and LAP2β in postmitotic chromosome association is caused by an α-specific nuclear targeting domain. *EMBO J.* **18,** 6370–6384 (1999).
31. Dechat, T. *et al.* Detergent-salt resistance of LAP2α in interphase nuclei and phosphorylation-dependent association with chromosomes early in nuclear assembly implies functions in nuclear structure dynamics. *EMBO J.* **17,** 4887–4902 (1998).
32. Vlcek, S., Korbei, B. & Foisner, R. Distinct functions of the unique C terminus of LAP2α in cell proliferation and nuclear assembly. *J. Biol. Chem.* **277,** 18898–18907 (2002).
33. Loewinger, L. & McKeon, F. Mutations in the nuclear lamin proteins resulting in their aberrant assembly in the cytoplasm. *EMBO J.* **7,** 2301–2309 (1988).

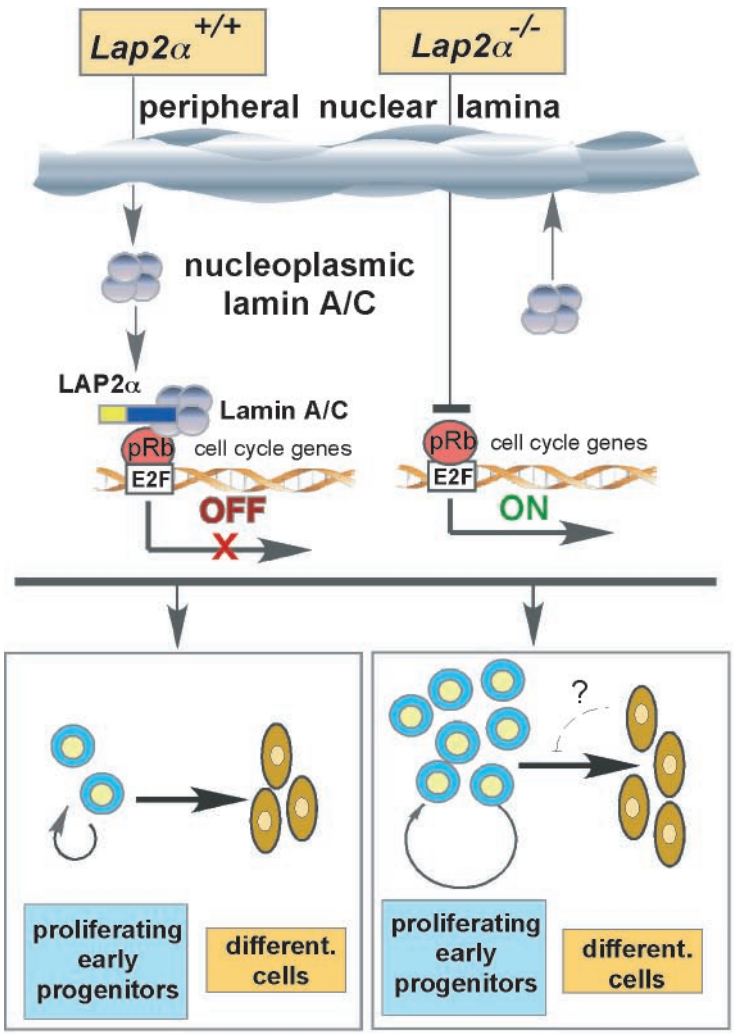

Figure S1 Model depicting the function of LAP2α. LAP2α targets a subfraction of lamin AC from the peripheral lamina to the nucleoplasm, where the complex interacts with pRb and represses the expression of pRb/E2F-dependent cell cycle regulatory genes. In the absence of LAP2α nucleoplasmic lamin A/C is lost and pRb's repressor activity is impaired. While cell proliferation and differentiation of early progenitor cells in regenerating tissues is balanced in wild-type tissues, LAP2α-deficient cells hyperproliferate due to the deregulated pRb pathway. Despite hyperproliferation, differentiation appears normal, but several control mechanisms (?) may keep the number of differentiated cells within a narrow window.

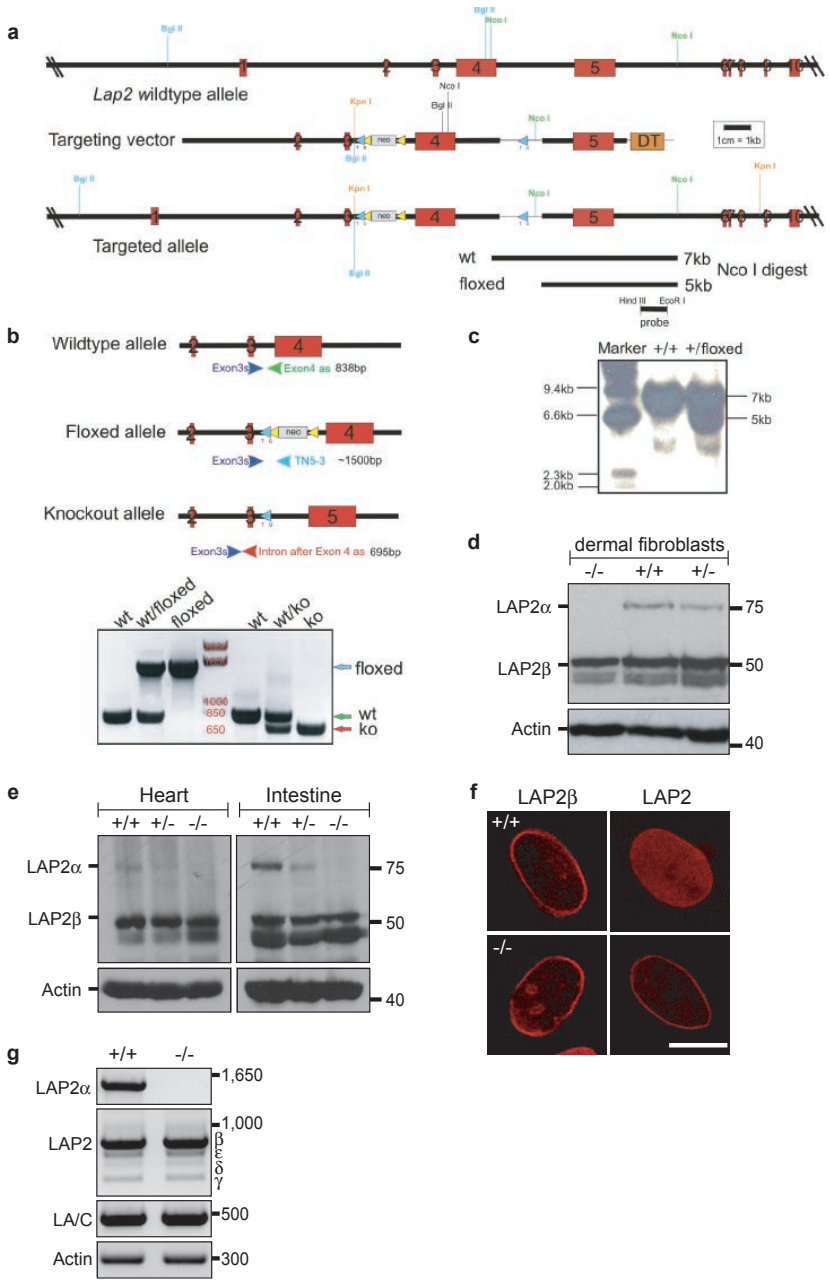

Figure S2 Targeted inactivation of *Lap2α*. (**a**) Schematic representation of the *Lap2* gene locus, the targeting vector, and the targeted allele. NcoI restriction sites, FRT (yellow triangles) and loxP (blue triangles) recombination sites, exons (boxes), the Pgk-neo and the diphtheria toxin cassette (DT) are shown. The position of the probe used for Southern blotting and the expected fragments are indicated. (**b**) PCR analysis of genomic DNA prepared from tail biopsies of wild-type (wt), heterozygous floxed (wt/floxed), homozygous floxed (floxed), heterozygous (wt/ko) and homozygous knockout (ko) mice. A schematic drawing of the wild-type, floxed and deleted *Lap2* alleles is shown and positions of primers are indicated. (**c**) Southern blot analysis of NcoI-digested genomic DNA from wild-type (+/+) and heterozygous floxed (+/floxed) ES cell clones, using the probe shown in (**a**). (**d**, **e**) Immunoblot analyses of lysates from primary fibroblasts (**d**) isolated from newborn wild-type (+/+), heterozygous (+/–) and homozygous knockout (–/–) mice, and from heart and intestine tissue (**e**) prepared from 2 months old mice, using pan LAP2 antibody, detecting all LAP2 isoforms. Actin was stained as a loading control. Numbers indicate molecular masses of marker proteins in kDa. (**f**) Immunofluorescence of wild-type (+/+) or LAP2α knockout (–/–) fibroblasts stained with antibodies to LAP2β or LAP2. Confocal images are shown. Bar, 10 μm. (**g**) Reverse transcriptase (RT-) PCR of mRNA from primary fibroblasts using primers for LAP2α, LAP2 isoforms (indicated on the right), lamin A/C, and actin to normalize for mRNA amounts. Numbers denote corresponding marker bands and their length in bp.

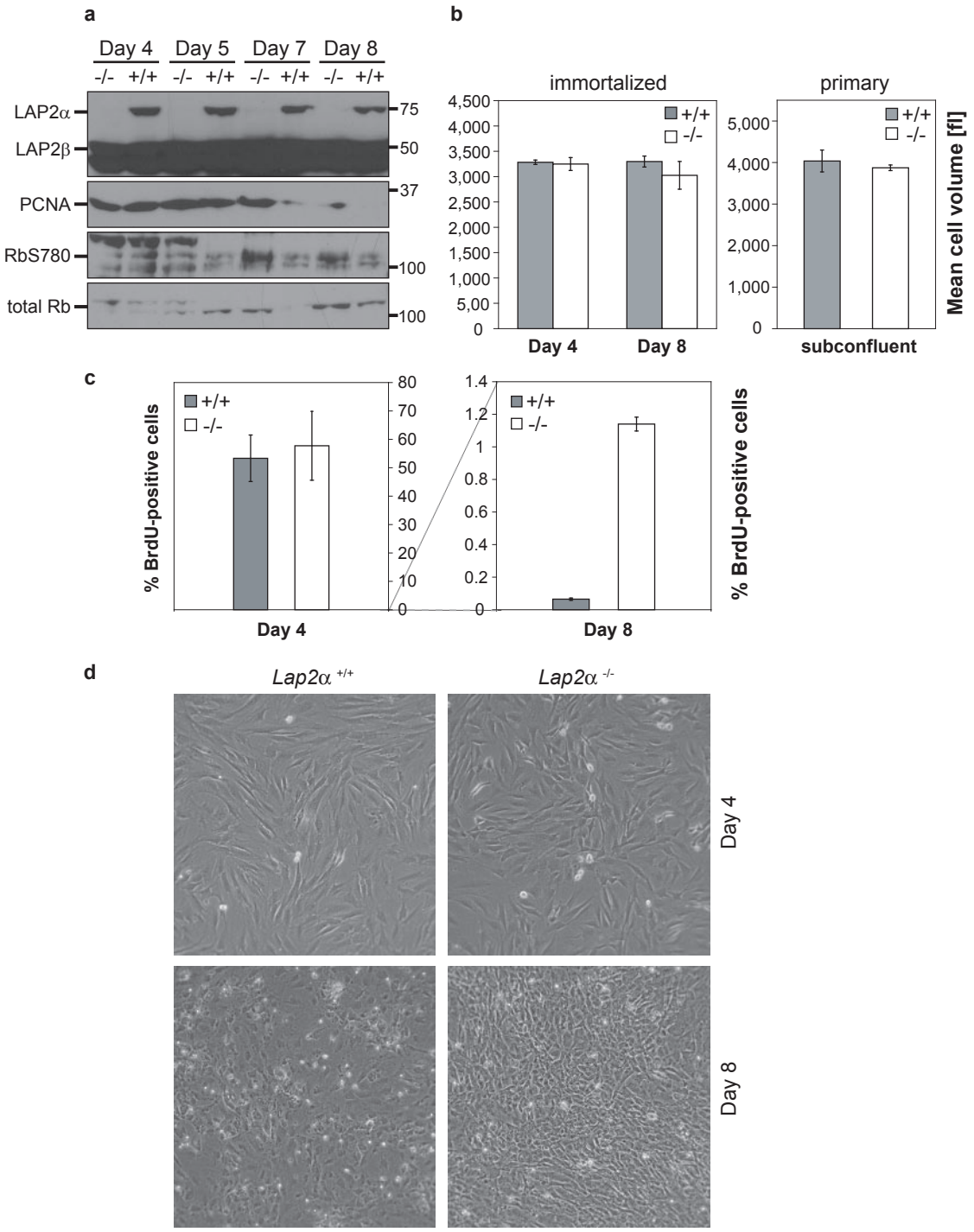

Figure S3 Immortalized LAP2α knockout fibroblasts show impaired cell cycle arrest upon contact inhibition. Immortalized skin fibroblasts from LAP2α knockout mice and wild-type littermates were seeded at equal cell numbers and grown to confluency. Proliferating (Day 4 and 5) or contact inhibited (Day 7 and 8) cells were either lysed and processed for immunoblotting using antibodies to the indicated antigens (**a**) or used for BrdU-labeling assays (**c**). Numbers in (**a**) indicate molecular masses of marker proteins in kDa. (**b**) Mean cell volumes of primary and immortalized fibroblasts were determined using a Casy cell counter and plotted in a bar graph. Means ± s. d. from 3 independent experiments are shown in (**b**) and (**c**). (**d**) Pictures of cells from the indicated time points (see a) were obtained using a Zeiss microscope equipped with a Canon digital camera; Magnification: 100x.

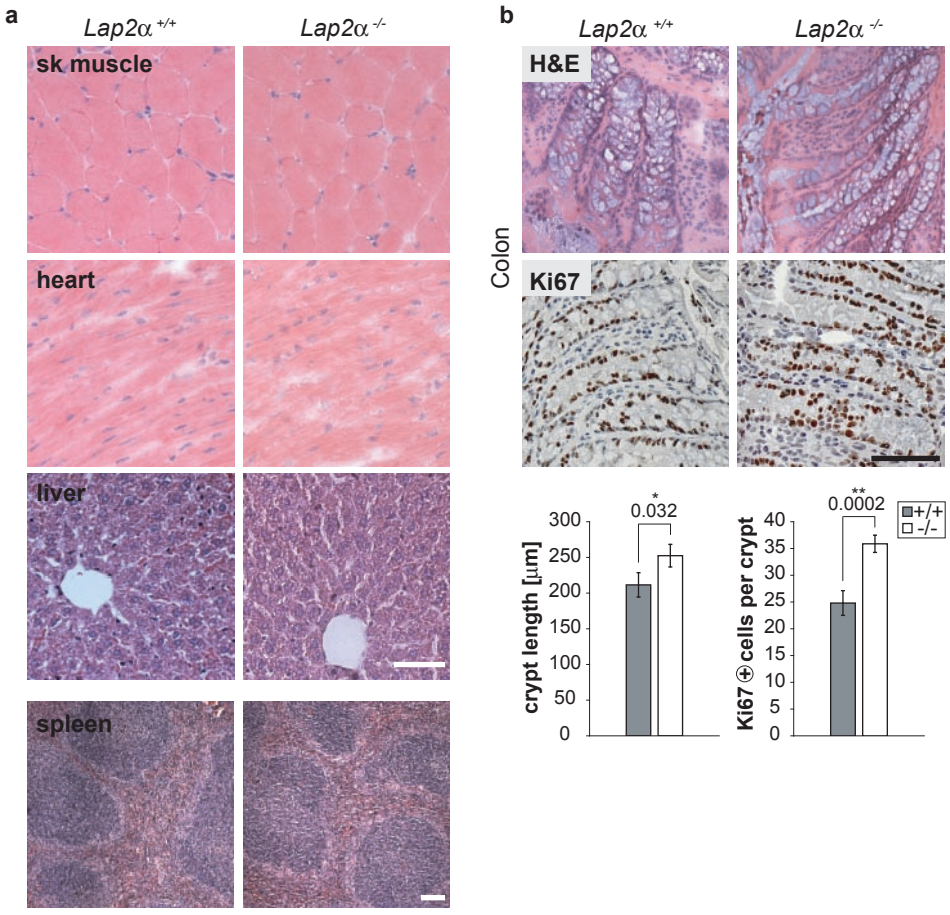

Figure S4 LAP2α-null mice show no overt pathologies in muscle, heart and liver, but enhanced proliferation of progenitors in intestinal tissue. (**a**) Paraffin- or cryosections of indicated tissues isolated from wild-type (+/+) and LAP2 α knockout (–/–) mice were stained with haematoxylin/eosin. Bar, 50 µm. (**b**) Cryosections of colon were stained with haematoxylin/eosin (upper panels) or processed for immunohistochemistry using an antibody to Ki67 (lower panels). Bar, 50 µm. Bar graphs show the length of the crypt axis (n = 10) as determined by Axiovision imaging software (left graphs) or the number of Ki67-positive cells per crypt (right graphs; n = 8). Means ± s. e. m. are shown; p-values are indicated; ** highly significant; * significant.

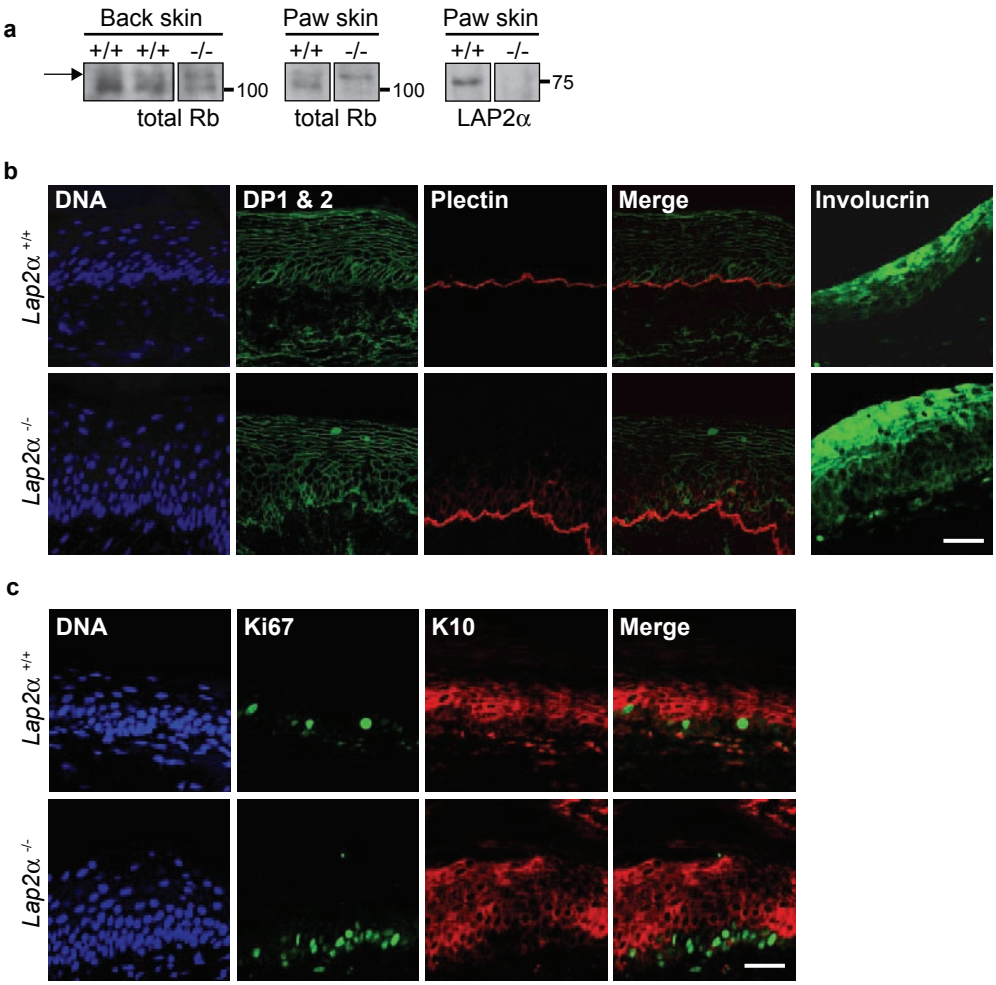

Figure S5 *Lap2α*$^{-/-}$ epidermal progenitors have hyperphosphorylated pRb, but differentiate normally. (**a**) Total pRb was immunoprecipitated from whole lysates of paw skin and back skin of *LAP2α* knockout (–/–) or wild-type control mice (+/+). Precipitates were processed for immunoblotting using antibodies to total pRb or LAP2. Arrow denotes phosphorylated pRb. Numbers indicate molecular masses of marker proteins in kDa. (**b**, **c**) Tissue sections of paw epidermis from *Lap2*$^{+/+}$ and $^{-/-}$ mice were analyzed by immunofluorescence microscopy using antibodies to desmoplakin (DP) 1 and 2, plectin, involucrin, keratin 10 (K10) or Ki67 as indicated. DNA was stained with Hoechst. Confocal images are shown. Bar, 50 μm.

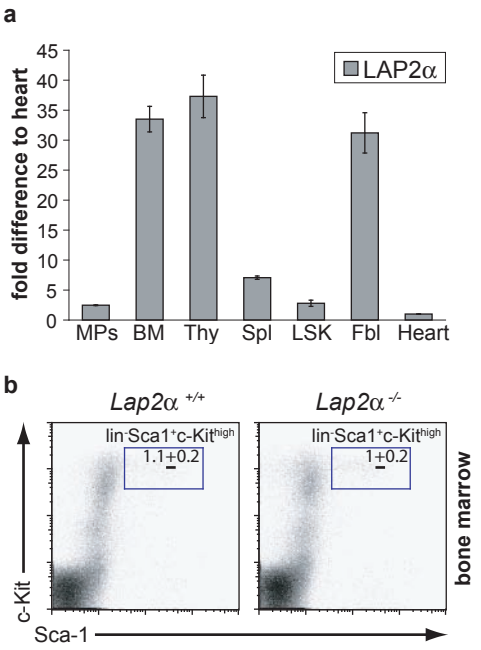

Figure S6 The haematopoietic stem and multipotent progenitor cell compartment is not affected in LAP2α knockout mice. (**a**) Quantitative realtime PCR of cDNAs obtained from mRNA of bone-marrow derived macrophages (MPs), whole bone marrow (BM), thymus (Thy), spleen (Spl), lin-Sca-1^{+}c-Kit^{high} hematopoietic stem and progenitor cells (LSK), skin fibroblasts (Fbl) and heart. Values are depicted as fold difference to heart expression levels and represent means ± s. d. from 3 biological replicates. (**b**) Representative flow cytometric profiles of lineage marker negative, Sca-1/c-Kit double positive (lin- Sca-1^{+}c-Kit^{high}) haematopoietic stem and progenitor cells in bone marrow of *Lap2α*$^{-/-}$ mice and wild-type littermate controls. LSK fraction of total lineage negative bone marrow cells in % is depicted. Values represent means ± s.e.m. (n = 3).

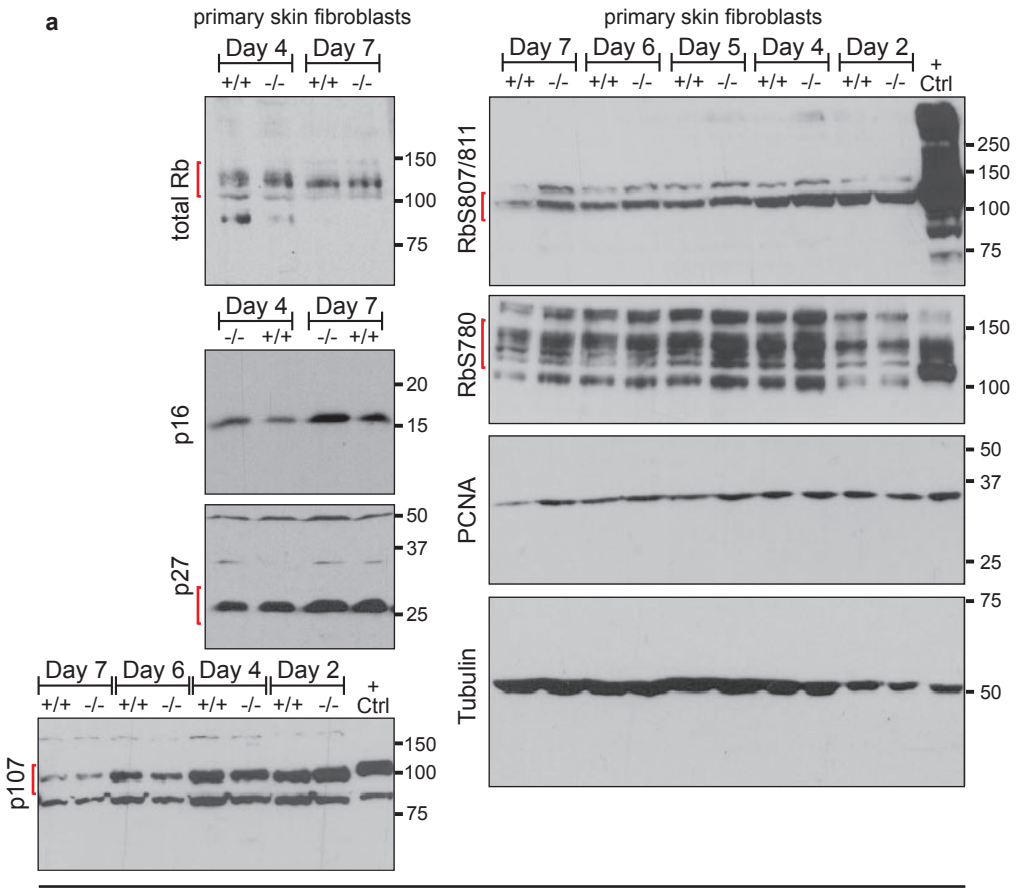

corresponding figure panel: 2b

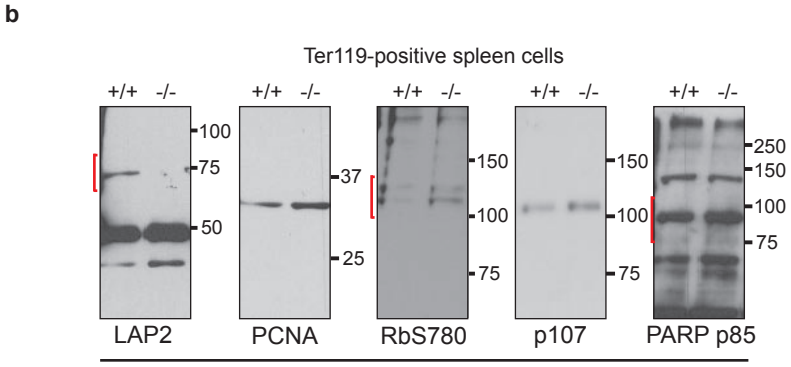

corresponding figure panel: 5b

Figure S7 Full scans of key Western data. (**a**, **b**) Full scans of immunoblot gels presented in Figure 2b (**a**) and 5b (**b**) of the manuscript are shown. (**a**) Primary skin fibroblasts from LAP2α knockout mice (–/–) and wild-type (+/+) littermates were seeded at equal cell numbers and grown to confluency. Lysates were prepared at the indicated time points (see also Figure 2a). (**b**) Ter119+ spleen cells obtained by magnetic cell sorting from LAP2α knockout and wild-type control mice were lysed and processed for immunoblotting. Antibodies are indicated on the left (**a**) or below (**b**) gels. Red parentheses denote bands shown in the Figures of the manuscript, if other unspecific bands are detectable. Numbers indicate molecular masses of marker proteins in kDa. + Ctrl: positive control.

SUPPLEMENTARY METHODS

Cloning of the LAP2α targeting construct

For construction of the targeting vector we used a BAC clone (Genome Systems, LAP2-genomic 22427, accession #g238), derived from strain 129 DNA. Oligonucleotide pair 5'-CCCCCGCGGATAACTTCGTATAATGTAAGCTATACGAAGTTATCCATGGCCC-3', 5-GGGCCATGGARAACTTCGTATAGCATACATTATACGAAGTTATCCGCGGGGG-3' containing a loxP site, and 5'-CCCCCATGGAGATCTGATATCCCCGGATCCCCCGGGGGG-3', 5'-CCCCCCGGGGGATCCGGGGATATCAGATCTCCATGGGGG-3', containing required restriction sites were cloned into pBSKS+ (Stratagene, La Jolla, USA) via SacII/KpnI, and 5'-CCCGAGCTCGCGGCCGCGAATTCGGGGGTACCGGGCCGCGGCCC-3', 5'-GGGCCGCGGCCCGGTACCCCCGAATTCGCGGCCGCGAGCTCGGG-3' inserted into the generated construct via SacI/SacII resulting in pBK9. Plasmid pDTα containing the diphtheria toxin (DT) gene was cut with EcoRI, treated with Klenow enzyme, cut with BamHI and the DT gene was inserted into pBK9 via EcoRV/BamHI generating intermediate construct 1. A BglII-cut genomic DNA fragment containing exon 5 was inserted at the BglII site of intermediate 1 yielding intermediate construct 2. A fragment containing exon 3, obtained from a genomic clone by PCR using primer pair 5'-ACTGGCCGTCGTTTTAC-3' and 5'-CCCGGTACCAGATCTCACATAAACATGTAATATGGACC-3', and cut with PstI and KpnI was ligated together with an EcoRI/PstI genomic DNA fragment containing exon 2 into intermediate 2 resulting in intermediate construct 3. An EcoRI fragment of genomic DNA containing intron sequences downstream of exon 1 was inserted into this construct yielding intermediate construct 4. Plasmid pK-11 was digested with KpnI and SacII to yield a fragment containing the neomycin resistance cassette flanked with FRT sites and an upstream loxP site, which was inserted into intermediate construct 4 via KpnI/SacII to yield intermediate construct 5.

A PCR fragment containing parts of exon 4, obtained from genomic DNA with the primer pair 5'-GGAAACAGCTATGACCATG-3' and 5'-CCCGGTACCAGATCTCACATAAACA TGTAATATGGACC-3' and cut with ApaI was ligated with an EcoRI/ApaI-digested genomic DNA fragment containing exon 4 into pBKS+ via SacII/EcoRI. Next a BsmI/EcoRI and a BsmI/BglII fragment containing intron sequences downstream of exon 4 were inserted into pBSKS+ via EcoRI/NotI. This and the latter pBSKS+ derived construct were cut with SacII/EcoRI and inserted into pBSKS+ via SacII. The SacII fragment of this construct was cloned into intermediate construct 5 yielding the targeting construct.

The targeting vector was linearised with NotI and electroporated into W9.5 ES cells. Clones were picked, expanded, and screened for homologous recombinants by Southern blot analyses. Genomic DNA of ES cells was digested with NcoI and hybridized with a probe (see Fig. S1) containing intron sequences downstream of exon 5 and outside of the homology domain of the targeting construct. Southern blot analysis was performed according to standard protocols using the AlkPhos Direct CDP-Star System (GE Healthcare Biosciences, NJ, USA) for hybridization. Positive clones were injected into C57Bl/6 blastocysts, chimeras were derived and bred to produce recombinant offspring as described.

Genotyping of LAP2α knockout mice

For genotyping, genomic DNA was prepared from tail tips and PCR analyses were performed using puRE*Taq* Ready-To-Go PCR beads (GE Healthcare Biosciences, NJ, USA) in a PTC-200 Peltier Thermo Cycler (TJ Research). Primers used were:

Exon 4 as: 5'-CACAATCCCTAGAGGACTTCACTT-3'

Intron after Exon 4 as: 5'-CTGTGACTTTGCTGGCCTTCCAGTCTA-3'

Exon 3 s: 5'-CAGGGAACTGAATCGAGATCCTCTAC-3'

TN5-3: 5'-GCCCTGAATGAACTGCAGGACG-3'

Primers used for expression analysis

LAP2α/LAP2:

LAP2f: 5'-GTGGGAACAACCAGGAAGCTATATGA-3'

LAP2αr: 5'-TGAGTGCCTGCTGTGCATCACTA-3'

LAP2r: 5'-TTCTGACTTGACATCTGCCAAGG-3'

Lamin A/C:

LACf: 5'-CATCAAGCTGGCCCTGGACATGGAG-3'

LACr: 5'-TGCGCCTTCCACACCAAGTCAGTAG-3'

PCNA:

PCNAf: 5'-GATGCCGTCGGGTGAATTTG-3'

PCNAr: 5'-TGGTTACCGCCTCCTCTT CT-3'

E2F1:

E2F1f: 5'-ACGCTATGAAACCTCACTAAA-3'

E2F1r: 5'-AGGACATTGGTGATGTCATA-3'

Immunohistochemistry of tissues

For immunohistochemistry, frozen sections were fixed in 3.7% formaldehyde (Merck, NJ, USA) in PBS, washed, permeabilised and treated with 2% H_2O_2 in PBS plus 0.3% goat serum for 15 minutes. After blocking with goat serum (Vectastain; Vector Labs, Burlingame, CA, USA), primary antibodies diluted in 0.1% gelatine/0.1% Triton-X 100 in PBS were applied either 1 hour at room temperature or overnight at 4°C. Samples were then washed and incubated in biotinylated secondary antibodies (Vector Laboratories). Sections were washed in PBS and Elite ABC Reagent (Vectastain Elite ABC Kit from Vector Laboratories) was applied for 30 minutes. Sections were treated for 2-10 minutes with DAB staining solution (DAB substrate kit for peroxidase from Vector Laboratories), counterstained in haematoxylin (Sigma), washed thoroughly, dehydrated and mounted in Entellan (Merck).

Quantitative PCR analyses

For quantitative PCR of LAP2α expression levels, cDNAs from different tissues were produced as described in the Methods section. PCR amplification was performed using the MESA GREEN qPCR MasterMix Plus for SYBR Assay I TTP (Eurogentec, Seraing, Belgium) and primers specific for mouse LAP2α (see above) on the MasterCycler ep realplex (Eppendorf, Hamburg, Germany).

Immunoprecipitation of pRb from skin lysates

Paw and back skin from LAP2α-deficient mice and wild-type littermates was isolated and homogenised in mouse lysis buffer (25 mM HEPES pH 7.5, 25 mM Tris-HCl pH 7.5, 100 mM NaCl, 5 mM $MgCl_2$, 10 mM EGTA, 0.1% Tween-20, 0.5% NP-40, 0.4% Triton X-100, 1 mM PMSF, 1 mM DTT, 20 μm cytochalasin B, 0.25 mg/ml DNAse I, 0.05 mg/ml RNAse A, protease inhibitor cocktail from Roche, 0.5 mM β-glycerol phosphate, 1 mM sodium-orthovanadate) using the precellys 24 homogenizer with 2.8 mm ceramic beads (Peqlab, Erlangen, Germany). 2 mg protein from total lysates were imunoprecipitated using antibodies to pRb (G3-245 from BD Biosciences, Franklin Lakes, NJ, USA) and fast flow sepharose G (Sigma, Munich, Germany) according to standard protocols. Immunoprecipitates were washed three times in lysis buffer and processed for Western blotting.

Microscopy equipment and settings

Microscopy of haematoxylin/eosin stained sections was done on a Zeiss Axio Imager.M1 equipped with a Zeiss AxioCam MRc5 and Axiovision LE software, version 4.5. All immunofluorescence microscopy samples were viewed in a Zeiss Axiovert 200M microscope equipped with a Zeiss LSM510META confocal laser-scanning unit, an alpha Plan-Fluor 100x/1,45 Oil (a=0,11mm) and a Plan-Apochromat 63x/1.40 Oil DIC MC27 (a=0.19mm) objective (Zeiss) using LSM imaging software (Zeiss). Images were prepared with Adobe

Photoshop software. Fluorochromes used were either Texas Red (Jackson Immuno Research, West-Grove, USA) or Alexa Fluor 488 (Molecular Probes, Inc., Eugene, OR, USA), coupled to appropriate secondary antibodies.

4 References

1. Evans DE, Bryant JA, Hutchison C. The nuclear envelope: a comparative overview. *Symp Soc Exp Biol.* 2004(56):1-8.

2. Gruenbaum Y, Margalit A, Goldman RD, Shumaker DK, Wilson KL. The nuclear lamina comes of age. *Nat Rev Mol Cell Biol.* 2005;6(1):21-31.

3. Hutchison CJ, Worman HJ. A-type lamins: guardians of the soma? *Nat Cell Biol.* 2004;6(11):1062-1067.

4. Herrmann H, Bar H, Kreplak L, Strelkov SV, Aebi U. Intermediate filaments: from cell architecture to nanomechanics. *Nat Rev Mol Cell Biol.* 2007;8(7):562-573.

5. McKeon FD, Kirschner MW, Caput D. Homologies in both primary and secondary structure between nuclear envelope and intermediate filament proteins. *Nature.* 1986;319(6053):463-468.

6. Ben-Harush K, Wiesel N, Frenkiel-Krispin D, Moeller D, Soreq E, Aebi U, Herrmann H, Gruenbaum Y, Medalia O. The supramolecular organization of the C. elegans nuclear lamin filament. *J Mol Biol.* 2009;386(5):1392-1402.

7. Margalit A, Vlcek S, Gruenbaum Y, Foisner R. Breaking and making of the nuclear envelope. *J Cell Biochem.* 2005;95(3):454-465.

8. Burke B, Stewart CL. The laminopathies: the functional architecture of the nucleus and its contribution to disease. *Annu Rev Genomics Hum Genet.* 2006;7:369-405.

9. Lin F, Worman HJ. Structural organization of the human gene encoding nuclear lamin A and nuclear lamin C. *J Biol Chem.* 1993;268(22):16321-16326.

10. Machiels BM, Zorenc AH, Endert JM, Kuijpers HJ, van Eys GJ, Ramaekers FC, Broers JL. An alternative splicing product of the lamin A/C gene lacks exon 10. *J Biol Chem.* 1996;271(16):9249-9253.

11. Alsheimer M, von Glasenapp E, Schnolzer M, Heid H, Benavente R. Meiotic lamin C2: the unique amino-terminal hexapeptide GNAEGR is essential for nuclear envelope association. *Proc Natl Acad Sci U S A.* 2000;97(24):13120-13125.

12. Rusinol AE, Sinensky MS. Farnesylated lamins, progeroid syndromes and farnesyl transferase inhibitors. *J Cell Sci.* 2006;119(Pt 16):3265-3272.

13. Gotzmann J, Foisner R. A-type lamin complexes and regenerative potential: a step towards understanding laminopathic diseases? *Histochem Cell Biol.* 2006;125(1-2):33-41.

14. Stewart C, Burke B. Teratocarcinoma stem cells and early mouse embryos contain only a single major lamin polypeptide closely resembling lamin B. *Cell.* 1987;51(3):383-392.

15. Rober RA, Sauter H, Weber K, Osborn M. Cells of the cellular immune and hemopoietic system of the mouse lack lamins A/C: distinction versus other somatic cells. *J Cell Sci.* 1990;95 (Pt 4):587-598.

16. Harborth J, Elbashir SM, Bechert K, Tuschl T, Weber K. Identification of essential genes in cultured mammalian cells using small interfering RNAs. *J Cell Sci.* 2001;114(Pt 24):4557-4565.

17. Dechat T, Pfleghaar K, Sengupta K, Shimi T, Shumaker DK, Solimando L, Goldman RD. Nuclear lamins: major factors in the structural organization and function of the nucleus and chromatin. *Genes Dev.* 2008;22(7):832-853.

18. Wagner N, Krohne G. LEM-Domain proteins: new insights into lamin-interacting proteins. *Int Rev Cytol.* 2007;261:1-46.

19. Chen S, Wang QL, Nie Z, Sun H, Lennon G, Copeland NG, Gilbert DJ, Jenkins NA, Zack DJ. Crx, a novel Otx-like paired-homeodomain protein, binds to and transactivates photoreceptor cell-specific genes. *Neuron.* 1997;19(5):1017-1030.

20. Berger R, Theodor L, Shoham J, Gokkel E, Brok-Simoni F, Avraham KB, Copeland NG, Jenkins NA, Rechavi G, Simon AJ. The characterization and localization of the mouse thymopoietin/lamina-associated polypeptide 2 gene and its alternatively spliced products. *Genome Res.* 1996;6(5):361-370.

21. Dechat T, Vlcek S, Foisner R. Review: lamina-associated polypeptide 2 isoforms and related proteins in cell cycle-dependent nuclear structure dynamics. *J Struct Biol.* 2000;129(2-3):335-345.

22. Dechat T, Korbei B, Vaughan OA, Vlcek S, Hutchison CJ, Foisner R. Lamina-associated polypeptide 2alpha binds intranuclear A-type lamins. *J Cell Sci.* 2000;113 Pt 19:3473-3484.

23. Vlcek S, Korbei B, Foisner R. Distinct functions of the unique C terminus of LAP2alpha in cell proliferation and nuclear assembly. *J Biol Chem.* 2002;277(21):18898-18907.

24. Snyers L, Vlcek S, Dechat T, Skegro D, Korbei B, Gajewski A, Mayans O, Schofer C, Foisner R. Lamina-associated polypeptide 2-alpha forms homo-trimers via its C terminus, and oligomerization is unaffected by a disease-causing mutation. *J Biol Chem.* 2007;282(9):6308-6315.

25. Bradley CM, Jones S, Huang Y, Suzuki Y, Kvaratskhelia M, Hickman AB, Craigie R, Dyda F. Structural basis for dimerization of LAP2alpha, a component of the nuclear lamina. *Structure.* 2007;15(6):643-653.

26. Schirmer EC, Foisner R. Proteins that associate with lamins: many faces, many functions. *Exp Cell Res.* 2007;313(10):2167-2179.

27. Prufert K, Winkler C, Paulin-Levasseur M, Krohne G. The lamina-associated polypeptide 2 (LAP2) genes of zebrafish and chicken: no LAP2alpha isoform is synthesised by non-mammalian vertebrates. *Eur J Cell Biol.* 2004;83(8):403-411.

28. Taylor MR, Slavov D, Gajewski A, Vlcek S, Ku L, Fain PR, Carniel E, Di Lenarda A, Sinagra G, Boucek MM, Cavanaugh J, Graw SL, Ruegg P, Feiger J, Zhu X, Ferguson DA, Bristow MR, Gotzmann J, Foisner R, Mestroni L. Thymopoietin (lamina-associated polypeptide 2) gene mutation associated with dilated cardiomyopathy. *Hum Mutat.* 2005;26(6):566-574.

29. Dorner D, Gotzmann J, Foisner R. Nucleoplasmic lamins and their interaction partners, LAP2alpha, Rb, and BAF, in transcriptional regulation. *Febs J.* 2007;274(6):1362-1373.

30. Dorner D, Vlcek S, Foeger N, Gajewski A, Makolm C, Gotzmann J, Hutchison CJ, Foisner R. Lamina-associated polypeptide 2alpha regulates cell cycle progression and differentiation via the retinoblastoma-E2F pathway. *J Cell Biol.* 2006;173(1):83-93.

31. Markiewicz E, Dechat T, Foisner R, Quinlan RA, Hutchison CJ. Lamin A/C binding protein LAP2alpha is required for nuclear anchorage of retinoblastoma protein. *Mol Biol Cell.* 2002;13(12):4401-4413.

32. Naetar N, Korbei B, Kozlov S, Kerenyi MA, Dorner D, Kral R, Gotic I, Fuchs P, Cohen TV, Bittner R, Stewart CL, Foisner R. Loss of nucleoplasmic LAP2alpha-lamin A complexes causes erythroid and epidermal progenitor hyperproliferation. *Nat Cell Biol.* 2008;10(11):1341-1348.

33. Suzuki Y, Yang H, Craigie R. LAP2alpha and BAF collaborate to organize the Moloney murine leukemia virus preintegration complex. *Embo J.* 2004;23(23):4670-4678.

34. Snyers L, Schofer C. Lamina-associated polypeptide 2alpha forms complexes with heat shock proteins Hsp70 and Hsc70 in vivo. *Biochem Biophys Res Commun.* 2008;368(3):767-771.

35. Kenny MK, Mendez F, Sandigursky M, Kureekattil RP, Goldman JD, Franklin WA, Bases R. Heat shock protein 70 binds to human apurinic/apyrimidinic endonuclease and stimulates endonuclease activity at abasic sites. *J Biol Chem.* 2001;276(12):9532-9536.

36. Hunt CR, Dix DJ, Sharma GG, Pandita RK, Gupta A, Funk M, Pandita TK. Genomic instability and enhanced radiosensitivity in Hsp70.1- and Hsp70.3-deficient mice. *Mol Cell Biol.* 2004;24(2):899-911.

37. Furukawa K, Pante N, Aebi U, Gerace L. Cloning of a cDNA for lamina-associated polypeptide 2 (LAP2) and identification of regions that specify targeting to the nuclear envelope. *Embo J.* 1995;14(8):1626-1636.

38. Nili E, Cojocaru GS, Kalma Y, Ginsberg D, Copeland NG, Gilbert DJ, Jenkins NA, Berger R, Shaklai S, Amariglio N, Brok-Simoni F, Simon AJ, Rechavi G. Nuclear membrane protein LAP2beta mediates transcriptional repression alone and together with its binding partner GCL (germ-cell-less). *J Cell Sci.* 2001;114(Pt 18):3297-3307.

39. Somech R, Shaklai S, Geller O, Amariglio N, Simon AJ, Rechavi G, Gal-Yam EN. The nuclear-envelope protein and transcriptional repressor LAP2beta interacts with HDAC3 at the nuclear periphery, and induces histone H4 deacetylation. *J Cell Sci.* 2005;118(Pt 17):4017-4025.

40. Kimura T, Ito C, Watanabe S, Takahashi T, Ikawa M, Yomogida K, Fujita Y, Ikeuchi M, Asada N, Matsumiya K, Okuyama A, Okabe M, Toshimori K, Nakano T. Mouse germ cell-less as an essential component for nuclear integrity. *Mol Cell Biol.* 2003;23(4):1304-1315.

41. Martins S, Eikvar S, Furukawa K, Collas P. HA95 and LAP2 beta mediate a novel chromatin-nuclear envelope interaction implicated in initiation of DNA replication. *J Cell Biol.* 2003;160(2):177-188.

42. Shaklai S, Somech R, Gal-Yam EN, Deshet-Unger N, Moshitch-Moshkovitz S, Hirschberg K, Amariglio N, Simon AJ, Rechavi G. LAP2zeta binds BAF and suppresses LAP2beta-mediated transcriptional repression. *Eur J Cell Biol.* 2008;87(5):267-278.

43. Lin F, Blake DL, Callebaut I, Skerjanc IS, Holmer L, McBurney MW, Paulin-Levasseur M, Worman HJ. MAN1, an inner nuclear membrane protein that shares the LEM domain with lamina-associated polypeptide 2 and emerin. *J Biol Chem.* 2000;275(7):4840-4847.

44. Lin F, Morrison JM, Wu W, Worman HJ. MAN1, an integral protein of the inner nuclear membrane, binds Smad2 and Smad3 and antagonizes transforming growth factor-beta signaling. *Hum Mol Genet.* 2005;14(3):437-445.

45. Pan D, Estevez-Salmeron LD, Stroschein SL, Zhu X, He J, Zhou S, Luo K. The integral inner nuclear membrane protein MAN1 physically interacts with the R-Smad proteins to repress signaling by the transforming growth factor-{beta} superfamily of cytokines. *J Biol Chem.* 2005;280(16):15992-16001.

46. Ishimura A, Ng JK, Taira M, Young SG, Osada S. Man1, an inner nuclear membrane protein, regulates vascular remodeling by modulating transforming growth factor beta signaling. *Development.* 2006;133(19):3919-3928.

47. Bione S, Maestrini E, Rivella S, Mancini M, Regis S, Romeo G, Toniolo D. Identification of a novel X-linked gene responsible for Emery-Dreifuss muscular dystrophy. *Nat Genet.* 1994;8(4):323-327.

48. Liu J, Lee KK, Segura-Totten M, Neufeld E, Wilson KL, Gruenbaum Y. MAN1 and emerin have overlapping function(s) essential for chromosome segregation and cell division in Caenorhabditis elegans. *Proc Natl Acad Sci U S A.* 2003;100(8):4598-4603.

49. Markiewicz E, Tilgner K, Barker N, van de Wetering M, Clevers H, Dorobek M, Hausmanowa-Petrusewicz I, Ramaekers FC, Broers JL, Blankesteijn WM, Salpingidou G, Wilson RG, Ellis JA, Hutchison CJ. The inner nuclear membrane protein emerin regulates beta-catenin activity by restricting its accumulation in the nucleus. *Embo J.* 2006;25(14):3275-3285.

50. Willert K, Jones KA. Wnt signaling: is the party in the nucleus? *Genes Dev.* 2006;20(11):1394-1404.

51. Sullivan T, Escalante-Alcalde D, Bhatt H, Anver M, Bhat N, Nagashima K, Stewart CL, Burke B. Loss of A-type lamin expression compromises nuclear envelope integrity leading to muscular dystrophy. *J Cell Biol.* 1999;147(5):913-920.

52. Fong LG, Ng JK, Lammerding J, Vickers TA, Meta M, Cote N, Gavino B, Qiao X, Chang SY, Young SR, Yang SH, Stewart CL, Lee RT, Bennett CF, Bergo MO, Young SG. Prelamin A and lamin A appear to be dispensable in the nuclear lamina. *J Clin Invest.* 2006;116(3):743-752.

53. Raharjo WH, Enarson P, Sullivan T, Stewart CL, Burke B. Nuclear envelope defects associated with LMNA mutations cause dilated cardiomyopathy and Emery-Dreifuss muscular dystrophy. *J Cell Sci.* 2001;114(Pt 24):4447-4457.

54. Holaska JM, Kowalski AK, Wilson KL. Emerin caps the pointed end of actin filaments: evidence for an actin cortical network at the nuclear inner membrane. *PLoS Biol.* 2004;2(9):E231.

55. Libotte T, Zaim H, Abraham S, Padmakumar VC, Schneider M, Lu W, Munck M, Hutchison C, Wehnert M, Fahrenkrog B, Sauder U, Aebi U, Noegel AA, Karakesisoglou I. Lamin A/C-dependent localization of Nesprin-2, a giant scaffolder at the nuclear envelope. *Mol Biol Cell.* 2005;16(7):3411-3424.

56. Zhang Q, Skepper JN, Yang F, Davies JD, Hegyi L, Roberts RG, Weissberg PL, Ellis JA, Shanahan CM. Nesprins: a novel family of spectrin-repeat-containing proteins that localize to the nuclear membrane in multiple tissues. *J Cell Sci.* 2001;114(Pt 24):4485-4498.

57. Haque F, Lloyd DJ, Smallwood DT, Dent CL, Shanahan CM, Fry AM, Trembath RC, Shackleton S. SUN1 interacts with nuclear lamin A and cytoplasmic nesprins to provide a physical connection between the nuclear lamina and the cytoskeleton. *Mol Cell Biol.* 2006;26(10):3738-3751.

58. Ivorra C, Kubicek M, Gonzalez JM, Sanz-Gonzalez SM, Alvarez-Barrientos A, O'Connor JE, Burke B, Andres V. A mechanism of AP-1 suppression through interaction of c-Fos with lamin A/C. *Genes Dev.* 2006;20(3):307-320.

59. Chinenov Y, Kerppola TK. Close encounters of many kinds: Fos-Jun interactions that mediate transcription regulatory specificity. *Oncogene.* 2001;20(19):2438-2452.

60. Maraldi NM, Capanni C, Lattanzi G, Camozzi D, Facchini A, Manzoli FA. SREBP1 interaction with prelamin A forms: a pathogenic mechanism for lipodystrophic laminopathies. *Adv Enzyme Regul.* 2008;48:209-223.

61. Jagatheesan G, Thanumalayan S, Muralikrishna B, Rangaraj N, Karande AA, Parnaik VK. Colocalization of intranuclear lamin foci with RNA splicing factors. *J Cell Sci.* 1999;112 (Pt 24):4651-4661.

62. Duband-Goulet I, Courvalin JC, Buendia B. LBR, a chromatin and lamin binding protein from the inner nuclear membrane, is proteolyzed at late stages of apoptosis. *J Cell Sci.* 1998;111 (Pt 10):1441-1451.

63. Makatsori D, Kourmouli N, Polioudaki H, Shultz LD, McLean K, Theodoropoulos PA, Singh PB, Georgatos SD. The inner nuclear membrane protein lamin B receptor forms distinct microdomains and links epigenetically marked chromatin to the nuclear envelope. *J Biol Chem.* 2004;279(24):25567-25573.

64. Hoffmann K, Dreger CK, Olins AL, Olins DE, Shultz LD, Lucke B, Karl H, Kaps R, Muller D, Vaya A, Aznar J, Ware RE, Sotelo Cruz N, Lindner TH, Herrmann H, Reis A, Sperling K. Mutations in the gene encoding the lamin B receptor produce an altered nuclear morphology in granulocytes (Pelger-Huet anomaly). *Nat Genet.* 2002;31(4):410-414.

65. Waterham HR, Koster J, Mooyer P, Noort Gv G, Kelley RI, Wilcox WR, Wanders RJ, Hennekam RC, Oosterwijk JC. Autosomal recessive HEM/Greenberg skeletal dysplasia is caused by 3 beta-hydroxysterol delta 14-reductase deficiency due to mutations in the lamin B receptor gene. *Am J Hum Genet.* 2003;72(4):1013-1017.

66. Shultz LD, Lyons BL, Burzenski LM, Gott B, Samuels R, Schweitzer PA, Dreger C, Herrmann H, Kalscheuer V, Olins AL, Olins DE, Sperling K, Hoffmann K. Mutations at the mouse ichthyosis locus are within the lamin B receptor gene: a single gene model for human Pelger-Huet anomaly. *Hum Mol Genet.* 2003;12(1):61-69.

67. Malhas AN, Lee CF, Vaux DJ. Lamin B1 controls oxidative stress responses via Oct-1. *J Cell Biol.* 2009;184(1):45-55.

68. Malhas AN, Vaux DJ. Transcription factor sequestration by nuclear envelope components. *Cell Cycle.* 2009;8(7):959-960.

69. Pines J, Rieder CL. Re-staging mitosis: a contemporary view of mitotic progression. *Nat Cell Biol.* 2001;3(1):E3-6.

70. Heald R, McKeon F. Mutations of phosphorylation sites in lamin A that prevent nuclear lamina disassembly in mitosis. *Cell.* 1990;61(4):579-589.

71. Gruenbaum Y, Goldman RD, Meyuhas R, Mills E, Margalit A, Fridkin A, Dayani Y, Prokocimer M, Enosh A. The nuclear lamina and its functions in the nucleus. *Int Rev Cytol.* 2003;226:1-62.

72. Gajewski A, Csaszar E, Foisner R. A phosphorylation cluster in the chromatin-binding region regulates chromosome association of LAP2alpha. *J Biol Chem.* 2004;279(34):35813-35821.

73. Foisner R, Gerace L. Integral membrane proteins of the nuclear envelope interact with lamins and chromosomes, and binding is modulated by mitotic phosphorylation. *Cell.* 1993;73(7):1267-1279.

74. Dechat T, Gajewski A, Korbei B, Gerlich D, Daigle N, Haraguchi T, Furukawa K, Ellenberg J, Foisner R. LAP2alpha and BAF transiently localize to telomeres and specific regions on chromatin during nuclear assembly. *J Cell Sci.* 2004;117(Pt 25):6117-6128.

75. Ellenberg J, Siggia ED, Moreira JE, Smith CL, Presley JF, Worman HJ, Lippincott-Schwartz J. Nuclear membrane dynamics and reassembly in living cells: targeting of an inner nuclear membrane protein in interphase and mitosis. *J Cell Biol.* 1997;138(6):1193-1206.

76. Worman HJ, Bonne G. "Laminopathies": a wide spectrum of human diseases. *Exp Cell Res.* 2007;313(10):2121-2133.

77. Zhang X, Chen S, Yoo S, Chakrabarti S, Zhang T, Ke T, Oberti C, Yong SL, Fang F, Li L, de la Fuente R, Wang L, Chen Q, Wang QK. Mutation in nuclear pore component NUP155 leads to atrial fibrillation and early sudden cardiac death. *Cell.* 2008;135(6):1017-1027.

78. Zhang Q, Bethmann C, Worth NF, Davies JD, Wasner C, Feuer A, Ragnauth CD, Yi Q, Mellad JA, Warren DT, Wheeler MA, Ellis JA, Skepper JN, Vorgerd M, Schlotter-Weigel B, Weissberg PL, Roberts RG, Wehnert M, Shanahan CM. Nesprin-1 and -2 are involved in the pathogenesis of Emery Dreifuss muscular dystrophy and are critical for nuclear envelope integrity. *Hum Mol Genet.* 2007;16(23):2816-2833.

79. Broers JL, Ramaekers FC, Bonne G, Yaou RB, Hutchison CJ. Nuclear lamins: laminopathies and their role in premature ageing. *Physiol Rev.* 2006;86(3):967-1008.

80. Muchir A, Bonne G, van der Kooi AJ, van Meegen M, Baas F, Bolhuis PA, de Visser M, Schwartz K. Identification of mutations in the gene encoding lamins A/C in autosomal dominant limb girdle muscular dystrophy with atrioventricular conduction disturbances (LGMD1B). *Hum Mol Genet.* 2000;9(9):1453-1459.

81. van der Kooi AJ, van Meegen M, Ledderhof TM, McNally EM, de Visser M, Bolhuis PA. Genetic localization of a newly recognized autosomal dominant limb-girdle muscular dystrophy with cardiac involvement (LGMD1B) to chromosome 1q11-21. *Am J Hum Genet.* 1997;60(4):891-895.

82. Bonne G, Di Barletta MR, Varnous S, Becane HM, Hammouda EH, Merlini L, Muntoni F, Greenberg CR, Gary F, Urtizberea JA, Duboc D, Fardeau M, Toniolo D, Schwartz K. Mutations in the gene encoding lamin A/C cause autosomal dominant Emery-Dreifuss muscular dystrophy. *Nat Genet.* 1999;21(3):285-288.

83. Dubowitz V. 68th ENMC international workshop (5th international workshop): On congenital muscular dystrophy, 9-11 April 1999, Naarden, The Netherlands. *Neuromuscul Disord.* 1999;9(6-7):446-454.

84. Quijano-Roy S, Mbieleu B, Bonnemann CG, Jeannet PY, Colomer J, Clarke NF, Cuisset JM, Roper H, De Meirleir L, D'Amico A, Ben Yaou R, Nascimento A, Barois A, Demay L, Bertini E, Ferreiro A, Sewry CA, Romero NB, Ryan M, Muntoni F, Guicheney P, Richard P, Bonne G, Estournet B. De novo LMNA mutations cause a new form of congenital muscular dystrophy. *Ann Neurol.* 2008;64(2):177-186.

85. Perrot A, Hussein S, Ruppert V, Schmidt HH, Wehnert MS, Duong NT, Posch MG, Panek A, Dietz R, Kindermann I, Bohm M, Michalewska-Wludarczyk A, Richter A, Maisch B, Pankuweit S, Ozcelik C. Identification of mutational hot spots in LMNA encoding lamin A/C in patients with familial dilated cardiomyopathy. *Basic Res Cardiol.* 2008.

86. Zhang YQ, Sarge KD. Sumoylation regulates lamin A function and is lost in lamin A mutants associated with familial cardiomyopathies. *J Cell Biol.* 2008;182(1):35-39.

87. Basson CT, Solomon SD, Weissman B, MacRae CA, Poznanski AK, Prieto F, Ruiz de la Fuente S, Pease WE, Levin SE, Holmes LB, et al. Genetic heterogeneity of heart-hand syndromes. *Circulation.* 1995;91(5):1326-1329.

88. Sinkovec M, Petrovic D, Volk M, Peterlin B. Familial progressive sinoatrial and atrioventricular conduction disease of adult onset with sudden death, dilated cardiomyopathy, and brachydactyly. A new type of heart-hand syndrome? *Clin Genet.* 2005;68(2):155-160.

89. Renou L, Stora S, Yaou RB, Volk M, Sinkovec M, Demay L, Richard P, Peterlin B, Bonne G. Heart-hand syndrome of Slovenian type: a new kind of laminopathy. *J Med Genet.* 2008;45(10):666-671.

90. Vigouroux C, Capeau J. A-type lamin-linked lipodystrophies. *Novartis Found Symp.* 2005;264:166-177; discussion 177-182, 227-130.

91. Young J, Morbois-Trabut L, Couzinet B, Lascols O, Dion E, Bereziat V, Feve B, Richard I, Capeau J, Chanson P, Vigouroux C. Type A insulin resistance syndrome revealing a novel lamin A mutation. *Diabetes.* 2005;54(6):1873-1878.

92. Goizet C, Yaou RB, Demay L, Richard P, Bouillot S, Rouanet M, Hermosilla E, Le Masson G, Lagueny A, Bonne G, Ferrer X. A new mutation of the lamin A/C gene leading to autosomal dominant axonal neuropathy, muscular dystrophy, cardiac disease, and leuconychia. *J Med Genet.* 2004;41(3):e29.

93. Novelli G, Muchir A, Sangiuolo F, Helbling-Leclerc A, D'Apice MR, Massart C, Capon F, Sbraccia P, Federici M, Lauro R, Tudisco C, Pallotta R, Scarano G, Dallapiccola B, Merlini L, Bonne G. Mandibuloacral dysplasia is caused by a mutation in LMNA-encoding lamin A/C. *Am J Hum Genet.* 2002;71(2):426-431.

94. Garg A, Cogulu O, Ozkinay F, Onay H, Agarwal AK. A novel homozygous Ala529Val LMNA mutation in Turkish patients with mandibuloacral dysplasia. *J Clin Endocrinol Metab.* 2005;90(9):5259-5264.

95. Agarwal AK, Fryns JP, Auchus RJ, Garg A. Zinc metalloproteinase, ZMPSTE24, is mutated in mandibuloacral dysplasia. *Hum Mol Genet.* 2003;12(16):1995-2001.

96. Navarro CL, De Sandre-Giovannoli A, Bernard R, Boccaccio I, Boyer A, Genevieve D, Hadj-Rabia S, Gaudy-Marqueste C, Smitt HS, Vabres P, Faivre L, Verloes A, Van Essen T, Flori E, Hennekam R, Beemer FA, Laurent N, Le Merrer M, Cau P, Levy N. Lamin A and ZMPSTE24 (FACE-1) defects cause nuclear disorganization and identify restrictive dermopathy as a lethal neonatal laminopathy. *Hum Mol Genet.* 2004;13(20):2493-2503.

97. Caux F, Dubosclard E, Lascols O, Buendia B, Chazouilleres O, Cohen A, Courvalin JC, Laroche L, Capeau J, Vigouroux C, Christin-Maitre S. A new clinical condition linked to a novel mutation in lamins A and C with generalized lipoatrophy, insulin-resistant diabetes, disseminated leukomelanodermic papules, liver steatosis, and cardiomyopathy. *J Clin Endocrinol Metab.* 2003;88(3):1006-1013.

98. van Engelen BG, Muchir A, Hutchison CJ, van der Kooi AJ, Bonne G, Lammens M. The lethal phenotype of a homozygous nonsense mutation in the lamin A/C gene. *Neurology.* 2005;64(2):374-376.

99. Nikolova V, Leimena C, McMahon AC, Tan JC, Chandar S, Jogia D, Kesteven SH, Michalicek J, Otway R, Verheyen F, Rainer S, Stewart CL, Martin D, Feneley MP, Fatkin D. Defects in nuclear structure and function promote dilated cardiomyopathy in lamin A/C-deficient mice. *J Clin Invest.* 2004;113(3):357-369.

100. Melcon G, Kozlov S, Cutler DA, Sullivan T, Hernandez L, Zhao P, Mitchell S, Nader G, Bakay M, Rottman JN, Hoffman EP, Stewart CL. Loss of emerin at the nuclear envelope disrupts the Rb1/E2F and MyoD pathways during muscle regeneration. *Hum Mol Genet.* 2006;15(4):637-651.

101. Frock RL, Kudlow BA, Evans AM, Jameson SA, Hauschka SD, Kennedy BK. Lamin A/C and emerin are critical for skeletal muscle satellite cell differentiation. *Genes Dev.* 2006;20(4):486-500.

102. Rudnicki MA, Braun T, Hinuma S, Jaenisch R. Inactivation of MyoD in mice leads to up-regulation of the myogenic HLH gene Myf-5 and results in apparently normal muscle development. *Cell.* 1992;71(3):383-390.

103. Novitch BG, Spicer DB, Kim PS, Cheung WL, Lassar AB. pRb is required for MEF2-dependent gene expression as well as cell-cycle arrest during skeletal muscle differentiation. *Curr Biol.* 1999;9(9):449-459.

104. Johnson BR, Nitta RT, Frock RL, Mounkes L, Barbie DA, Stewart CL, Harlow E, Kennedy BK. A-type lamins regulate retinoblastoma protein function by promoting subnuclear localization and preventing proteasomal degradation. *Proc Natl Acad Sci U S A.* 2004;101(26):9677-9682.

105. De Sandre-Giovannoli A, Chaouch M, Kozlov S, Vallat JM, Tazir M, Kassouri N, Szepetowski P, Hammadouche T, Vandenberghe A, Stewart CL, Grid D, Levy N. Homozygous defects in LMNA, encoding lamin A/C nuclear-envelope proteins, cause autosomal recessive axonal neuropathy in human (Charcot-Marie-Tooth disorder type 2) and mouse. *Am J Hum Genet.* 2002;70(3):726-736.

106. Mejat A, Decostre V, Li J, Renou L, Kesari A, Hantai D, Stewart CL, Xiao X, Hoffman E, Bonne G, Misteli T. Lamin A/C-mediated neuromuscular junction defects in Emery-Dreifuss muscular dystrophy. *J Cell Biol.* 2009;184(1):31-44.

107. Alsheimer M, Liebe B, Sewell L, Stewart CL, Scherthan H, Benavente R. Disruption of spermatogenesis in mice lacking A-type lamins. *J Cell Sci.* 2004;117(Pt 7):1173-1178.

108. Arimura T, Helbling-Leclerc A, Massart C, Varnous S, Niel F, Lacene E, Fromes Y, Toussaint M, Mura AM, Keller DI, Amthor H, Isnard R, Malissen M, Schwartz K, Bonne G. Mouse model carrying H222P-Lmna mutation develops muscular dystrophy and dilated cardiomyopathy similar to human striated muscle laminopathies. *Hum Mol Genet.* 2005;14(1):155-169.

109. Mounkes LC, Kozlov SV, Rottman JN, Stewart CL. Expression of an LMNA-N195K variant of A-type lamins results in cardiac conduction defects and death in mice. *Hum Mol Genet.* 2005;14(15):2167-2180.

110. Wang Y, Herron AJ, Worman HJ. Pathology and nuclear abnormalities in hearts of transgenic mice expressing M371K lamin A encoded by an LMNA mutation causing Emery-Dreifuss muscular dystrophy. *Hum Mol Genet.* 2006;15(16):2479-2489.

111. Mounkes LC, Kozlov S, Hernandez L, Sullivan T, Stewart CL. A progeroid syndrome in mice is caused by defects in A-type lamins. *Nature.* 2003;423(6937):298-301.

112. Yang SH, Bergo MO, Toth JI, Qiao X, Hu Y, Sandoval S, Meta M, Bendale P, Gelb MH, Young SG, Fong LG. Blocking protein farnesyltransferase improves nuclear blebbing in mouse fibroblasts with a targeted Hutchinson-Gilford progeria syndrome mutation. *Proc Natl Acad Sci U S A.* 2005;102(29):10291-10296.

113. Varga R, Eriksson M, Erdos MR, Olive M, Harten I, Kolodgie F, Capell BC, Cheng J, Faddah D, Perkins S, Avallone H, San H, Qu X, Ganesh S, Gordon LB, Virmani R, Wight TN, Nabel EG, Collins FS. Progressive vascular smooth muscle cell defects in a mouse

model of Hutchinson-Gilford progeria syndrome. *Proc Natl Acad Sci U S A.* 2006;103(9):3250-3255.

114. Pendas AM, Zhou Z, Cadinanos J, Freije JM, Wang J, Hultenby K, Astudillo A, Wernerson A, Rodriguez F, Tryggvason K, Lopez-Otin C. Defective prelamin A processing and muscular and adipocyte alterations in Zmpste24 metalloproteinase-deficient mice. *Nat Genet.* 2002;31(1):94-99.

115. Bergo MO, Gavino B, Ross J, Schmidt WK, Hong C, Kendall LV, Mohr A, Meta M, Genant H, Jiang Y, Wisner ER, Van Bruggen N, Carano RA, Michaelis S, Griffey SM, Young SG. Zmpste24 deficiency in mice causes spontaneous bone fractures, muscle weakness, and a prelamin A processing defect. *Proc Natl Acad Sci U S A.* 2002;99(20):13049-13054.

116. Stewart CL, Kozlov S, Fong LG, Young SG. Mouse models of the laminopathies. *Exp Cell Res.* 2007;313(10):2144-2156.

117. Yang SH, Meta M, Qiao X, Frost D, Bauch J, Coffinier C, Majumdar S, Bergo MO, Young SG, Fong LG. A farnesyltransferase inhibitor improves disease phenotypes in mice with a Hutchinson-Gilford progeria syndrome mutation. *J Clin Invest.* 2006;116(8):2115-2121.

118. Fong LG, Frost D, Meta M, Qiao X, Yang SH, Coffinier C, Young SG. A protein farnesyltransferase inhibitor ameliorates disease in a mouse model of progeria. *Science.* 2006;311(5767):1621-1623.

119. Yang SH, Qiao X, Farber E, Chang SY, Fong LG, Young SG. Eliminating the synthesis of mature lamin A reduces disease phenotypes in mice carrying a Hutchinson-Gilford progeria syndrome allele. *J Biol Chem.* 2008;283(11):7094-7099.

120. Yang SH, Andres DA, Spielmann HP, Young SG, Fong LG. Progerin elicits disease phenotypes of progeria in mice whether or not it is farnesylated. *J Clin Invest.* 2008;118(10):3291-3300.

121. Fong LG, Ng JK, Meta M, Cote N, Yang SH, Stewart CL, Sullivan T, Burghardt A, Majumdar S, Reue K, Bergo MO, Young SG. Heterozygosity for Lmna deficiency eliminates the progeria-like phenotypes in Zmpste24-deficient mice. *Proc Natl Acad Sci U S A.* 2004;101(52):18111-18116.

122. Ozawa R, Hayashi YK, Ogawa M, Kurokawa R, Matsumoto H, Noguchi S, Nonaka I, Nishino I. Emerin-lacking mice show minimal motor and cardiac dysfunctions with nuclear-associated vacuoles. *Am J Pathol.* 2006;168(3):907-917.

123. Vergnes L, Peterfy M, Bergo MO, Young SG, Reue K. Lamin B1 is required for mouse development and nuclear integrity. *Proc Natl Acad Sci U S A.* 2004;101(28):10428-10433.

124. Espada J, Varela I, Flores I, Ugalde AP, Cadinanos J, Pendas AM, Stewart CL, Tryggvason K, Blasco MA, Freije JM, Lopez-Otin C. Nuclear envelope defects cause stem cell dysfunction in premature-aging mice. *J Cell Biol.* 2008;181(1):27-35.

125. Scaffidi P, Misteli T. Lamin A-dependent misregulation of adult stem cells associated with accelerated ageing. *Nat Cell Biol.* 2008;10(4):452-459.

126. Buckingham M. Myogenic progenitor cells and skeletal myogenesis in vertebrates. *Curr Opin Genet Dev.* 2006;16(5):525-532.

127. Bryson-Richardson RJ, Currie PD. The genetics of vertebrate myogenesis. *Nat Rev Genet.* 2008;9(8):632-646.

128. Chen AE, Ginty DD, Fan CM. Protein kinase A signaling via CREB controls myogenesis induced by Wnt proteins. *Nature.* 2005;433(7023):317-322.

129. Amthor H, Otto A, Macharia R, McKinnell I, Patel K. Myostatin imposes reversible quiescence on embryonic muscle precursors. *Dev Dyn.* 2006;235(3):672-680.

130. Le Grand F, Rudnicki MA. Skeletal muscle satellite cells and adult myogenesis. *Curr Opin Cell Biol.* 2007;19(6):628-633.

131. Zammit PS. All muscle satellite cells are equal, but are some more equal than others? *J Cell Sci.* 2008;121(Pt 18):2975-2982.

132. Kuang S, Kuroda K, Le Grand F, Rudnicki MA. Asymmetric self-renewal and commitment of satellite stem cells in muscle. *Cell.* 2007;129(5):999-1010.

133. Peault B, Rudnicki M, Torrente Y, Cossu G, Tremblay JP, Partridge T, Gussoni E, Kunkel LM, Huard J. Stem and progenitor cells in skeletal muscle development, maintenance, and therapy. *Mol Ther.* 2007;15(5):867-877.

134. Gopinath SD, Rando TA. Stem cell review series: aging of the skeletal muscle stem cell niche. *Aging Cell.* 2008;7(4):590-598.

135. Bischoff R. Interaction between satellite cells and skeletal muscle fibers. *Development.* 1990;109(4):943-952.

136. Conboy IM, Conboy MJ, Smythe GM, Rando TA. Notch-mediated restoration of regenerative potential to aged muscle. *Science.* 2003;302(5650):1575-1577.

137. Robert L, Labat-Robert J. Aging of connective tissues: from genetic to epigenetic mechanisms. *Biogerontology.* 2000;1(2):123-131.

138. Sartorelli V, Caretti G. Mechanisms underlying the transcriptional regulation of skeletal myogenesis. *Curr Opin Genet Dev.* 2005;15(5):528-535.

139. De Falco G, Comes F, Simone C. pRb: master of differentiation. Coupling irreversible cell cycle withdrawal with induction of muscle-specific transcription. *Oncogene.* 2006;25(38):5244-5249.

140. Megeney LA, Kablar B, Garrett K, Anderson JE, Rudnicki MA. MyoD is required for myogenic stem cell function in adult skeletal muscle. *Genes Dev.* 1996;10(10):1173-1183.

141. Lee EY, Chang CY, Hu N, Wang YC, Lai CC, Herrup K, Lee WH, Bradley A. Mice deficient for Rb are nonviable and show defects in neurogenesis and haematopoiesis. *Nature.* 1992;359(6393):288-294.

142. Huh MS, Parker MH, Scime A, Parks R, Rudnicki MA. Rb is required for progression through myogenic differentiation but not maintenance of terminal differentiation. *J Cell Biol.* 2004;166(6):865-876.

143. Muralikrishna B, Dhawan J, Rangaraj N, Parnaik VK. Distinct changes in intranuclear lamin A/C organization during myoblast differentiation. *J Cell Sci.* 2001;114(Pt 22):4001-4011.

144. Markiewicz E, Ledran M, Hutchison CJ. Remodeling of the nuclear lamina and nucleoskeleton is required for skeletal muscle differentiation in vitro. *J Cell Sci.* 2005;118(Pt 2):409-420.

145. Favreau C, Higuet D, Courvalin JC, Buendia B. Expression of a mutant lamin A that causes Emery-Dreifuss muscular dystrophy inhibits in vitro differentiation of C2C12 myoblasts. *Mol Cell Biol.* 2004;24(4):1481-1492.

146. Bakay M, Wang Z, Melcon G, Schiltz L, Xuan J, Zhao P, Sartorelli V, Seo J, Pegoraro E, Angelini C, Shneiderman B, Escolar D, Chen YW, Winokur ST, Pachman LM, Fan C, Mandler R, Nevo Y, Gordon E, Zhu Y, Dong Y, Wang Y, Hoffman EP. Nuclear envelope dystrophies show a transcriptional fingerprint suggesting disruption of Rb-MyoD pathways in muscle regeneration. *Brain.* 2006;129(Pt 4):996-1013.

147. Brodsky GL, Bowersox JA, Fitzgerald-Miller L, Miller LA, Maclean KN. The prelamin A pre-peptide induces cardiac and skeletal myoblast differentiation. *Biochem Biophys Res Commun.* 2007;356(4):872-879.

148. Bassel-Duby R, Olson EN. Signaling pathways in skeletal muscle remodeling. *Annu Rev Biochem.* 2006;75:19-37.

149. Hughes SM, Koishi K, Rudnicki M, Maggs AM. MyoD protein is differentially accumulated in fast and slow skeletal muscle fibres and required for normal fibre type balance in rodents. *Mech Dev.* 1997;61(1-2):151-163.

150. Ekmark M, Gronevik E, Schjerling P, Gundersen K. Myogenin induces higher oxidative capacity in pre-existing mouse muscle fibres after somatic DNA transfer. *J Physiol.* 2003;548(Pt 1):259-269.

151. Ekmark M, Rana ZA, Stewart G, Hardie DG, Gundersen K. De-phosphorylation of MyoD is linking nerve-evoked activity to fast myosin heavy chain expression in rodent adult skeletal muscle. *J Physiol.* 2007;584(Pt 2):637-650.

152. Wu H, Naya FJ, McKinsey TA, Mercer B, Shelton JM, Chin ER, Simard AR, Michel RN, Bassel-Duby R, Olson EN, Williams RS. MEF2 responds to multiple calcium-regulated signals in the control of skeletal muscle fiber type. *Embo J.* 2000;19(9):1963-1973.

153. Kitamura T, Kitamura YI, Funahashi Y, Shawber CJ, Castrillon DH, Kollipara R, DePinho RA, Kitajewski J, Accili D. A Foxo/Notch pathway controls myogenic differentiation and fiber type specification. *J Clin Invest.* 2007;117(9):2477-2485.

154. Fischer A, Gessler M. Delta-Notch--and then? Protein interactions and proposed modes of repression by Hes and Hey bHLH factors. *Nucleic Acids Res.* 2007;35(14):4583-4596.

155. Hong JS, Ki CS, Kim JW, Suh YL, Kim JS, Baek KK, Kim BJ, Ahn KJ, Kim DK. Cardiac dysrhythmias,cardiomyopathy and muscular dystrophy in patients with Emery-Dreifuss muscular dystrophy and limb-girdle muscular dystrophy type 1B. *J Korean Med Sci.* 2005;20(2):283-290.

156. Mittelbronn M, Hanisch F, Gleichmann M, Stotter M, Korinthenberg R, Wehnert M, Bonne G, Rudnik-Schoneborn S, Bornemann A. Myofiber degeneration in autosomal dominant

Emery-Dreifuss muscular dystrophy (AD-EDMD) (LGMD1B). *Brain Pathol.* 2006;16(4):266-272.

157. Srivastava D. Making or breaking the heart: from lineage determination to morphogenesis. *Cell.* 2006;126(6):1037-1048.

158. Black BL. Transcriptional pathways in second heart field development. *Semin Cell Dev Biol.* 2007;18(1):67-76.

159. Srivastava D, Thomas T, Lin Q, Kirby ML, Brown D, Olson EN. Regulation of cardiac mesodermal and neural crest development by the bHLH transcription factor, dHAND. *Nat Genet.* 1997;16(2):154-160.

160. Lin Q, Schwarz J, Bucana C, Olson EN. Control of mouse cardiac morphogenesis and myogenesis by transcription factor MEF2C. *Science.* 1997;276(5317):1404-1407.

161. von Both I, Silvestri C, Erdemir T, Lickert H, Walls JR, Henkelman RM, Rossant J, Harvey RP, Attisano L, Wrana JL. Foxh1 is essential for development of the anterior heart field. *Dev Cell.* 2004;7(3):331-345.

162. Laugwitz KL, Moretti A, Lam J, Gruber P, Chen Y, Woodard S, Lin LZ, Cai CL, Lu MM, Reth M, Platoshyn O, Yuan JX, Evans S, Chien KR. Postnatal isl1+ cardioblasts enter fully differentiated cardiomyocyte lineages. *Nature.* 2005;433(7026):647-653.

163. Moretti A, Caron L, Nakano A, Lam JT, Bernshausen A, Chen Y, Qyang Y, Bu L, Sasaki M, Martin-Puig S, Sun Y, Evans SM, Laugwitz KL, Chien KR. Multipotent embryonic isl1+ progenitor cells lead to cardiac, smooth muscle, and endothelial cell diversification. *Cell.* 2006;127(6):1151-1165.

164. McGill CJ, Brooks G. Cell cycle control mechanisms and their role in cardiac growth. *Cardiovasc Res.* 1995;30(4):557-569.

165. Papadimou E, Menard C, Grey C, Puceat M. Interplay between the retinoblastoma protein and LEK1 specifies stem cells toward the cardiac lineage. *Embo J.* 2005;24(9):1750-1761.

166. MacLellan WR, Garcia A, Oh H, Frenkel P, Jordan MC, Roos KP, Schneider MD. Overlapping roles of pocket proteins in the myocardium are unmasked by germ line deletion of p130 plus heart-specific deletion of Rb. *Mol Cell Biol.* 2005;25(6):2486-2497.

167. Flink IL, Oana S, Maitra N, Bahl JJ, Morkin E. Changes in E2F complexes containing retinoblastoma protein family members and increased cyclin-dependent kinase inhibitor activities during terminal differentiation of cardiomyocytes. *J Mol Cell Cardiol.* 1998;30(3):563-578.

168. Afilalo J, Sebag IA, Chalifour LE, Rivas D, Akter R, Sharma K, Duque G. Age-related changes in lamin A/C expression in cardiomyocytes. *Am J Physiol Heart Circ Physiol.* 2007;293(3):H1451-1456.

169. Gupta S, Das B, Sen S. Cardiac hypertrophy: mechanisms and therapeutic opportunities. *Antioxid Redox Signal.* 2007;9(6):623-652.

170. Rafael JA, Nitta Y, Peters J, Davies KE. Testing of SHIRPA, a mouse phenotypic assessment protocol, on Dmd(mdx) and Dmd(mdx3cv) dystrophin-deficient mice. *Mamm Genome.* 2000;11(9):725-728.

171. Shefer G, Yablonka-Reuveni Z. Isolation and culture of skeletal muscle myofibers as a means to analyze satellite cells. *Methods Mol Biol.* 2005;290:281-304.

172. Amalfitano A, Chamberlain JS. The mdx-amplification-resistant mutation system assay, a simple and rapid polymerase chain reaction-based detection of the mdx allele. *Muscle Nerve.* 1996;19(12):1549-1553.

173. Yan Z, Choi S, Liu X, Zhang M, Schageman JJ, Lee SY, Hart R, Lin L, Thurmond FA, Williams RS. Highly coordinated gene regulation in mouse skeletal muscle regeneration. *J Biol Chem.* 2003;278(10):8826-8836.

174. Moran AL, Warren GL, Lowe DA. Soleus and EDL muscle contractility across the lifespan of female C57BL/6 mice. *Exp Gerontol.* 2005;40(12):966-975.

175. Metzler B, Mair J, Lercher A, Schaber C, Hintringer F, Pachinger O, Xu Q. Mouse model of myocardial remodeling after ischemia: role of intercellular adhesion molecule-1. *Cardiovasc Res.* 2001;49(2):399-407.

176. Dixon RW, Harris JB. Myotoxic activity of the toxic phospholipase, notexin, from the venom of the Australian tiger snake. *J Neuropathol Exp Neurol.* 1996;55(12):1230-1237.

177. Xin M, Davis CA, Molkentin JD, Lien CL, Duncan SA, Richardson JA, Olson EN. A threshold of GATA4 and GATA6 expression is required for cardiovascular development. *Proc Natl Acad Sci U S A.* 2006;103(30):11189-11194.

178. Bisping E, Ikeda S, Kong SW, Tarnavski O, Bodyak N, McMullen JR, Rajagopal S, Son JK, Ma Q, Springer Z, Kang PM, Izumo S, Pu WT. Gata4 is required for maintenance of postnatal cardiac function and protection from pressure overload-induced heart failure. *Proc Natl Acad Sci U S A.* 2006;103(39):14471-14476.

179. van Oort RJ, van Rooij E, Bourajjaj M, Schimmel J, Jansen MA, van der Nagel R, Doevendans PA, Schneider MD, van Echteld CJ, De Windt LJ. MEF2 activates a genetic program promoting chamber dilation and contractile dysfunction in calcineurin-induced heart failure. *Circulation.* 2006;114(4):298-308.

180. Kerkela R, Pikkarainen S, Majalahti-Palviainen T, Tokola H, Ruskoaho H. Distinct roles of mitogen-activated protein kinase pathways in GATA-4 transcription factor-mediated regulation of B-type natriuretic peptide gene. *J Biol Chem.* 2002;277(16):13752-13760.

181. Morin S, Charron F, Robitaille L, Nemer M. GATA-dependent recruitment of MEF2 proteins to target promoters. *Embo J.* 2000;19(9):2046-2055.

182. Pipes GC, Creemers EE, Olson EN. The myocardin family of transcriptional coactivators: versatile regulators of cell growth, migration, and myogenesis. *Genes Dev.* 2006;20(12):1545-1556.

183. Kuwahara K, Teg Pipes GC, McAnally J, Richardson JA, Hill JA, Bassel-Duby R, Olson EN. Modulation of adverse cardiac remodeling by STARS, a mediator of MEF2 signaling and SRF activity. *J Clin Invest.* 2007;117(5):1324-1334.

184. Kuisk IR, Li H, Tran D, Capetanaki Y. A single MEF2 site governs desmin transcription in both heart and skeletal muscle during mouse embryogenesis. *Dev Biol.* 1996;174(1):1-13.

185. Hasegawa K, Lee SJ, Jobe SM, Markham BE, Kitsis RN. cis-Acting sequences that mediate induction of beta-myosin heavy chain gene expression during left ventricular hypertrophy due to aortic constriction. *Circulation.* 1997;96(11):3943-3953.

186. Pikkarainen S, Tokola H, Kerkela R, Ruskoaho H. GATA transcription factors in the developing and adult heart. *Cardiovasc Res.* 2004;63(2):196-207.

187. Wiesner RJ, Ehmke H, Faulhaber J, Zak R, Ruegg JC. Dissociation of left ventricular hypertrophy, beta-myosin heavy chain gene expression, and myosin isoform switch in rats after ascending aortic stenosis. *Circulation.* 1997;95(5):1253-1259.

188. Monreal G, Nicholson LM, Han B, Joshi MS, Phillips AB, Wold LE, Bauer JA, Gerhardt MA. Cytoskeletal remodeling of desmin is a more accurate measure of cardiac dysfunction than fibrosis or myocyte hypertrophy. *Life Sci.* 2008;83(23-24):786-794.

189. MacLellan WR, Schneider MD. Genetic dissection of cardiac growth control pathways. *Annu Rev Physiol.* 2000;62:289-319.

190. Chien KR, Knowlton KU, Zhu H, Chien S. Regulation of cardiac gene expression during myocardial growth and hypertrophy: molecular studies of an adaptive physiologic response. *Faseb J.* 1991;5(15):3037-3046.

191. Bulfield G, Siller WG, Wight PA, Moore KJ. X chromosome-linked muscular dystrophy (mdx) in the mouse. *Proc Natl Acad Sci U S A.* 1984;81(4):1189-1192.

192. Quinlan JG, Hahn HS, Wong BL, Lorenz JN, Wenisch AS, Levin LS. Evolution of the mdx mouse cardiomyopathy: physiological and morphological findings. *Neuromuscul Disord.* 2004;14(8-9):491-496.

193. Danialou G, Comtois AS, Dudley R, Karpati G, Vincent G, Des Rosiers C, Petrof BJ. Dystrophin-deficient cardiomyocytes are abnormally vulnerable to mechanical stress-induced contractile failure and injury. *Faseb J.* 2001;15(9):1655-1657.

194. Bruning JC, Michael MD, Winnay JN, Hayashi T, Horsch D, Accili D, Goodyear LJ, Kahn CR. A muscle-specific insulin receptor knockout exhibits features of the metabolic syndrome of NIDDM without altering glucose tolerance. *Mol Cell.* 1998;2(5):559-569.

195. Stanley EG, Biben C, Elefanty A, Barnett L, Koentgen F, Robb L, Harvey RP. Efficient Cre-mediated deletion in cardiac progenitor cells conferred by a 3'UTR-ires-Cre allele of the homeobox gene Nkx2-5. *Int J Dev Biol.* 2002;46(4):431-439.

196. Zammit PS, Golding JP, Nagata Y, Hudon V, Partridge TA, Beauchamp JR. Muscle satellite cells adopt divergent fates: a mechanism for self-renewal? *J Cell Biol.* 2004;166(3):347-357.

197. Sicinski P, Geng Y, Ryder-Cook AS, Barnard EA, Darlison MG, Barnard PJ. The molecular basis of muscular dystrophy in the mdx mouse: a point mutation. *Science.* 1989;244(4912):1578-1580.

198. Cerletti M, Jurga S, Witczak CA, Hirshman MF, Shadrach JL, Goodyear LJ, Wagers AJ. Highly efficient, functional engraftment of skeletal muscle stem cells in dystrophic muscles. *Cell.* 2008;134(1):37-47.

199. Shefer G, Van de Mark DP, Richardson JB, Yablonka-Reuveni Z. Satellite-cell pool size does matter: defining the myogenic potency of aging skeletal muscle. *Dev Biol.* 2006;294(1):50-66.

200. Lyons GE, Muhlebach S, Moser A, Masood R, Paterson BM, Buckingham ME, Perriard JC. Developmental regulation of creatine kinase gene expression by myogenic factors in embryonic mouse and chick skeletal muscle. *Development.* 1991;113(3):1017-1029.

201. Kim YK, Suarez J, Hu Y, McDonough PM, Boer C, Dix DJ, Dillmann WH. Deletion of the inducible 70-kDa heat shock protein genes in mice impairs cardiac contractile function and calcium handling associated with hypertrophy. *Circulation.* 2006;113(22):2589-2597.

202. Marber MS, Mestril R, Chi SH, Sayen MR, Yellon DM, Dillmann WH. Overexpression of the rat inducible 70-kD heat stress protein in a transgenic mouse increases the resistance of the heart to ischemic injury. *J Clin Invest.* 1995;95(4):1446-1456.

203. Keller C, Hansen MS, Coffin CM, Capecchi MR. Pax3:Fkhr interferes with embryonic Pax3 and Pax7 function: implications for alveolar rhabdomyosarcoma cell of origin. *Genes Dev.* 2004;18(21):2608-2613.

204. Seale P, Sabourin LA, Girgis-Gabardo A, Mansouri A, Gruss P, Rudnicki MA. Pax7 is required for the specification of myogenic satellite cells. *Cell.* 2000;102(6):777-786.

205. Relaix F, Montarras D, Zaffran S, Gayraud-Morel B, Rocancourt D, Tajbakhsh S, Mansouri A, Cumano A, Buckingham M. Pax3 and Pax7 have distinct and overlapping functions in adult muscle progenitor cells. *J Cell Biol.* 2006;172(1):91-102.

206. Totsuka Y, Nagao Y, Horii T, Yonekawa H, Imai H, Hatta H, Izaike Y, Tokunaga T, Atomi Y. Physical performance and soleus muscle fiber composition in wild-derived and laboratory inbred mouse strains. *J Appl Physiol.* 2003;95(2):720-727.

207. Nishijo K, Hosoyama T, Bjornson CR, Schaffer BS, Prajapati SI, Bahadur AN, Hansen MS, Blandford MC, McCleish AT, Rubin BP, Epstein JA, Rando TA, Capecchi MR, Keller C. Biomarker system for studying muscle, stem cells, and cancer in vivo. *Faseb J.* 2009.

208. Stoykova A, Gruss P. Roles of Pax-genes in developing and adult brain as suggested by expression patterns. *J Neurosci.* 1994;14(3 Pt 2):1395-1412.

5 Acknowledgment

To those who believed in me and pushed me forward.

Thank you

6 Curriculum vitae

EUROPEAN CURRICULUM VITAE FORMAT

PERSONAL INFORMATION

Name	**GOTIC, IVANA**
Address	**2/25 HERNALSER GUERTEL, 1080 VIENNA, AUSTRIA**
E-mail	**ivana.gotic@univie.ac.at**
Nationality	Croatian
Date of birth	13.08.1980

EDUCATION AND TRAINING

• Dates	December 2004 onwards
• Name and type of organization providing education and training	Max F. Perutz Laboratories, Department of Medical Biochemistry, Medical University of Vienna, Dr. Bohr-Gasse 9, A-1030 Vienna, Austria. University of Vienna, Faculty of Life Science, Department of Molecular Biology, Vienna, Austria.
• Title of qualification awarded	**PhD in Molecular Biology expected in 2009**
• Principal subjects/occupational skills covered	Thesis Title: *Role of lamina-associated polypeptide 2α in muscle differentiation and regeneration* Research experience in: ▪ molecular and cellular biology ▪ mouse anatomy and physiology ▪ histology ▪ transgenic mouse models

• Dates	October 2003 – July 2004
• Name and type of organization providing education and training	Laboratory for Experimental Cancerology, Department of Molecular Biology, Ruđer Bošković Institute, Zagreb, Croatia.
• Principal subjects/occupational skills covered	Diploma Thesis Title: "*Telomerase activity during growth of HeLa cells*". Research experience in molecular and cellular biology.

• Dates	July 1999 – July 2004
• Name and type of organization providing education and training	University of Zagreb, Faculty of Science, Department of Biology, Zagreb, Croatia.
• Principal subjects/occupational skills covered	Eight semesters of lectures and laboratory courses completed in June 2003
• Title of qualification awarded	**Diploma in Molecular Biology**

Additional Certificates

"Deutsches Sprachdiplom, zweite Stufe", an international diploma of German language acquired in 1999, recognized as fulfilling German language entry requirements by German universities.
"First certificate in English" grade A – certificate of competence in English awarded by university of Cambridge for candidates whose mother tongue is not English, acquired in 1999.

SCIENTIFIC PUBLICATIONS

- Ivana Gotic, Michael Leschnik, Ursula Kolm, Mato Markovic, Bernhard J. Haubner, Katarzyna Biadasiewicz, Bernhard Metzler, Colin L. Stewart and Roland Foisner:**.**
  LAP2α loss impairs heart function and stress response in mice. *Submitted manuscript*

- Ivana Gotic, Wolfgang M. Schmidt, Katarzyna Biadasiewicz, Michael Leschnik, Rita Spilka, Juliane Braun, Colin L. Stewart and Roland Foisner
  Loss of LAP2α Delays Satellite Cell Differentiation and Affects Postnatal Fibre Type Determination. *Submitted manuscript*

- Naetar, Nana; Korbei, Barbara; Kozlov, Serguei; Dorner, Daniela;Kerenyi, Marc; Kral, Rosana; Gotic, Ivana; Fuchs, Peter; Cohen Tanya; Bittner Reginald; Stewart, Colin L. and Foisner, Roland**.**
  Loss of nucleoplasmic LAP2α–lamin A complexescauses erythroid and epidermal progenitor hyperproliferation. *Nat Cell Biol. 2008 Nov;10 (11):1341-8*

- Ćukušić, Andrea; Ivanković, Milena; Škrobot, Nikolina; Ferenac, Marina; Gotić, Ivana; Matijašić, Mario; Polančec, Denis; Rubelj, Ivica.
  Spontaneous senescence in MDA-MB-231 cell line. *Cell proliferation*. **39** (2006): 205-216.
- Ivanković, Milena; Ćukušić, Andrea; Gotić, Ivana; Škrobot, Nikolina; Matijašić, Mario; Polančec, Denis; Rubelj, Ivica.
  Telomerase activity in HeLa cervical carcinoma cell line proliferation. *Biogerontology*. **8(2)** (2007): 163-172.

SCIENTIFIC ORAL PRESENTATIONS

- **Role of Lamina-associated polypeptide 2α in striated muscle differentiation and regeneration**
  The Multiple Faces of Lamins in Aging & Disease, EMBO Workshop, January 6-9, 2009, Vienna Austria
- **Role of Lap2α – Lamin A complexes in muscle differentiation and regeneration.**
  Annual Euro-laminopathies Meeting, March 22-24, 2007, Rome, Italy.
- **Role of Lap2α – Lamin A complexes in muscle differentiation and regeneration.**
  Anatomy and Embryology of the Mouse, EMBO Practical Course, September 9-17, 2006, Zagreb, Croatia.

SCIENTIFIC POSTER PRESENTATIONS

- Ivana Gotic and Roland Foisner: **Role of Lap2α – Lamin A complexes in muscle differentiation and regeneration.**
  Advances in Stem Cell Research, EMBO Conference Series, October 12-14, 2007, Stockholm, Sweden.
- Ivana Gotic and Roland Foisner: **Role of Lap2α – Lamin A complexes in muscle differentiation and regeneration.**
  Muscle Development and Regeneration Workshop, Myores Network of Excellence, September 19-22, 2007, Berlin, Germany.
- Ivana Gotic and Roland Foisner: **Role of Lap2α – Lamin A complexes in muscle differentiation and regeneration.**
  International PhD conference, June 24-26, 2007, Cambridge, UK.
- Ivana Gotic and Roland Foisner: **Role of Lap2α – Lamin A complexes in muscle differentiation and regeneration.**
  3. PhD-Symposium of the Medical University of Vienna, June 21-22, 2007, Vienna, Austria.
- Andrea Ćukušić, Milena Ivanković, Ivana Gotić, Ivica Rubelj: **Isolation and characterization of senescent cells from immortal human cell line MDA-MB-231.**
  Second congress of Croatian geneticists. September 24-27, 2005, Supetar, Brač, Croatia.
- Milena Ivanković, Ivana Gotić, Andrea Ćukušić, Ivica Rubelj: **Telomerase activity during growth of HeLa cells**. Second conress of Croatian geneticists. September 24-27, 2005, Supetar, Brač, Croatia.

SCIENTIFIC WORKSHOPS

- **EMBO Practical Course** Anatomy and Embryology of the Mouse, September 9-17, 2006, Zagreb, Croatia.
- **EMBO Workshop** The Multiple Faces of Lamins in Aging & Disease, January 6-9, 2009, Vienna Austria

SCIENTIFIC SYMPOSIA

Participated in organization of 2 Vienna Biocenter PhD student symposia:

- **Timing age,** 4th VBC PhD Student Symposium, Vienna, Austria, November 2-3, 2006
- **Molecules to Mind,** 5th VBC PhD Student Symposium, Vienna, Austria, November 15-16, 2007

MOTHER TONGUE **Croatian**

OTHER LANGUAGES

English

• Reading skills	excellent
• Writing skills	excellent
• Verbal skills	excellent

German

• Reading skills	excellent
• Writing skills	excellent
• Verbal skills	excellent

French

• Reading skills	basic
• Writing skills	basic
• Verbal skills	basic

Spanish

• Reading skills	basic
• Writing skills	basic
• Verbal skills	basic

TECHNICAL SKILLS AND COMPETENCES

COMPETENT WITH MOST MICROSOFT OFFICE AND ADOBE PC APPLICATIONS

DRIVING LICENCE

Category B

SOCIAL SKILLS AND COMPETENCES

TEAM WORK, TOLERANCE, FLEXIBILITY, PATIENCE, DISCIPLINE, COMMUNICATION, RESPONSIBILITY